HORIZON NUCLEAR POWER

WYLFA NEWYDD

ENERGY WORKING FOR BRITAIN

Wylfa Newydd Project

6.4.90 ES Volume D - WNDA Development App D13-8 - Marine Hydrodynamic Modelling Report - Wylfa Newydd Development Area

PINS Reference Number: EN010007

Application Reference Number: 6.4.90

June 2018

Revision 1.0

Regulation Number: 5(2)(a)

Planning Act 2008
Infrastructure Planning (Applications: Prescribed Forms and Procedure) Regulations 2009

Horizon Internal DCRM Number: WN0902-JAC-EPT-REP-00001

[This page is intentionally blank]

Wylfa Newydd Project

Marine hydrodynamic modelling report

60PO8077/AQE/REP/008 | 3.0

WN0902-JAC-PAC-REP-00056

1st March 2018

Document history and status

Revision	Date	Description	By	Review	Approved
0	3rd Aug 2017	Marine modelling report – draft (note no reference list provided)	Matt Robson / Andy Moores	Rob Bromley	Rob Bromley
1	16th Aug 2017	Updated to address comments	Matt Robson/ Andy Moores	Rob Bromley	Rob Bromley
2	12th January 2018	Updated to address comments and additional sensitivity section added	Isabel Lee-Elliott	Matt Robson	Rob Bromley
3	1st March	Update to suspended solid modelling results	Isabel Lee-Elliott	Rob Bromley	Rob Bromley

Distribution of copies

Revision	Issue approved	Date issued	Issued to	Comments

Wylfa Newydd

Project No:	60PO8077
Document Title:	Marine hydrodynamic modelling report
Document No.:	60PO8077/AQE/REP/008
Document Reference:	WN0902-JAC-PAC-REP-00056
Revision:	3
Date:	1st March 2018
Client Name:	Horizon Nuclear Power Ltd
Author:	Matt Robson / Andy Moores

Jacobs UK Ltd
Kenneth Dibben House
Enterprise Road
Southampton Science Park
Chilworth
SO16 7NS

Contents

Executive Summary

This report provides a summary of the findings of a series of marine hydrodynamic modelling simulations of the Cooling Water (CW) discharge from the Wylfa Newydd Power Station. The hydrodynamic model simulated the mixing of the thermal and biocide components of the CW discharge within the receiving coastal waters. The simulations provided predicted mixing zones for both temperature and Total Residual Oxidant (TRO) for an average CW discharge of 126 m^3/s with a temperature rise of 12 °C (ΔT +12 °C) and a TRO concentration at the point of discharge of 0.1 mg/l. The marine layout used in the model was based on a western breakwater design of 400m in length.

The approach taken was to model seasonally appropriate TRO decay rates and surface heat loss coefficients. These scenarios were modelled without the influence of wind stress on the water surface. Sensitivity studies were then completed using the average observed wind speed from each of the north, east, south and west sectors. Sensitivity to surface heat loss and representation of the near-field were also investigated.

The extent of the temperature mixing zone was similar for all four seasons modelled. However, the size of the TRO mixing zone varied between the different seasons, with the largest potential surface mixing zone occurring during the summer. The sensitivity of the predicted mixing zones to surface heat flux was examined by modelling scenarios where the heat loss rate varied by 10 $W/m^2/K$ around a base-case of 22 $W/m^2/K$. The predicted thermal mixing zone was shown to be insensitive to the surface heat loss rate. The insensitivity to surface heat loss rate is considered to be due to the dominance of the mixing processes over surface heat exchange at this site, and explains why the thermal mixing zones for all four seasonal base cases are similar.

The model was also run with constant wind inputs from the north, east, south and west sectors. The wind strength used was the average observed from each sector of the RAF Valley 2003 to 2012 data set. With a constant wind from the north, the mixing zone was slightly smaller when compared to the base case. The degree of recirculation increased slightly (0.17 °C increase over the base-case of 0.63 °C). For a constant wind from the east, the mixing zone reduced slightly; however, recirculation remained similar to that of the base case (-0.46 °C). For a constant wind from the south, the size of the mixing zone was reduced, as was the degree of recirculation (by 0.13 °C). A constant wind from the west also resulted in a slight reduction in the size of the mixing zone, but did not change the degree of recirculation.

Therefore, for all wind directions, the inclusion of wind stress in the model resulted in a reduction in size of the mixing zones. The most common wind directions in the RAF Valley data set were from the south and west. While long duration winds from any direction are relatively rare, the sensitivity studies provided confidence that excluding wind stress in the base case simulations was unlikely to have resulted in the under-prediction of the size and temperatures of the mixing zone. A no wind-stress assumption is likely to result in conservative modelling outputs.

Sensitivity runs were also undertaken to examine the influence of the initial assumptions with regard to the near-field mixing on the predicted temperature and TRO fields. The output of the modelling showed that for a short near-field (where the CW discharge was introduced into the model at the actual location of the outfall) the size of the 2 °C mixing zone at the surface was approximately 75% of that predicted in the base case; however, there was no change in the degree of recirculation. With a near-field 100 m longer than in the base case there was slight reduction in the size of the mixing zone and a small increase (0.06 °C) in recirculation. The modelling showed the predicted temperatures and TRO concentrations away from the outfall to be relatively insensitive to the assumptions made for the near-field mixing. It was considered that this was as a result of the geometry of the coastline around the outfall at Porth Wnal, such that it effectively channels and directs the discharge offshore. The relative insensitivity to the near-field representation gives confidence in the final model prediction of the mixing zones.

Simulations were also completed to examine the sensitivity of the predicted mixing zones to the inclusion of wave forcing in the model. The model pulled in boundary wave data from the Project's SWAN wave model for the desired wave condition, which was selected as a wave from the southwest (most common wave direction), with a wave height of 1.5m. Typical and extreme winter wave conditions were also modelled. The resulting model output showed that the addition of waves resulted in a reduced surface mixing zone when compared to the without wave base case.

The report also provides a summary of the modelling work completed to aid assessment of the thermal influence on water quality, specifically dissolved oxygen and un-ionised ammonia, and the formation of chlorinated by-products.

The modelling suggests that operation of the CW discharge is unlikely to affect the Water Framework Directive (WFD) classification on the basis of dissolved oxygen, with predicted levels likely to be reflective of a High status water body. Similarly, the modelling showed that the proposed discharge is unlikely to result in an increase of un-ionised ammonia that would change the classification of the water body. Based on the predicted TRO discharge modelling, baseline water quality measurements and estimates from other UK Power Station discharges, the discharge levels for chloroform and bromoform are likely to be well below the relevant Environmental Quality Standards.

The report also discusses the modelling scenarios used to inform the coastal processes studies, particularly the effects on bed shear stress. The modelling outputs suggest that the Power Station will have limited effects on the bed shear stress during typical wave conditions, although some differences may result during stronger winter wave conditions. However, conditions immediately seaward of the Cemlyn lagoon shingle ridge are not affected by the Power Station.

Modelling was also completed to predicted the dispersion and deposition of suspended solids released as a result of dredging activity and construction drainage. The model outputs showed that the release of fugitive material from dredging activities resulted in elevated suspended solids concentrations and the deposition of material on the bed. However, these elevated levels were very localised, and low when compared to natural deposition rates (MarLin). Suspended solids concentrations and deposited material resulting from construction drainage discharges were localised and very low.

1. Introduction

Horizon Nuclear Power Wylfa Limited (Horizon) is a UK energy company developing a new generation of Nuclear Power Stations to help meet the country's need for stable and sustainable low carbon energy. The Wylfa Newydd Development Area has been listed as an approved site for the construction of a new nuclear facility in the National Policy Statement for Nuclear Power Generation (EN-6) (NPS EN-6), (Department for Energy and Climate Change (DECC), 2011). The approved site (termed the Wylfa NPS Site) comprises a 254 hectare area of land to the south of the existing Magnox Nuclear Power Station (the Existing Power Station, which ceased operation in December 2015).

The development of the Wylfa Newydd Project (the Project) will require a number of applications to be made under different legislations to different regulators. As the Wylfa Newydd Power Station constitutes a Nationally Significant Infrastructure Project, Horizon intends to make an application for a Marine Licence and Development Consent Order (DCO) to the Secretary of State under the *Planning Act 2008* to authorise its construction and operation.

The Project includes the Wylfa Newydd Power Station and Associated Developments. The Wylfa Newydd Power Station includes two UK Advanced Boiling Water Reactors to be supplied by Hitachi-GE Nuclear Energy Ltd, associated plant and ancillary structures and features. In addition to the reactors, development would include steam turbines, control and service buildings, operational plant, radioactive waste storage buildings, ancillary structures, offices and coastal developments. The coastal developments would include Cooling Water (CW) intakes and pumphouse, outfall structures, a breakwater arrangement for CW intake wave protection and a Marine Off-Loading Facility (MOLF (See A1-1 in chapter A1 of the Environmental Statement).

The CW system (CWS) consists of circulating water, reactor service water and turbine service water which would likely require the addition of biocide (i.e. sodium hypochlorite) to control biofouling. The Cooling Water, once having passed through the CWS would therefore be returned to the sea warmer than ambient and likely contain residual biocide. As a result, the Environmental Permitting Regulations would be applicable to the Project in relation to emissions to surface waters (discharge consenting)[1].

This document presents the findings of a series of marine hydrodynamic modelling simulations of the CW discharge from the Wylfa Newydd Power Station, undertaken to support the Environmental Permitting, DCO and Marine Licence for the Project. The hydrodynamic model simulated the mixing of the thermal and biocide components of the CW discharge. The simulations provided predicted mixing zones for both temperature and Total Residual Oxidant (TRO) for an average CW discharge of 126 m^3/s with a CW temperature rise of 12 °C (ΔT +12 °C) and a TRO concentration at the point of discharge of 0.1 mg/l. The TRO percentile modelled and presented was as stipulated by the UK EQS (expressed as available chlorine) which is a 95 percentile concentration (of 0.01 mg/l) (Water Framework Directive, 2015) while for temperature a 98 percentile is used for presentation in-line with various guidance documents.

There are no legal temperature standards in coastal environments in the UK. Draft guidance prepared for WFD and presented in BEEMS (2011b) and expanded in Wither *et al*. (2012) propose absolute limits and elevation above ambient limits outside of mixing zones depending on the WFD status of a water body. Despite the lack of specific temperature standards modelling work for the Wylfa Newydd Project presents predicted +3°C and +2°C uplifts outside of mixing zones in line with the above guidance. The results are also interpreted in terms of an absolute temperature of 23°C, which is the thermal limit recommended in Wither *et al* (2012) for high to good status water bodies. Of note is draft guidance presented by Water Quality Technical Advisory Group (WQTAG) (WQTAG160) which presents draft temperature standards developed for Habitats Regulations Assessment. These values relate to Special Protection Areas (SPAs) with values at +2°C above ambient outside of the mixing zone and absolute temperatures of 28°C and Special Areas of Conservation (SACs) designated for estuaries or embayment habitats and/or salmonid species. These areas do not exist around north Anglesey and are therefore not applicable, nevertheless values proposed are +2°C above ambient outside of the mixing zone and absolute temperatures of 21.5°C.

In addition to the model results this report also provides background information on the setup of the model and selection of the individual modelling scenarios.

[1] See: The Environmental Permitting (England and Wales) Regulations 2016 No. 1154

The modelling approach follows that as detailed in the *Marine Modelling and Assessment Methodology* (Horizon, 2014).

This report covers model scenarios based on a breakwater design of 400 m. This report supersedes the results presented in Jacobs (2017a) in which all modelling was undertaken using a breakwater design of 541 m.

2. Overview of Model Setup, Calibration and Audit

The Wylfa Newydd hydrodynamic model has been developed over a number of years. The main calibration and validation process occurred in 2010/11 (Horizon, 2014). Additional validation work has been undertaken as part of an independent audit process in early 2016.

The bathymetry in the calibrated model was constructed using data from marine surveys commissioned by Horizon in the coastal waters centred on the Wylfa Newydd Development Area (see Horizon 2012a), in combination with digital survey and chart data sets. The initial model grid was derived from the Dutch Coastal Model via the model developer Deltares. Tidal elevations obtained from the Dutch Coastal Model were imposed at the model boundaries.

The model was developed in two phases starting in 2010, the current model being the result of the second of these phases. The model has three nested grids, an outer 2D grid and two 3D inner grids (these cover the north coast of Anglesey). The resolution of the grids (mesh size) increases from 350 m in the outer grid to 70 m in the mid grid and to 23m in the inner-most grid (Horizon 2012a).

The model was calibrated using baseline data collected at four fixed moorings, boat-based Acoustic Doppler Current Profiler and thermal plume surveys, drogue studies and an aerial infrared plume survey.

Development of the Wylfa Newydd hydrodynamic model has been subject to an external audit by ABPmer. The audit concluded the model was fit for purpose.

Documents that have been produced or published externally during development and validation of the model include the following.

- *H1 Annex D-Basic Surface water discharges.* (Environment Agency, 2011).
- *Wylfa Hydrodynamic Survey: Development of a statistical model of seawater temperature* (Moores, 2011a)
- *Hydrodynamic Modelling for Wylfa: Phase 1 Calibration Study*. (Moores, 2011b)
- *Hydrodynamic Modelling of Wylfa wave enhanced mixing* (Moores, 2011c).
- *Hydrodynamic Modelling for Wylfa: Wind and Heat Transfer* (Horizon, 2011a).
- *Chlorine Decay Measurements in Saline waters from Wylfa Power Station during Autumn* (Horizon, 2011b).
- *Consultancy Report Wylfa Water Quality Surveys*. (Jacobs UK Ltd, 2012).
- *Wylfa Oceanography Interpretive Report* (Titan, 2012).
- *Wylfa Hydrodynamic and Water Quality Modelling: Phase 2 model build, Calibration and Validation* (Horizon, 2012a).
- *Infra-Red Survey Draft Report* (APEM Ltd, 2012).
- *Chlorine Decay Measurements in Saline waters from Wylfa Power Station during Winter* (Horizon, 2012b).
- *Chlorine Decay Measurements in Saline waters from Wylfa Power Station during Summer* (Horizon, 2012c).
- *Chlorine Decay Measurements in Saline waters from Wylfa Power Station during Spring* (Horizon, 2012d).
- *Hydrology Modelling and Assessment Methodology Memo* (Jacobs UK Ltd, 2014).
- *Audit of the Wylfa Hydrodynamic Model Second Review* (ABPmer, 2016)

3. Modifications to the Validated Model

Changes were necessary to the bathymetry in the validated (Phase 2) model to reflect the Wylfa Newydd Power Station design. These and the representation of wind, surface heat loss coefficients and CW discharge are described in the following sections.

3.1 Changes to the Bathymetry

The model used to predict mixing of the CW discharge includes changes to the bathymetry to reflect the proposed CWS intake and outfall. The CWS intake includes a breakwater and Marine Off-Loading-Facility (MOLF). The design assumed was that as of February 2015[2]. The changes in bathymetry implied by the breakwater, the MOLF and intake dredge were added to the validated model bathymetry to create the bathymetry used in modelling scenarios.

3.2 Heat Flux used in the Modelling

Modelling of the CWS discharge has been undertaken using the so-called 'Excess Temperature' method following the advice of Natural Resources Wales (NRW) and its predecessors, the Countryside Council for Wales (CCW) and the Environment Agency (EA). In this approach to modelling the mixing of the CWS discharge, the hydrodynamic model is used to predict the change in water temperature that occurs.

When using the excess temperature method, the model is set up to simulate a defined surface heat loss coefficient. Heat transfer (or loss) coefficients have been calculated for the waters around Wylfa Head using ten years of meteorology and seawater data. The meteorology data used were collected at RAF Valley (2003 to 2012), while seawater temperature data were obtained from the Existing Power Station's CWS intake for the same period.

The calculation of the heat transfer coefficients involved first calculating the full heat flux that occurred each month over the ten year period (2003 to 2012). The calculations were then repeated with the seawater temperature increased by 1 °C. The difference between the heat fluxes for these two cases were then used as the heat transfer coefficient (Moores, 2016e).

The seasonal average seawater temperatures, wind speeds and surface heat transfer coefficients are tabulated below (Table 1).

Table 1 Seasonal average sea temperature, wind speed and surface heat transfer.

Season	Month	Sea temperature (ºC)	Wind speed (m/s)	Surface heat transfer coefficient ($W/m^2/K$)
Spring	March, April and May	9.0	6.0	19.7
Summer	June, July and August	14.6	5.6	21.7
Autumn	September, October and November	14.3	6.8	24.0
Winter	December, January and February	8.5	6.9	21.4

[2] *HNGE drawing MD-400-AR-001*

The sensitivity of the predicted temperature rise to the surface heat transfer coefficient was explored by running two additional simulations of the summer case. In these two additional runs the coefficient was changed by 10W/m^2/K and 13 W/m^2/K for the low flux and high flux, to 12 and 35 W/m^2/K respectively.

3.3 Wind Conditions

The base-cases used the seasonal average wind speed, although the surface drag coefficient was set to zero so that the wind did not influence the hydrodynamics. This is a common modelling approach which results in a constant surface heat loss rate; use of a variable wind speed results in a variable surface heat loss.

To explore the influence of wind on the hydrodynamics, additional sensitivity studies were undertaken with winds from each of the four main sectors. The average wind for each sector was assumed to blow throughout the duration of the simulation. Analysis of the RAF Valley meteorology data (Moores, 2016b) showed that long duration wind events were infrequent; hence it was deemed appropriate to use a mean wind speed rather than a maximum. A constant wind from a single direction allows the maximum potential influence on the hydrodynamics to develop and is considered an extreme case in itself, hence modelling a long-term wind of the maximum observed speed would be unreasonable as it is a combination of two extremes.

3.4 Total Residual Oxidant (TRO) Decay Rates

A biocide is proposed to be used in the CWS to control the growth of marine organisms. The decay of TRO has been modelled as a first order decay process, under the advice of NRW and its predecessors, CCW and the EA. The decay rates were obtained from measurements using seawater samples collected from the Existing Power Station's CWS intake and dosed with biocide at differing temperatures in the laboratory (Moores, 2014).

For each of the seasonal simulations, decay rates appropriate for the seawater temperature were used (Table 2), the maximum being when sea surface heat transfer coefficient is the highest (i.e. autumn). The different rates used in each simulation allowed the predicted TRO mixing zones' sensitivity to assumed decay rates to be explored.

Table 2 Seasonal TRO decay rates.

Season	TRO decay rate (per day)
Winter	4.75
Spring	11.15
Summer	10.08
Autumn	36.81

3.5 Representation of the CWS Discharge in the Model

The hydrodynamic modelling used the Delft3d software package. The physics implemented in Delft3d, in common with other hydrodynamic codes and typical grid resolutions, limits the ability of the hydrodynamic model to simulate the near-field mixing of the discharge (the near-field being the zone where the design features of the outfall such as the number of ports and the discharge jet momentum are the dominant determinant of mixing). As the hydrodynamic model does not reproduce the details of the near-field mixing, it is good practice to use an alternative tool to simulate the near-field mixing characteristics and add the discharge to the model in such a way as to simulate the discharge at the end of the near-field.

The CORMIX software tool has been used to predict the near-field mixing of the discharge from the Wylfa Newydd CWS outfall (Moores, 2016a). The outfall design assumed was that as of February 2015[3]. In addition to the near-field representation provided by the CORMIX study, two other representations have been used in a sensitivity study. One sensitivity study assumed a longer near-field, which involved moving the basic CWS

[3] HNGE document HA-HG-2015-006 (pending approval)

discharge distribution offshore by approximately 100 m. The second sensitivity study used a short near-field, whereby the CWS discharge was introduced at the physical location of the outfall.

4. Model Runs

The modelling assumed an average CWS flow rate of 126 m^3/s, and a ΔT of 12 ºC. For each simulation the model was run for a warm-up period to allow the long-term heat and biocide fields to develop. The time allowed for the heat and biocide fields to develop was longer than the time necessary to allow the hydrodynamic conditions to settle.

The hydrodynamic model was set up to simulate the full load CWS discharge from the Wylfa Newydd Power Station over a spring-neap cycle using surface heat flux and TRO decay rates representative of the summer. The simulation included use of a conservative tracer in the discharge to allow dilution factors to be calculated if required (for example by the H1 screening process).

The model output was processed in MATLAB® to generate statistics of the temperature rise and TRO concentration at each model cell. The minimum, mean, maximum and percentile values were calculated. In line with the relevant environmental quality standard (EQS) for TRO (0.01 mg/l) and the chosen temperature uplift of +2 ºC, a different percentile was calculated for both temperature and TRO (98^{th} and 95^{th} percentile, respectively).

Recirculation occurs when a Power Station draws in water that has already been warmed by the CWS discharge. Unlike a river, where the flow is unidirectional and siting the intake a suitable distance upstream for the discharge should prevent recirculation, the potential for recirculation is to be expected in a tidal environment. The mean, 98^{th} percentile and maximum temperature rise above ambient at the intake were calculated to identify the potential for recirculation.

5. Model Output

5.1 Tidal Variation of the CW plume

The CW discharge is buoyant and will form a buoyant plume which will be advected by the tide. While the tidal flow north of Wylfa Head is relatively simple with an essentially east to west tidal current (Titan, 2012), the presence of the headland results in a complex flow region in the bays either side.

To illustrate the tidal variation of the CW plume surface and bed temperature rise has been plotted for both a neap and a spring tide in the following sections. The model run simulated long-term operation of the Power Station CW discharge under surface heat loss conditions, typical of average summer conditions.

The figures are included to illustrate the evolution of the thermal plume from the Power Station and not for comparison against temperature standards.

5.1.1 Plume Evolution over a Neap Tide

Surface and bed temperature rise data are plotted for times at high water, mid ebb, low water and mid flood in Figure 1 to Figure 8 below. The dotted lines on the figures represent the two cross-sectional areas at Cemaes Bay (left line) and the outfall location (right line).

At high water on a neap tide (Figure 1) the plume is beginning to be advected to the west as the tide begins to ebb. Temperature rises of greater than 5 °C are predicted west of Wylfa Head at the surface while a plume of water of 1 °C above ambient extends 2.5 km from the outfall. At the same time the temperature rise at the bed is lower than at the surface with a rise of around 0.4 °C in Cemlyn Bay and 0.3 °C in Cemaes Bay to the east of Wylfa Head (Figure 2). A comparison of the predicted rise at the bed (Figure 2) and at the surface (Figure 1) illustrates the influence of buoyancy on the mixing of the CW discharge. Within Cemlyn and Cemaes Bays away from the plume the water is well mixed and surface and bed temperatures are similar. The increase of around 0.3 to 0.4 °C is due to the long-term operation of the CW discharge.

At mid ebb on a neap tide (Figure 3) the CW plume at the surface has been advected to the west of the outfall. Compared to the High Water (HW) case (Figure 1) the plume is shorter with the 1 °C rise extending 1.5 km from the outfall. Temperatures close to the outfall and around the west of Wylfa Head are warmer than in the HW case.

The predicted temperature rise at the bed at mid ebb on a neap tide (Figure 4) is lower than at the water surface (shown as Figure 3). Compared to the HW case the area of the bed with a rise greater than 0.5 °C is somewhat larger.

At low water (Figure 5) the plume extends to the west of the outfall with the 1 °C rise reaching 2.2 km from the outfall. At the same time the predicted temperature rise at the bed (Figure 6) is lower than at the water's surface. In general the long-term well mixed temperature rise in Cemaes and Cemlyn Bays are as the other cases (0.3 and 0.4 °C respectively) although there is an area of the bed in Cemlyn Bay where the temperature rise is predicted to exceed 0.5 °C.

At mid ebb the surface temperature rise (Figure 7) shows the plume being advected to the east past Wylfa Head. The 1 °C contour extends approximately 3.5 km from the outfall. There are isolated patches of water of 1 °C or more in Cemlyn Bay. The difference between the surface and bed (Figure 8) temperature rise at mid ebb again shows the influence of the plume buoyancy. In general the temperature rise at the bed is less than 0.5 °C away from the vicinity of the outfall although there are patches of bed in Cemlyn and Cemaes Bays with an increase of more than 0.5 °C.

5.1.2 Plume Evolution over a Spring Tide

Surface and bed temperature rise data are plotted for times at high water, mid ebb, low water and mid flood on a spring tide (Figure 9 to Figure 16). The dotted lines on the figures represent the two cross-sectional areas at Cemaes Bay (left line) and the outfall location (right line).

At HW on a spring tide (Figure 9) the plume is beginning to be advected to the west as the tide begins to ebb. Temperature rises of greater than 5 °C are predicted west of Wylfa Head at the surface while a plume of water of 1 °C above ambient extends a few hundred meters from the outfall. At the same time the temperature rise at the bed is lower than at the surface with a rise of around 0.4 °C in Cemlyn Bay and 0.3 °C in Cemaes Bay to the east of Wylfa Head (Figure 10). A comparison of the predicted rise at the bed (Figure 10) and at the surface (Figure 9) illustrates the influence of buoyancy on the mixing of the CW discharge. Within Cemlyn and Cemaes Bays away from the plume the water is well mixed and surface and bed temperatures are similar. The increase of around 0.3 to 0.4 °C is due to the long-term operation of the CW discharge.

At mid ebb on a spring tide (Figure 11) the CW plume at the surface has been advected to the west of the outfall. Compared to the HW case (Figure 9) the plume is more elongate. Temperatures close to the outfall and around the west of Wylfa Head are similar to the HW case.

At low water (Figure 13) the plume extends to the west of the outfall with the 0.5 °C rise contour reaching 2 km from the outfall and the 1 °C rise extending 1.3 km. At the same time the predicted temperature rise at the bed (Figure 14) is lower than at the water surface. In general the long-term well mixed rise in Cemaes and Cemlyn Bays are as the other cases (0.3 and 0.4 °C respectively).

At mid flood the surface temperature rise (Figure 15) shows the plume being advected to the east past Wylfa Head. The 1 °C contour extends approximately 1.7 km from the outfall. The difference between the surface and bed temperature rise at mid ebb again shows the influence of the plume buoyancy. In general the temperature rise at the bed is less than 0.5 °C away from the vicinity of the outfall.

5.1.3 Comparison of the Neap and Spring Tide Plume

There are similarities between how the plume develops over a spring and a neap tide. For both tidal states, the buoyancy of the CW plume limits the exposure of the bed to elevated temperatures. Other trends are similar for both tides with the plume being advected to the west on the ebb and east on the flood tide.

However, there are differences between the evolution of the plume on the neap and the spring tide, with the plume having a larger extent on the neap tide. On the neap tide there are areas of 0.5 °C to 1 °C water at the surface in Cemlyn Bay, which are remnants of the low water plume that are not seen on the spring tide.

These differences can be explained by the higher current magnitudes on a spring tide compared to a neap tide. The higher currents promote shear and hence greater mixing of the CW discharge. Hence, the extent of a given temperature rise contour is greater on the neap tide compared to a spring.

5.1.4 Plume Cross Section

A series of north-south cross-section plots through the vertical are shown at high water, mid ebb, low water and mid flood through i) the outfall and ii) Cemlyn Bay on a neap tide in Figure 17 to Figure 22. In these plots, the viewer is effectively facing east so that the shoreline is on the right hand side of each image, giving a depiction of the how the plume temperatures vary throughout the vertical. A neap tide has been presented as the temperature rise is higher on a neap than a spring tide. The horizontal and the vertical scales differ for the cross section through the outfall and through Cemlyn Bay. The simulation conditions were as per the summer base case.

The temperature cross section near the outfall at high water (Figure 17) shows a rise of around 9 °C close to the outfall. The plume penetrates furthest offshore at low water (Figure 19), with temperature rises of 4 to 5 °C predicted within the upper 4 to 5 m. For the other tidal states the predicted temperature rise is similar, although with reduced offshore penetration.

The temperature cross section through Cemlyn Bay at high water (Figure 21) shows a buoyant plume which is located offshore, with maximum temperatures of around 1 °C with a thickness of 3 to 4 m in water of at least 10 m depth (i.e. no contact of the plume with the bed). At mid ebb (Figure 22) the predicted rise shows the plume is constrained more inshore, although still with no contact to the bed.

The predicted temperatures at low water across Cemlyn Bay (Figure 23) show a more extensive lateral plume extent than at other tidal states, with the plume penetrating inshore but again with no contact with the bed. At mid flood the plume has for the most part been advected to the east by the turning tide; however, an area of temperature rise of less than 1 °C lingers within Cemlyn Bay.

Read in combination with the surface and bed temperature rise plots for the neap tide (Figure 1 to Figure 8); the vertical profiles provide a view on the vertical mixing of the CW discharge. They show that the plume is limited to the upper layers of the water body except in the vicinity of the outfall where the bed maps indicate higher temperatures.

5.1.5 Vertical Profile at the Transition from 3D to 2D grid

An important consideration for the simulation of CW plumes in a model with a mixed 3D and 2D grid is ensuring that the extent of the 3D grid is adequate to capture the vertical profile of the CW plume. During operation the CW discharge from Wylfa Newydd is consistently warmer than the ambient and is therefore buoyant. Buoyancy is an important mixing mechanism and also acts to limit the temperature rise experienced at the bed. Predicting the mixing of the CW discharge in the mid field where buoyancy is important is therefore a three dimensional problem. However, with distance from the outfall the plume will tend to mix well vertically. At this point further mixing can be well represented by a 2D model. When designing the final version of the Wylfa Newydd model grids, different extents of the 3D grids (see Section 2) were tested to ensure that they were adequate to capture the buoyancy of the plume.

To identify where the plume becomes well mixed in the vertical, the maximum difference between surface and bed concentration of a conservative tracer has been plotted in Figure 25. To provide context, the maximum concentration at the surface has been plotted in Figure 26. The tracer was included in the summer base case simulation with a concentration at the outfall of 100units /m^3. The simulation included the influence of the buoyancy of the CW discharge and hence the tracer concentration is greater at the surface than at the bed. Hourly values of concentration were saved over a spring-neap cycle and then processed to generate the statistics of the hourly difference between the surface and bed.

The maximum difference between the surface and bed at the boundary of the 3D grid is 0.3 to 0.5 units /m^3 at an area along the western boundary where the maximum concentration is around 2.5 units /m^3. The 98 percentile difference at the same location on the boundary between the 3D and 2D grid is around 0.1 units /m^3. The maximum surface tracer concentration at the boundary is less than 3% of the discharge concentration.

The tracer is essentially well mixed at the edge of the 3D grid leading to the conclusion that the extent of the grid is adequate to capture the buoyant mixing of the plume.

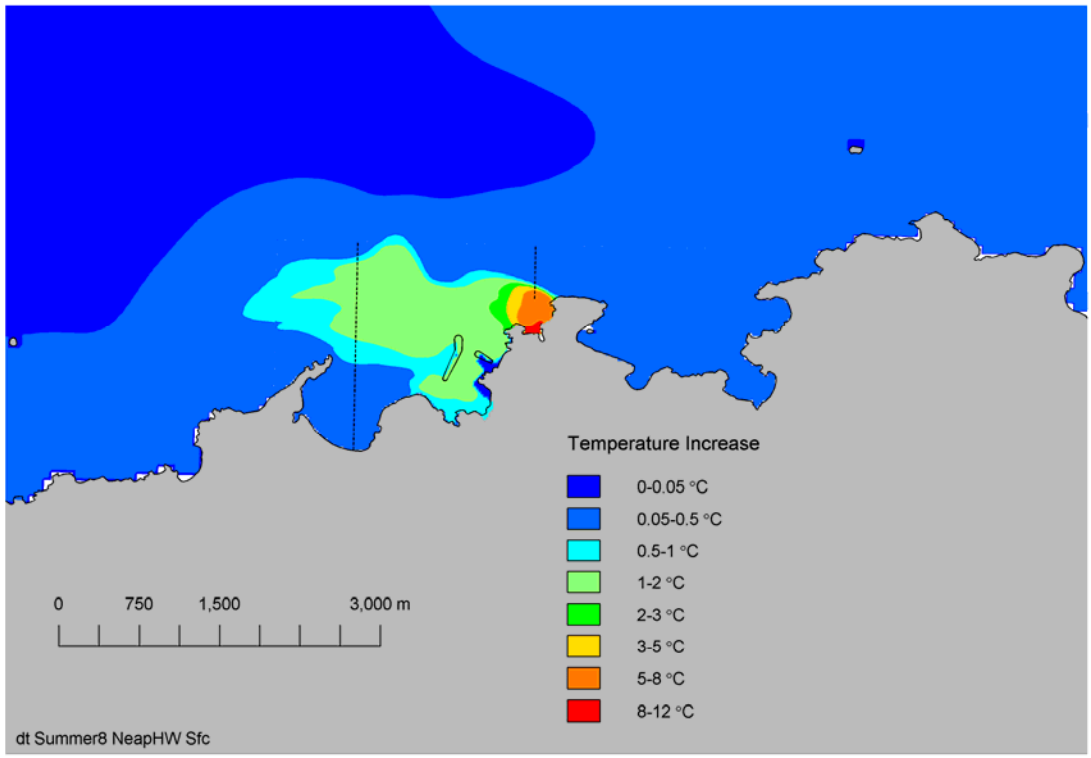

Figure 1 Rise in surface temperature at high water –Neap tide (dotted lines indicate cross-section location).

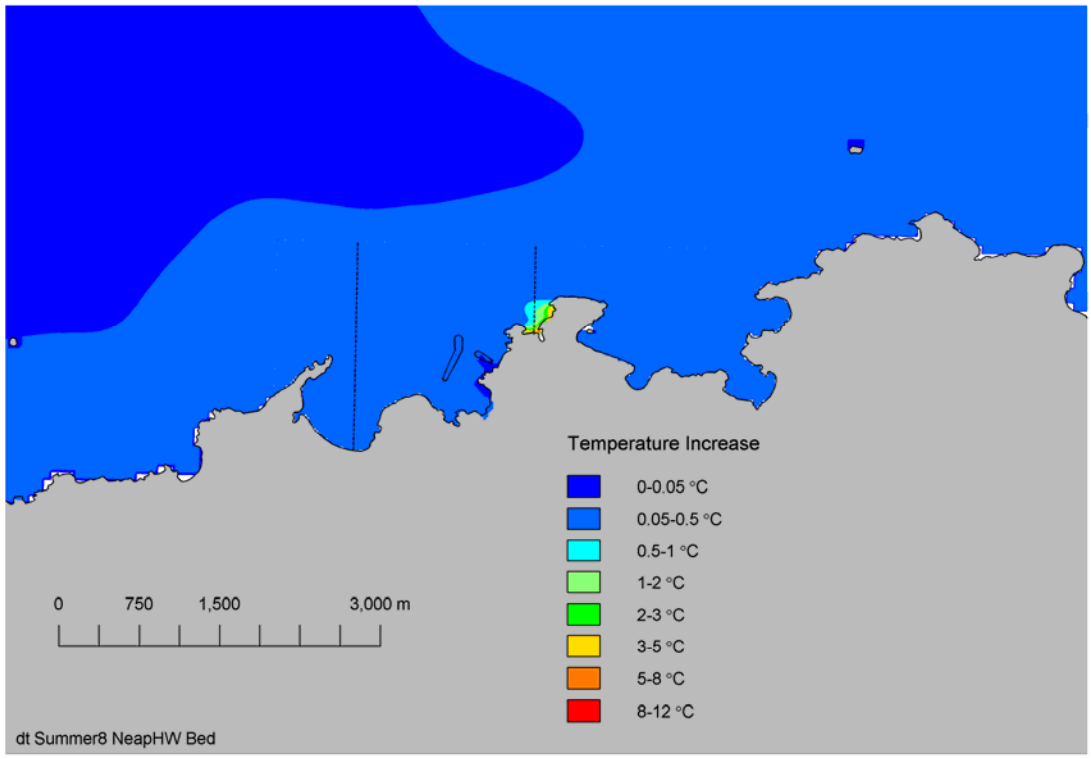

Figure 2 Rise in bed temperature at high water –Neap tide (dotted lines indicate cross-section location).

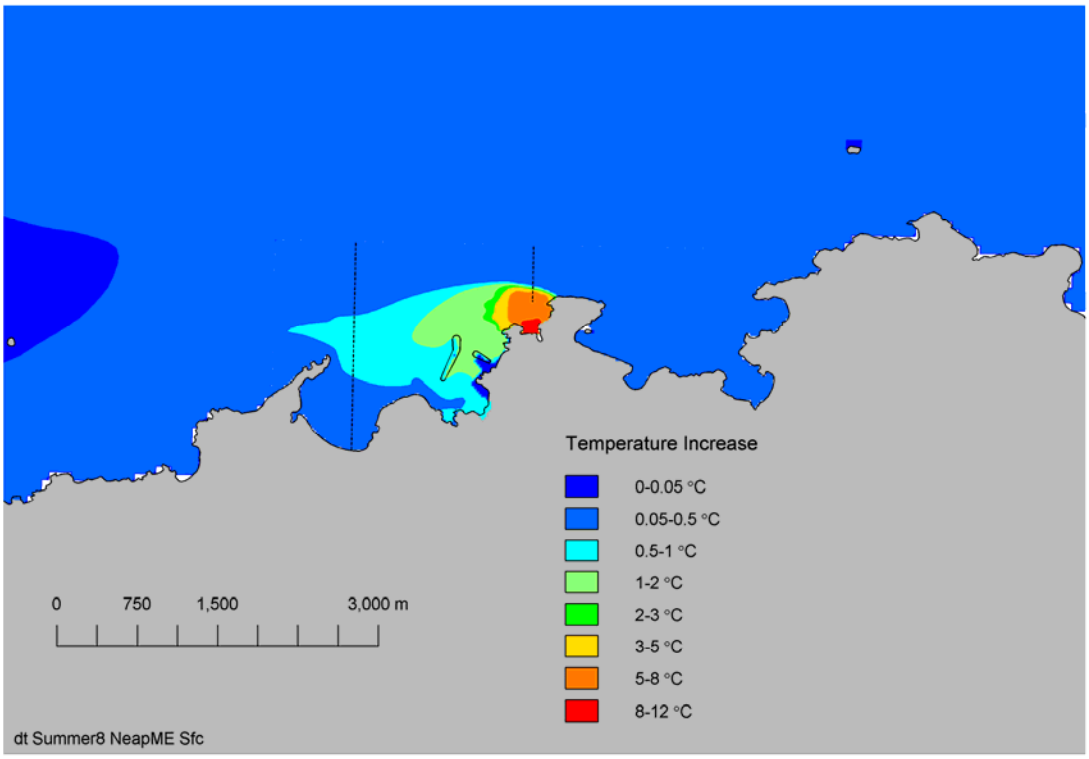

Figure 3 Rise in surface temperature at mid ebb – Neap tide (dotted lines indicate cross-section location).

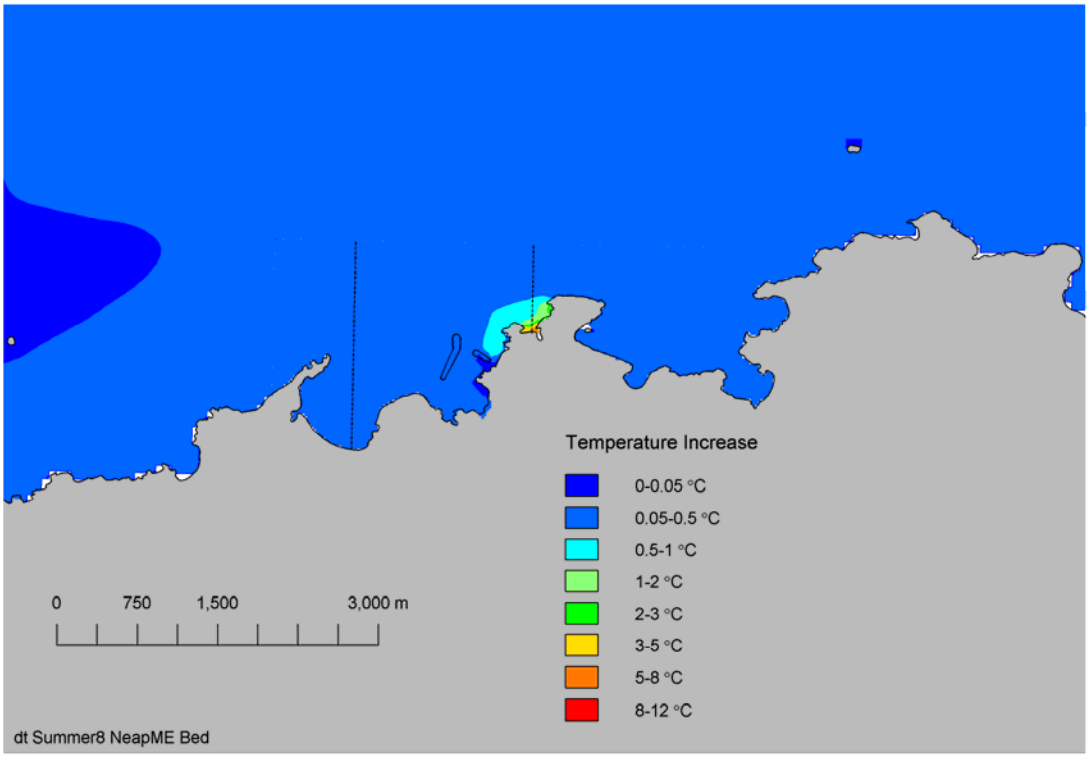

Figure 4 Rise in bed temperature at mid ebb–Neap tide (dotted lines indicate cross-section location).

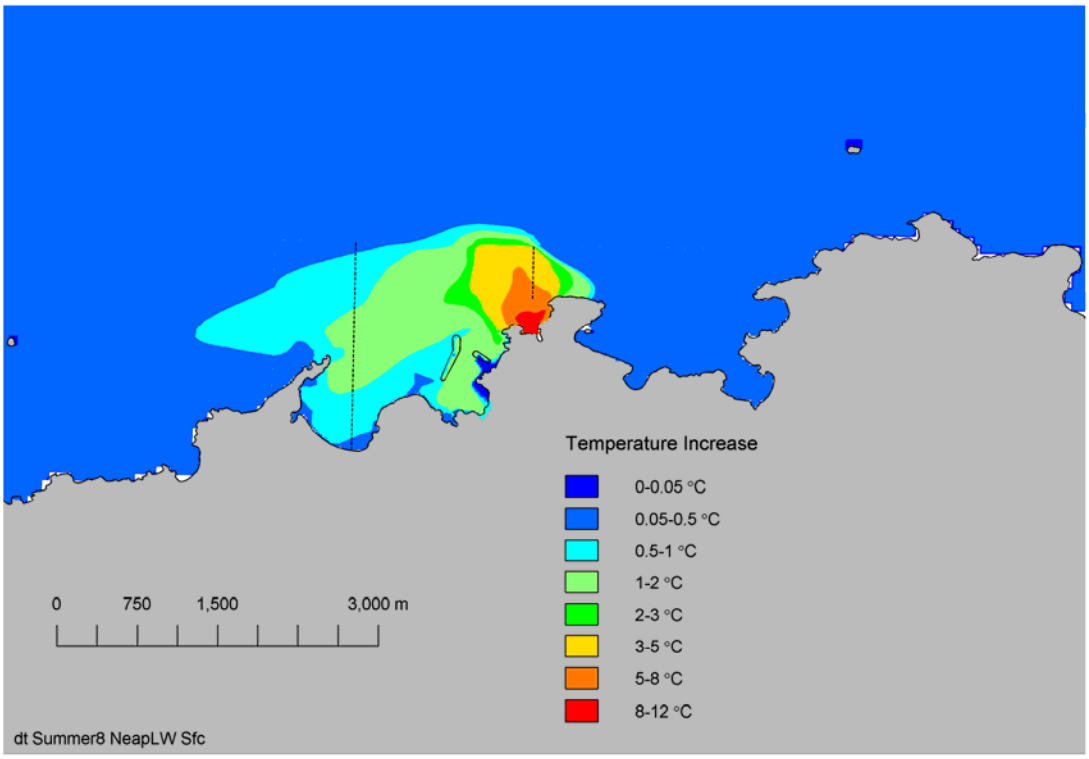

Figure 5 Rise in surface temperatures at low water – Neap tide (dotted lines indicate cross-section location).

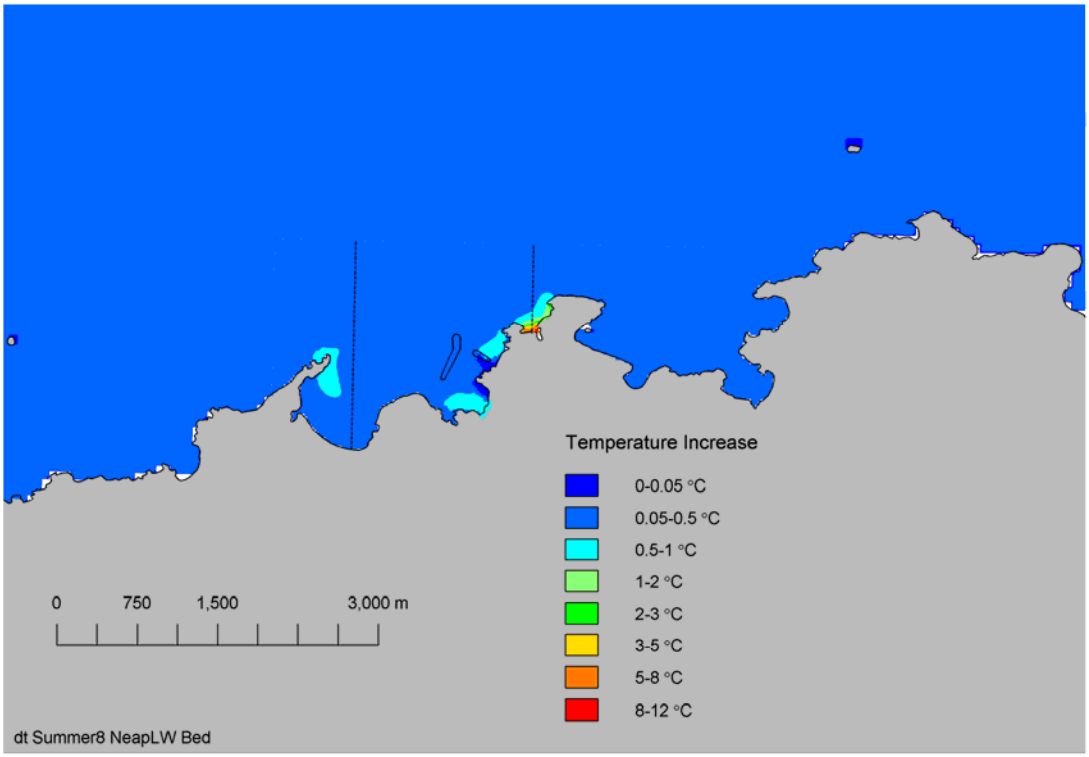

Figure 6 Rise in bed temperature at low water – Neap tide (dotted lines indicate cross-section location).

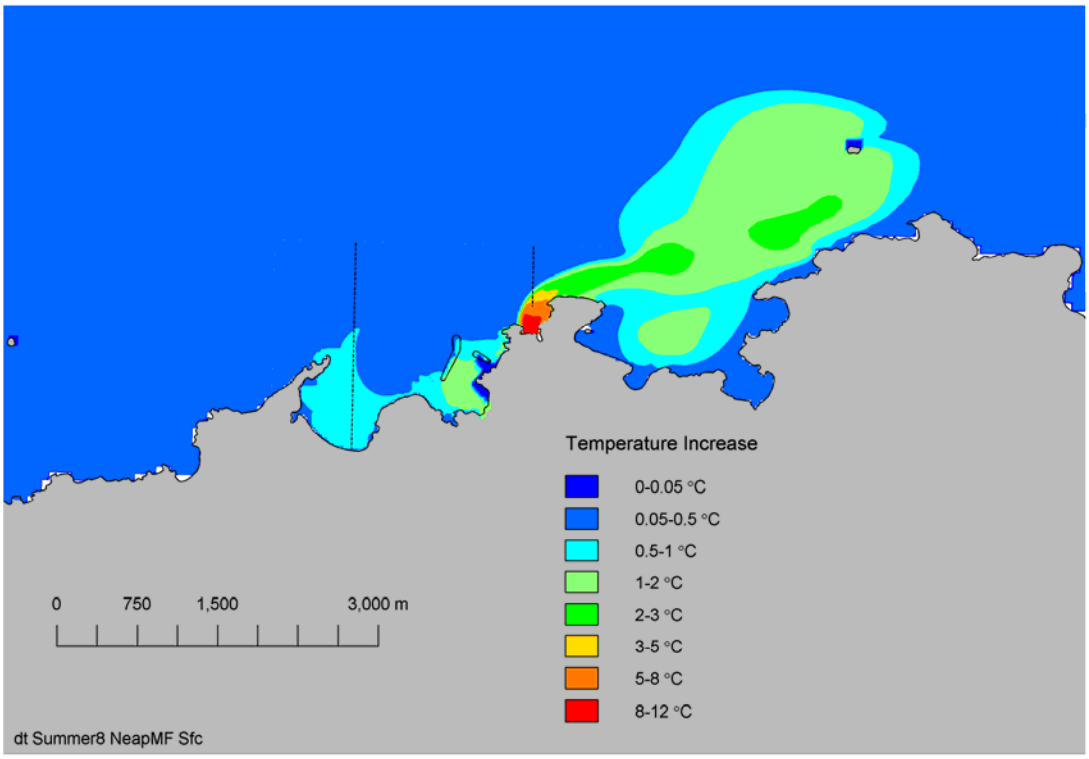

Figure 7 Rise in surface temperature at mid flood – Neap tide (dotted lines indicate cross-section location).

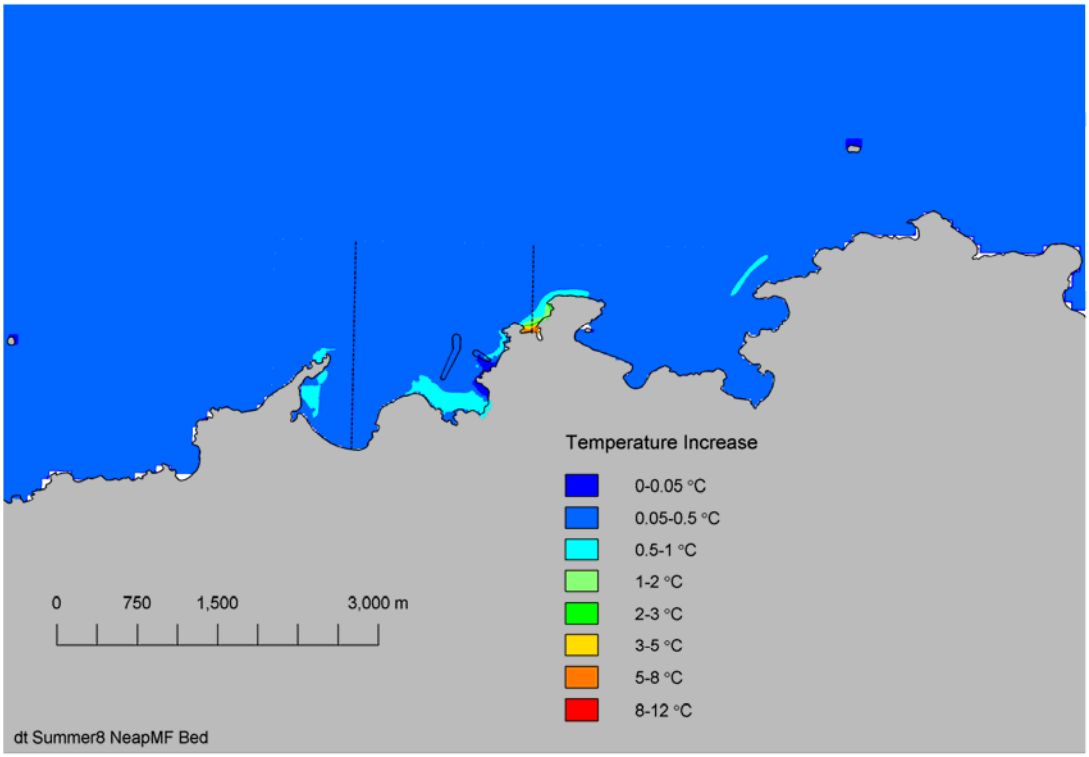

Figure 8 Rise in bed temperature at mid flood – Neap tide (dotted lines indicate cross-section location).

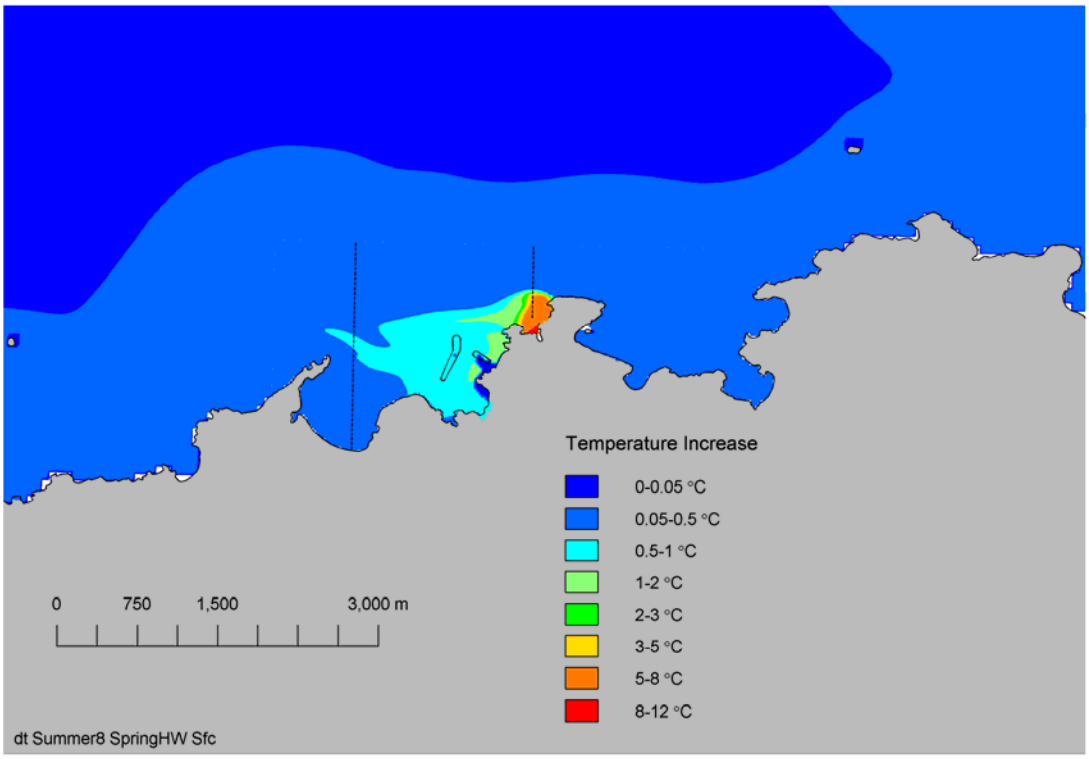

Figure 9 Rise in surface temperature at high water – Spring tide (dotted lines indicate cross-section location).

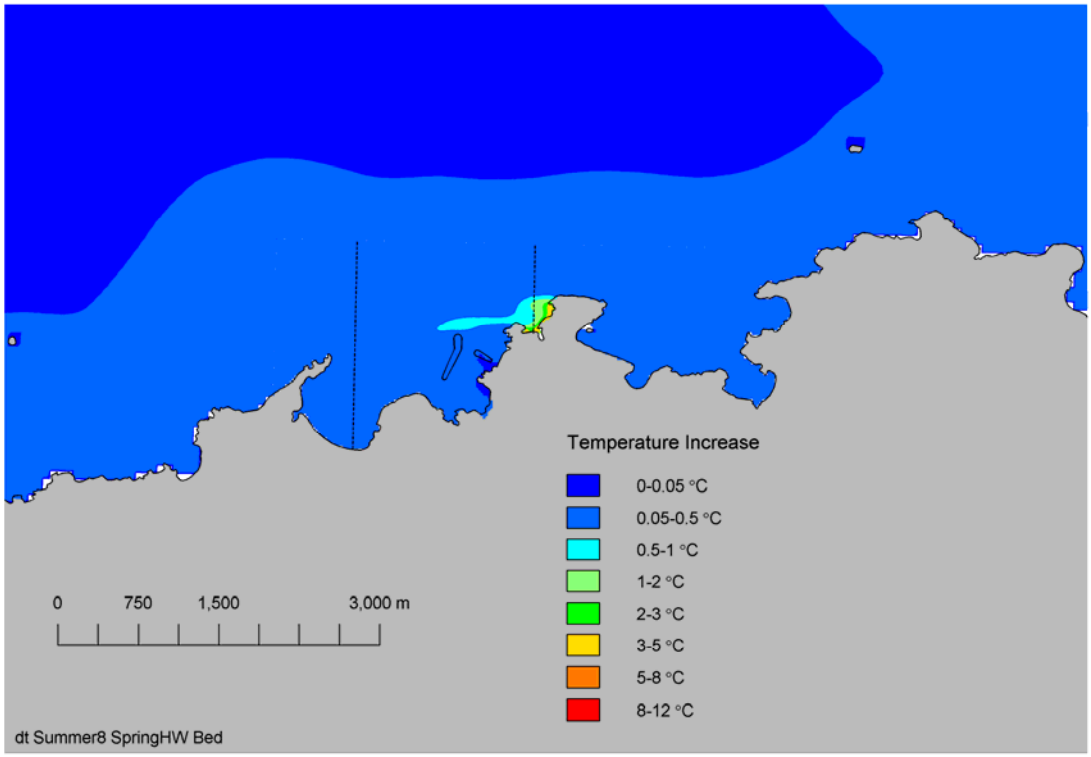

Figure 10 Rise in bed temperature at high water – Spring tide (dotted lines indicate cross-section location).

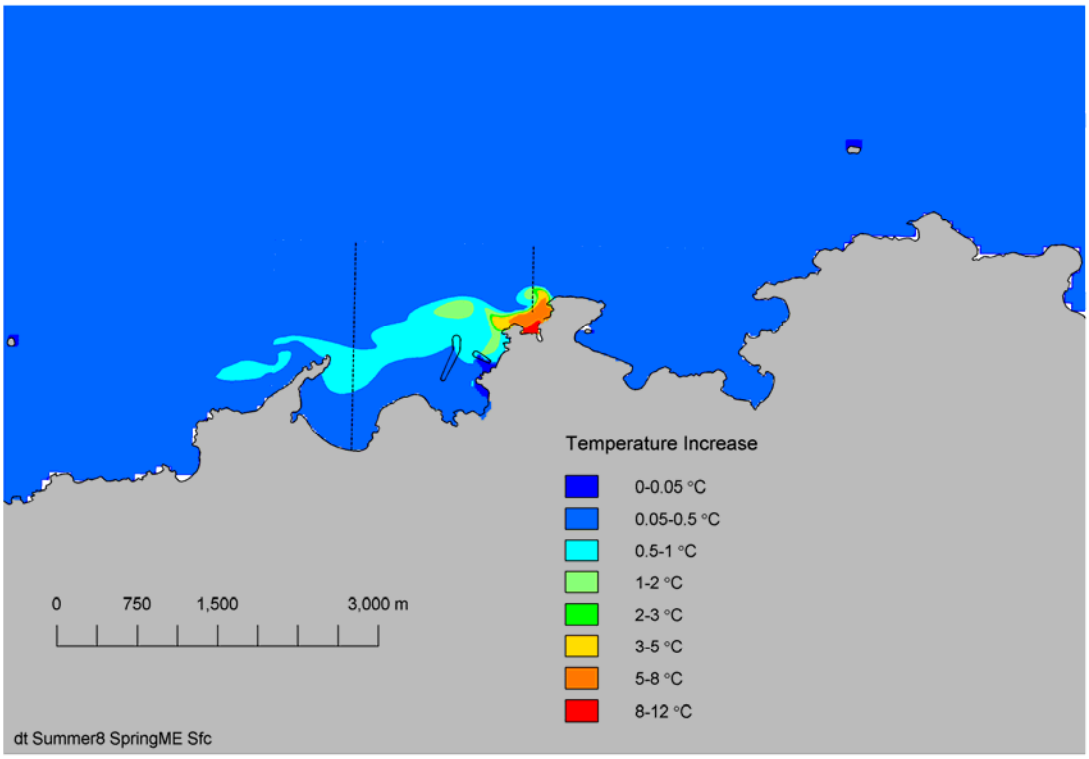

Figure 11 Rise in surface temperature at mid ebb – Spring tide (dotted lines indicate cross-section location).

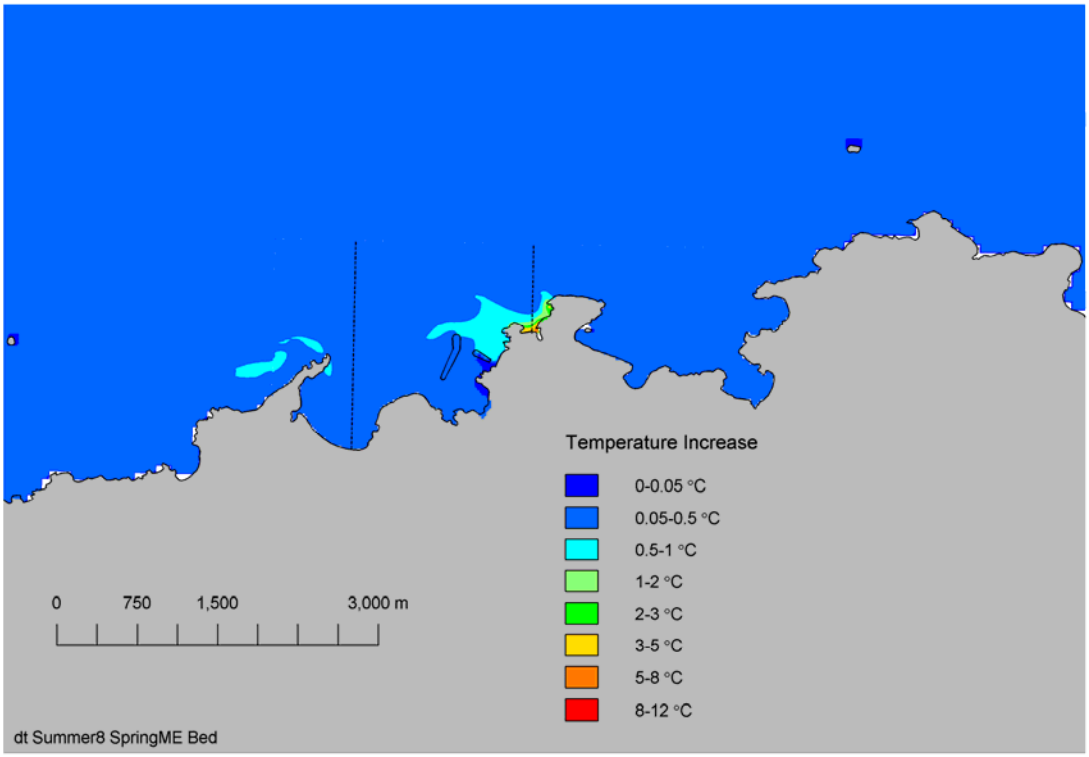

Figure 12 Rise in bed temperature at mid ebb – Spring tide (dotted lines indicate cross-section location).

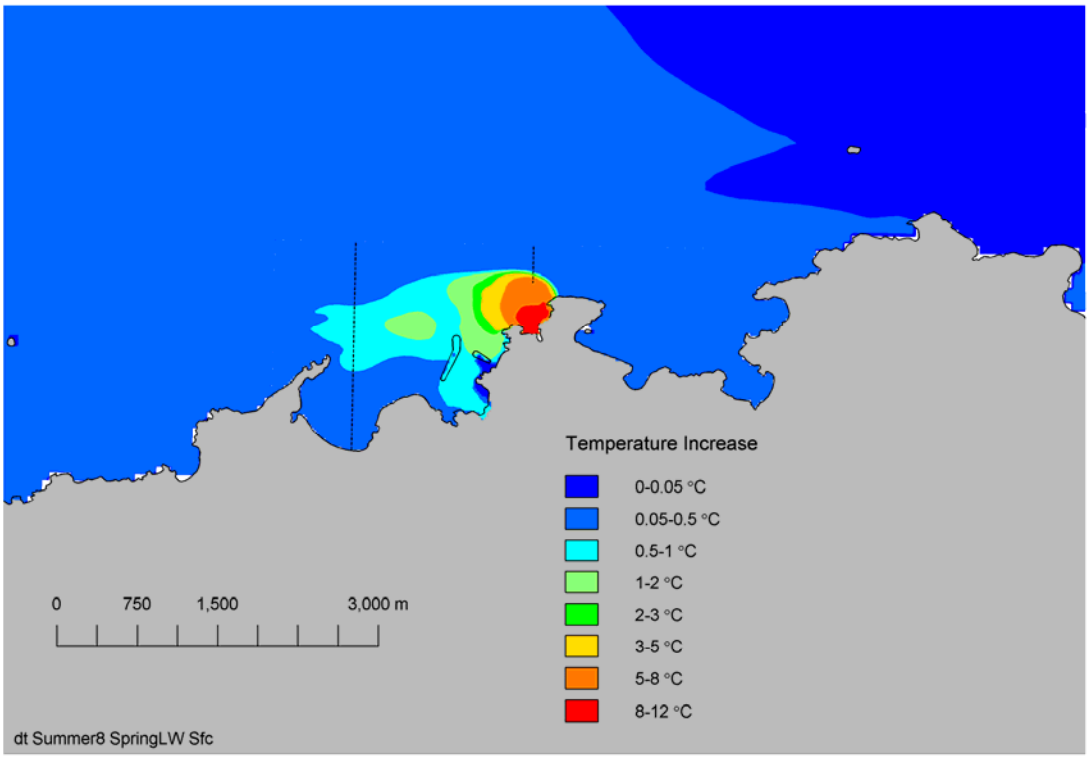

Figure 13 Rise in surface temperature at low water – Spring tide (dotted lines indicate cross-section location).

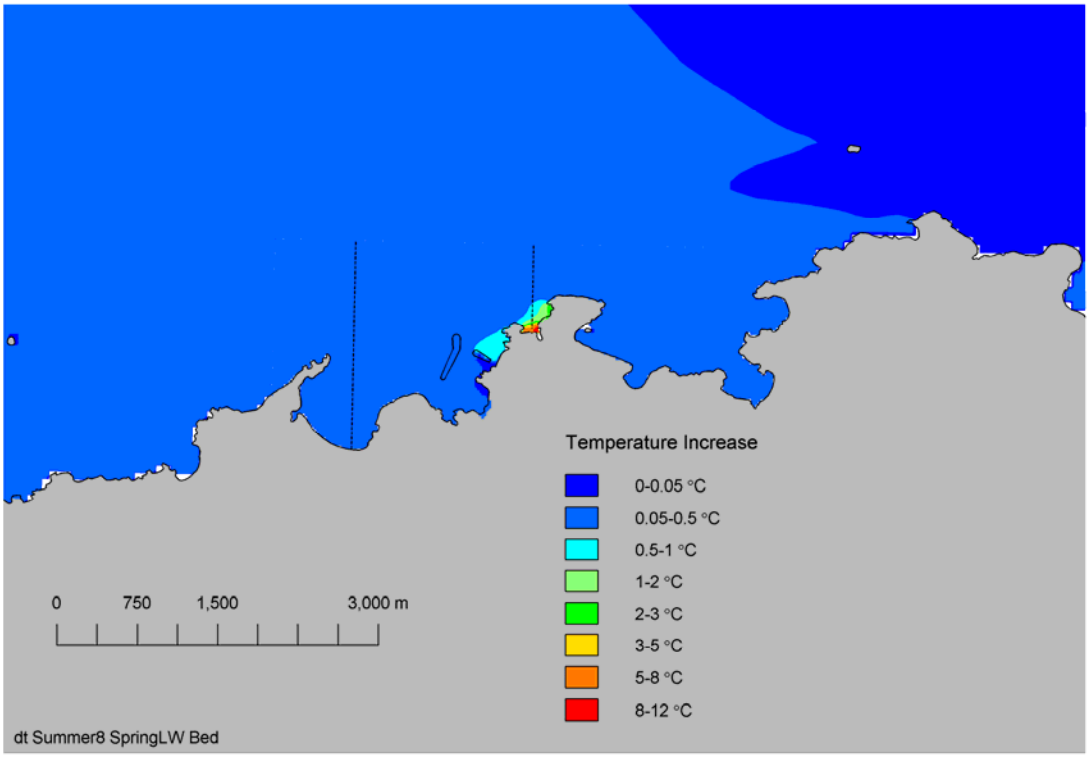

Figure 14 Rise in bed temperature at low water – Spring tide (dotted lines indicate cross-section location).

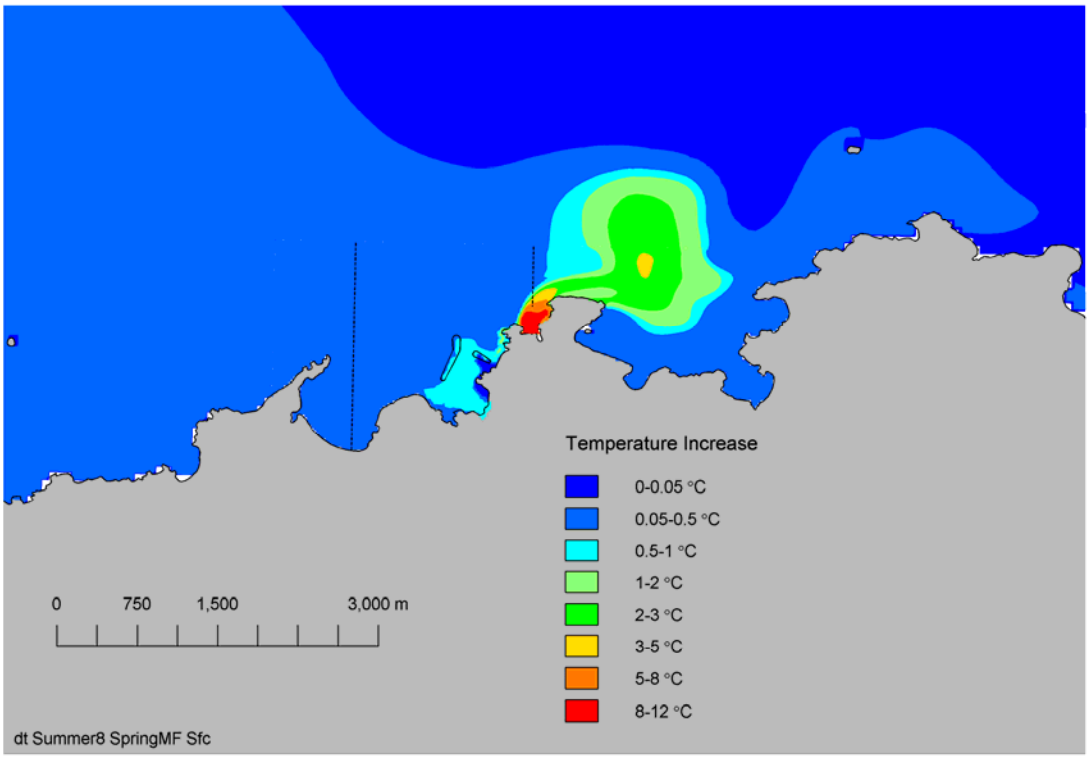

Figure 15 Rise in surface temperature at mid flood – Spring tide (dotted lines indicate cross-section location).

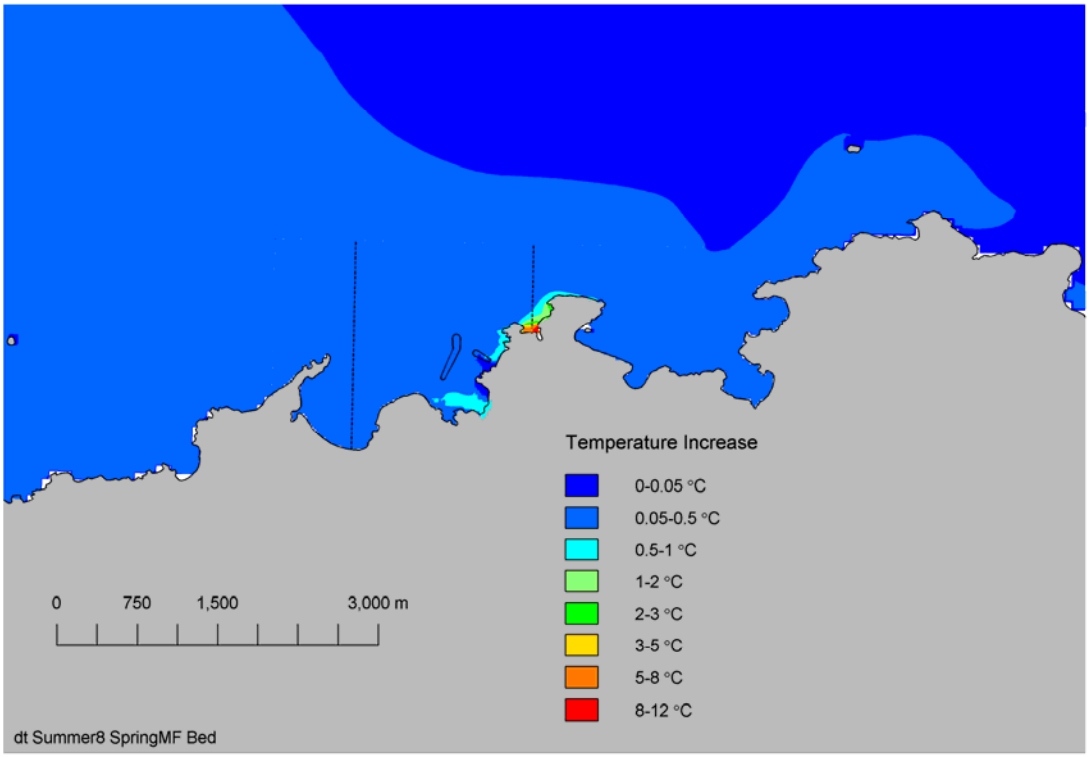

Figure 16 Rise in bed temperature at mid flood – Spring tide (dotted lines indicate cross-section location).

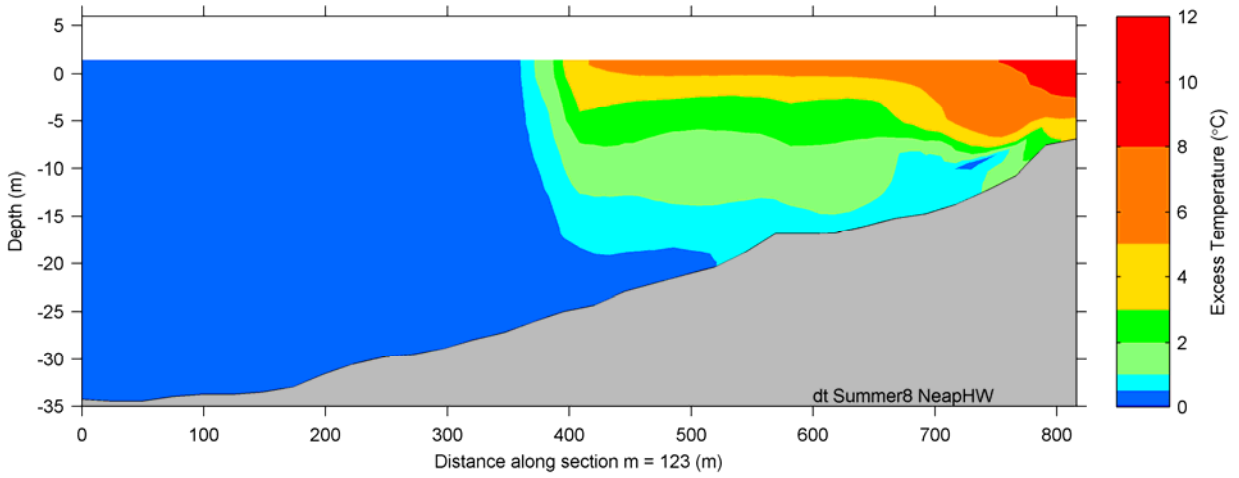

Figure 17 Vertical temperature profile at the outfall location at high water – Neap tide.

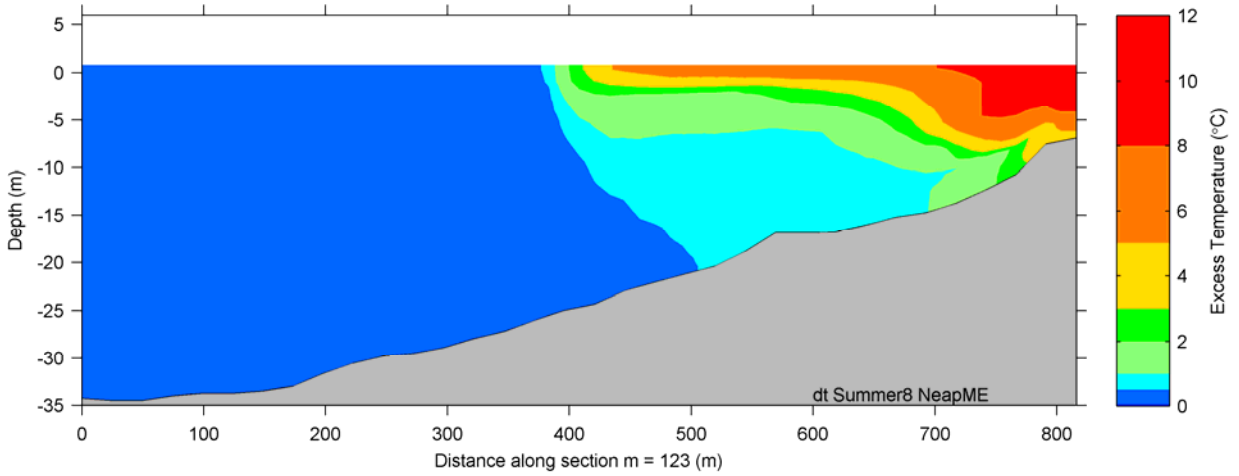

Figure 18 Vertical temperature profile at the outfall location at mid ebb – Neap tide.

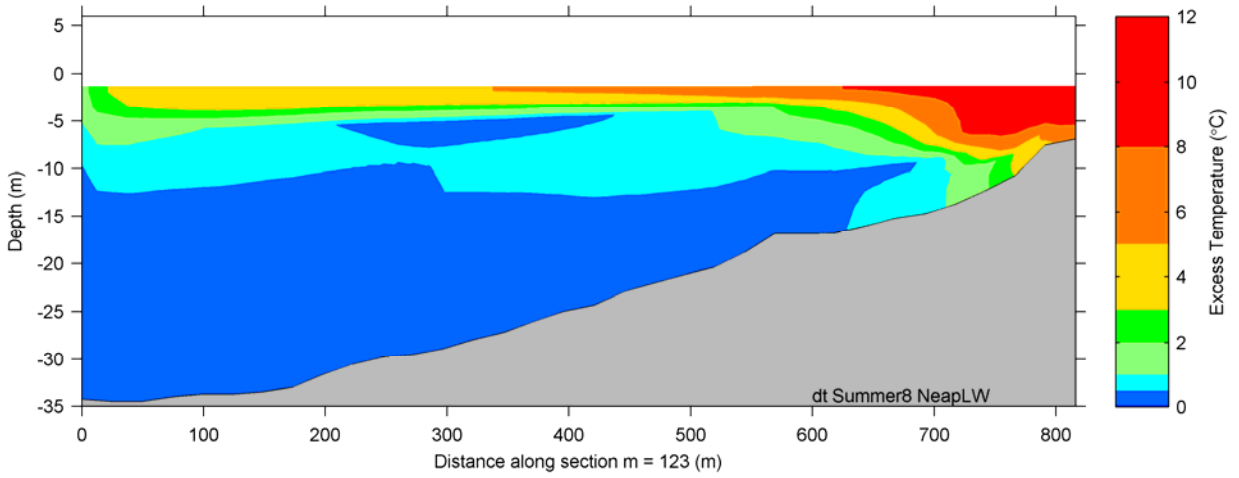

Figure 19 Vertical temperature profile at the outfall location at low water – Neap tide.

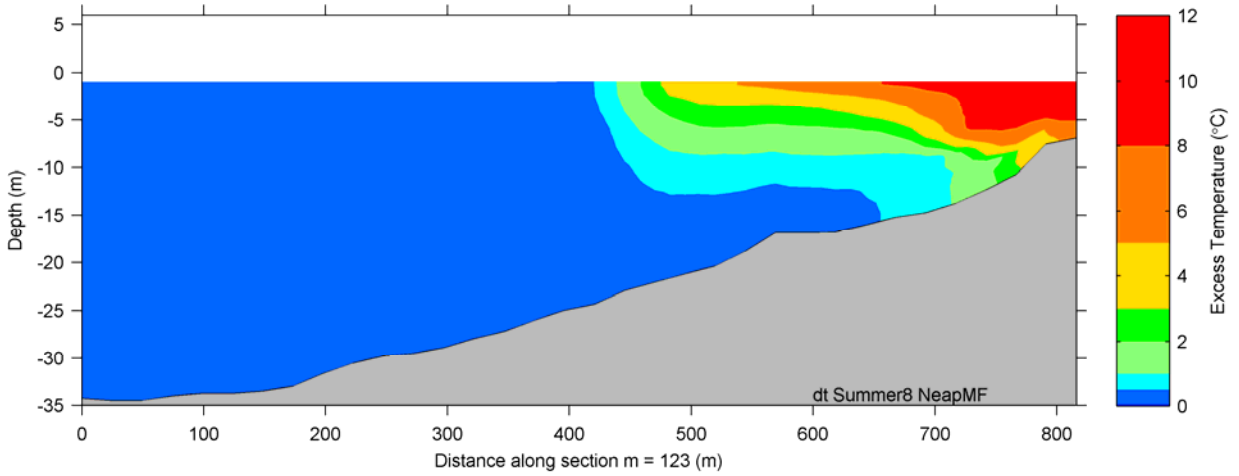

Figure 20 Vertical temperature profile at the outfall location at mid flood – Neap tide.

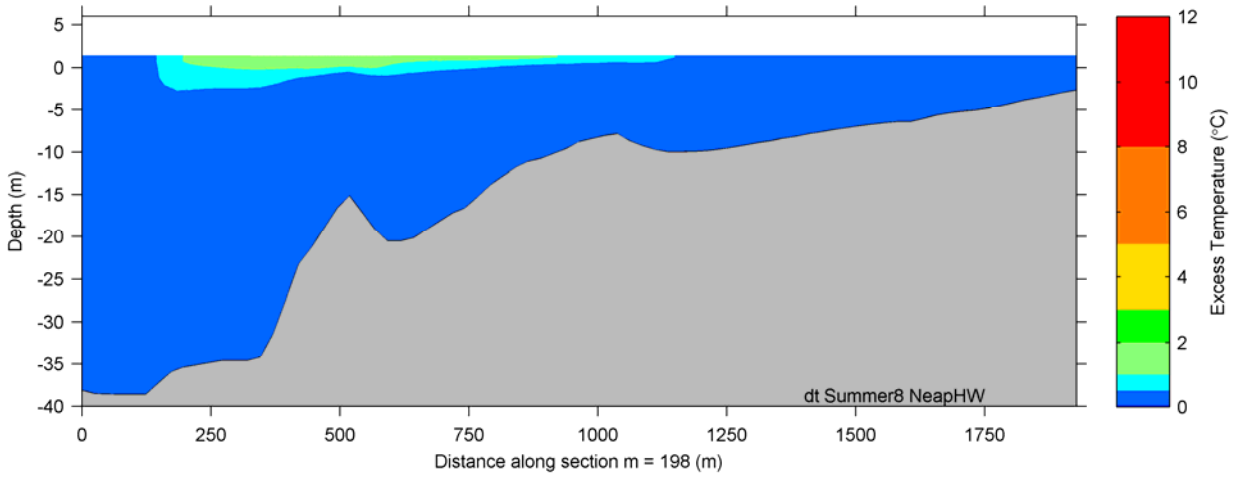

Figure 21 Vertical temperature profile at Cemlyn Bay at high water – Neap tide.

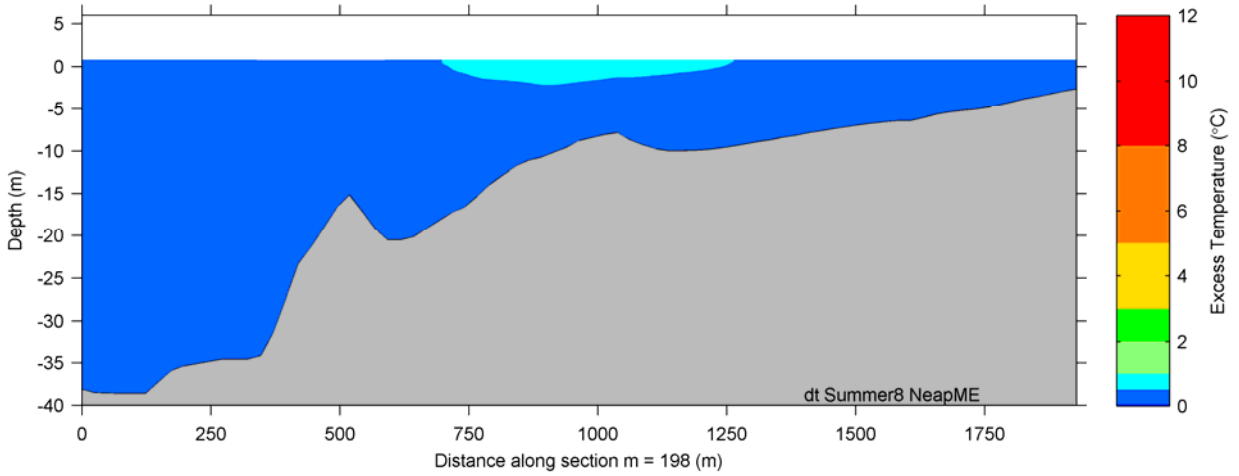

Figure 22 Vertical temperature profile at Cemlyn Bay at mid ebb – Neap tide.

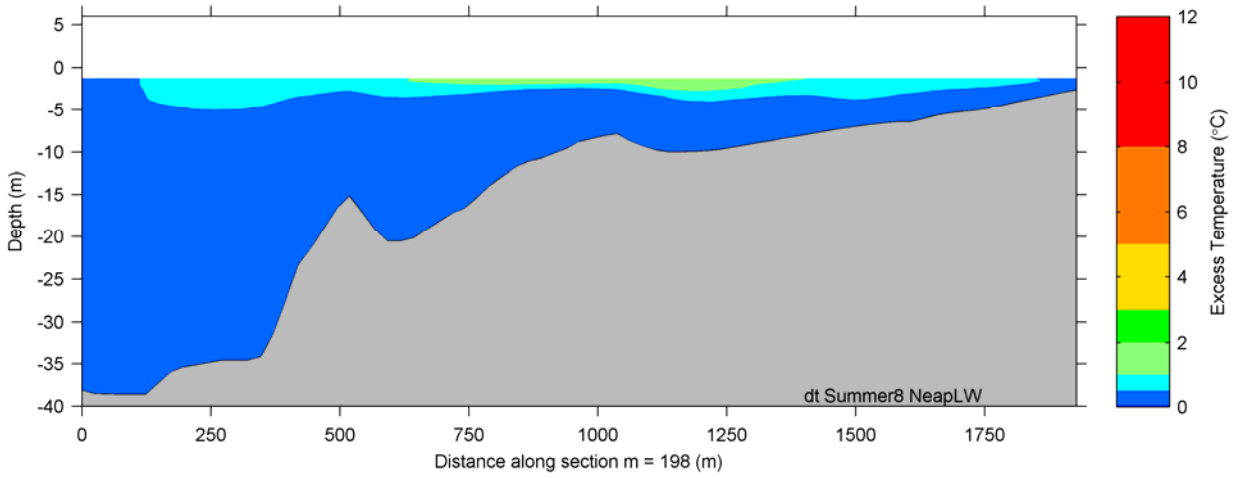

Figure 23 Vertical temperature profile at Cemlyn Bay at low water – Neap tide.

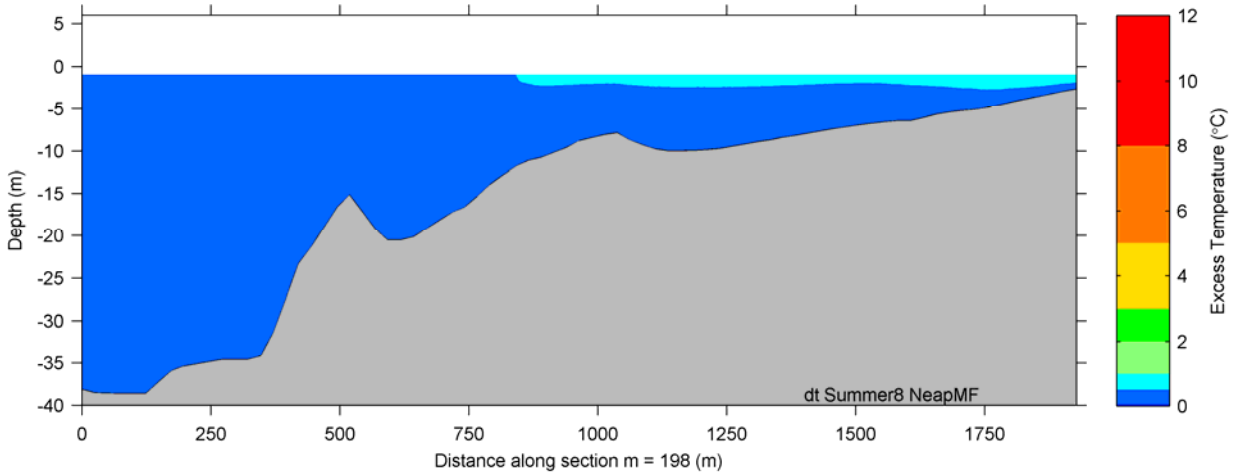

Figure 24 Vertical temperature profile at Cemlyn Bay at mid flood – Neap tide.

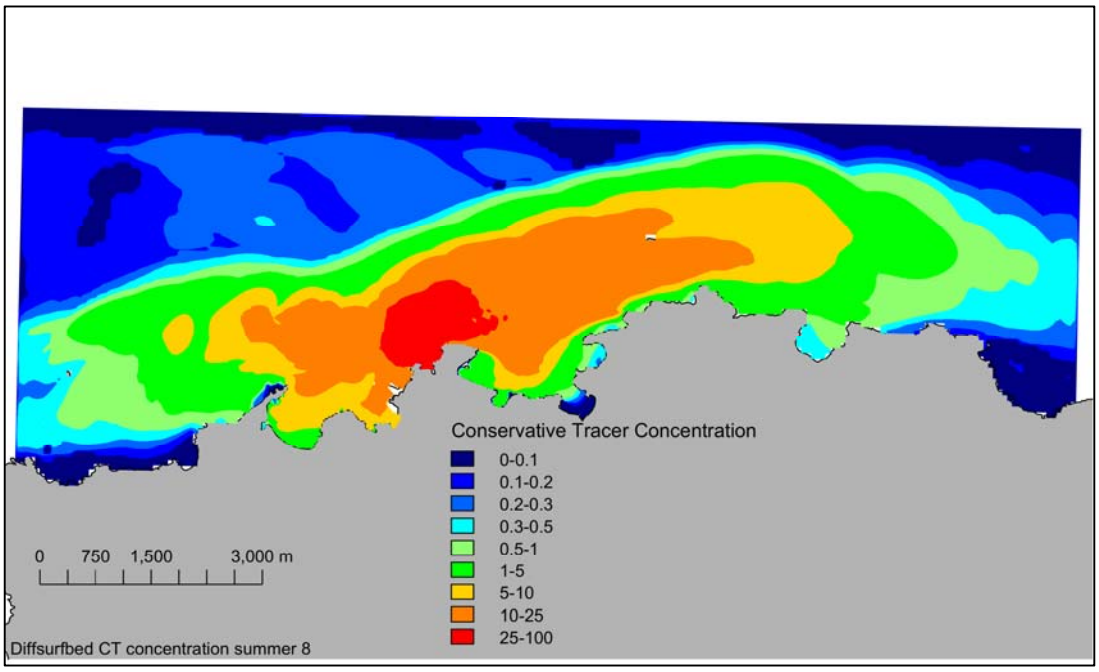

Figure 25 Maximum difference between surface and bed tracer concentration.

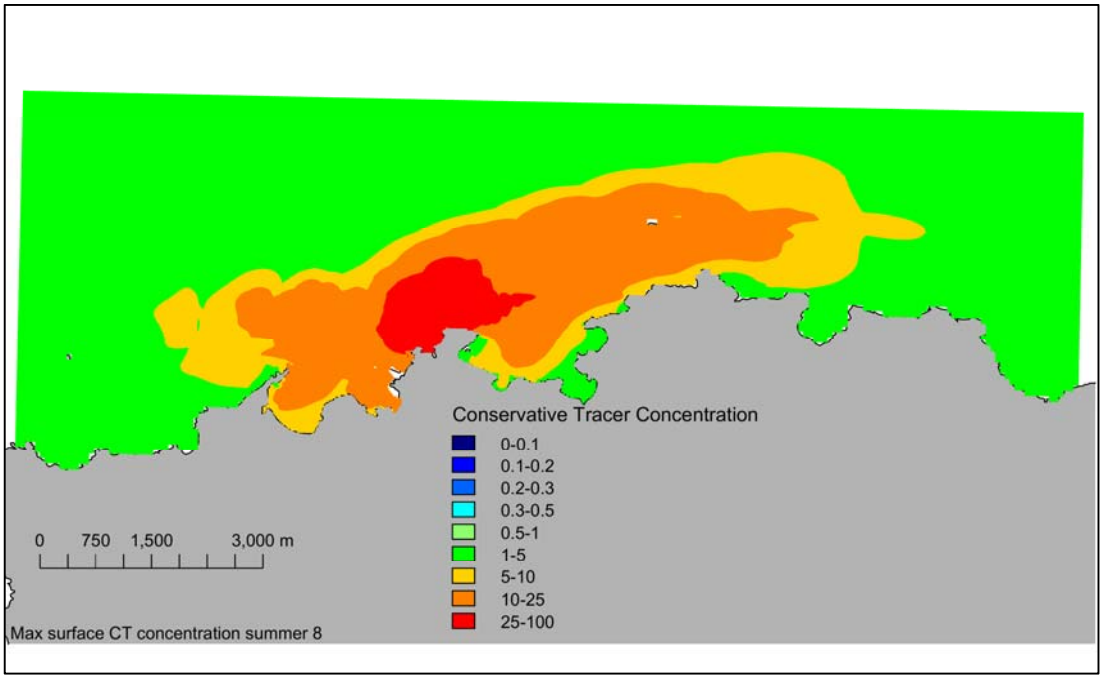

Figure 26 Maximum tracer concentration at the surface.

6. Sensitivity Studies

The approach taken with modelling the Wylfa Newydd CW discharge has been to develop base case simulations and then to include studies to examine the sensitivity of the predicted temperature rise and TRO concentrations to the assumption in those cases.

Sensitivity studies have been undertaken to look at the influence of the following parameters.

- Seasonal variation in surface heat flux and decay rates.
- Intra-seasonal variation in surface heat flux.How the CW discharge is represented in the model:
    - length of the near field; and
    - dependence of the CW flow on the tide.
- Influence of the wind, with both a:
    - fixed wind from each of north, east, south and west sectors; and
    - Variable wind speed and direction.
- Influence of waves
- Influence of dilution
- Influence of an increased intake aperture length, increased dredge depth of intake channel, a continuous quay wall and change in the east/west orientation of the western breakwater.

6.1 Seasonal Temperature and TRO mixing zones

The model used included a representation of the proposed breakwater and intake systems. For all cases the model was spun up[4] and the long-term heat field and hydrodynamics were allowed to develop before saving data for analysis. The model output was processed in Matlab to generate statistics of the temperature rise and TRO at each active (non-dry) model cell. The minimum, mean, maximum and percentile values have been calculated.

The following sections cover the base case simulations of the summer, autumn, winter and spring seasons. In all cases, the hydrodynamic model was set up to simulate the full load CW discharge from Wylfa Newydd over a spring-neap cycle using surface heat flux and TRO decay rates representative of the season. The simulations were undertaken without the influence of wind stress.

6.1.1 Summer Base Case

The ambient seawater temperature was representative of the summer at 14.6 °C. The model was run in excess temperature mode with a wind speed of 5.6 m/s which is the mean measured at RAF Valley for the summer season, although the influences of wind drag on the water were not included in the simulation. The surface heat flux was 21.7 W/m^2/K , again representative of the average for the season. The TRO decay rate was set to an appropriate value for the summer season (10.08 per day).

The model was allowed to warm up over the period 25 June 2011 to 1 August 2011 with the CW discharge operating to allow the thermal and TRO fields to develop. After the initial warm-up period the model was run for a further period and set to record data at hourly intervals for each model cell. Data at each model cell was stored for a full spring-neap cycle over the period 15 August 2011 to 1 September 2011.

[4] Spun up/spin up refers to stabilisation of the model.

6.1.1.1 Summer Base Case – Temperature Rise

The mixing zone implied by the extent of the 3 °C 98 percentile rise at the surface (Figure 27) has an approximate area of 88.7 hectares, while the 2 °C 98 percentile rise has an area of approximately 227 hectares and the 1 °C 98 percentile rise at the surface has an approximate area of 741 hectares. Highest temperatures occur closer to the outfall, with temperatures reducing with distance offshore. The mixing zone is elongated WSW to ENE by the action of the currents around Wylfa Head.

The mixing zone implied by the extent of the 3 °C 98 percentile rise at the bed (Figure 28) is limited to an area around the proposed outfall and along the western edge of Wylfa Head, with an area of approximately 2.7 hectares. The area of the 2 °C 98ile rise at the bed has an area of approximately 3.5 hectares while the 1 °C rise area is approximately 6.6 hectares. The difference in the size of the mixing zone at the surface and bed is primarily due to the buoyancy of the CW discharge.

6.1.1.2 Summer Base Case – TRO

The mixing zone implied by the extent of the 10 µg/l 95 percentile contour (Figure 29) has an approximate area of 313 hectares. As for temperature, highest TRO concentrations occur closer to the outfall. The mixing zone is elongated WSW to ENE by the action of the currents around Wylfa Head.

The area of the bed with a TRO 95 percentile concentration greater than 10 µg/l is limited to the vicinity of the outfall (Figure 30) and a strip along the western side of Wylfa Head with an area of approximately 4.8 hectares. As with the temperature mixing zone, the difference in the size of the mixing zones at the surface and bed is due to the buoyancy of the CW discharge.

6.1.1.3 Summer Base Case – Full extent

The wider extent of the plume above the background is shown in Figure 31 to Figure 34. The extent of temperature increase above the background extends for a large area (approximately 60 km), predominantly to the north west of the intake/outfall area. However, this increase is small, with maximum increases of 0.2 °C. The same pattern can be seen for increase in TRO values; however, the extent is smaller (approximately 20 km). Here the maximum increase is 2.5 µg/l.

6.1.1.4 Summer Base Case – Recirculation

Recirculation occurs when a Power Station draws in water that has been warmed by the CW discharge. Unlike a river, where the flow is unidirectional and siting the intake a suitable distance upstream for the discharge should prevent recirculation, the potential for recirculation is to be expected in a tidal environment.

The depth-averaged temperature rise for a model cell (m=141, n=64) approximately in the middle of the CW forebay has been calculated from a simulation of the period 15 August 2011 to 1 September 2011.

In Table 3 the mean, 98 percentile and maximum temperature rise above ambient at the intake are listed.

Table 3 Recirculation statistics – Summer Base Case.

Statistic	Temperature rise above ambient (°C)
Average	0.46
98 percentile	0.78
Maximum	0.84

The average temperature increase above ambient at the intake was 0.46 °C with a maximum of 0.84 °C.

6.1.2 Autumn Base Case

The ambient seawater temperature was representative of the autumn: 14.3 °C. The model was run in excess temperature mode with a wind speed of 6.8 m/s which is the mean measured at RAF Valley for the autumn season although the wind drag was set to zero. The surface heat flux was 24 W/m^2/K again representative of the average for the season. The TRO decay rate was set to an appropriate value of decay (36.81 per day).

The model was allowed to warm up for the period 21 August 2011 to 21 September 2011 with the CW discharge operating to allow the thermal and TRO fields to develop. After this initial warm-up period the model was run for a further period and set to record data at hourly intervals for each model cell. Data at each model cell was stored for a full spring-neap cycle for the period 21st September 2011 to 6th October 2011.

6.1.2.1 Autumn Base Case – Temperature Rise

The mixing zone implied by the extent of the 3 °C 98 percentile rise at the surface (Figure 35) has an approximate area of 90.8 hectares. The 2 °C 98 percentile rise at the surface has an approximate area of 241 hectares, while the 1 °C 98 percentile rise has an area of approximately 750 hectares.

The mixing zone at the bed implied by the extent of the 3 °C 98 percentile rise area (Figure 36) is approximately 3.1 hectares and is limited to an area around the proposed outfall and along the western edge of Wylfa Head. The area of the 2 °C and 1 °C 98 percentile rise at the bed are approximately 3.9 hectares and 7.2 hectares respectively.

6.1.2.2 Autumn Base Case – TRO

The predicted 95 percentile TRO concentration at the surface and bed are plotted in Figure 37 and Figure 38, respectively. The mixing zone at the surface implied by the extent of the 10 µg/l 95 percentile contour has an approximate area of 288 hectares.

The area of the bed with a TRO 95 percentile concentration greater than 10 µg/lis limited to the vicinity of the outfall (Figure 38) and a strip along the western side of Wylfa Head with an area of approximately 5.1 hectares.

6.1.2.3 Autumn Base Case – Recirculation

The depth-averaged temperature rise for a model cell (m=141, n=64) approximately in the middle of the CW forebay has been calculated from a simulation of the period 21 September 2011 to 6 October 2011.

In the following table (Table 4) the mean, 98 percentile and maximum temperature rise above ambient at the intake are listed.

Table 4 Recirculation statistics – Autumn Base Case.

Statistic	Temperature rise above ambient (°C)
Average	0.50
98 percentile	0.84
Maximum	0.88

The average increase in the water temperature at the intake due to the long-term operation of the CWS discharge was 0.50 °C. The maximum increase of 0.88 °C was slightly higher than the summer base-case maximum.

6.1.3 Winter Base Case

The ambient seawater temperature was representative of the winter: 8.5 °C. The model was run in excess temperature mode with a wind speed of 6.9 m/s which is the mean measured at RAF Valley for the winter season although the wind drag was set to zero. The surface heat flux was 21.4 W/m^2/K again representative of the average for the season. The TRO decay rate was set to an appropriate value of decay (4.75per day).

The model was allowed to warm up for the period 1 December 2011 to 1 January 2012 with the CW discharge operating to allow the thermal and TRO fields to develop. After this initial warm-up period the model was run for a further period and set to record data at hourly intervals for each model cell. Data at each model cell were stored for a full spring-neap cycle for the period 11 January 2012 to 25 January 2012.

6.1.3.1 Winter Base Case – Temperature Rise

The mixing zone implied by the extent of the 3 °C 98 percentile rise at the surface (Figure 39) has an approximate area of 79 hectares, while the 2 °C 98 percentile rise and 1 °C 98 percentile rise cover areas of approximately 176 and 544 hectares, respectively.

The mixing zone implied by the extent of the 3 °C 98 percentile rise at the bed (Figure 40) is limited to an area around the proposed outfall and along the western edge of Wylfa Head, covering approximately 3.2 hectares. The area of the 2 °C 98 percentile rise at the bed has an area of approximately 4.1 hectares while the 1 °C rise area is approximately 7.9 hectares.

6.1.3.2 Winter Base Case – TRO

The mixing zone implied by the extent of the 10 µg/l 95 percentile contour (Figure 41) has an approximate area of 185.24 hectares.

The area of the bed with a TRO 95 percentile concentration greater than 10 µg/l is limited to the vicinity of the outfall (Figure 42) and a strip along the western side of Wylfa Head with an area of approximately 5.72 hectares

6.1.3.3 Winter Base Case – Recirculation

The depth-averaged temperature rise for a model cell (m=141, n=64) approximately in the middle of the CW forebay has been calculated from a simulation of the period 11 January 2012 to 25 January 2012.

In the following table (Table 5) the mean, 98 percentile and maximum temperature rise above ambient at the intake are listed.

Table 5 Recirculation statistics - Winter Base Case.

Statistic	Temperature rise above ambient (°C)
Average	0.44
98 percentile	0.64
Maximum	0.66

The average increase in the water temperature at the intake due to the long-term operation of the CWS discharge was 0.44 °C. The maximum increase of 0.66 °C was lower than the summer base-case maximum.

6.1.4 Spring Base Case

The ambient seawater temperature was representative of the winter: 9.0 °C. The model was run in excess temperature mode with a wind speed of 6 m/s which is the mean measured at RAF valley for the spring season

although the wind drag was set to zero. The surface heat flux was 19.7 W/m^2/K, again representative of the average for the season. The TRO decay rate was set to an appropriate value of decay (11.15 per day).

The model was allowed to warm up for the period 1 March 2011 to 1 April 2011 with the CW discharge operating to allow the thermal and TRO fields to develop. After this initial warm-up period the model was run for a further period and set to record data at hourly intervals for each model cell. Data at each model cell were stored for a full spring-neap cycle for the period 11 April 2011 to 25 April 2011.

6.1.4.1 Spring Base Case – Temperature Rise

The mixing zone implied by the extent of the 3 °C 98 percentile rise at the surface (Figure 43) has an approximate area of 88.8 hectares, while the 2 °C 98 percentile rise has an area of approximately 212 hectares. The 1 °C 98 percentile rise at the surface has an approximate area of 642 hectares.

The mixing zone implied by the extent of the 3 °C 98 percentile rise at the bed (Figure 44) is limited to an area around the proposed outfall and along the western edge of Wylfa Head. The area of the 3 °C 98 percentile rise at the bed has an area of approximately 3.2 hectares while the 2 °C rise area is approximately 4.1 hectares. The 1°C 98 percentile rise area is approximately 7.9 hectares.

6.1.4.2 Spring Base Case – TRO

The mixing zone implied by the extent of the 10 µg/l 95 percentile contour (Figure 45) has an approximate area of 223 hectares.

The area of the bed with a TRO 95 percentile concentration greater than 10 µg/l is limited to the vicinity of the outfall (Figure 46) and a strip along the western side of Wylfa Head with an area of approximately 5.5 hectares

6.1.4.3 Spring Base Case – Recirculation

The depth-averaged temperature rise for a model cell (m=141, n=64) approximately in the middle of the CW forebay has been calculated from a simulation of the period 11 April 2011 to 25 April 2011.

In Table 6 the mean, 98 percentile and maximum temperature rise above ambient at the intake are listed.

Table 6 Recirculation statistics – Spring Base Case.

Statistic	Temperature rise above ambient (°C)
Average	0.47
98 percentile	0.70
Maximum	0.76

The average increase in the water temperature at the intake due to the long-term operation of the CWS discharge was 0.47 °C. The maximum increase of 0.76 °C was lower than the summer base-case maximum (0.84 °C)

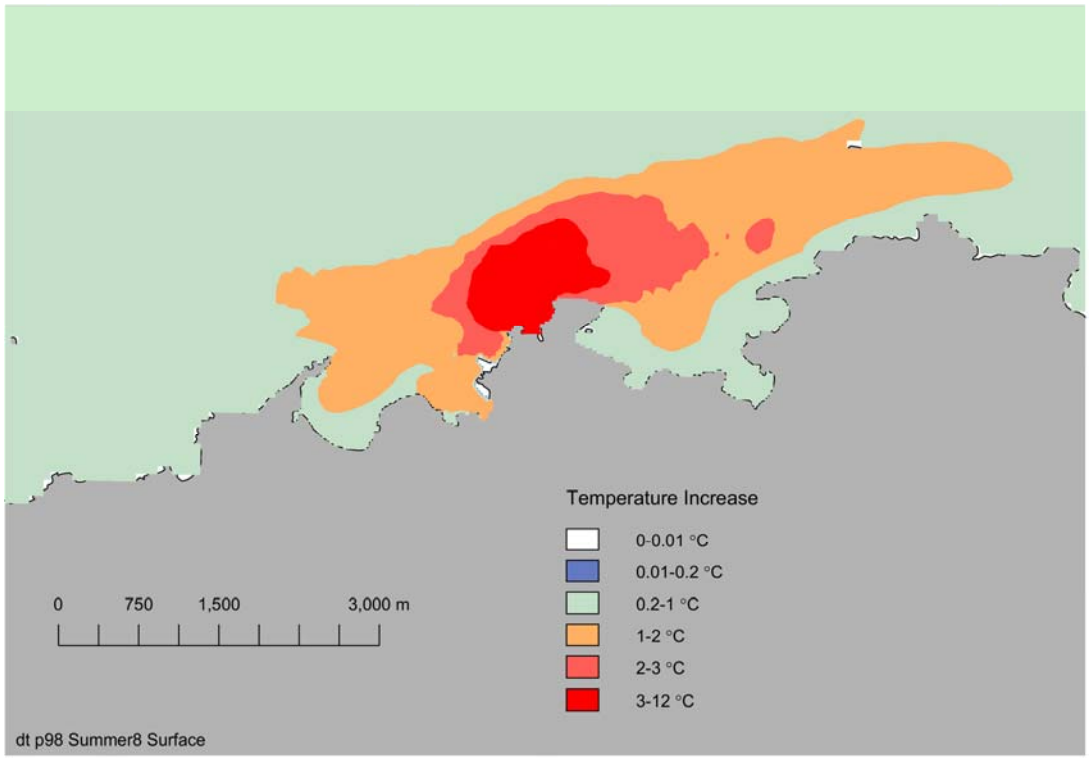

Figure 27 Surface temperature, 98 percentile – Summer base case.

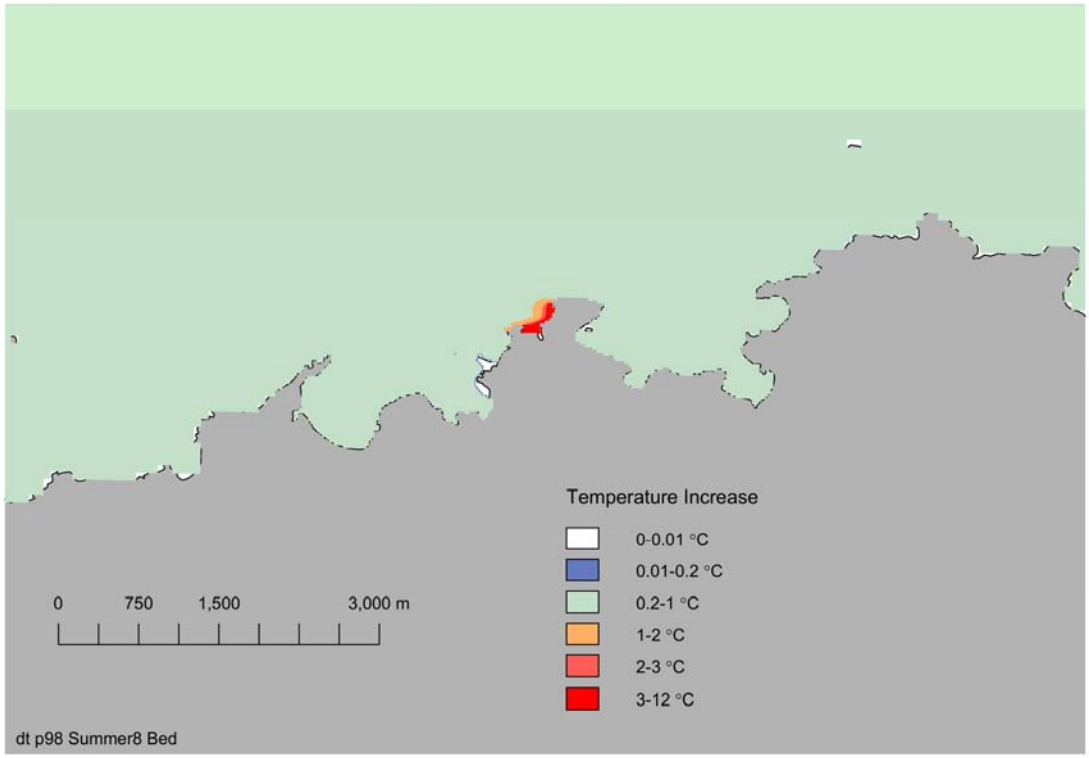

Figure 28 Bed temperature, 98 percentile – Summer base case.

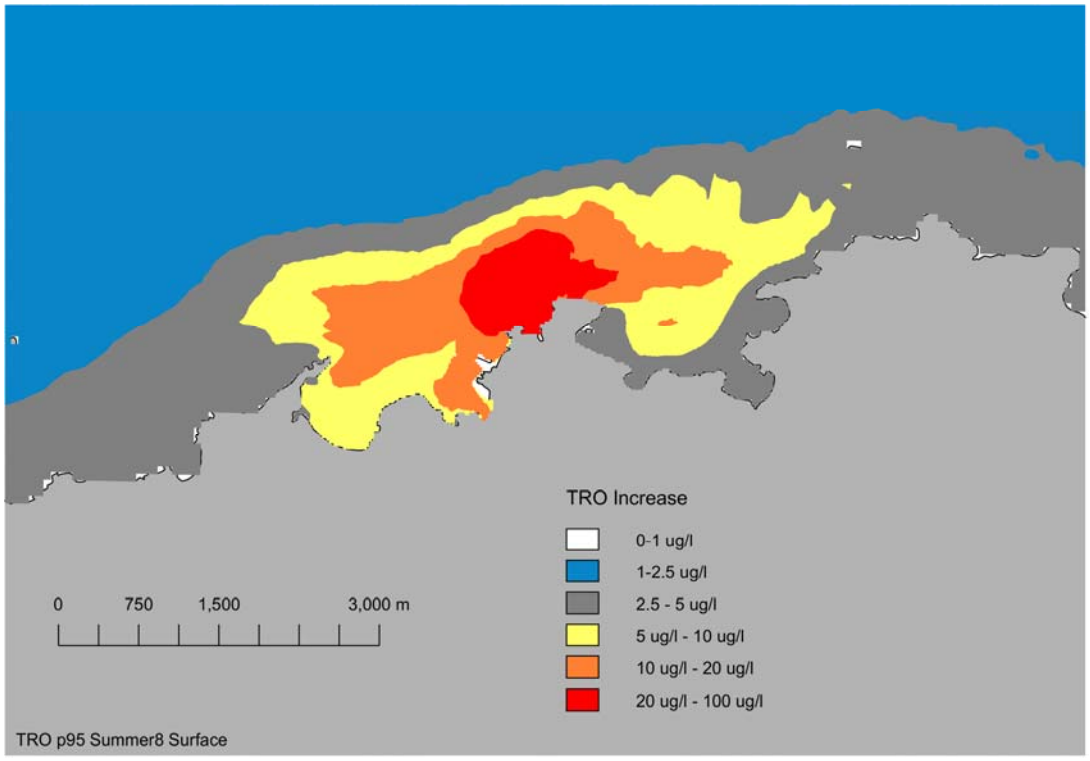

Figure 29 Surface TRO concentration, 95 percentile – Summer base case.

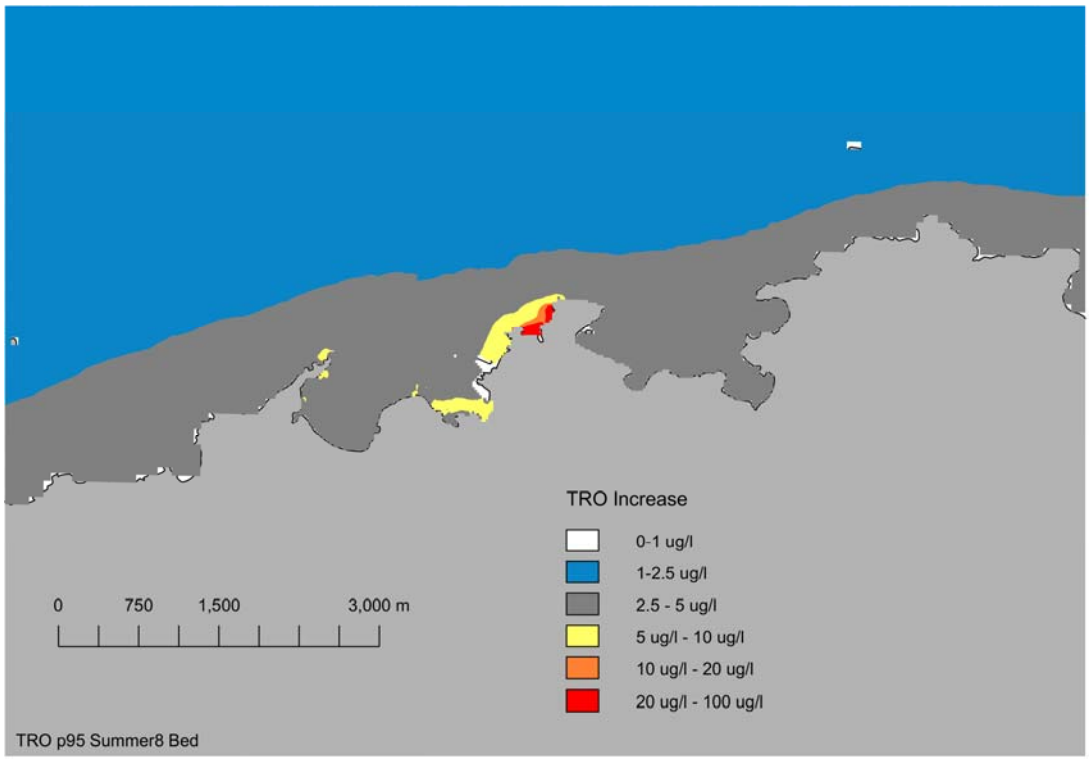

Figure 30 Bed TRO concentration, 95 percentile – Summer base case.

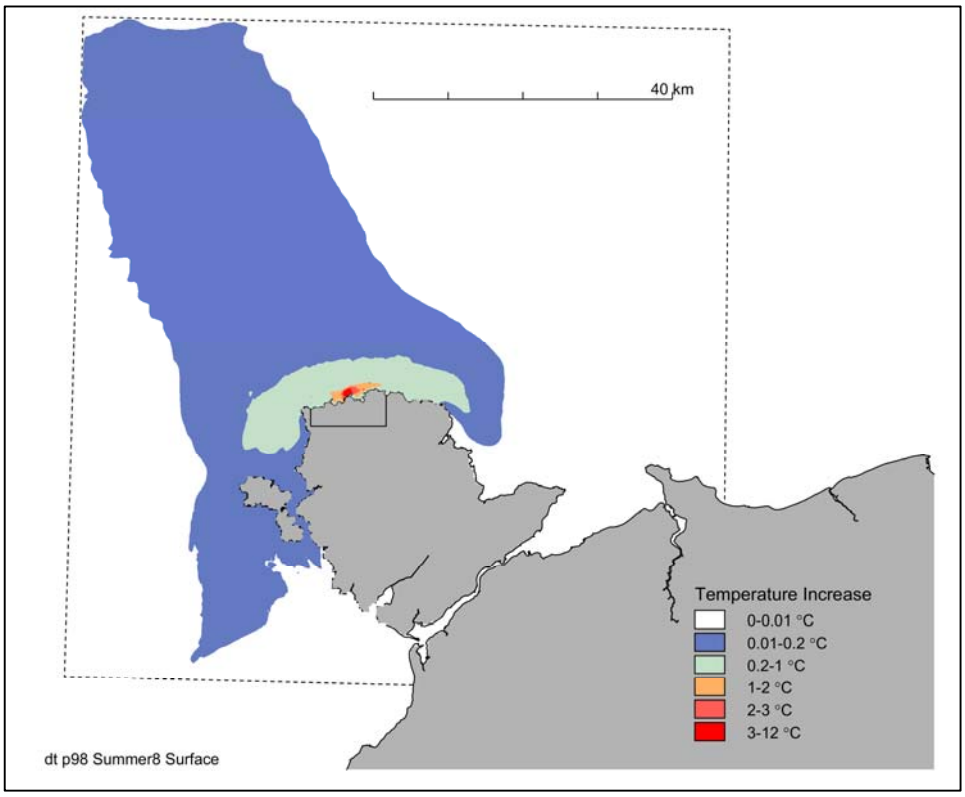

Figure 31 Surface temperature, 98 percentile – Summer base case, wide extent.

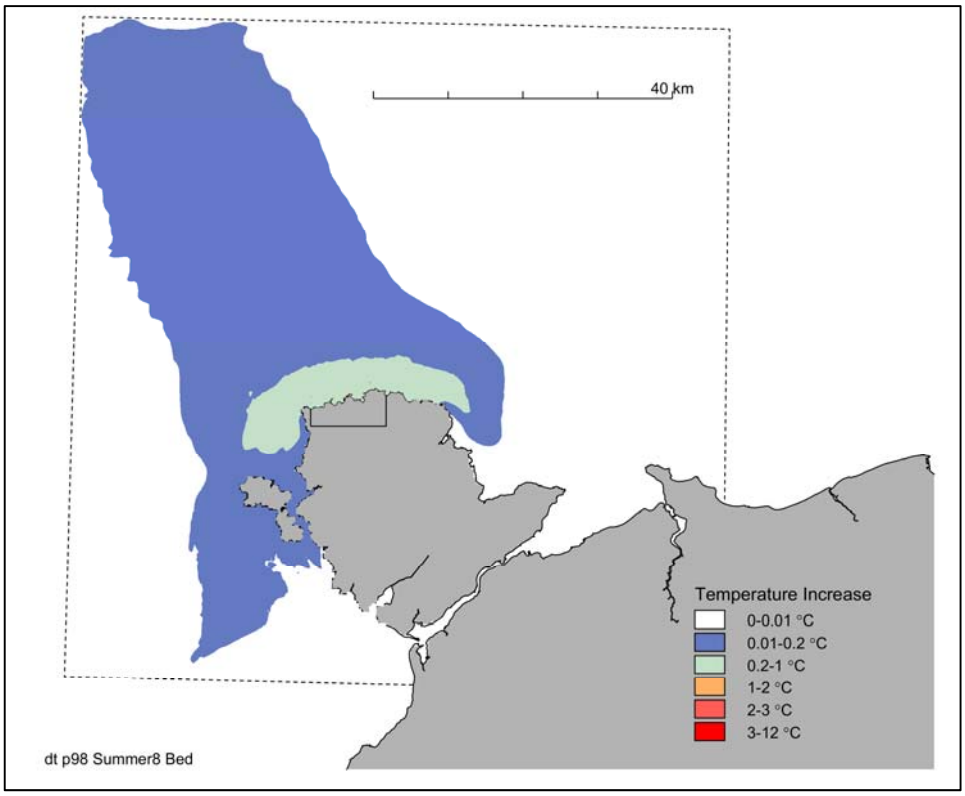

Figure 32 Bed temperature, 98 percentile – Summer base case, wide extent.

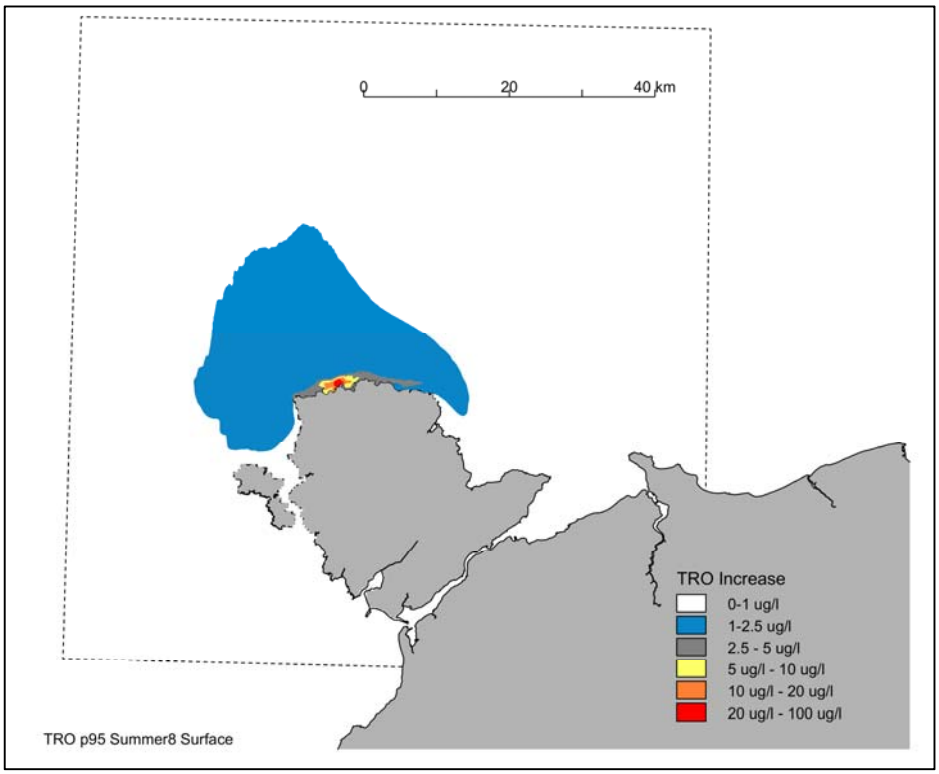

Figure 33 Surface TRO concentration, 95 percentile – Summer base case, wide extent.

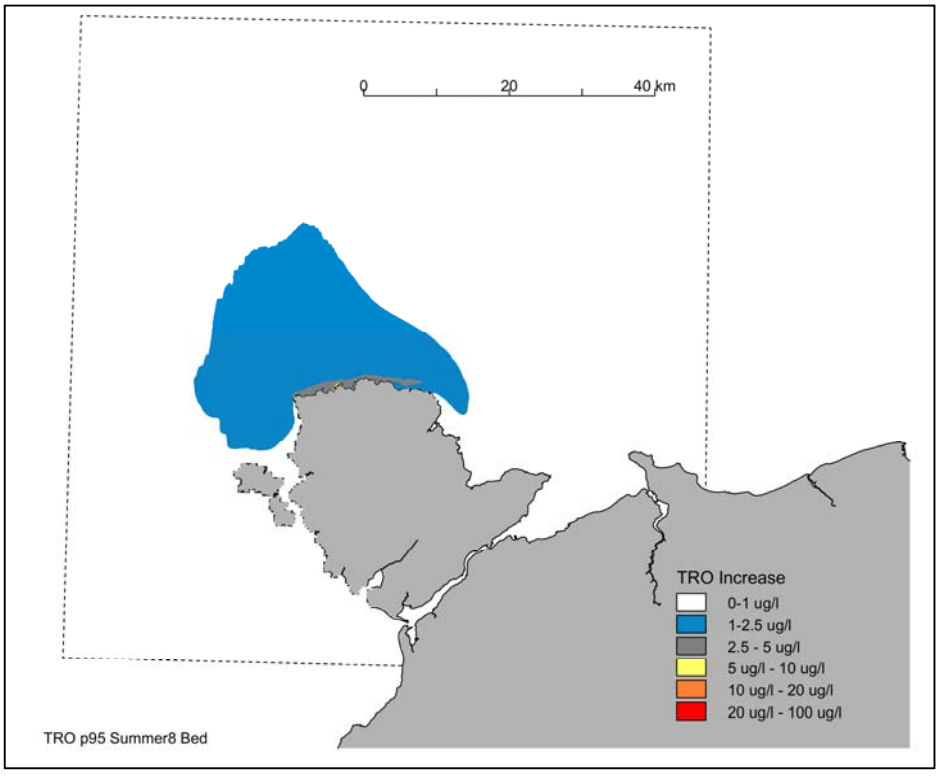

Figure 34 Bed TRO concentration, 95 percentile – Summer base case, wide extent.

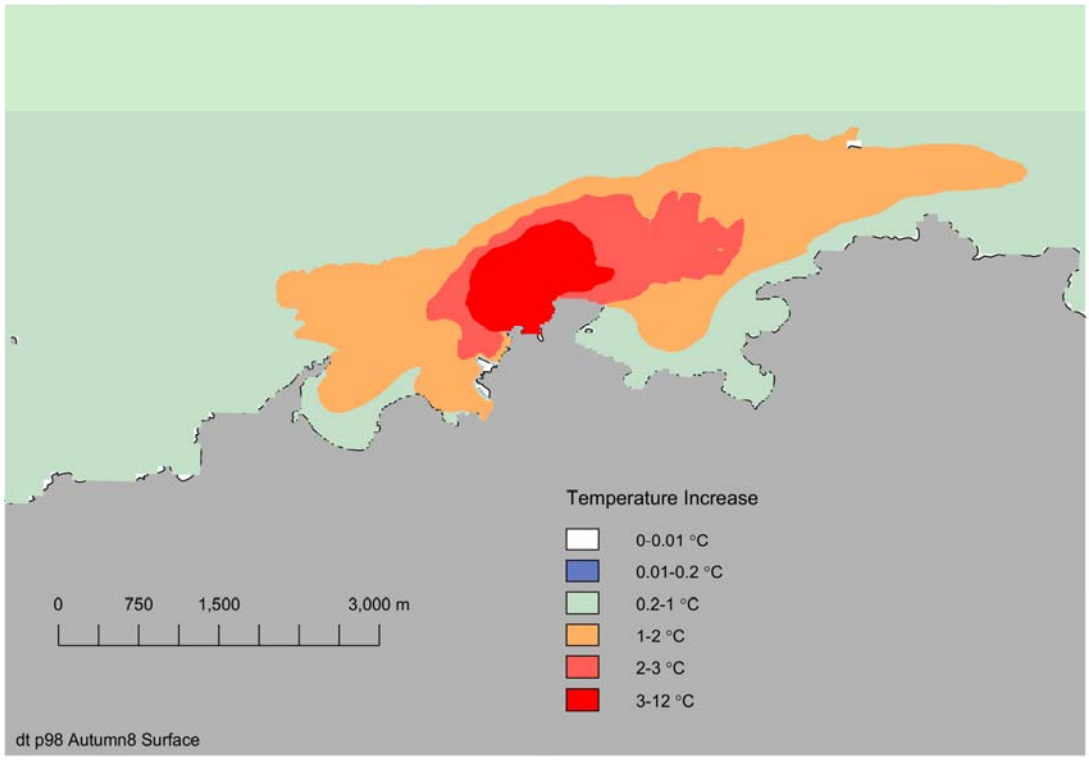

Figure 35 Surface temperature, 98 percentile – Autumn base case.

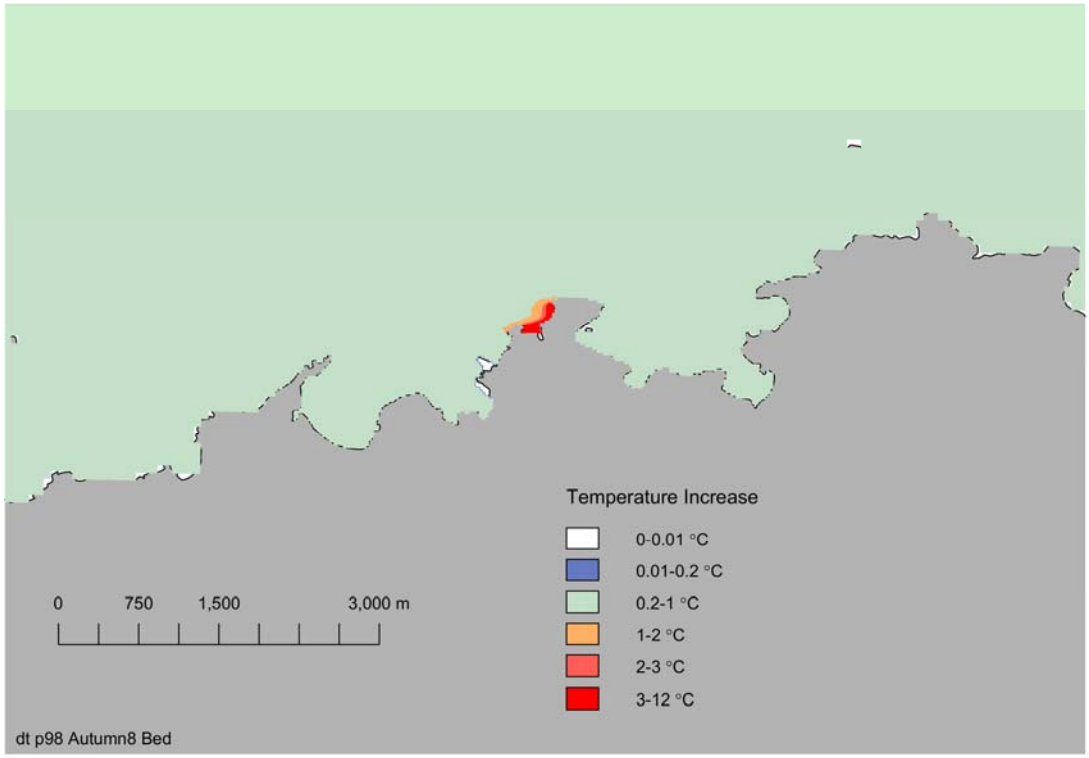

Figure 36 Bed temperature, 98 percentile – Autumn base case.

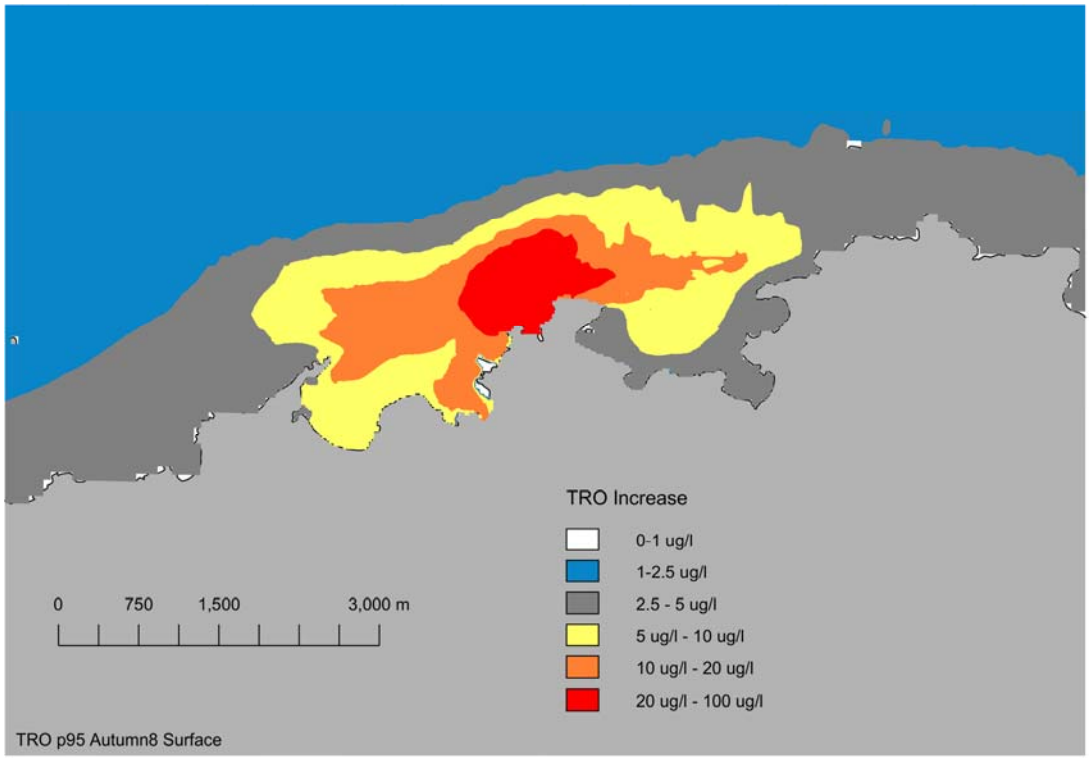

Figure 37 Surface TRO concentration, 95 percentile – Autumn base case.

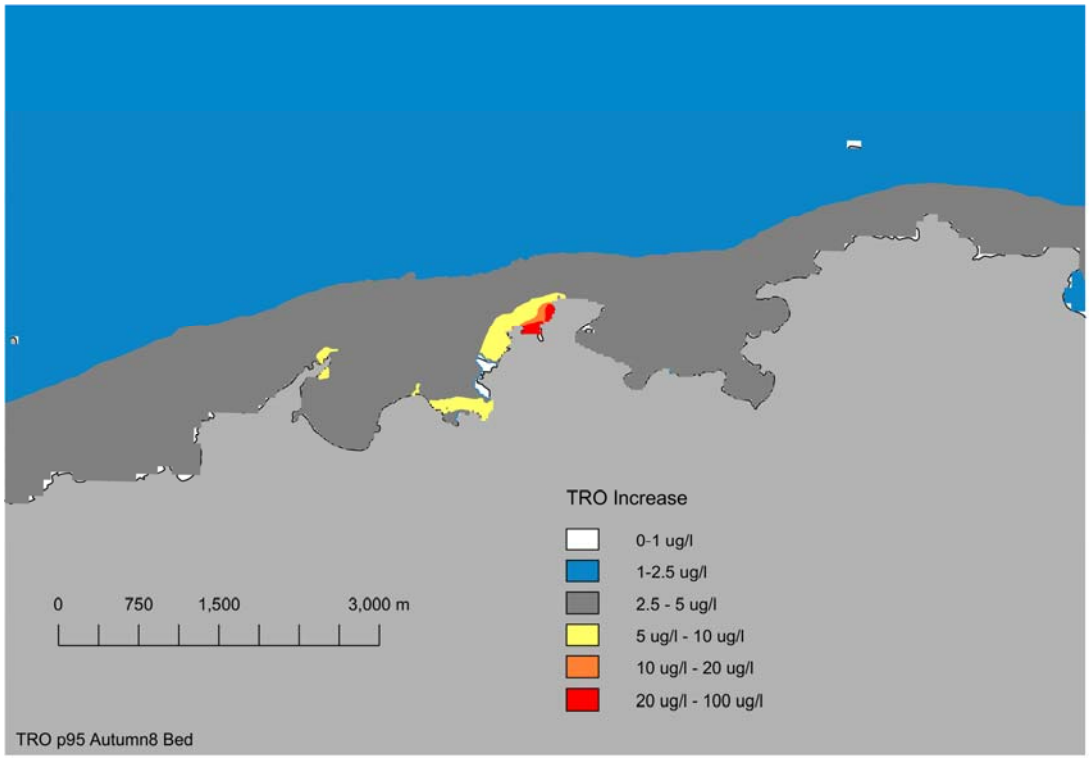

Figure 38 Bed TRO concentration, 95 percentile – Autumn base case.

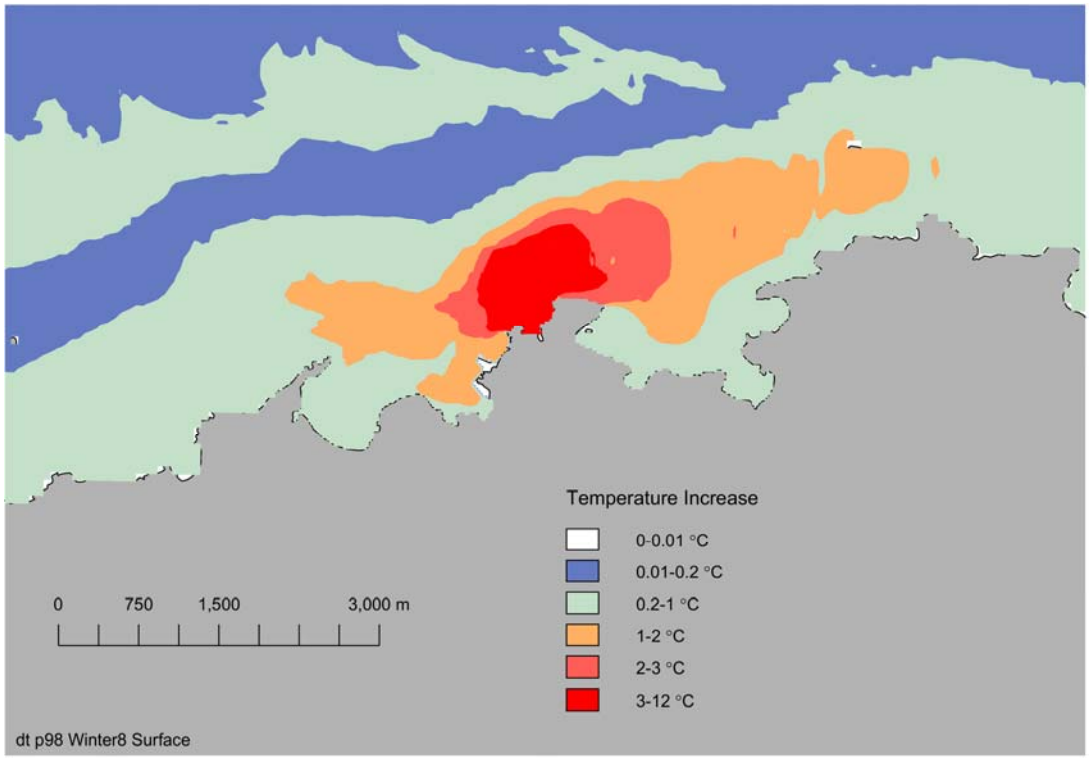

Figure 39 Surface temperature, 98 percentile – Winter base case.

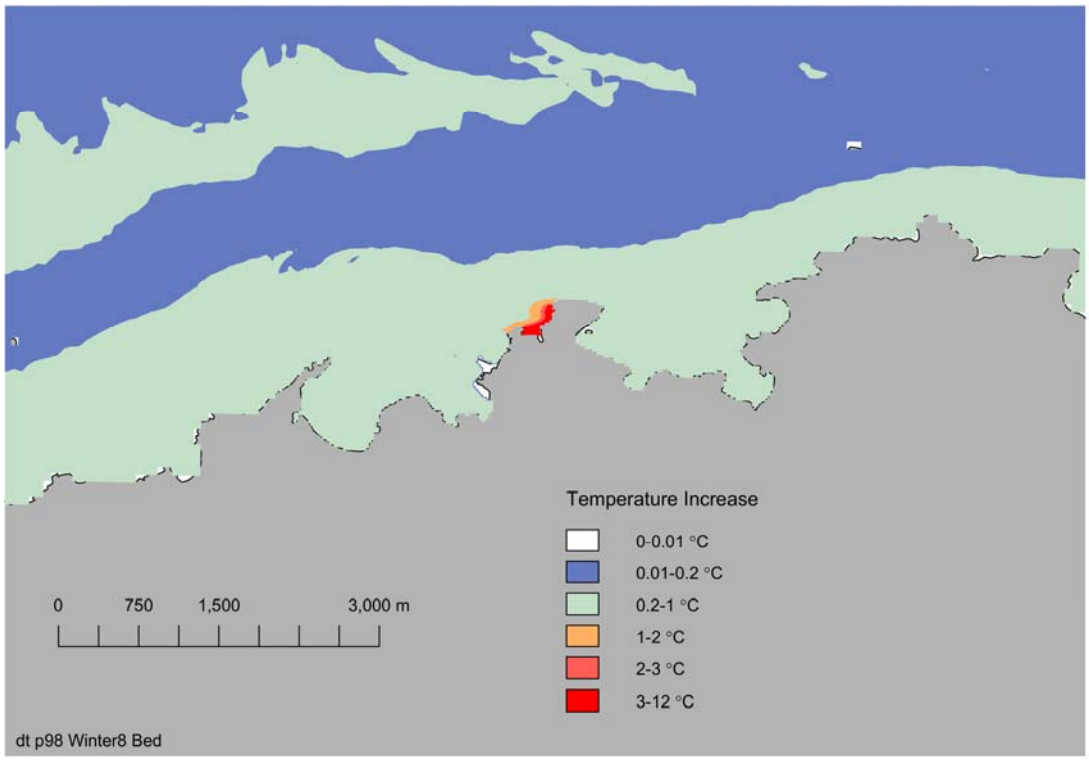

Figure 40 Bed temperature, 98 percentile – Winter base case.

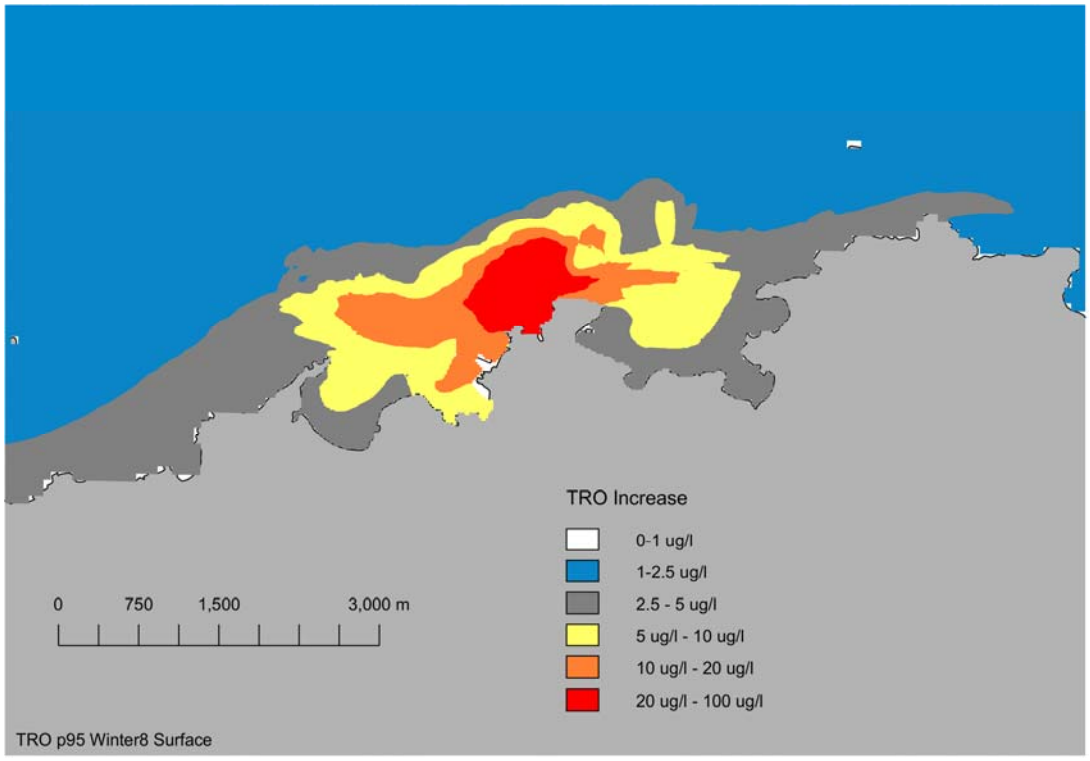

Figure 41 Surface TRO concentration, 95 percentile – Winter base case.

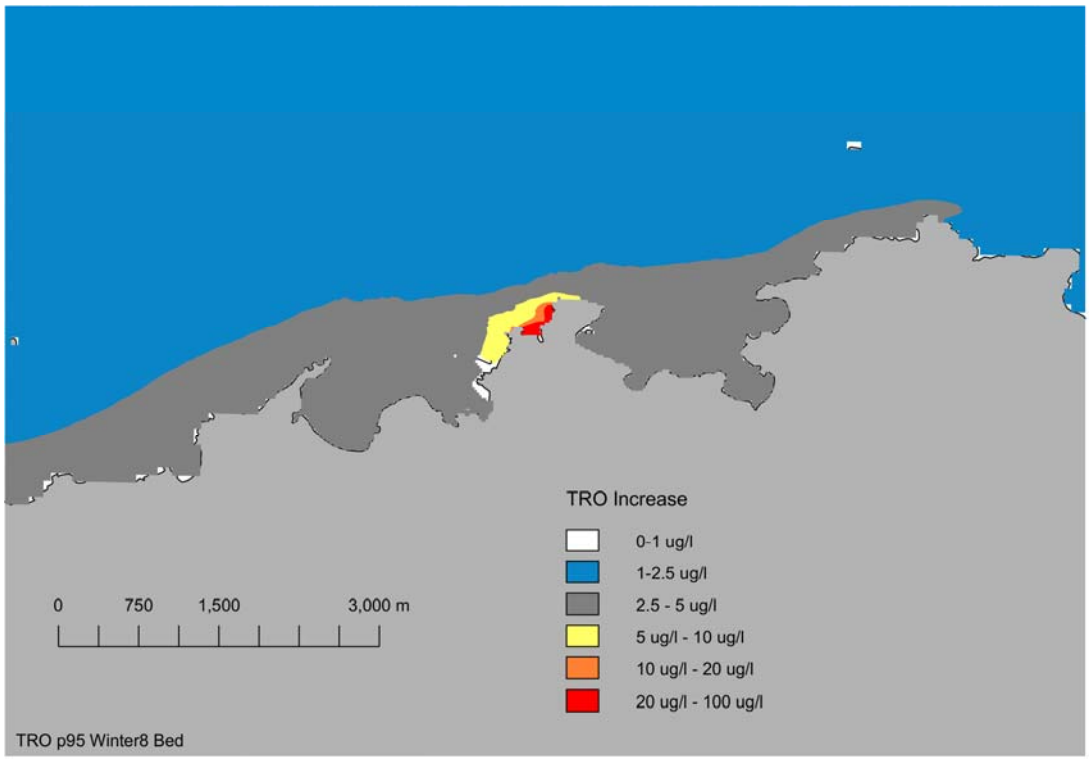

Figure 42 Bed TRO concentration, 95 percentile – Winter base case.

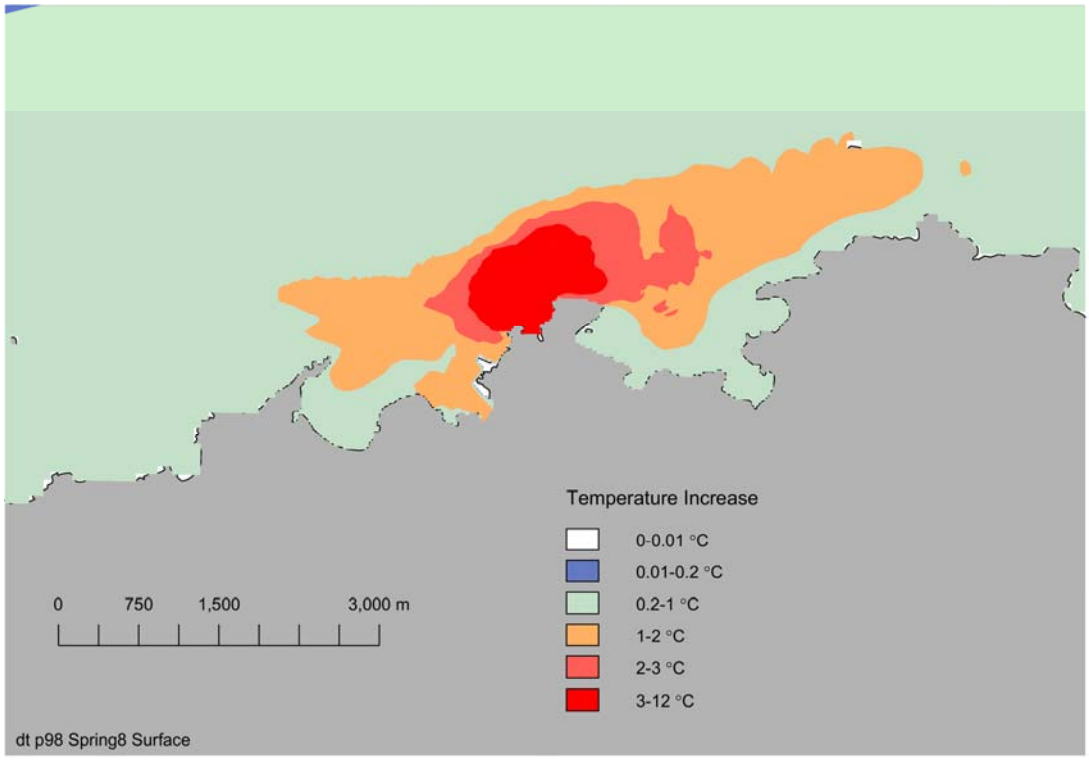

Figure 43 Surface temperature, 98 percentile – Spring base case.

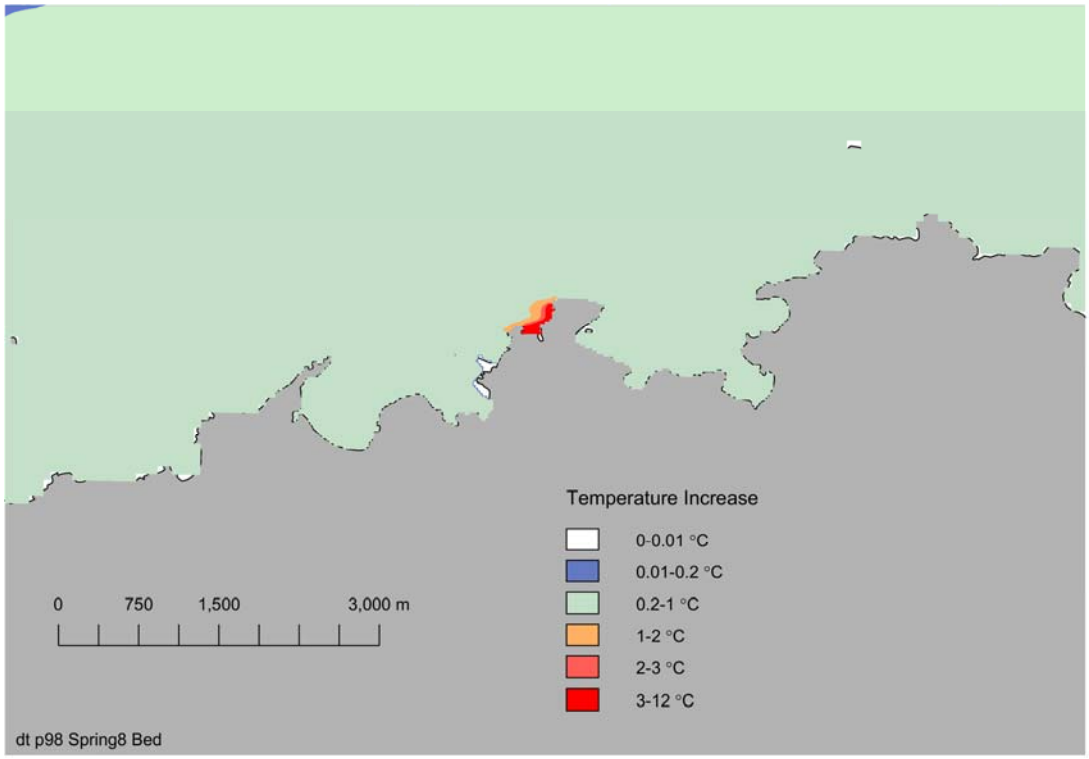

Figure 44 Bed temperature, 98 percentile – Spring base case.

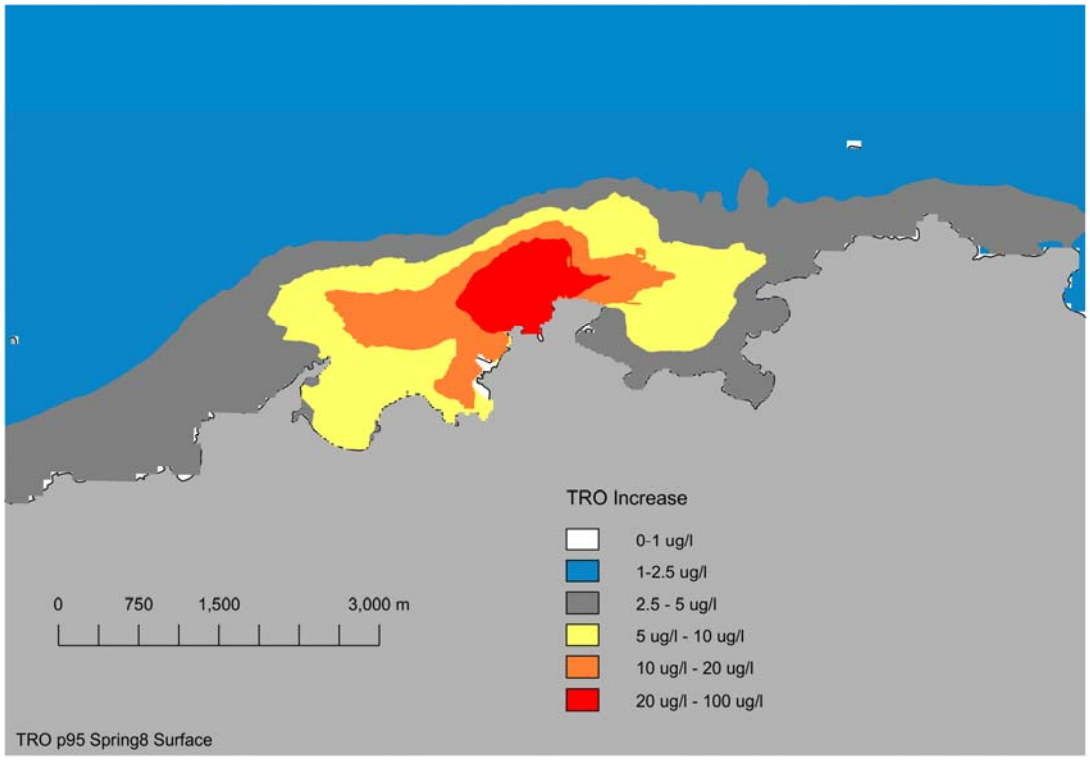

Figure 45 Surface TRO concentration, 95 percentile – Spring base case.

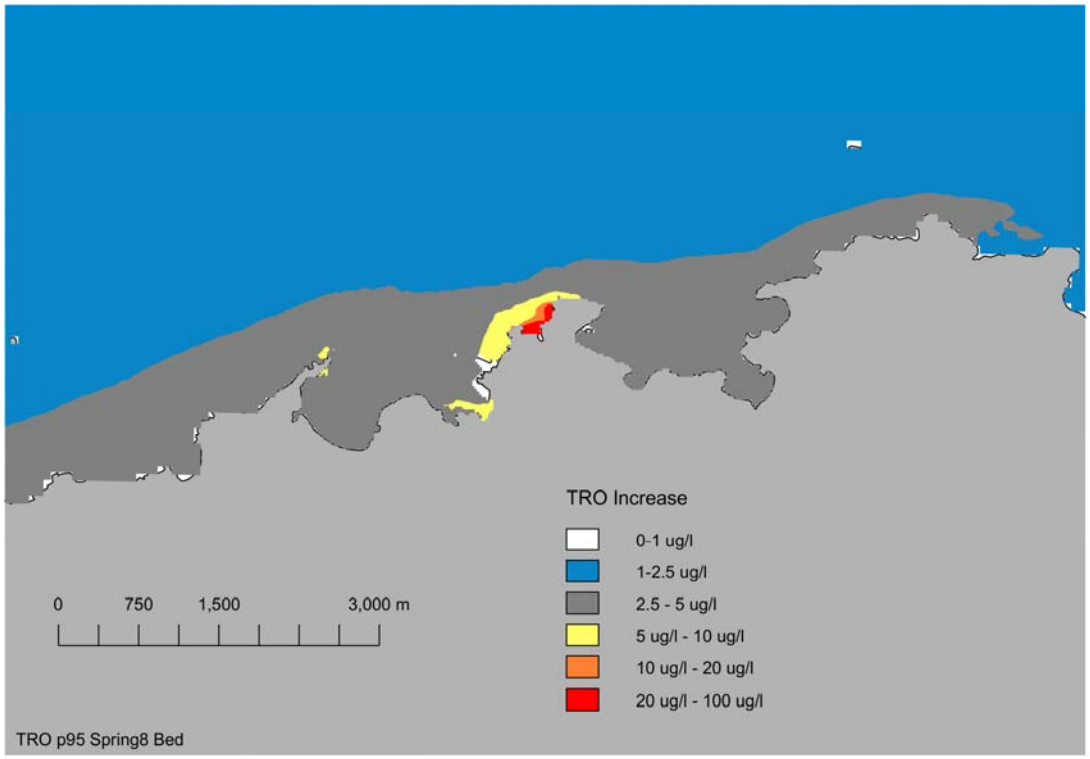

Figure 46 Bed TRO concentration, 95 percentile – Spring base case.

6.2 Heat Flux Sensitivity

Model simulations were undertaken with both low and high surface heat exchange coefficients. The low surface heat flux condition was 12 W/m^2/K (10 W/m^2/K lower than the summer base-case), while the high heat flux condition was 35 W/m^2/K (13 W/m^2/K higher than the summer base-case). Apart from the surface heat exchange coefficients the simulations were repeats of the summer base-case.

In the following sections the difference between the predicted temperature rise with the high and low heat flux conditions and the base-case are plotted for surface and bed.

6.2.1 Low Flux Model Setup

The simulation was a version of the summer base case in which the wind speed and area in the model were used to set the required surface heat flux in the model. The surface heat flux was 12 W/m^2/K , representative of a low surface heat flux (10 W/m^2/K lower than the base case surface heat flux). Other parameters such as the TRO decay rate were left as in the summer base case (10.08 per day).

The model was allowed to warm up for the period 25 June 2011 to 1 August 2011 with the CW discharge operating to allow the thermal and TRO fields to develop. After this initial warm-up period the model was run for a further period and set to record data at hourly intervals for each model cell. Data at each model cell were stored for a full spring-neap cycle for the period 15 August 2011 to 1 September 2011.

6.2.1.1 Summer Low Flux Case – Temperature Rise

The mixing zone implied by the extent of the 3 °C 98 percentile rise at the surface (Figure 47) has an approximate area of 91.1 hectares, while the 2 °C 98 percentile rise has an area of approximately 198 hectares. The 1 °C 98 percentile rise at the surface has an approximate area of 624 hectares.

The mixing zone implied by the extent of the 3 °C 98 percentile rise at the bed (Figure 48) is limited to an area around the proposed outfall and along the western edge of Wylfa Head, covering approximately 3.3 hectares. The area of the 2 °C 98 percentile rise at the bed has an area of approximately 4.4 hectares while the 1 °C 98 percentile rise area is approximately 9.2 hectares.

The output of the low heat flux and base cases has been processed to produce the mean difference between the two. In the data plotted in Figure 49 and Figure 50, a positive value occurs where the use of the low surface flux results in a higher predicted temperature rise compared to the base case at the surface and bed respectively. As expected the low surface heat loss results in general in elevated sea surface temperatures compared to the base case. However, differences are small and some areas of temperature reduction are also observed to occur further offshore, but only at the surface. In Cemlyn Bay the mean difference at the surface between the two cases is around 0.03 °C. The small differences between the two cases are indicative of the relative strength of the mixing processes compared to the surface heat loss in the waters surrounding Wylfa Head.

The mean differences in temperature rise at the bed between the low heat flux case and the base case are also small. In Cemlyn and Cemaes Bays the difference at the bed is around 0.02 °C.

6.2.1.2 Summer Low Flux Case – TRO

The mixing zone implied by the extent of the 10 µg/l 95 percentile contour (Figure 51) has an approximate area of 231 hectares.

The area of the bed with a TRO 95 percentile concentration greater than 10 µg/l is limited to the vicinity of the outfall (Figure 52) and a strip along the western side of Wylfa Head with an area of approximately 6.2 hectares

6.2.1.3 Summer Low Flux Case – Recirculation

The depth-averaged temperature rise for a model cell (m=141, n=64) approximately in the middle of the CW forebay has been calculated from a simulation of the period 15 August 2011 to 1 September 2011.

In Table 7 the mean, 98 percentile and maximum temperature rise above ambient at the intake are listed.

Table 7 Recirculation statistics – Low flux case.

Statistic	Temperature rise above ambient (°C)	Temperature difference to base case (°C)
Average	0.51	0.05
98 percentile	0.79	0.01
Maximum	0.84	0

The average recirculation for the low surface heat flux case is 0.51 °C which is 0.05 °C higher than the summer base case for the same period. This demonstrates that recirculation was relatively insensitive to the surface heat exchange coefficient.

6.2.2 High Flux Model Setup

The simulation was a version of the summer base case in which the wind speed and area in the model were used to set the required surface heat flux in the model. The surface heat flux was 35 W/m^2/K representative of a high surface heat flux (13 W/m^2/K higher than the base case surface heat flux). Other parameters such as the TRO decay rate were left as in the summer base case (10.08 per day).

The model was allowed to warm up for the period 25 June 2011 to 1 August 2011 with the CW discharge operating to allow the thermal and TRO fields to develop. After this initial warm-up period the model was run for a further period and set to record data at hourly intervals for each model cell. Data at each model cell were stored for a full spring-neap cycle for the period 15 August 2011 to 1 Sept 2011.

6.2.2.1 Summer High Flux Case – Temperature Rise

The mixing zone implied by the extent of the 3 °C 98 percentile rise at the surface (Figure 53) has an approximate area of 86.7 hectares, while the 2 °C 98 percentile rise has an area of approximately 318 hectares. The 1 °C 98 percentile rise at the surface has an approximate area of 727 hectares. These areas are slightly smaller than the equivalent areas for the summer base case (which were 88.7, 227 and 741 hectares for the 3, 2 and 1°C 98 percentile rise, respectively).

The mixing zone implied by the extent of the 3 °C 98 percentile rise at the bed (Figure 54) is limited to an area around the proposed outfall and along the western edge of Wylfa Head, with an area of approximately 3.1 hectares. The area of the 2 °C 98 percentile rise at the bed has an area of approximately 3.8 hectares while the 1 °C 98 percentile rise area is approximately 7.1 hectares.

The output of the high heat flux and base cases has been processed to produce the mean difference between the two at the surface and at the bed (Figure 55 and Figure 56). As expected the higher surface heat loss results in reduced sea surface temperatures compared to the base case. However, differences are in general small. In Cemlyn Bay the mean difference at the surface between the two cases is around -0.03 °C. These small differences between the two cases are indicative of the relative strength of the mixing processes compared to the surface heat loss at in the waters surrounding Wylfa Head. The mean differences in temperature rise at the bed between the two surface heat flux cases are also small. In Cemlyn and Cemaes Bays the difference at the bed is generally around -0.02 °C, with the difference in some near shore areas around 0.03 °C.

6.2.2.2 Summer High Flux Case – TRO

The mixing zone implied by the extent of the 10 µg/l 95 percentile contour (Figure 57) has an approximate area of 305 hectares.

The area of the bed with a TRO 95 percentile concentration greater than 10 µg/l is limited to the vicinity of the outfall (Figure 58) and a strip along the western side of Wylfa Head with an area of approximately 5.1 hectares

6.2.2.3 Summer High Flux Case – Recirculation

The depth-averaged temperature rise for a model cell (m=141, n=64) approximately in the middle of the CW forebay has been calculated from a simulation of the period 15 August 2011 to 1 September 2011.

In Table 8 the mean, 98 percentile and maximum temperature rise above ambient at the intake are listed.

Table 8 Recirculation statistics – High flux case.

Statistic	Temperature rise above ambient (°C)	Temperature difference to base case (°C)
Average	0.45	-0.01
98 percentile	0.76	-0.02
Maximum	0.81	-0.03

The average recirculation for the high surface heat flux case is 0.45 °C which is 0.01 °C lower than the summer base case for the same period. This demonstrates that recirculation was insensitive to the surface heat exchange coefficient.

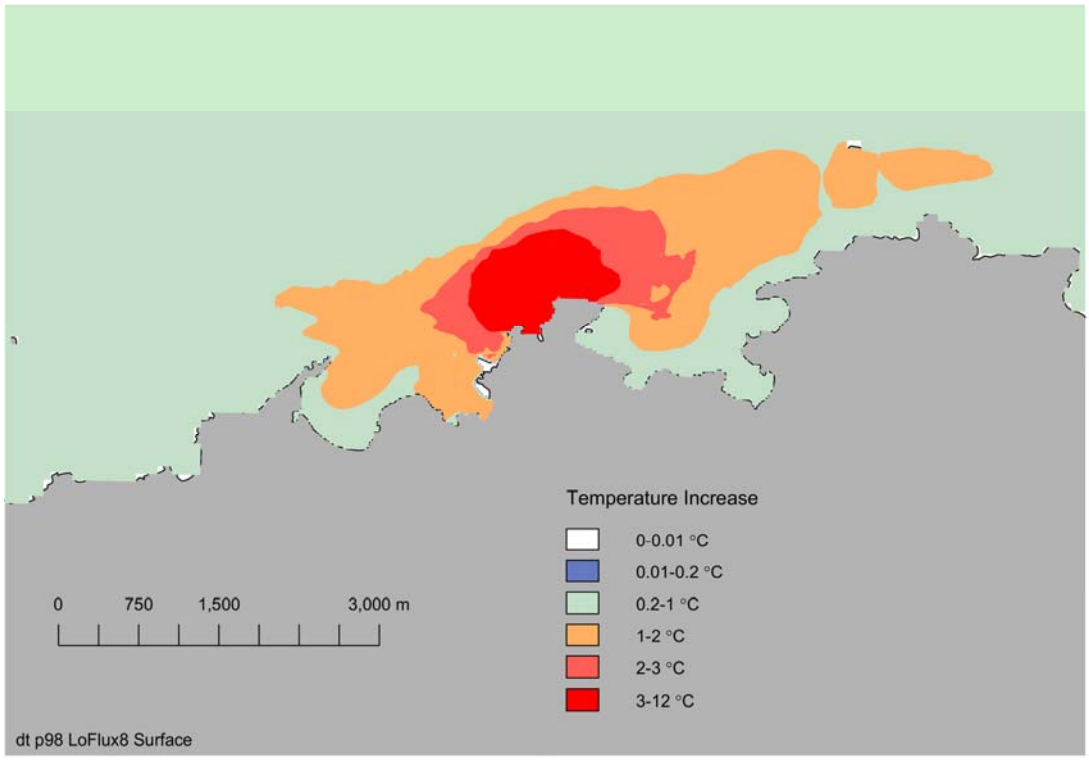

Figure 47 Surface temperature, 98 percentile – Low surface heat flux.

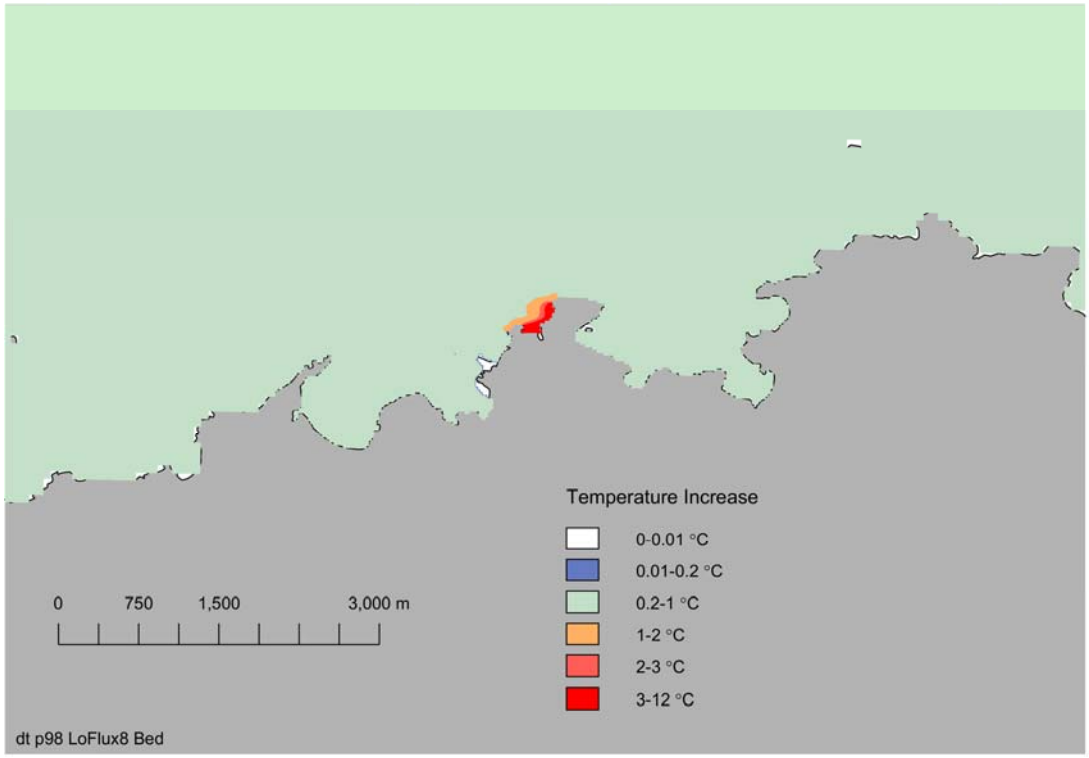

Figure 48 Bed temperature, 98 percentile – Low bed heat flux.

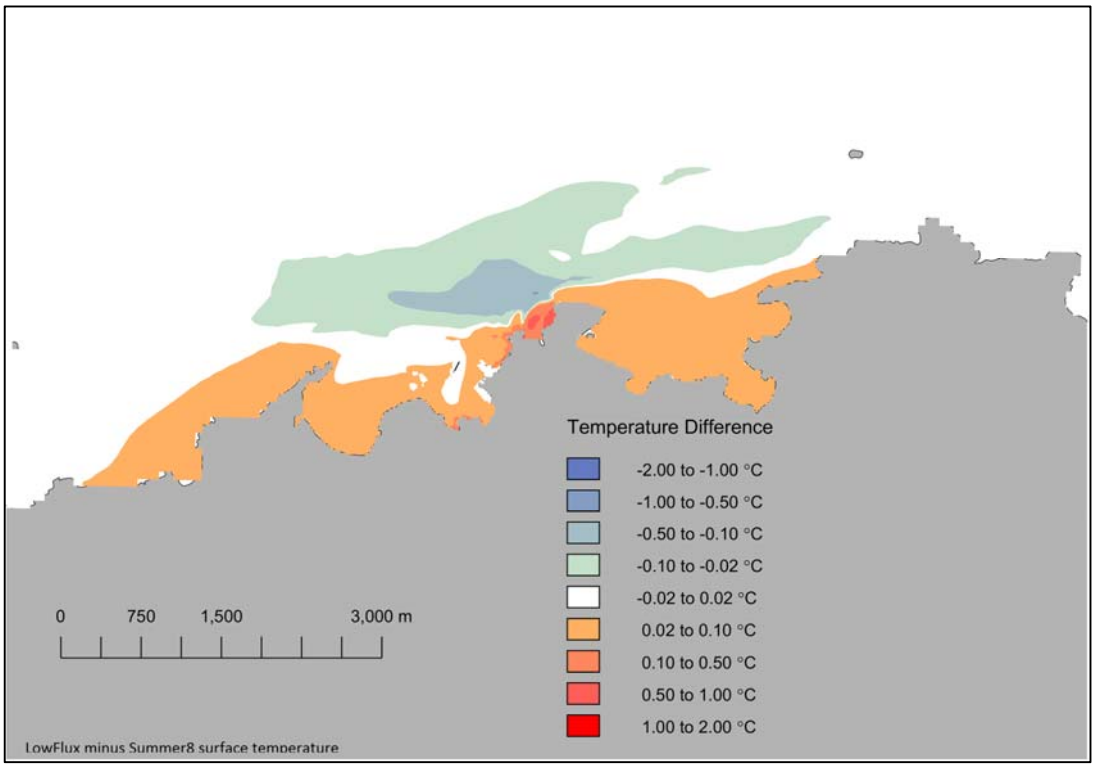

Figure 49 Surface temperature mean difference – Low surface heat flux.

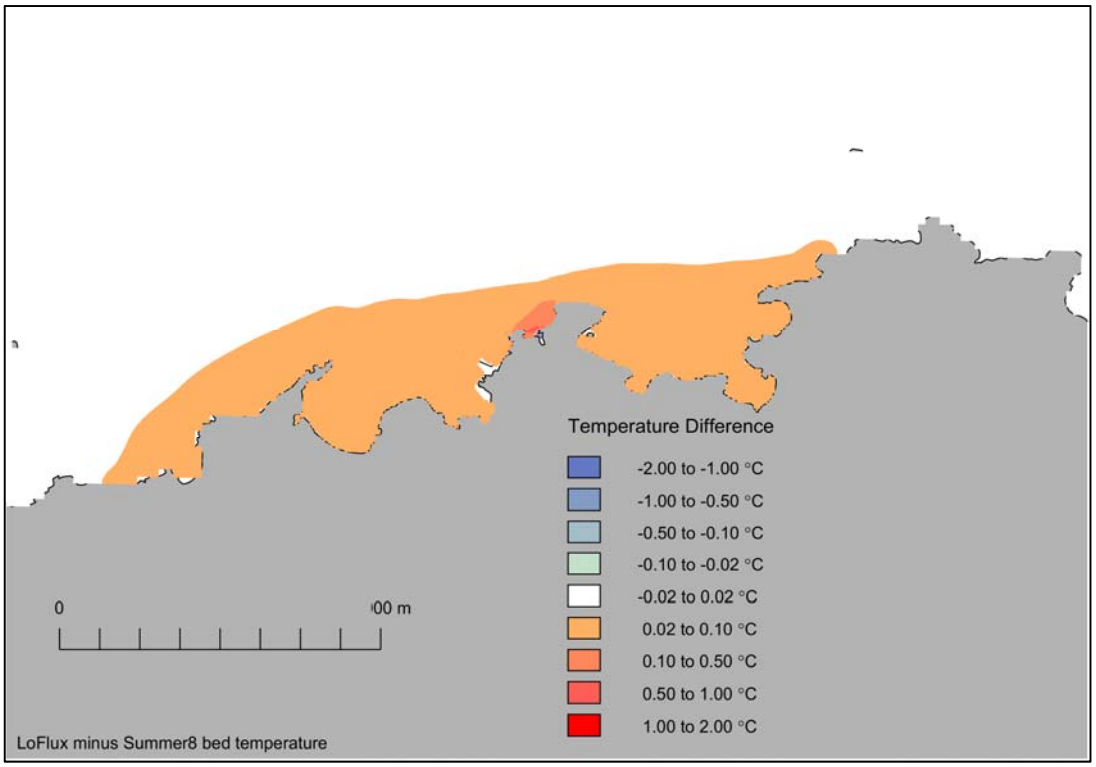

Figure 50 Bed temperature mean difference – Low bed heat flux.

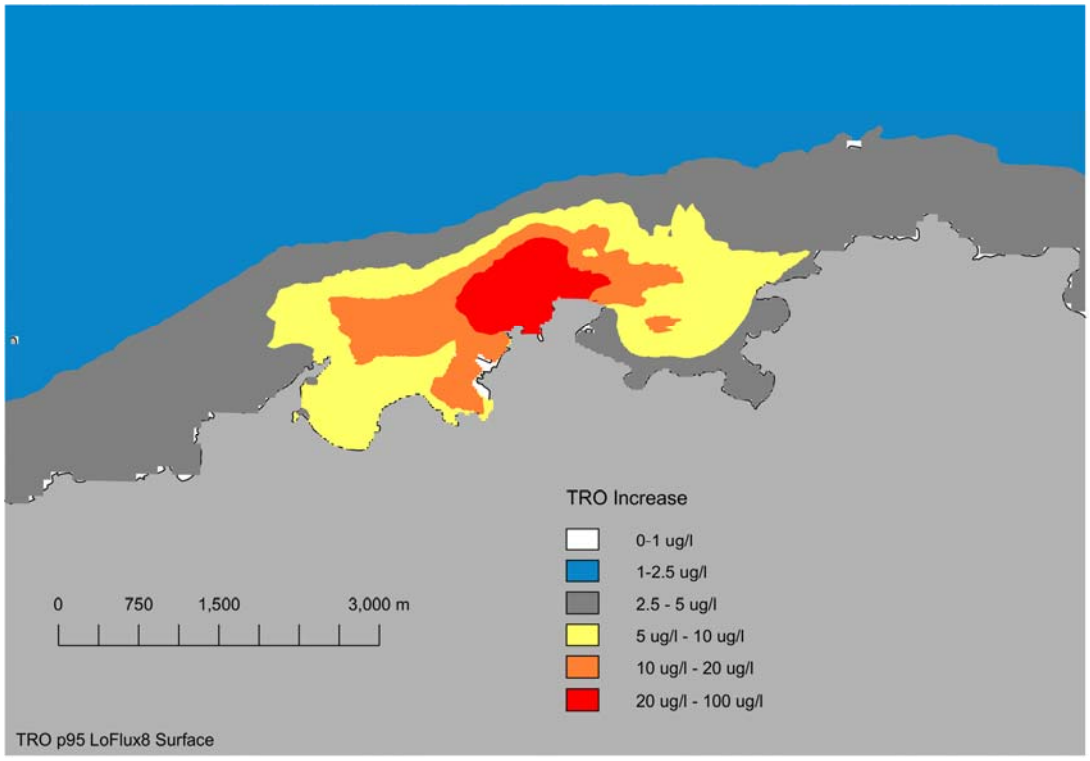

Figure 51 Surface TRO concentration, 95 percentile – Low surface heat flux.

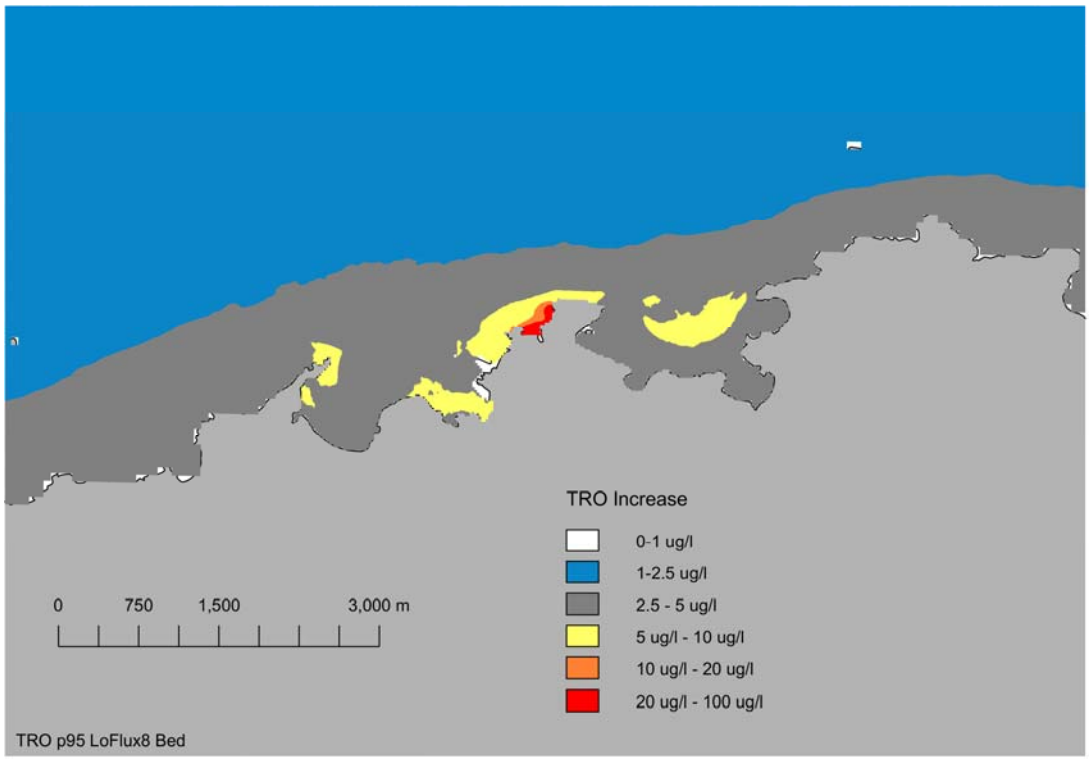

Figure 52 Bed TRO concentration, 95 percentile – Low bed heat flux.

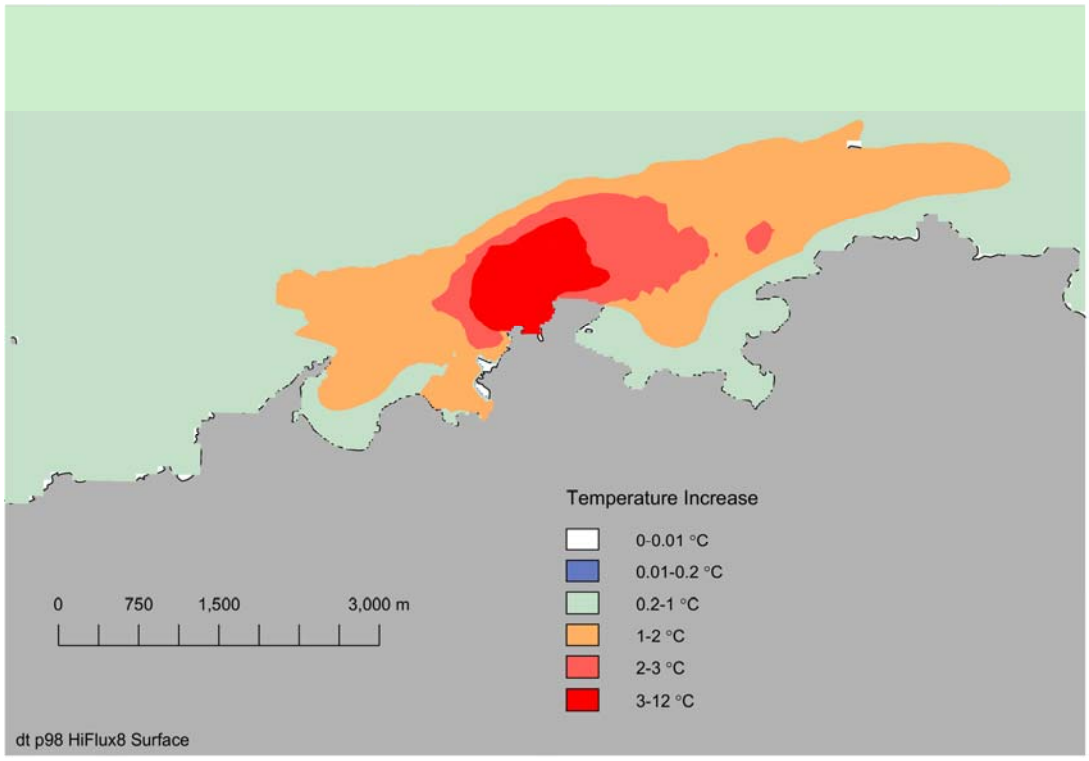

Figure 53 Surface temperature, 98 percentile – High surface heat flux.

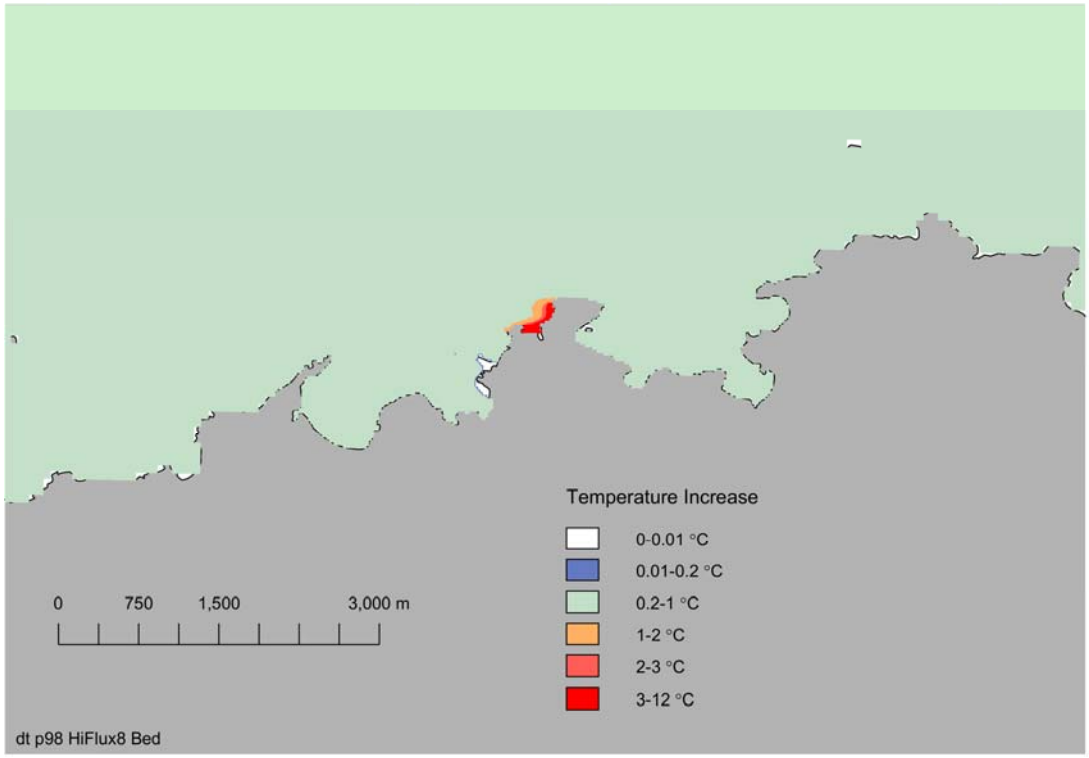

Figure 54 Bed temperature, 98 percentile – High bed heat flux.

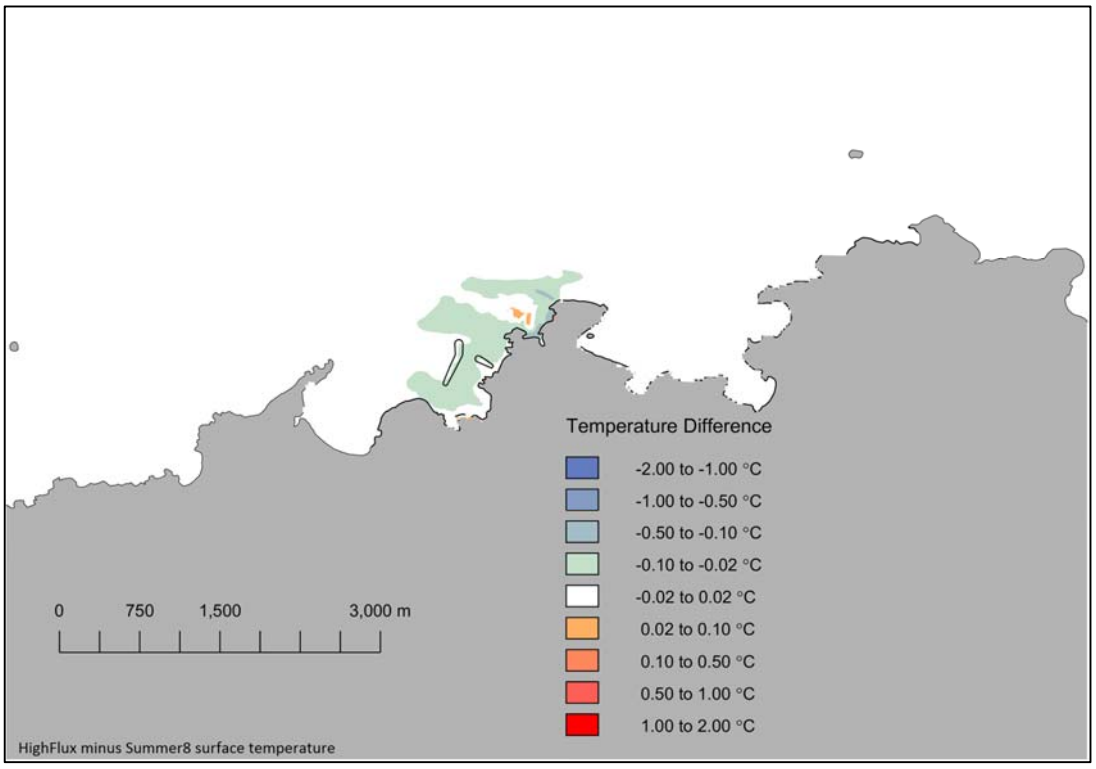

Figure 55 Surface temperature mean difference – High surface heat flux.

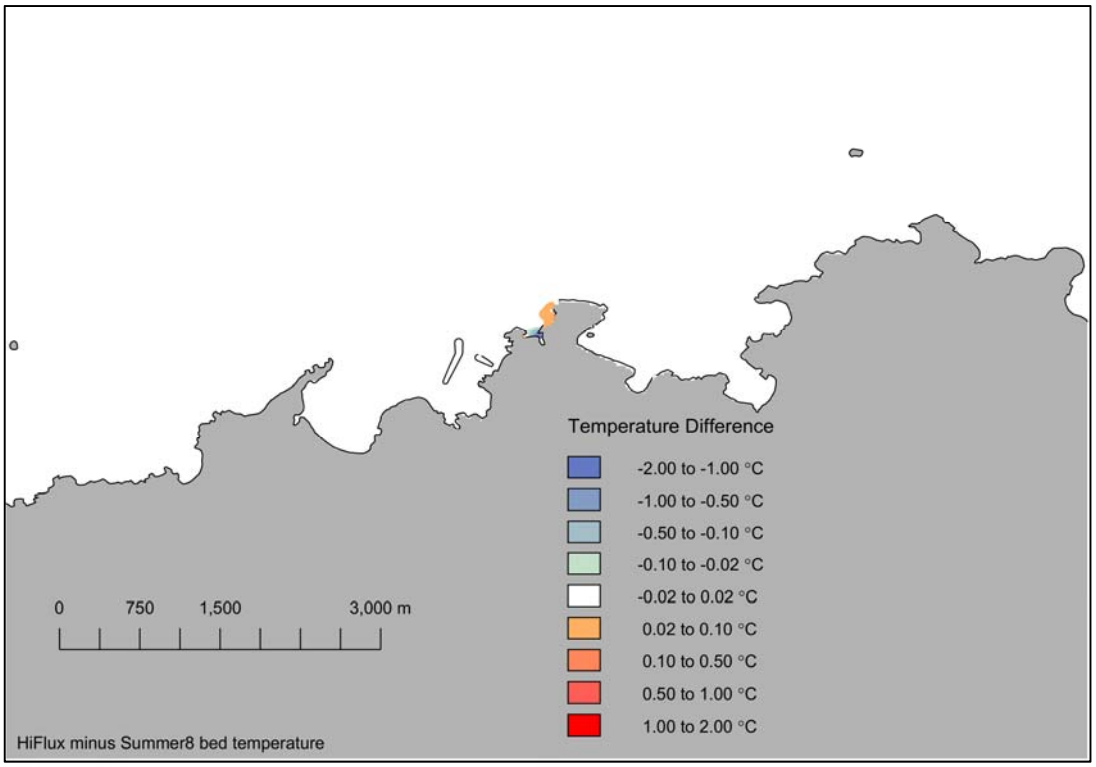

Figure 56 Bed temperature mean difference – High bed heat flux.

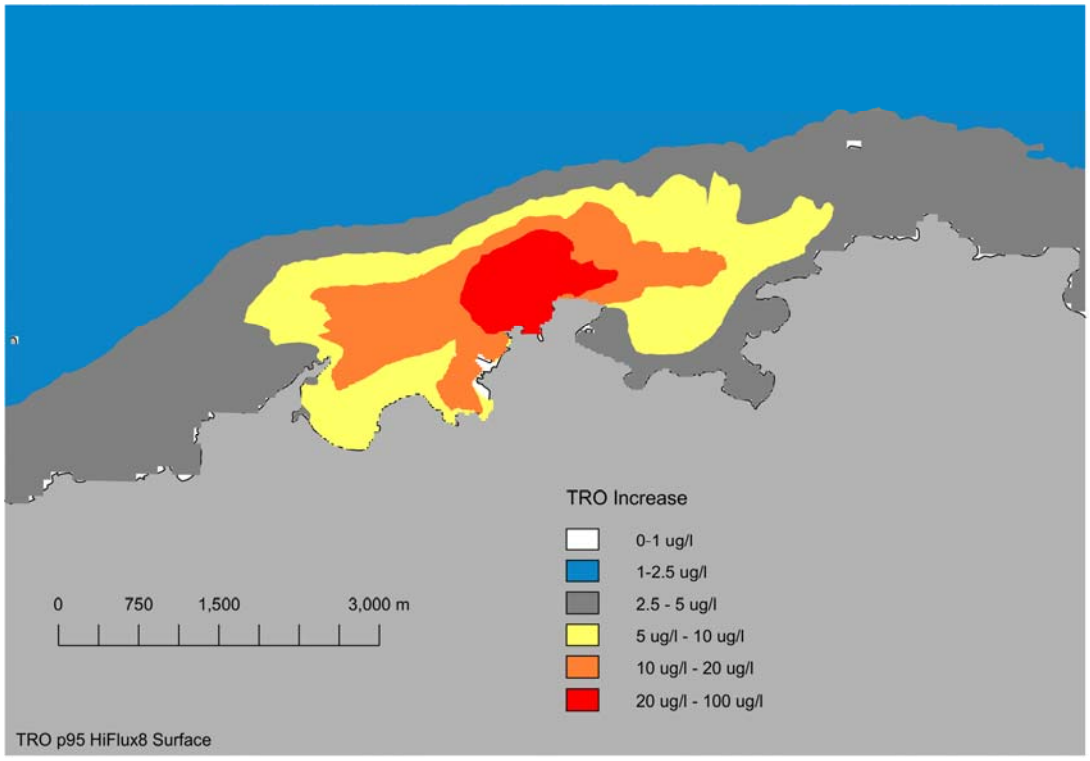

Figure 57 Surface TRO concentration, 95 percentile – High surface heat flux.

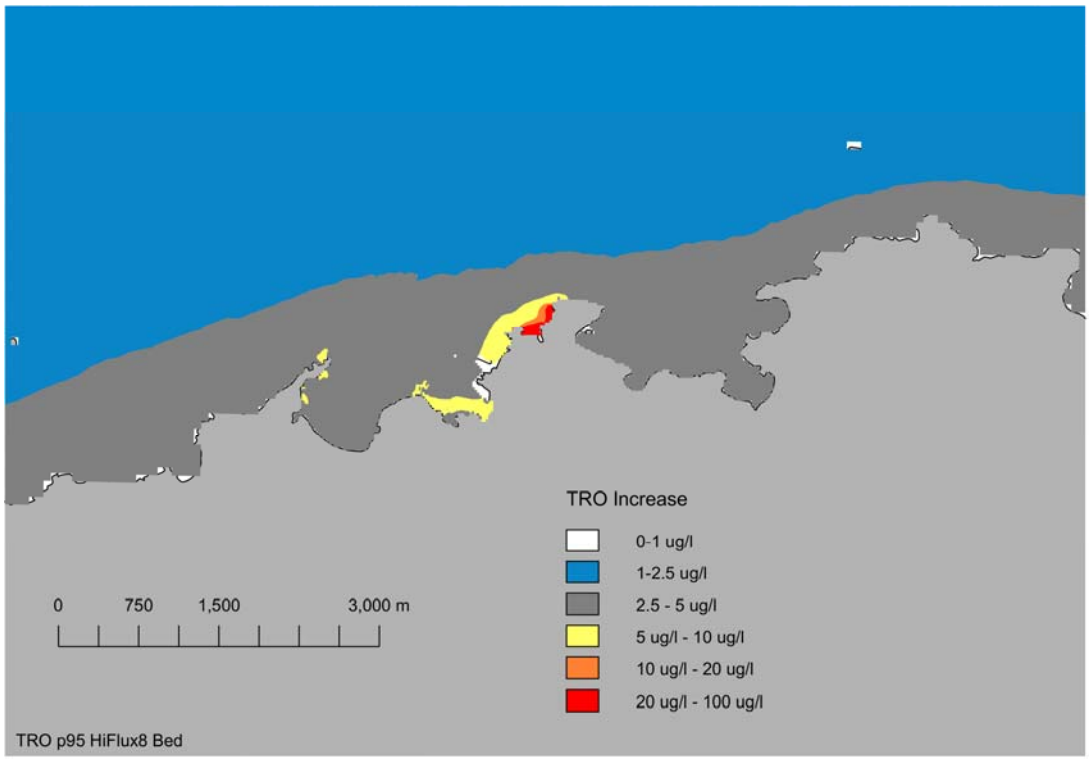

Figure 58 Bed TRO concentration, 95 percentile – High bed heat flux.

6.3 Source Sensitivity

In order to explore the sensitivity of the predicted mid and far field mixing to the representation of the near field, two CORMIX studies have been undertaken. One has a short near field where the CW discharge is introduced into the model at the location of the outfall structure; and the second simulates a situation where the near field is longer, with the discharge representation moved 100 m offshore. These two simulations were selected as boundaries on likely near field conditions (Moores, 2016c and 2016d).

6.3.1 Short Field

To simulate a case with a short, effectively zero length, near field, the Wylfa Newydd CW discharge was introduced into the model at the two cells at the end of the outfall structure.

The model was run for the period 29 June 2011 to 1 August 2011 with the CWS discharge operating to allow the thermal and TRO fields to develop. After the initial warm-up, which used the standard source representation, the model was run for a further period and set to record data at hourly intervals for each model cell. Data at each model cell were stored for a full spring-neap cycle for the period 15 August 2011 to 1 September 2011. The model was run for two weeks with the new two-cell source representation before data were recorded. The warm-up simulation using the standard source representation allowed the long-term thermal field to develop. The two weeks simulated with the modified source representation prior to data being recorded ensured that the influence of the standard representation on the shorter-term thermal field was eliminated.

6.3.1.1 Short Near Field – Temperature Rise

The mixing zone implied by the extent of the 3 °C 98 percentile rise at the surface (Figure 60) has an approximate area of 68.0 hectares. The 2 °C 98 percentile rise at the surface has an approximate area of 167 hectares, while the 1 °C 98 percentile rise has an area of approximately 716 hectares. The size of the 2°C mixing zone at the surface is approximately 75% of that predicted in the base case.

The mixing zone at the bed implied by the extent of the 2 °C 98 percentile rise area (Figure 61) is approximately 2.4 hectares and is limited to an area around the proposed outfall. The mixing zone is reduced compared to the summer base case and does not extend along the western edge of Wylfa Head. The area of the 3 °C and 1 °C 98 percentile rises at the bed are approximately 2.2 hectares and 5.7 hectares respectively.

6.3.1.2 Difference between Short Near Field and Standard Source Representation

The mean difference between the surface and bed temperature predicted using the simple and standard source representation is plotted in Figure 62 and Figure 63.

In general differences are small with values of more than +/- 0.02 °C constrained to an area within 2.5 km of the outfall. To the west of the outfall the surface (Figure 62) is warmer with the simple source by up to 2.5 °C, while to the east, the simple source results in predicted temperatures 2.1 °C cooler than the base case. The simple source is more constrained by Wylfa Head than the standard source representation and this explains the distribution of the differences observed.

In general the difference between the predicted bed temperatures (Figure 63) using the two source representations is small, with values of more than +/- 0.02 °C constrained to an area within 0.5 km of the outfall. Close to the outfall the simple source representation results in predicted temperatures 5 °C higher, while along the western edge of Wylfa Head temperatures are up to 1.4 °C lower. The increase close to the actual outfall at the bed compared to the base case is due to the differences in how the CW is introduced into both models. The simple source uses two cells at the outfall location and assumes a vertically well-mixed discharge. Given the grid size and CW flow higher bed temperatures at the point where the CW is introduced into the model are to be expected with the simple source representation.

6.3.1.3 Short Near Field – TRO Mixing Zone

The mixing zone implied by the extent of the 10 µg/l 95 percentile contour (Figure 64) has an approximate area of 292 hectares.

The area of the bed with a TRO 95 percentile concentration greater than 10 µg/l is limited to the vicinity of the outfall and a strip along the western side of Wylfa Head with an area of approximately 4.1 hectares (Figure 65).

6.3.1.4 Short Near Field – Recirculation

The depth-averaged temperature rise for a model cell (m=141, n=64) approximately in the middle of the CW forebay has been calculated from a simulation of the period from the 15 August 2011 to 1 September 2011.

In Table 9 the mean, 98 percentile and maximum temperature rise above ambient at the intake are listed.

Table 9 Recirculation statistics – Short near field case.

Statistic	Temperature rise above ambient (°C)	Temperature Difference between Short Near Field and Base Case (°C)
Average	0.46	0
98 percentile	0.74	-0.04
Maximum	0.79	-0.05

The average rise above the ambient at the intake for the short near field case is 0.46°C (which is unchanged from the base case). The 98 percentile and maximum rise were slightly less than the base case.

6.3.2 Long Near Field

The hydrodynamic model was set up to simulate the full load CW discharge from Wylfa Newydd over a spring-neap cycle using surface heat flux and TRO decay rates representative of the summer. The simulation includes a conservative tracer in the discharge to allow dilution factors to be calculated if required, for example, by the H1 screening process. The only difference to the summer base case is that the source representation has been moved approximately 100 m offshore. This simulated a longer near-field than was predicted using CORMIX.

The cells used for the summer base case and the source sensitivity study are listed and shown in Table 10 and Figure 59 respectively below.

Table 10 Cells used for the location of the source representation in the base and long near field source sensitivity cases.

Cell No.	Base case	Long Near Field
1	121,34	121,34
2	122,34	130,31
3	123,32	129,30
4	124,32	128,30
5	125,32	127,28
6	124,31	127,30

7	123,31	126,31
8	122,30	123,32

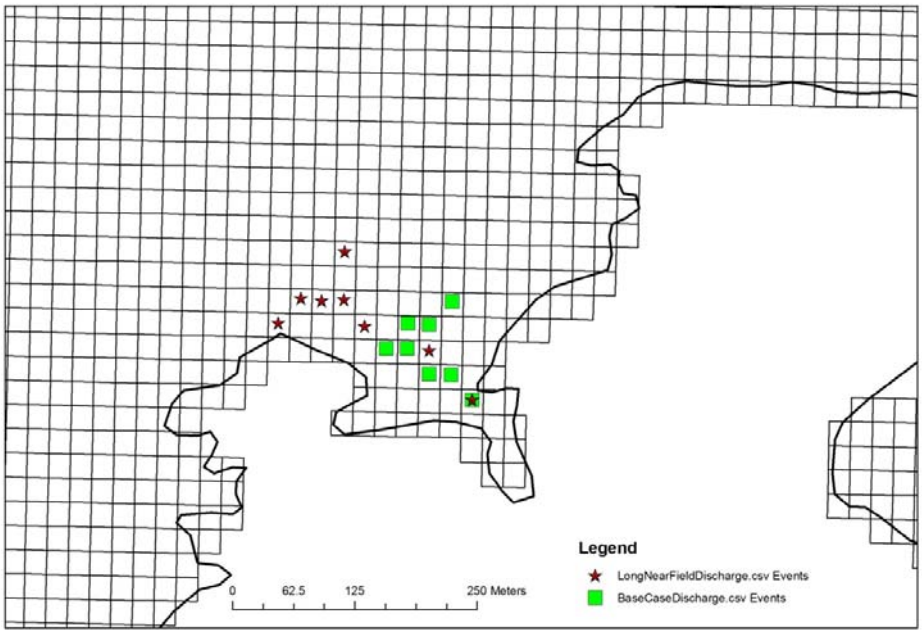

Figure 59 Cells used for the location of the source representation in the base and long near field source sensitivity cases.

6.3.2.1 Long Near Field – Temperature Rise

The mixing zone implied by the extent of the 2 °C 98 percentile rise at the surface (Figure 66) has an approximate area of 211 hectares, which is smaller than that for the base case.

The 3 °C 98 percentile rise at the surface has an approximate area of 79.7 hectares, while the 1 °C 98 percentile rise has an area of approximately 679 hectares.

The mixing zone at the bed implied by the extent of the 2 °C 98 percentile rise area (Figure 67) is approximately 4.8 hectares and is limited to an area around the proposed outfall and along the western edge of Wylfa Head. The area of the 3 °C and 1 °C 98 percentile rise at the bed is approximately 3.1 hectares and 9.0 hectares respectively.

6.3.2.2 Difference between Long Near Field and Standard Source Representation

The mean difference between the surface and bed temperature predicted using the simple and standard source representation is plotted in Figure 68 and Figure 69, respectively. A negative value implies that the long near field source representation results in a lower predicted temperature rise compared to the base case. Differences of more than 0.02 °C are constrained to an area within 2.5 km of the outfall. Temperatures are generally reduced for the long near field case, with largest reductions of more than 2 °C occurring to the north west of the outfall. This general reduction in predicted temperature rise is due to the more offshore source representation mixing the discharge in greater volumes of water, due to the greater depth. Within the inshore areas differences show a small increase in surface temperature rise, although these are typically less than 0.5 °C. These areas of

temperature increase result from the increased advection of the discharge from the more exposed offshore discharge location.

In general there is only a small difference in the mean between the bed temperature rise predicted using the long near field and the base case (Figure 69). In Cemaes and Cemlyn Bays the differences are around 0.02°C and 0.03°C respectively.

In Porth-y-pistyll the long near field simulation predicts a slightly higher bed temperature rise compared to the base case, with the mean difference being up to 0.09°C. West of Wylfa Head the long far field source results in slightly higher temperatures with a mean difference of up to 0.8°C. Near the actual outfall in Porth Wnal the mean difference between the long near field and base case is 1.4°C. This is because in the long near field case the discharge is introduced in cells further offshore reducing temperatures close to the location of the outfall structure, but increasing the potential for advection of the discharge by the tidal flow.

6.3.2.3 Long Near Field – TRO Mixing Zone

The mixing zone implied by the extent of the 10 µg/l 95 percentile contour (Figure 70) has an approximate area of 283 hectares.

The area of the bed with a TRO 95 percentile concentration greater than 10 µg/l is limited to the vicinity of the outfall and a strip along the western side of Wylfa Head with an area of approximately 6.4 hectares (Figure 71).

6.3.2.4 Long Near Field – Recirculation

The depth-averaged temperature rise for a model cell (m=141, n=64) approximately in the middle of the CW forebay has been calculated from a simulation of the period 15 August 2011 to 1 September 2011.

In Table 11 the mean, 98 percentile and maximum temperature rise above ambient at the intake and the temperature difference between the long near field and base case are listed.

Table 11 Recirculation statistics – Long near field.

Statistic	Temperature rise above ambient (°C)	Temperature Difference between Long Near Field and Base Case (°C)
Average	0.52	0.06
98 percentile	0.78	0
Maximum	0.82	-0.02

The long near field sensitivity simulations predict a slightly greater recirculation compared to the base case. The average recirculation in the sensitivity case was 0.52 °C which is 0.06 °C higher than the base case. This can be explained by the closer proximity of the outfall in the sensitivity case to the intake in comparison to the base case.

6.3.3 Summary of Source Sensitivity Studies

In general away from the vicinity of the outfall differences between the predicted surface and bed temperature rise using the two representations are small. The simple two-cell representation for the short near field results in higher predicted temperatures at the surface and bed close to the outfall location and a reduction in the predicted rise along the western edge of Wylfa Head. The difference between the predicted temperature rises reduces with distance from the outfall.

The mixing zone implied by the 2 °C temperature and the 0.01 mg/l 95 percentile TRO contours using the two-cell representation is somewhat smaller than that for the eight-cell representation.

Differences between the base case and a simulation with a long near field are also small. In part differences between the base case and long near field will be due to the further offshore source representation mixing the discharge in greater volumes of water, due to the greater depth. Closer to the outfall itself the differences are greater, with mean difference between the long near field representation and base case being more than 2 °C. Either side of the area of maximum negative difference there are two areas where the longer near field results in an increased surface temperature rise compared to the base case of up to 0.5 °C. These areas result from the enhanced advection of the discharge from the more exposed outfall location.

Overall the predicted temperature and TRO mixing zones are fairly insensitive to the source representation with differences of more than 0.02 °C constrained to within 2.5 km of the outfall location.

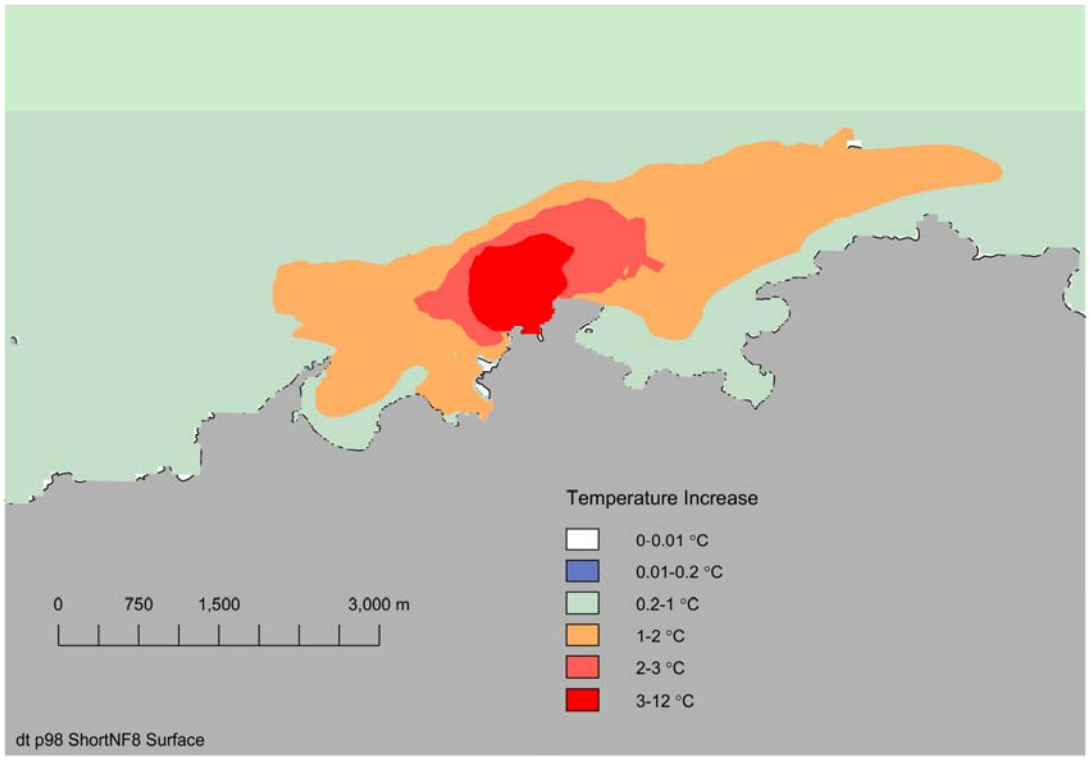

Figure 60 Surface temperature, 98 percentile – Short near field case.

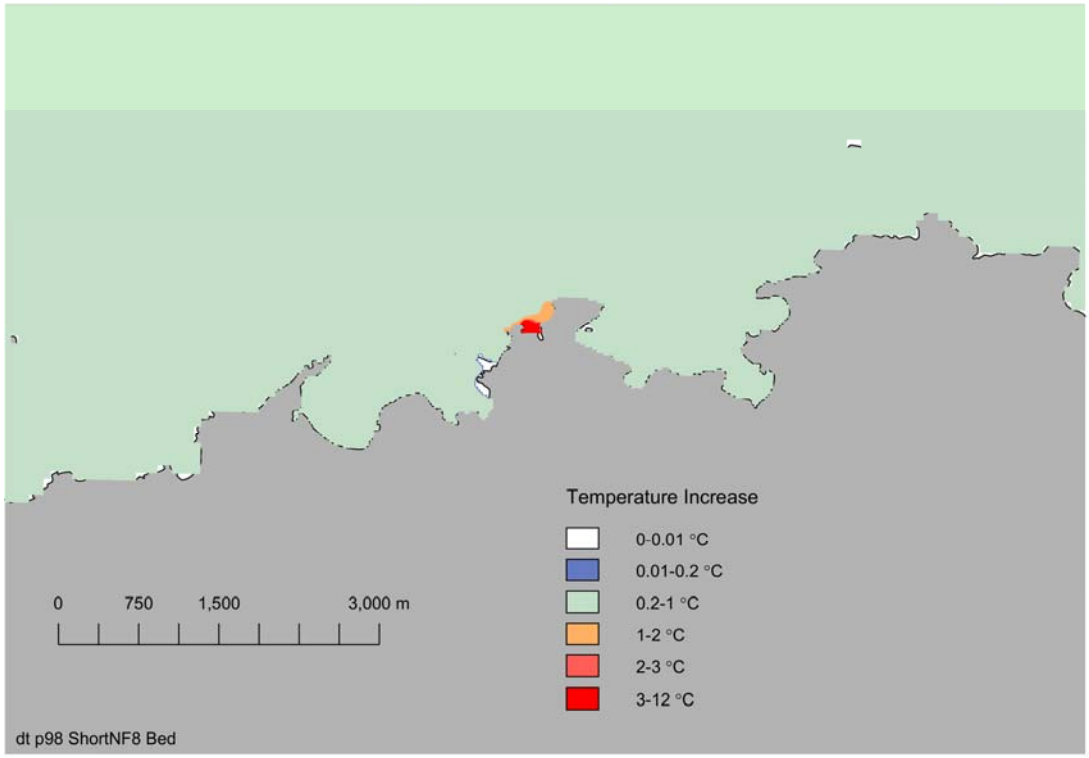

Figure 61 Bed temperature, 98 percentile – Short near field case.

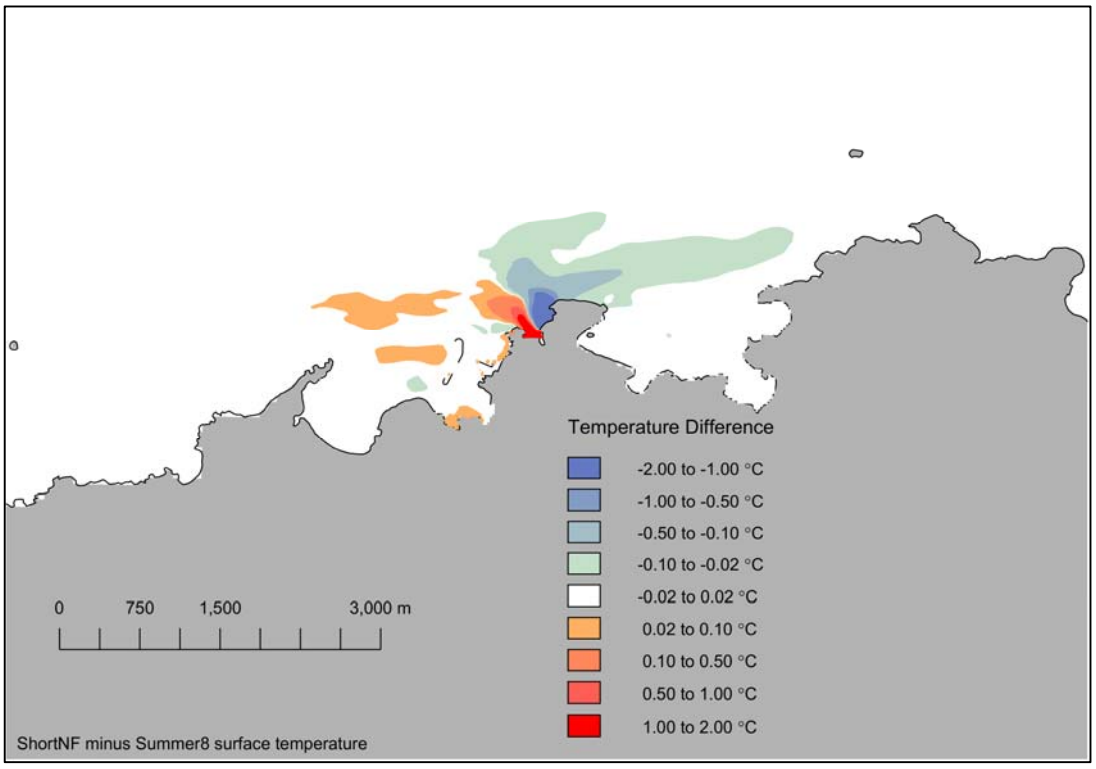

Figure 62 Surface temperature mean difference – Short near field and standard source.

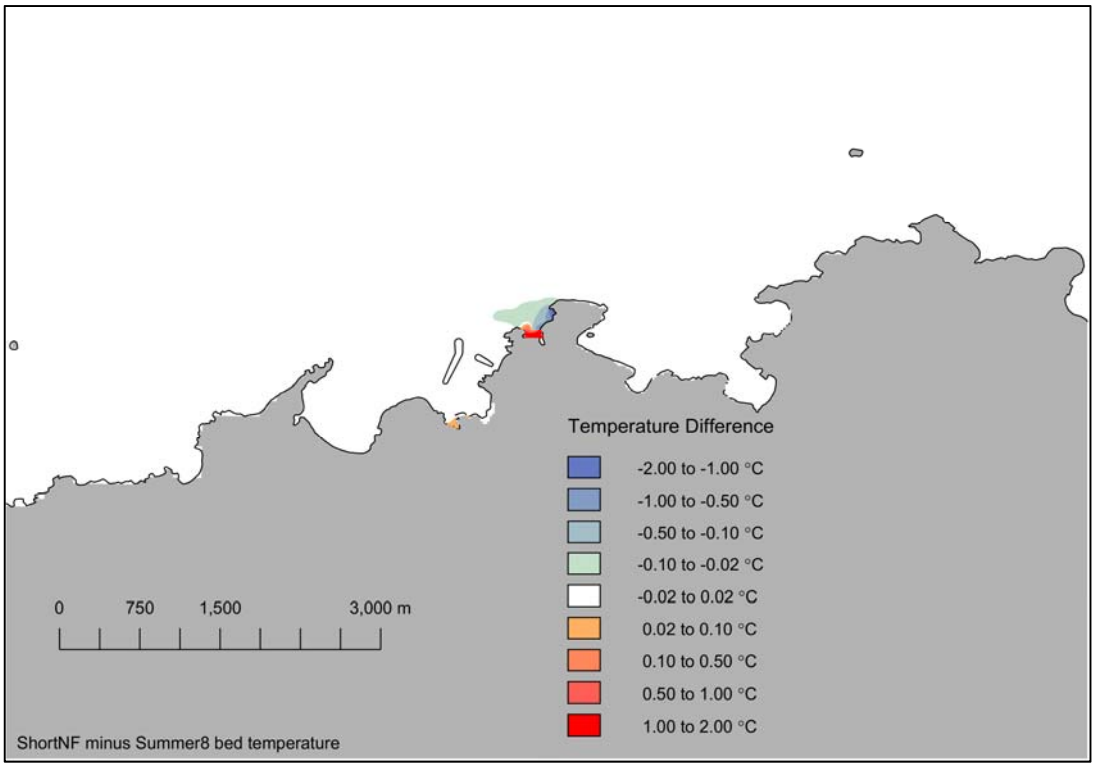

Figure 63 Bed temperature mean difference – Short near field and standard source.

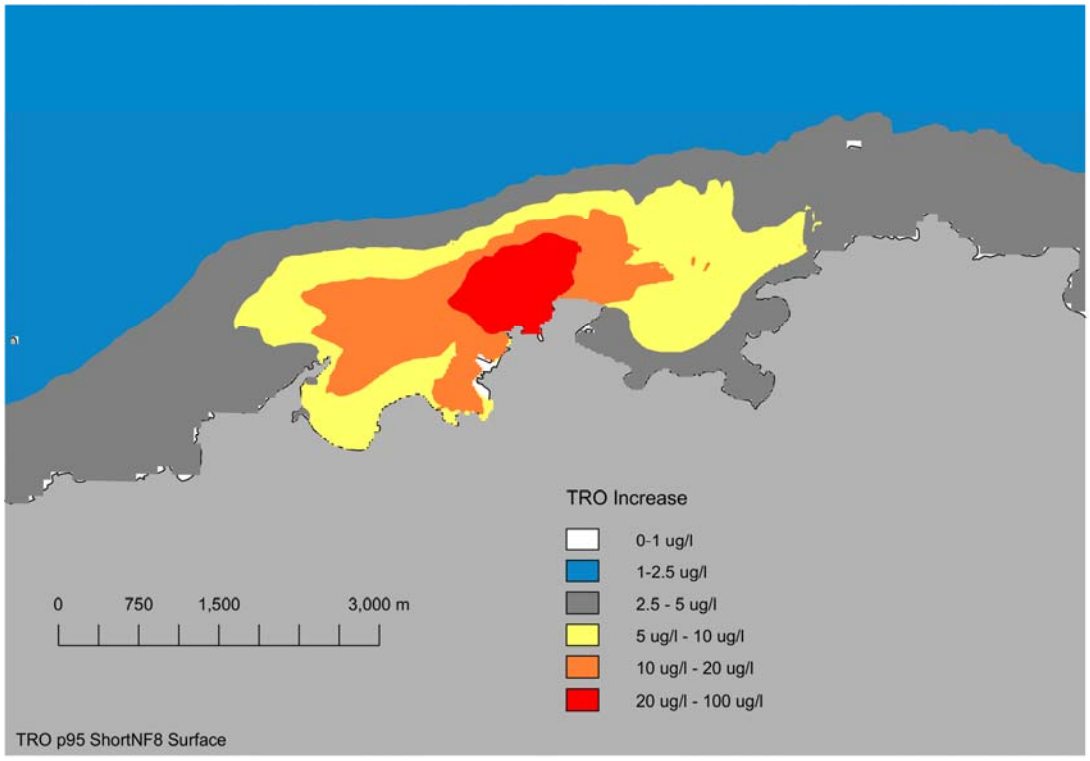

Figure 64 Surface TRO concentration, 95 percentile – Short near field case.

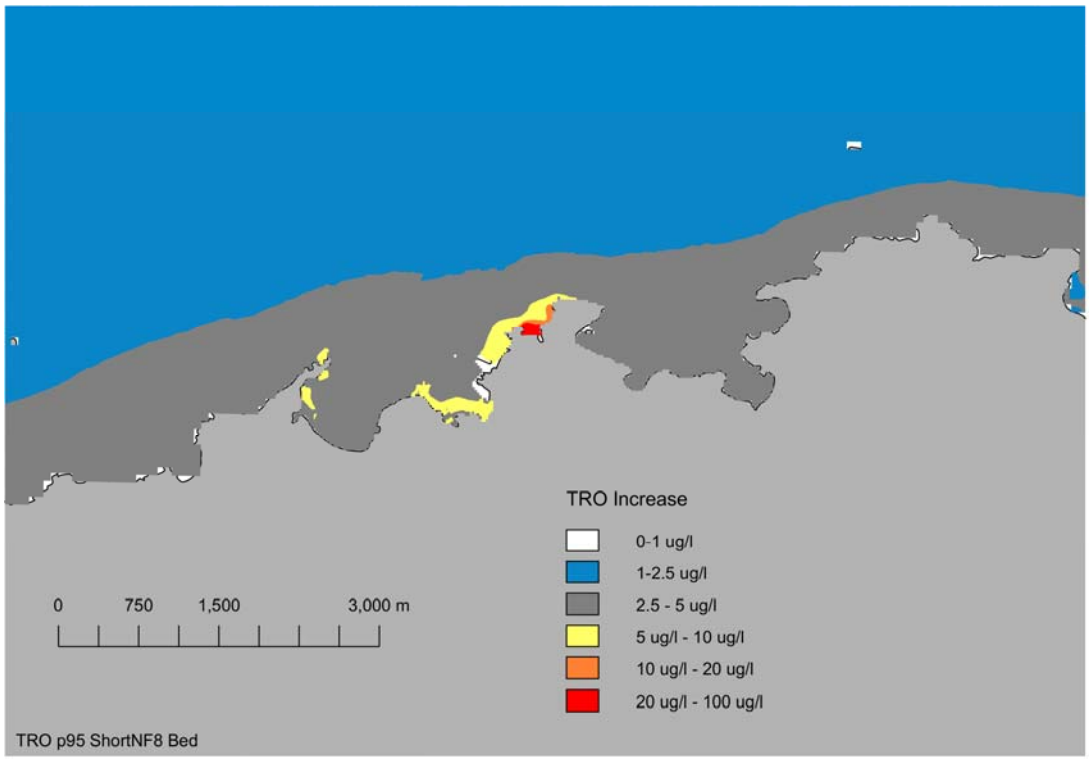

Figure 65 Bed TRO concentration, 95 percentile – Short near field case.

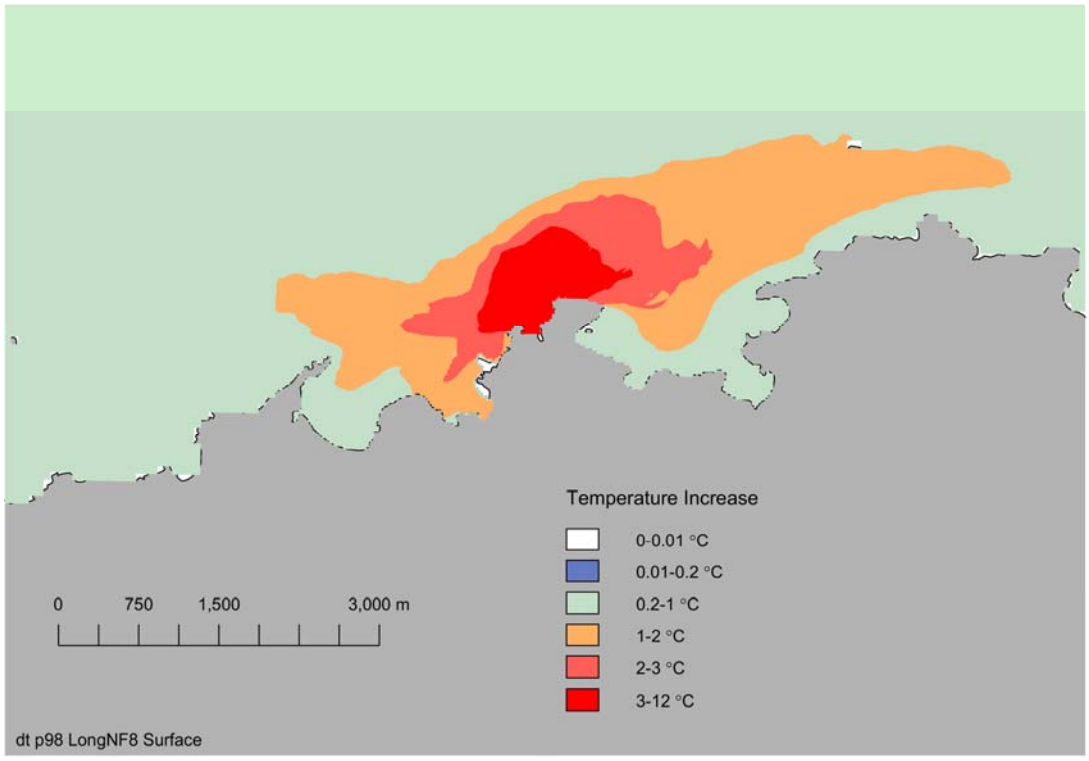

Figure 66 Surface temperature 98 percentile – Long near field case.

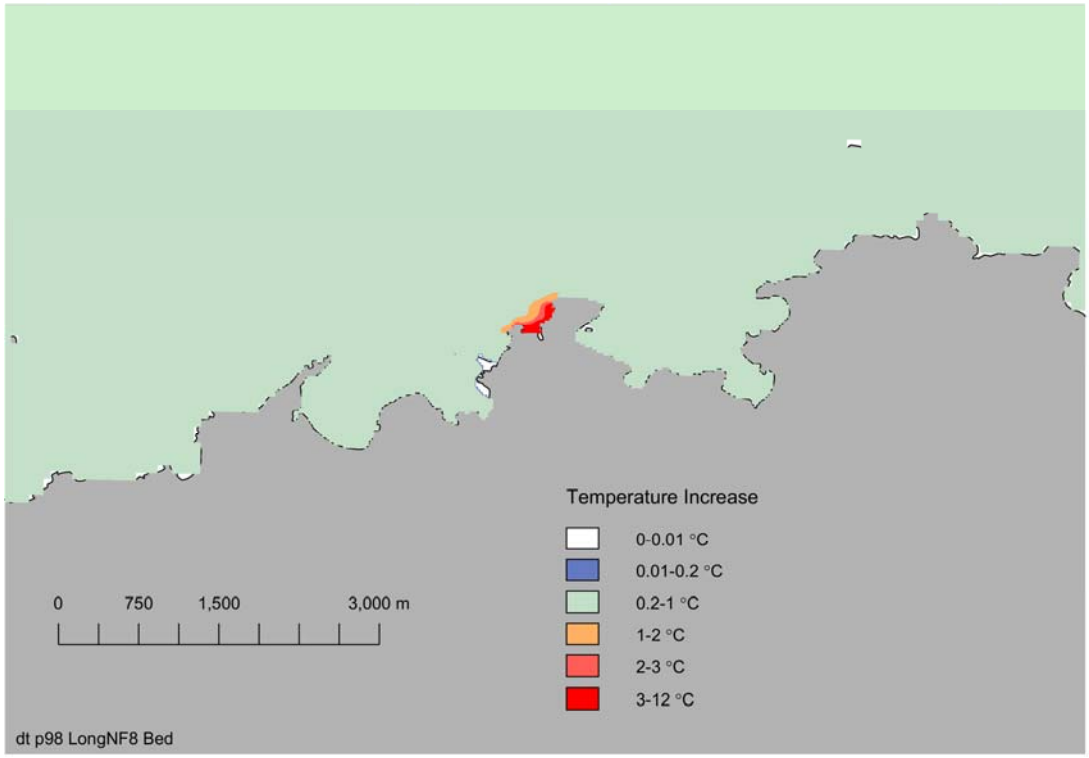

Figure 67 Bed temperature, 98 percentile – Long near field case.

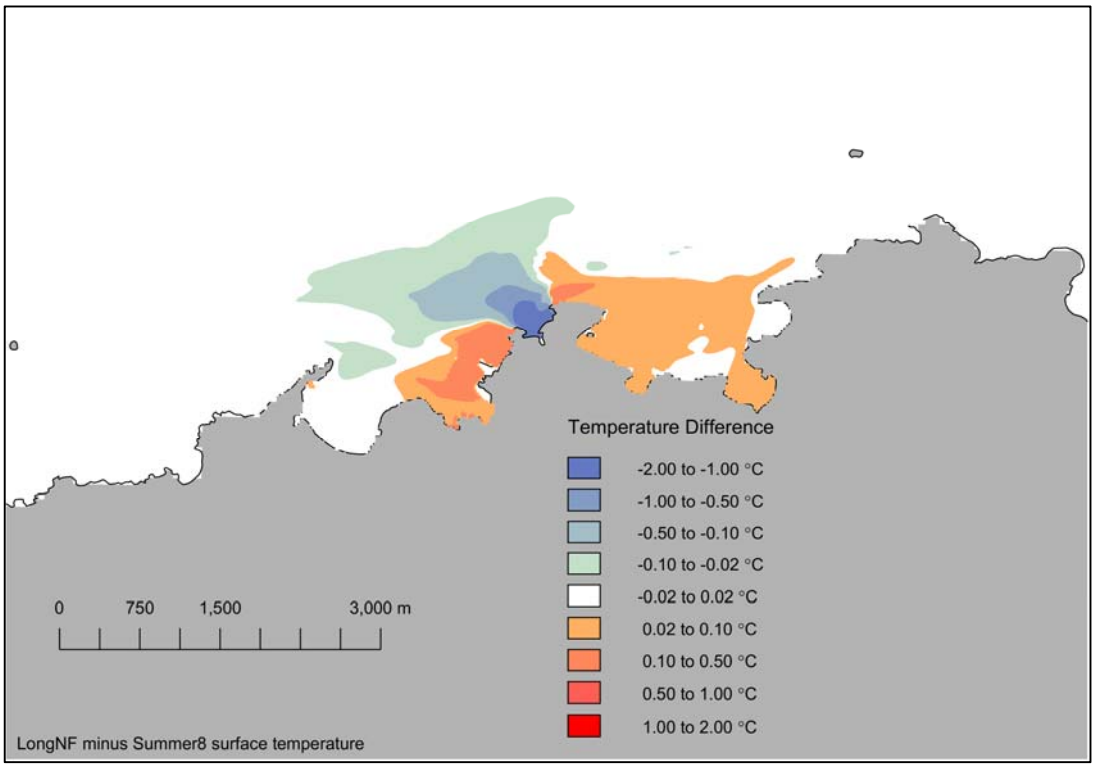

Figure 68 Surface temperature mean difference – Long near field and base case.

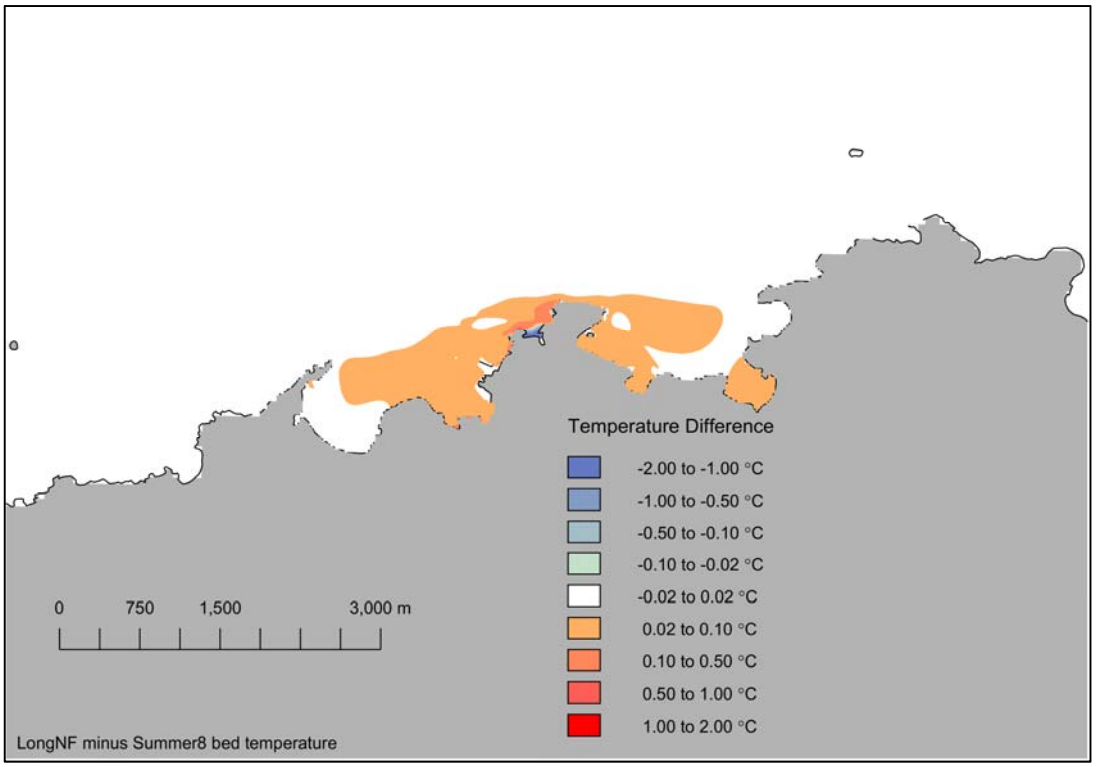

Figure 69 Bed temperature mean difference – Long near field and base case.

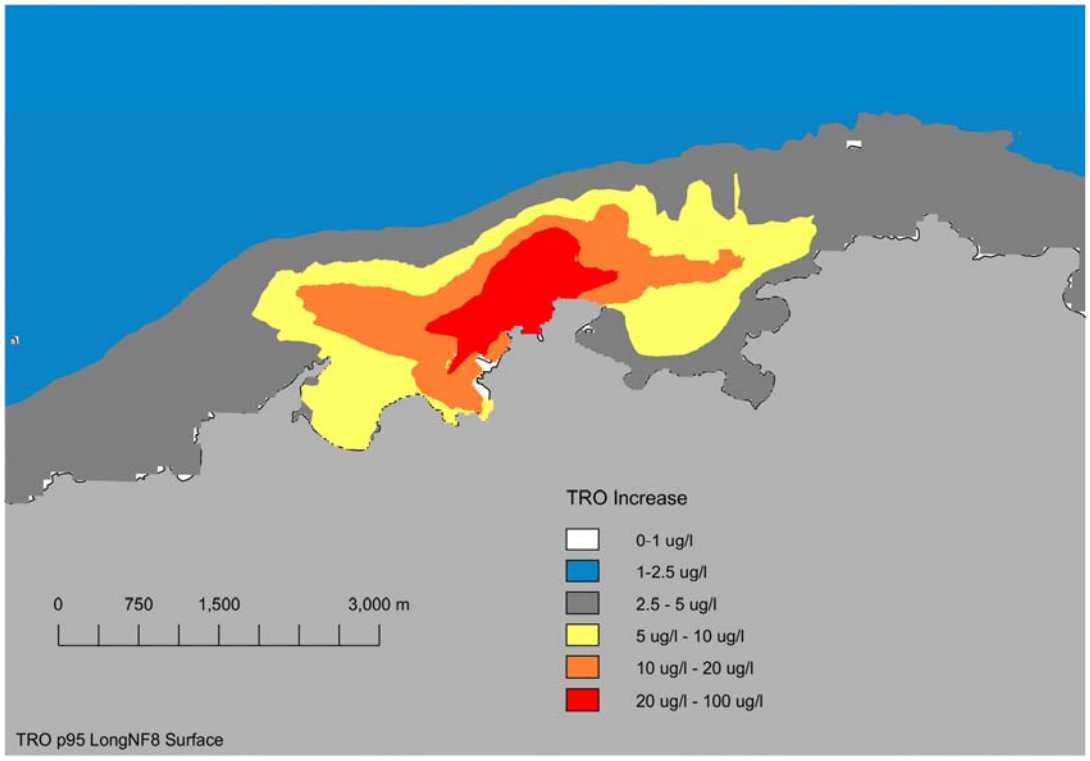

Figure 70 Surface TRO concentration, 95 percentile – Long near field case.

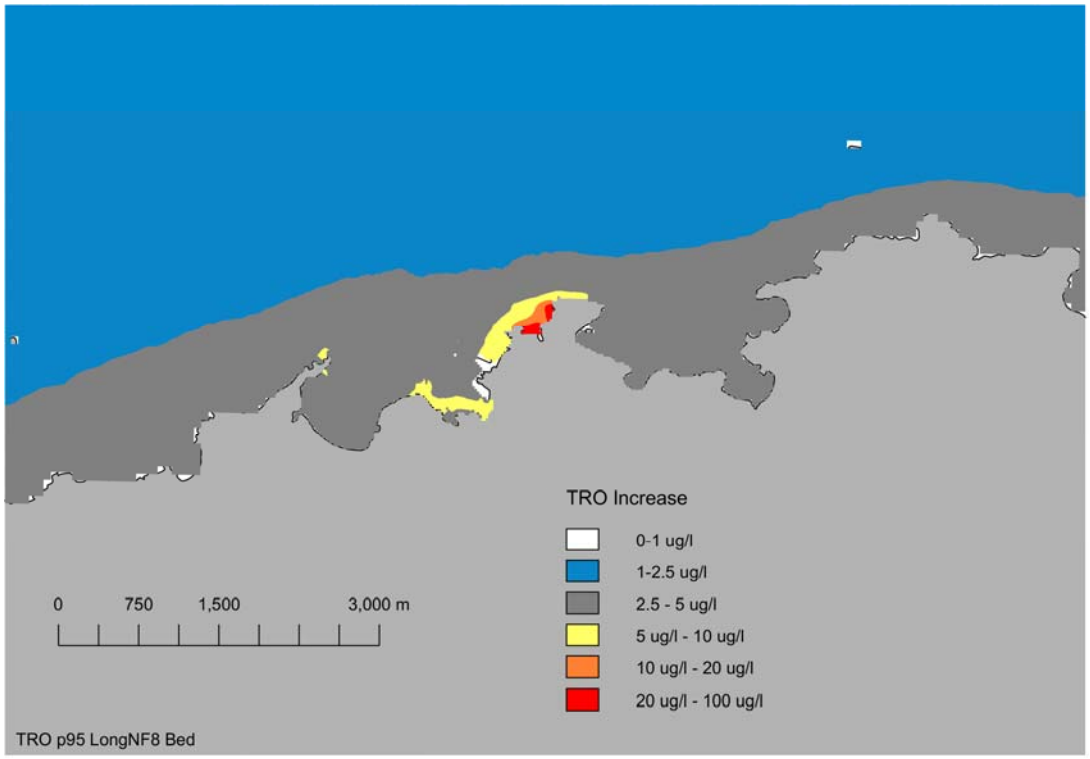

Figure 71 Bed TRO concentration, 95 percentile – Long near field case.

6.4 Wind Sensitivity studies

A number of model simulations have been undertaken to study the influence of wind on the predicted temperature rise and TRO concentrations. The following sections provide background information on the wind climate of the study area and the sensitivity studies undertaken.

Of the two data sets available for use in modelling studies, the RAF Valley data set is the most appropriate for the hydrodynamic modelling as it is a good representation of the prevailing conditions over the sea. An alternative data set that modelled conditions for Wylfa Newydd that were created for local air quality modelling purposes is discussed below.

The most common direction in the 2003-2012 RAF Valley wind data is from the south-southwest (see Figure 72 below) which for RAF Valley is from the sea. The least common wind direction for the 2003 to 2012 data plotted in Figure 72 is from the southeast.

The strength and duration of the wind will also determine the potential influence on the CW plume. In Figure 73 the average wind speed in each of the 10° bins[5] has been plotted for the RAF Valley 2003-2012 data set. The strongest winds are those from the south-southwest. The average wind speed from this direction is 8.8 m/s.

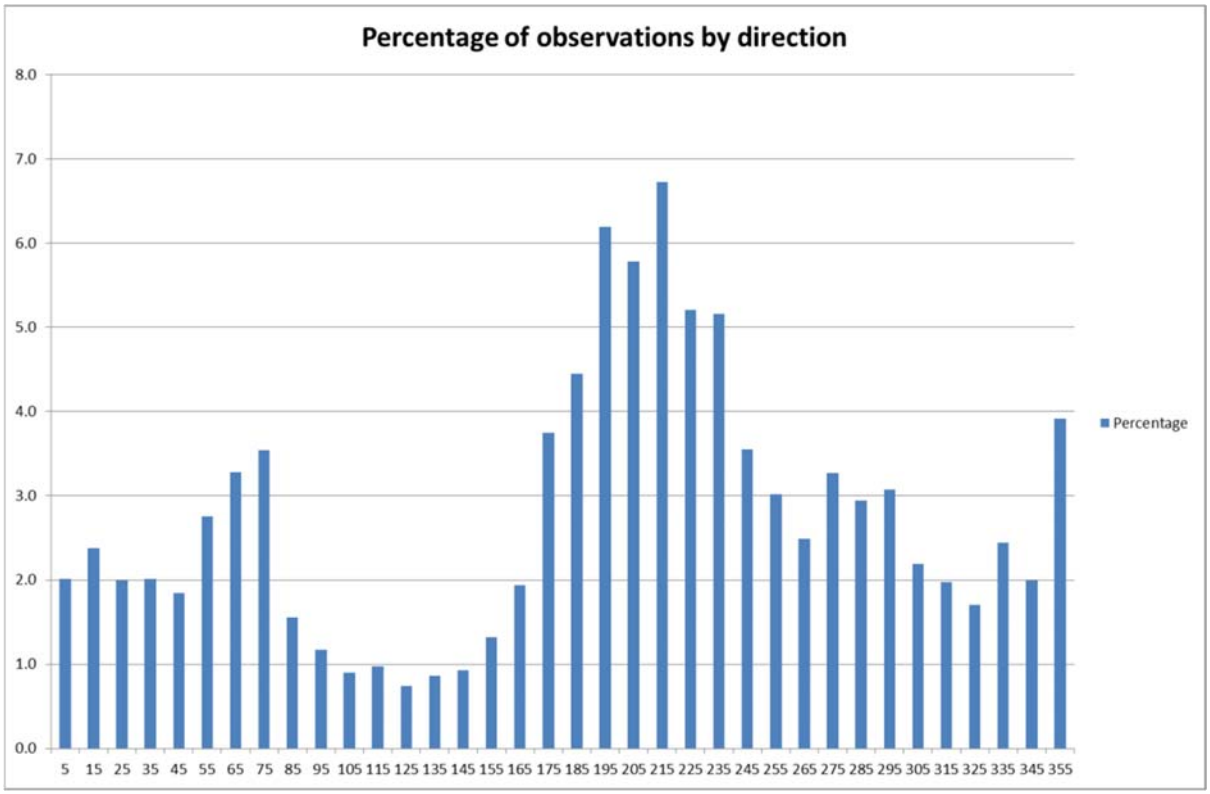

Figure 72 Percentage of observations (y axis) by direction (x axis) (RAF Valley Data, 2003-2012).

[5] Bins are categories for ranges of numbers

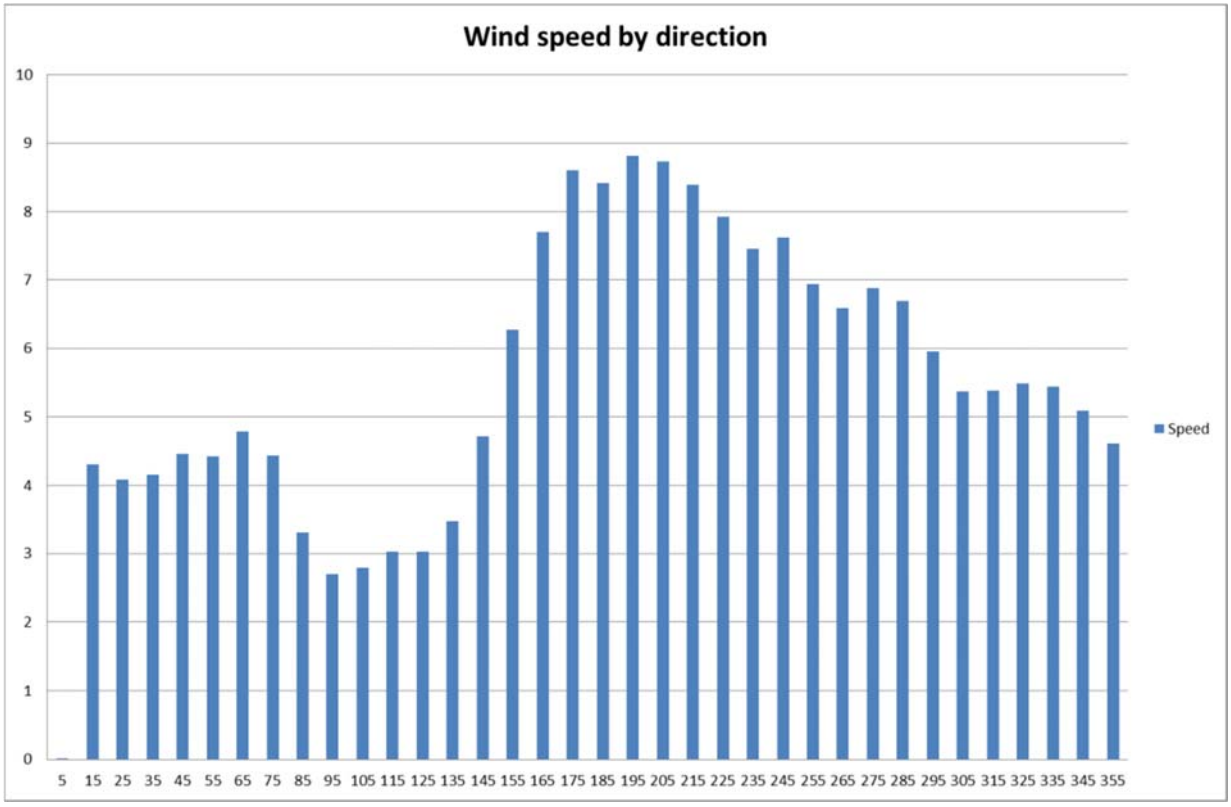

Figure 73 Wind speed (m/s) (y axis) by direction (x axis) (RAF Valley Data, 2003-2012).

Broadly, winds from the north will have the potential to move the CW plume onshore, while winds from the south will have the potential to move the plume offshore. Percentage of occurrences, average and 95 percentile wind speeds over a 90° sector are detailed in Table 12.

Table 12 Wind statistics 2003-2012 by sector (RAF Valley Data, 2003-2012).

Direction	Percentage Of Hours	Average (m/s)	95 percentile (m/s)
North	18.3	4.7	9.8
East	15.8	4.0	8.7
South	36.3	8.3	14.4
West	27.7	6.7	12.3

Note: The percentage of hours does not include those hours when no wind was recorded and the sum is therefore less than 100 %.

In addition to the wind speed the duration of wind events will also influence the potential for wind in a given sector to move the plume. Typically the probability of a wind from a given direction reduces with time. Long duration winds are relatively rare with short duration directional periods being the most common.

6.5 Simulation with a constant wind from the south

The model was run in excess temperature mode with a wind speed of 8.3 m/s which is the mean measured at RAF valley from the southern sector. The surface heat flux was 21.7 W/m^2/K, again representative of the average for the season and in accordance with other summer simulations.

The TRO concentration of the discharge was set to 0.1 mg/l over the intake. The TRO decay rate was set to 10.08 per day as with the summer base case

The model was run for the period 29 June 2011 to 1 August 2011 with the CW discharge operating to allow the thermal and TRO fields to develop. After this initial warm-up period the model was run for a further period and set to record data at hourly intervals for each model cell. Data at each model cell were stored for a full spring-neap cycle for the period 15 August 2011 to 1 September 2011.

6.5.1 South Wind – Temperature Rise

The mixing zone implied by the extent of the 3 °C 98 percentile rise at the surface (Figure 74) has an approximate area of 25.6 hectares, while the 2 °C 98 percentile rise has an area of approximately 47.8 hectares. The 3 °C 98 percentile rise at the surface has an approximate area of 155 hectares. The size of the mixing zone is reduced compared to the base (no wind stress) case.

The mixing zone implied by the extent of the 3 °C 98 percentile rise at the bed (Figure 75) is limited to an area around the proposed outfall and along the western edge of Wylfa Head, with an area of approximately 2.9 hectares. The area of the 2 °C 98 percentile rise at the bed has an area of approximately 3.7 hectares while the 1 °C 98 percentile rise area is approximately 5.9 hectares.

6.5.2 South Wind – TRO

The mixing zone implied by the extent of the 10 µg/l 95 percentile contour (Figure 76) has an approximate area of 80.0 hectares. The mixing zone is reduced compared to the base (no wind stress) case.

The area of the bed with a TRO 95 percentile concentration greater than 10 µg/l is limited to the vicinity of the outfall and a strip along the western side of Wylfa Head with an area of approximately 4.8 hectares (Figure 77).

6.5.3 South Wind – Recirculation

The depth-averaged temperature rise for a model cell (m=141, n=64) approximately in the middle of the CW forebay has been calculated from a simulation of the period 15 August 2011 to 1 September 2011.

In Table 13 the mean, 98 percentile and maximum temperature rise above ambient at the intake are listed.

Table 13 Recirculation statistics – south wind case.

Statistic	Temperature rise above ambient (°C)	Difference between south wind case and base case (°C)
Average	0.31	–0.15
98 percentile	0.40	–0.38
Maximum	0.42	–0.42

The average temperature rise above ambient at the intake for the south wind case is 0.31 °C (0.15 °C less than the no wind case). The 98 percentile and maximum rise were also less than the no wind stress case by 0.38 and 0.42 °C respectively.

Overall, the influence of a continuous wind from the south with a speed equal to the average from the southern sector has been to reduce both recirculation and the size of the temperature and TRO mixing zones at the surface. This is because the wind is tending to move the plume out into the area of faster currents north of Wylfa Head where mixing is stronger...

6.6 Simulation with a constant wind from the west

The model was run in excess temperature mode with a wind speed of 6.7 m/s which is the mean measured at RAF valley from the western sector. The surface heat flux was 21.7 W/m^2/K again representative of the average for the season. The TRO decay rate was set to 10.08 per day.

The model was run for the period 29 June 2011 to 1 August 2011 with the CW discharge operating to allow the thermal and TRO fields to develop. After this initial warm-up period the model was run for a further period and set to record data at hourly intervals for each model cell. Data at each model cell were stored for a full spring-neap cycle for the period 15 August 2011 to 1 September 2011.

6.6.1 West Wind – Temperature Rise

The mixing zone implied by the extent of the 3 °C 98 percentile rise at the surface (Figure 78) has an approximate area of 50.7 hectares, while the 2 °C 98 percentile rise has an area of approximately 97.8 hectares. The 1 °C 98 percentile rise at the surface has an approximate area of 311 hectares. The mixing zone is reduced compared to the base (no wind stress) case.

The mixing zone implied by the extent of the 3 °C 98 percentile rise at the bed (Figure 79) is limited to an area around the proposed outfall and along the western edge of Wylfa Head, with an area of 3.3 hectares. The area of the 2 °C 98 percentile rise at the bed has an area of approximately 4.2 hectares while the 1 °C rise area is approximately 11.7 hectares.

6.6.2 West Wind – TRO

The mixing zone implied by the extent of the 10 µg/l 95 percentile contour (Figure 80) has an approximate area of 139 hectares. The mixing zone is reduced compared to the base (no wind stress) case.

The area of the bed with a TRO 95 percentile concentration greater than 10 µg/l is limited to the vicinity of the outfall and a strip along the western side of Wylfa Head with an area of approximately 6.6 hectares (Figure 81).

6.6.3 West Wind – Recirculation

The depth-averaged temperature rise for a model cell (m=141, n=64) approximately in the middle of the CW forebay has been calculated from a simulation of the period 15 August 2011 to 1 September 2011.

In Table 14 the mean, 98 percentile and maximum temperature rise above ambient at the intake are listed.

Table 14 Recirculation statistics - West wind case.

Statistic	Temperature rise above ambient (°C)	Difference between west wind case and base case (°C)
Average	0.46	0
98 percentile	0.60	-0.18
Maximum	0.65	-0.19

The average temperature rise above ambient at the intake for the west wind case is 0.46 °C (the same as the no wind stress case). The 98 percentile and maximum temperature rises were less than the no wind stress case (by 0.18 °C and 0.19 °C, respectively)

Overall the imposition of a constant wind from the west reduced the size of the mixing zone and the maximum recirculation. The average recirculation was unchanged.

6.7 Simulation with a constant wind from the north

The model was run in excess temperature mode with a wind speed of 4.7 m/s which is the mean measured at RAF Valley from the northern sector. The surface heat flux was 21.7 W/m^2/K again representative of the average for the season. The TRO decay rate was set to 10.08 per day.

The model was run for the period 29 June 2011 to 1 August 2011 with the CW discharge operating to allow the thermal and TRO fields to develop. After this initial warm-up period the model was run for a further period and set to record data at hourly intervals for each model cell. Data at each model cell was stored for a full spring-neap cycle for the period 15 August 2011 to 1 September 2011.

6.7.1 North Wind – Temperature Rise

The mixing zone implied by the extent of the 3 °C 98 percentile rise at the surface (Figure 82) has an approximate area of 103 hectares, while the 2 °C 98 percentile rise has an area of approximately 225 hectares. The 1 °C 98 percentile rise at the surface has an approximate area of approximately 700 hectares. The mixing zone implied by the extent of the 3 °C contour is larger than for the no wind (base) case, while the mixing zone implied by the extent of the 2 °C and 1 °C contours are smaller than that for the no wind base case.

The mixing zone implied by the extent of the 3 °C 98 percentile rise at the bed (Figure 83) is limited to an area around the proposed outfall and along the western edge of Wylfa Head, covering an area of approximately 0.4 hectares. The area of the 2 °C 98 percentile rise at the bed has an area of approximately 0.7 hectares while the 1 °C rise area is approximately 2.7 hectares. The mixing zones at the bed are smaller than for the no wind base case.

6.7.2 North Wind – TRO

The mixing zone implied by the extent of the 10 µg/l 95 percentile contour (Figure 84) has an approximate area of 239 hectares. The mixing zone at the surface is smaller than that for the no wind base case.

The area of the bed with a TRO 95 percentile concentration greater than 10 µg/l is limited to the vicinity of the outfall and a strip along the western side of Wylfa Head with an area of approximately 7.7 hectares (Figure 85). The mixing zone at the bed is larger than that for the no wind base case.

6.7.3 North Wind – Recirculation

The depth-averaged temperature rise for a model cell (m=141, n=64) approximately in the middle of the CW forebay has been calculated from a simulation of the period 15 August 2011 to 1 September 2011.

In Table 15 the mean, 98 percentile and maximum temperature rise above ambient at the intake and the difference between the north wind and base case are listed.

Table 15 Recirculation statistics – north wind case.

Statistic	Temperature rise above ambient (°C)	Difference between north wind case and base case (°C)
Average	0.63	0.17
98 percentile	1.13	0.35
Maximum	1.28	0.44

The average temperature rise above ambient at the intake for the north wind case is 0.63 °C (0.17 °C greater than the no wind stress case). The 98 percentile and maximum rise were also larger than the no wind stress case (by 0.35 °C and 0.44 °C respectively)

Overall the imposition of wind stress from a continuous wind from the north with a speed equal to the average for that sector acts to drive the plume onshore, reducing plume advection away from the area. This results in an increase in the size of the surface mixing zone above 3 °C and increases recirculation.

6.8 Simulation with a constant wind from the east

The model was run in excess temperature mode with a wind speed of 4.0 m/s which is the mean measured at RAF valley from the southern sector. The surface heat flux was 21.7 W/m^2/K again representative of the average for the season. The TRO decay rate was set to 10.08 per day.

The model was run for the period 29 June 2011 to 1 August 2011 with the CW discharge operating to allow the thermal and TRO fields to develop. After this initial warm-up period the model was run for a further period and set to record data at hourly intervals for each model cell. Data at each model cell were stored for a full spring-neap cycle for the period 15 August 2011 to 1 September 2011.

6.8.1 East Wind – Temperature Rise

The mixing zone implied by the extent of the 3 °C 98 percentile rise at the surface (Figure 86) has an approximate area of 61 hectares, while the 2 °C 98 percentile rise has an area of approximately 154 hectares. The 1 °C 98 percentile rise at the surface has an approximate area of 545 hectares. The size of the mixing zone is reduced compared to the base (no wind stress) case.

The mixing zone implied by the extent of the 3 °C 98 percentile rise at the bed (Figure 87) is limited to an area around the proposed outfall and along the western edge of Wylfa Head, covering an area of approximately 2.8 hectares. The area of the 2 °C 98 percentile rise at the bed has an area of approximately 3.7 hectares while the 2 °C rise area is approximately 6.3 hectares.

6.8.2 East Wind – TRO

The mixing zone implied by the extent of the 10 µg/l 95 percentile contour (Figure 88) has an approximate area of 213 hectares. The mixing zone is reduced compared to the base (no wind stress) case.

The area of the bed with a TRO 95 percentile concentration greater than 10 µg/l is limited to the vicinity of the outfall and a strip along the western side of Wylfa Head with an area of approximately 4.8 hectares (Figure 89).

6.8.3 East Wind – Recirculation

The depth-averaged temperature rise for a model cell (m=141, n=64) approximately in the middle of the CW forebay has been calculated from a simulation of the period 15 August 2011 to 1 September 2011.

In Table 16 the mean, 98 percentile and maximum temperature rise above ambient at the intake and the difference between the east wind and base case are listed.

Table 16 Recirculation statistics – east wind case.

Statistic	Temperature rise above ambient (°C)	Difference between east wind case and base case (°C)
Average	0.44	-0.02
98 percentile	0.70	-0.08
Maximum	0.74	-0.10

The average temperature rise above ambient at the intake for the eastern wind case is 0.44 °C (a reduction of 0.02 °C compared to the no wind stress case). The 98 percentile and maximum rise were both slightly less than the no wind stress case (by 0.08 °C and 0.10 °C, respectively).

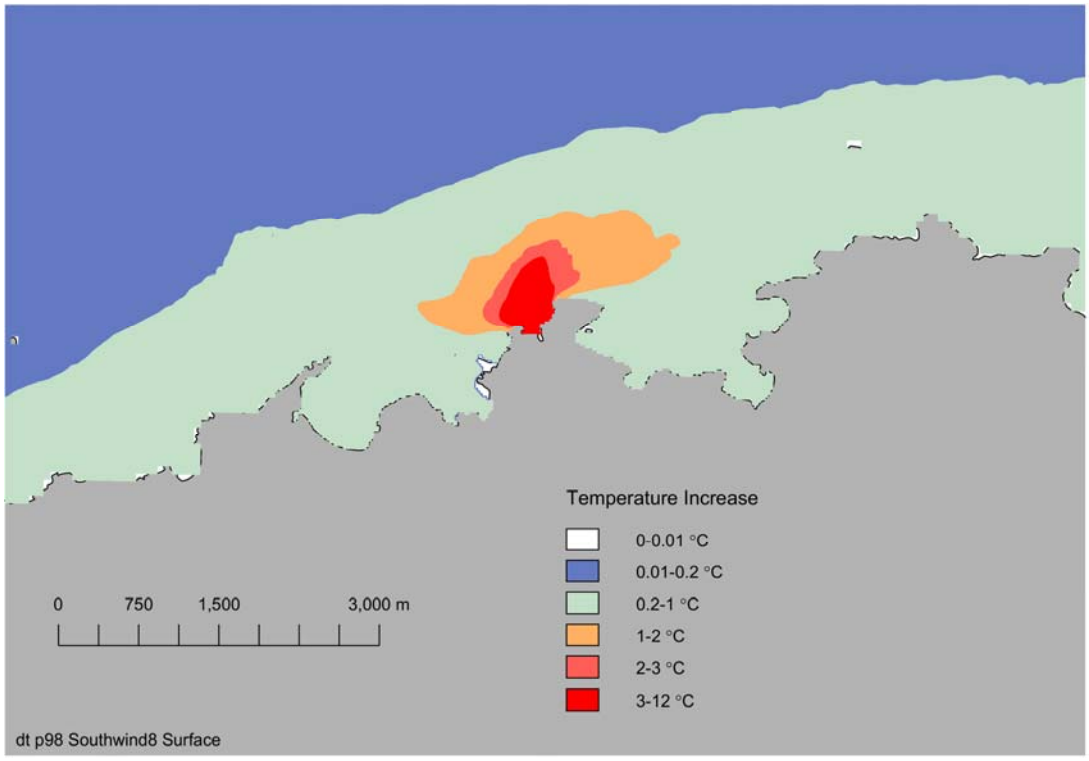

Figure 74 Surface temperature, 98 percentile – South wind case.

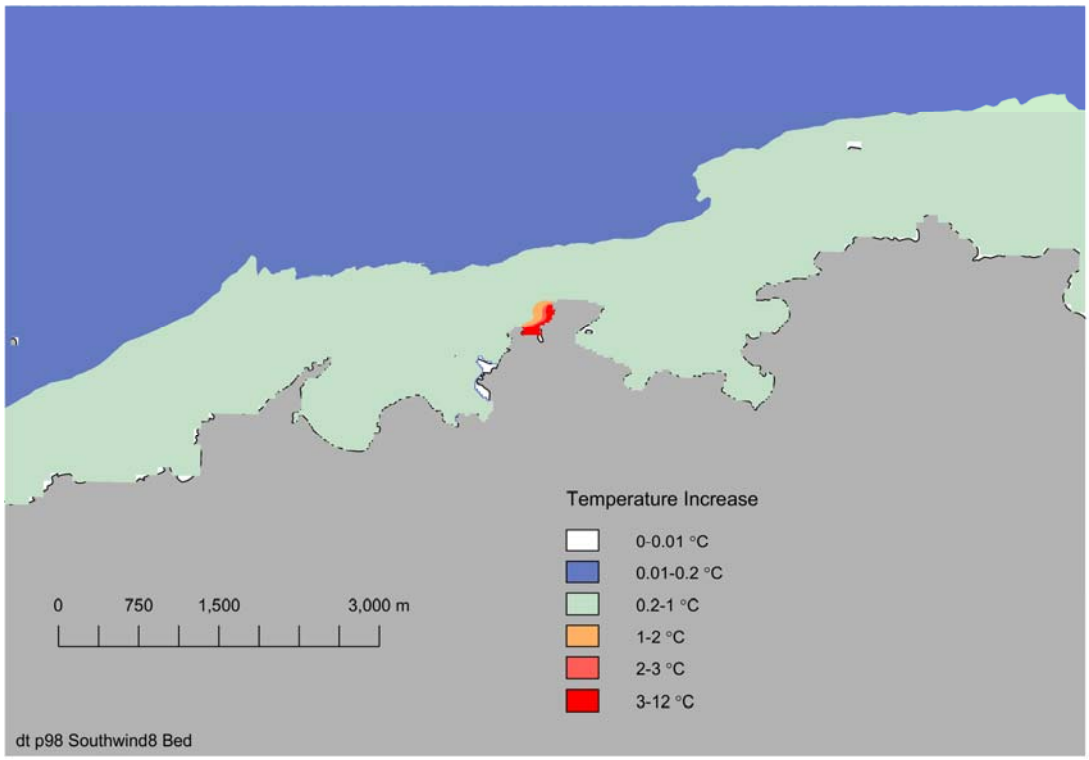

Figure 75 Bed temperature, 98 percentile– South wind case.

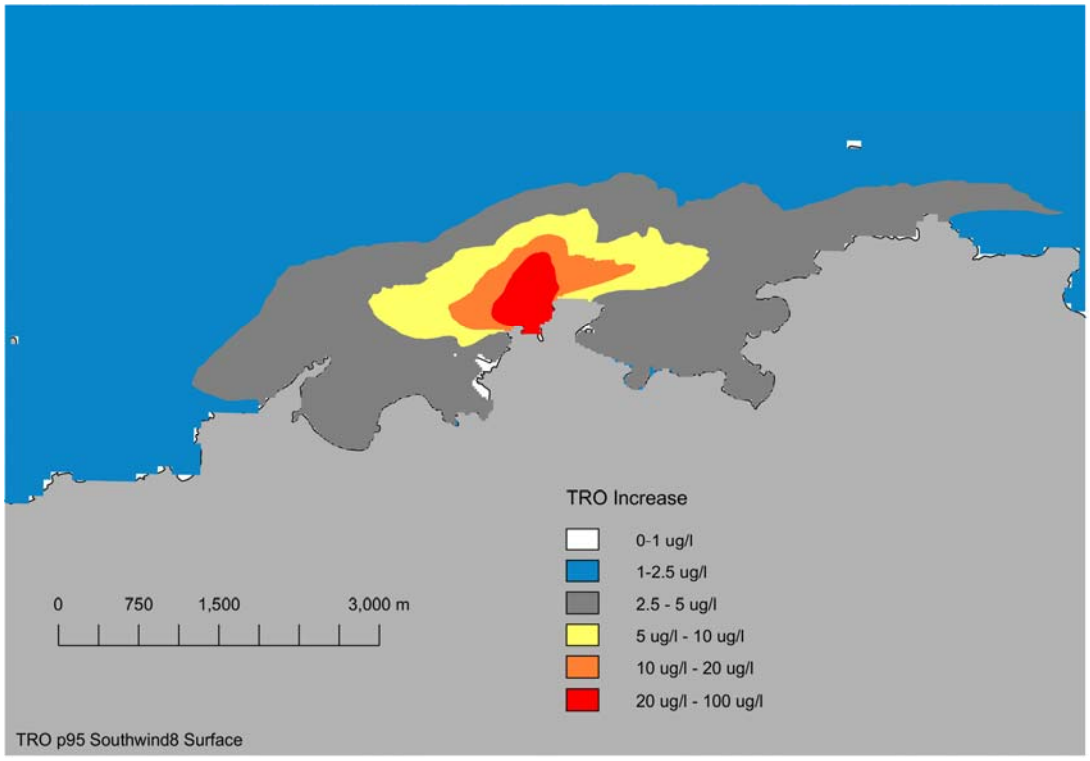

Figure 76 Surface TRO concentration, 95 percentile – South wind case.

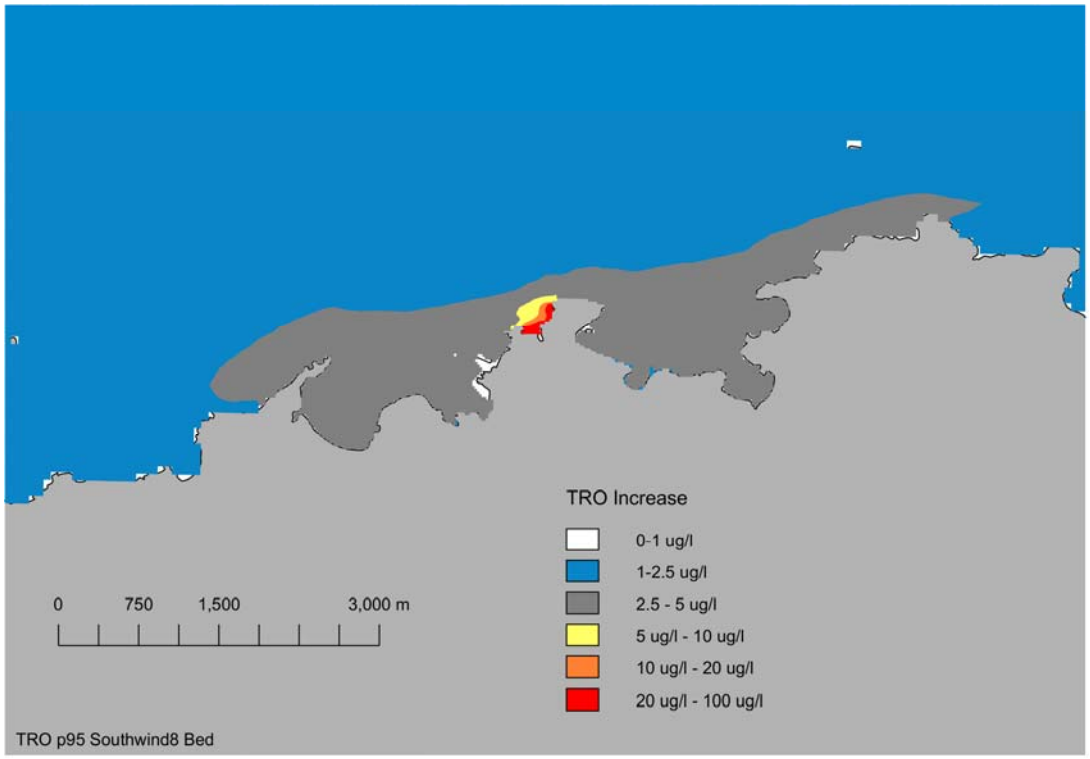

Figure 77 Bed TRO concentration, 95 percentile – South wind case.

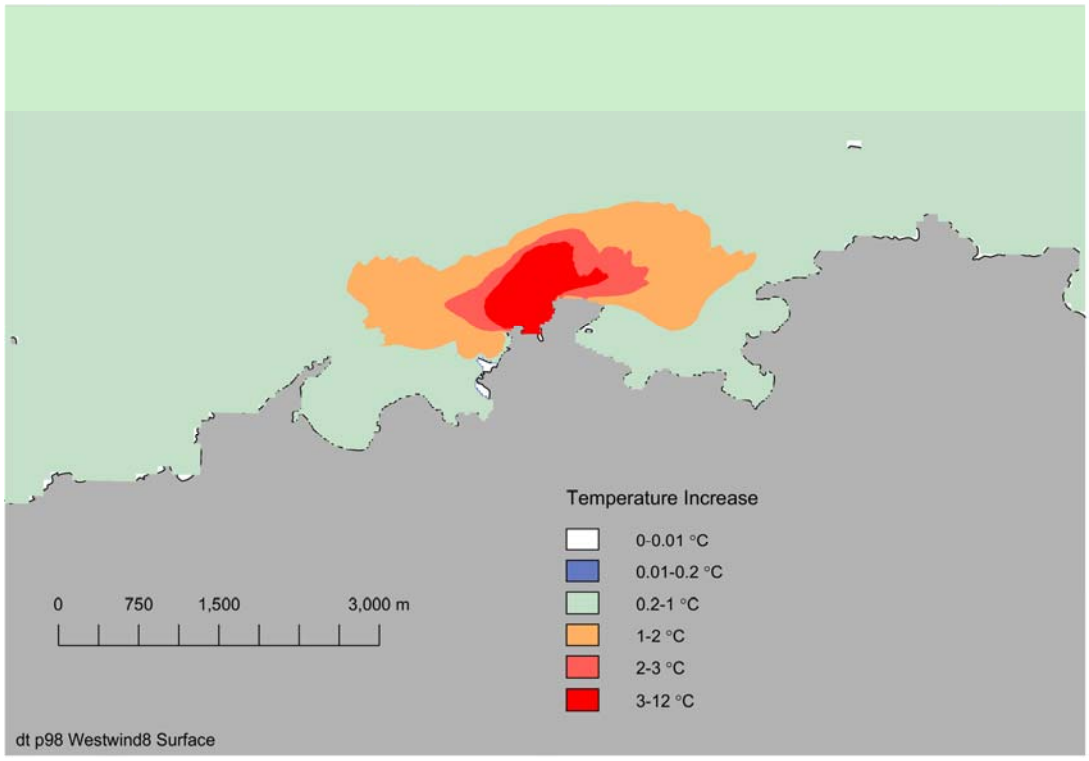

Figure 78 Surface temperature, 98 percentile – West wind case.

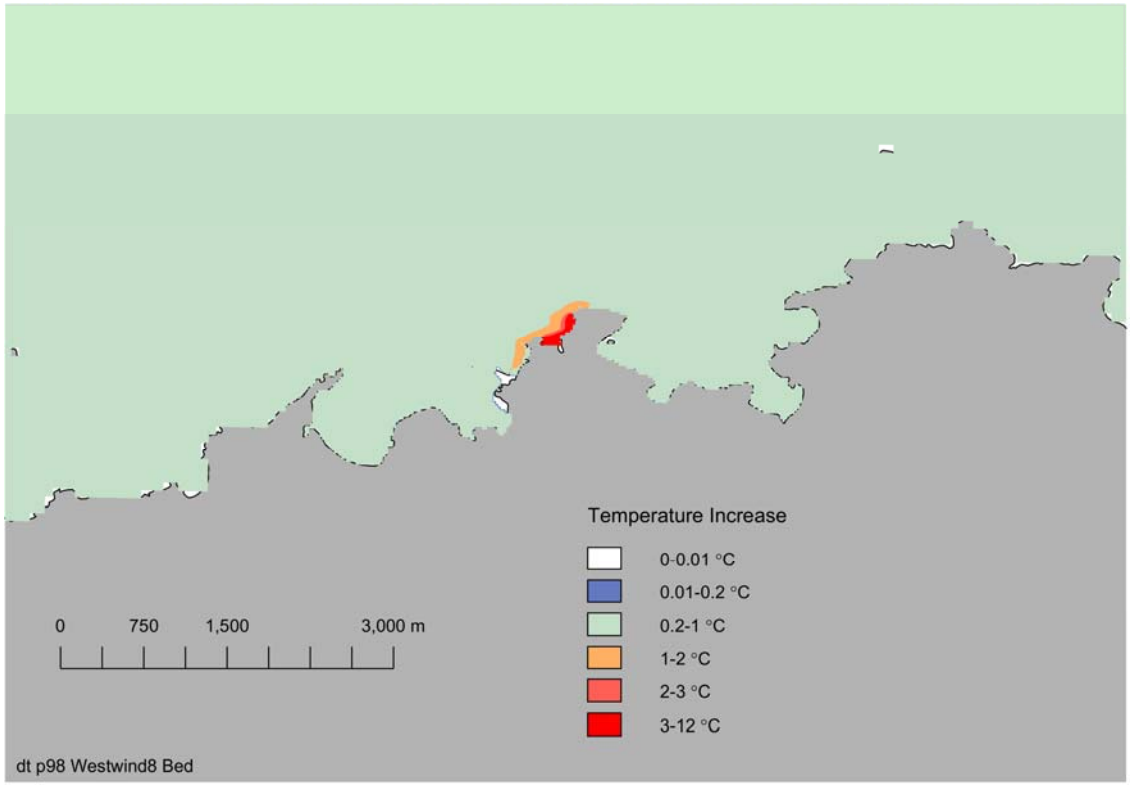

Figure 79 Bed temperature, 98 percentile – West wind case.

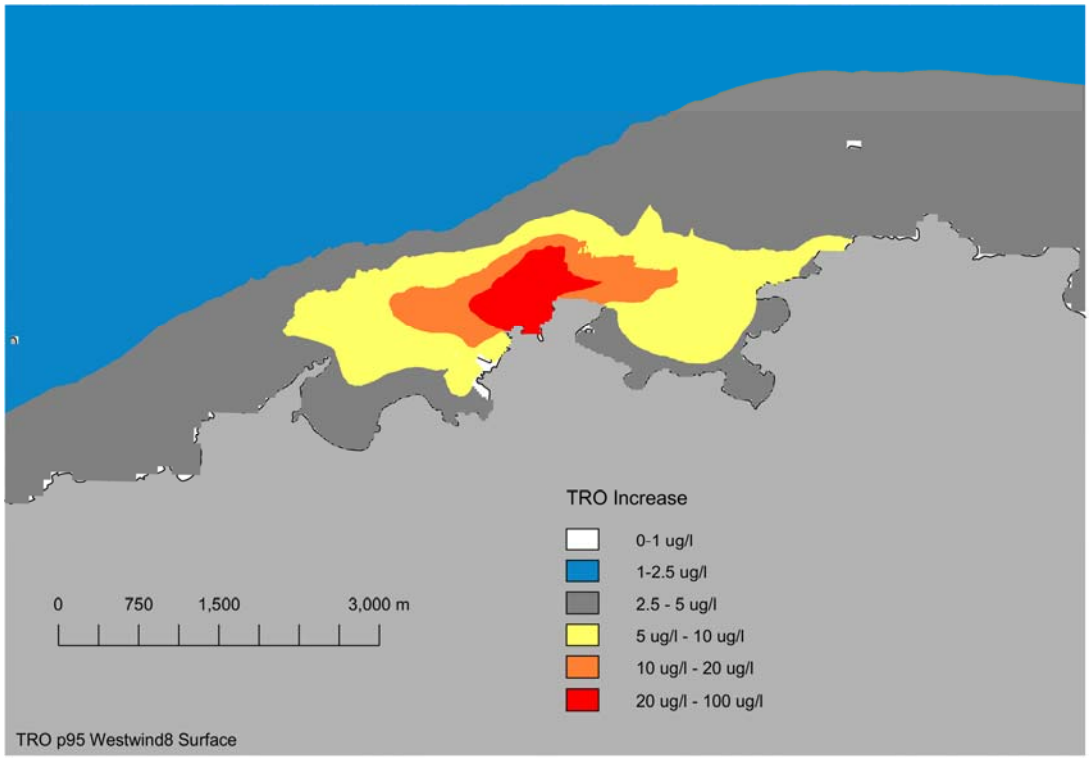

Figure 80 Surface TRO concentration, 95 percentile – West wind case

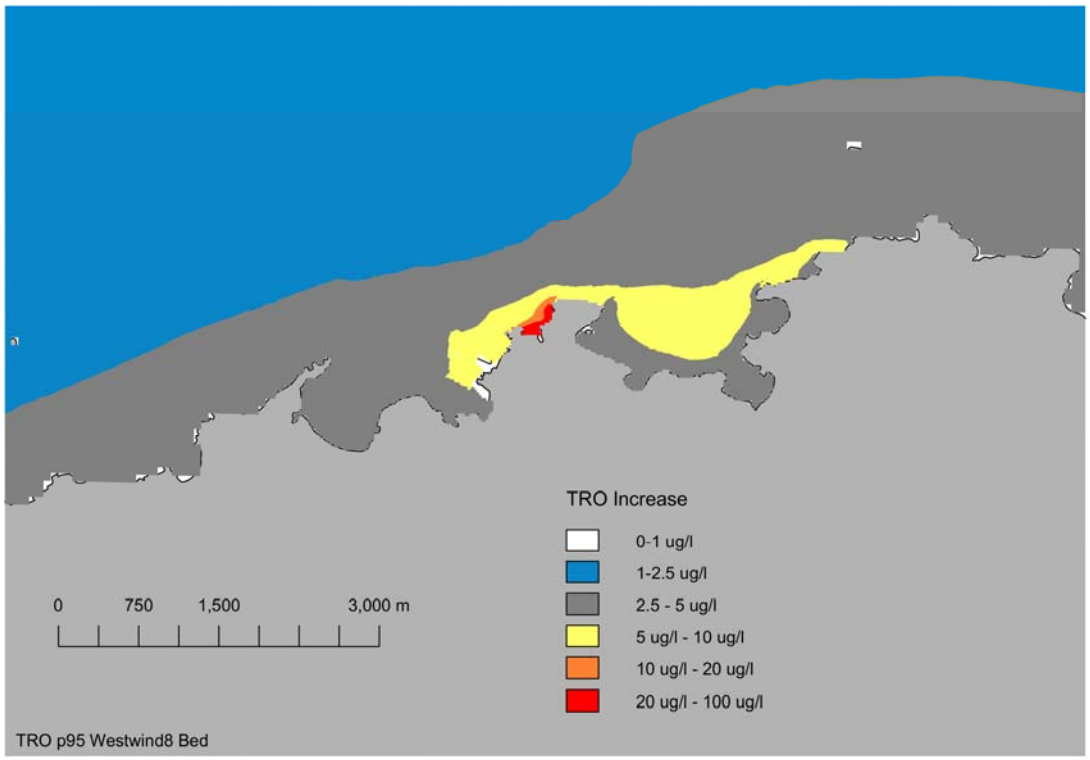

Figure 81 Bed TRO concentration, 95 percentile – West wind case.

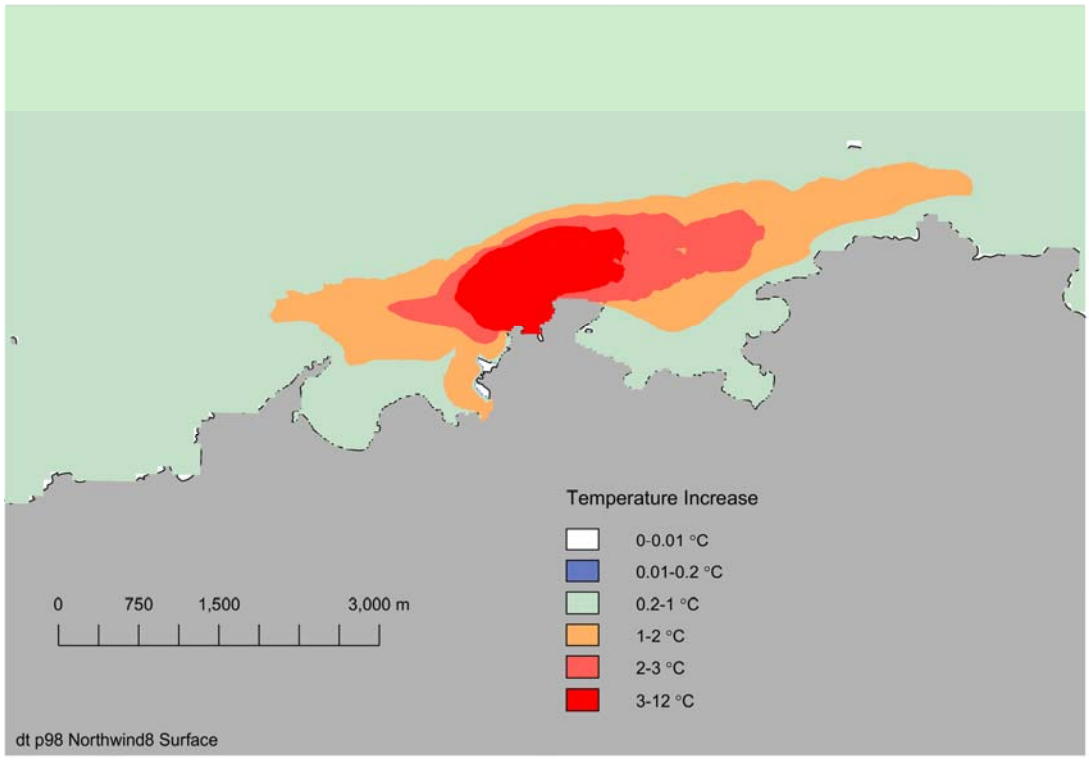

Figure 82 Surface temperature, 98 percentile – North wind case.

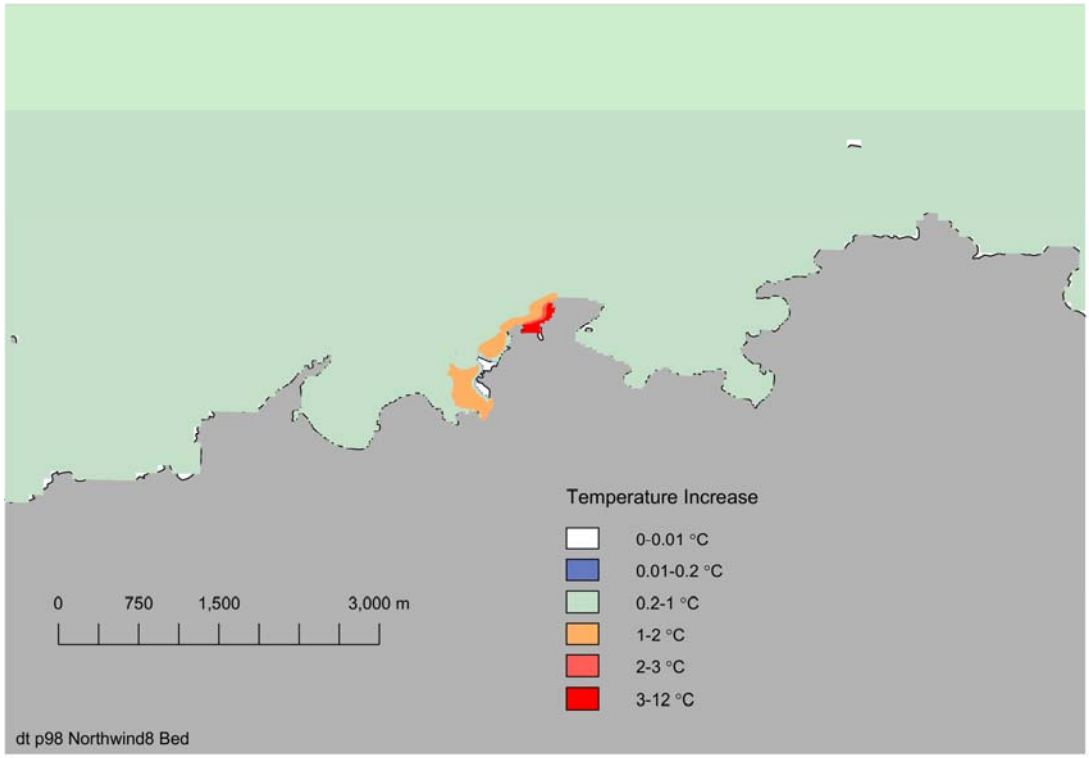

Figure 83 Bed temperature, 98 percentile – North wind case.

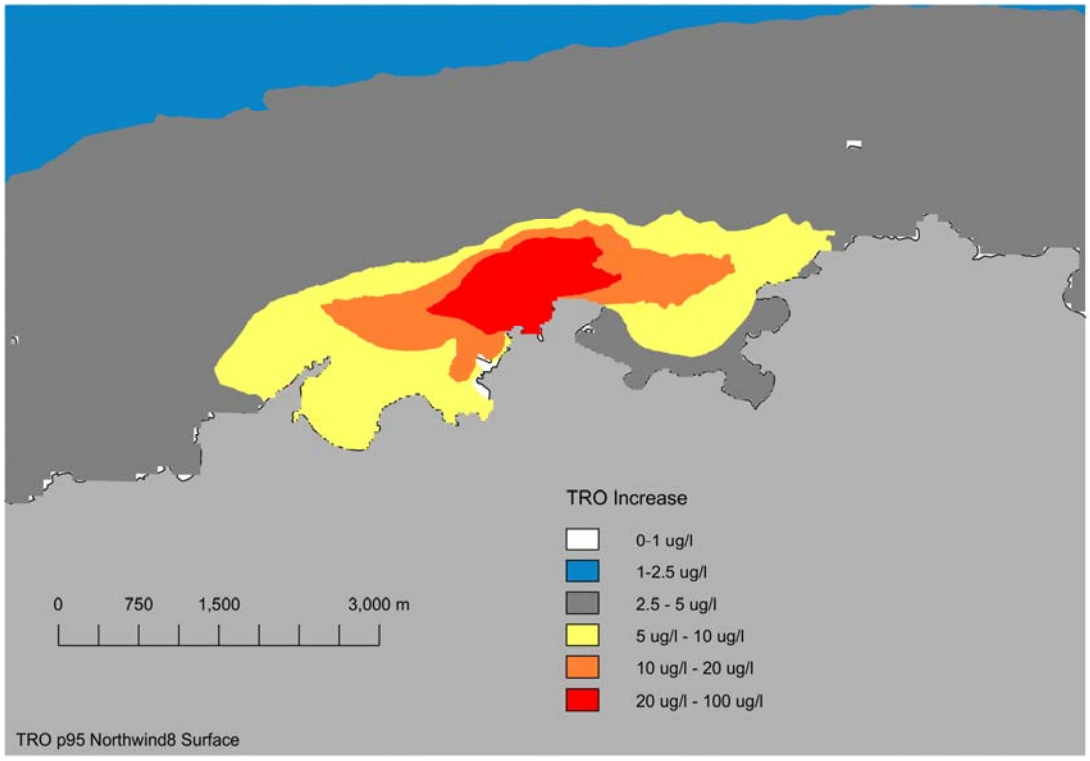

Figure 84 Surface TRO concentration, 95 percentile – North wind case.

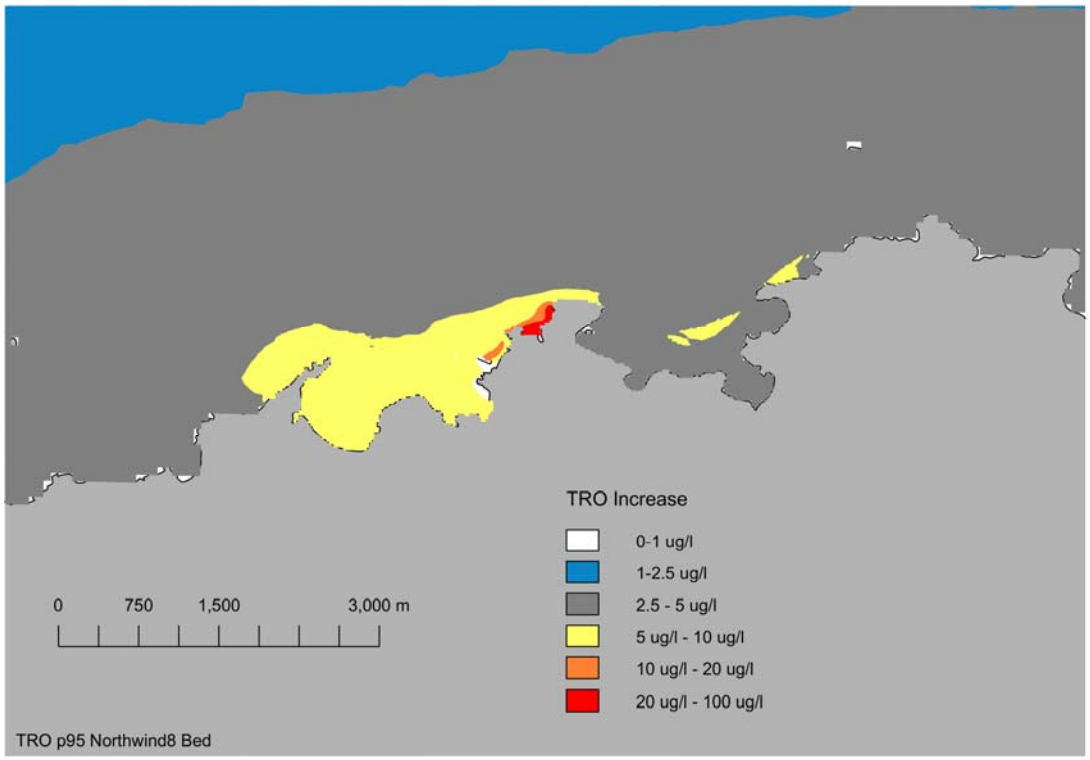

Figure 85 Bed TRO concentration, 95 percentile – North wind case.

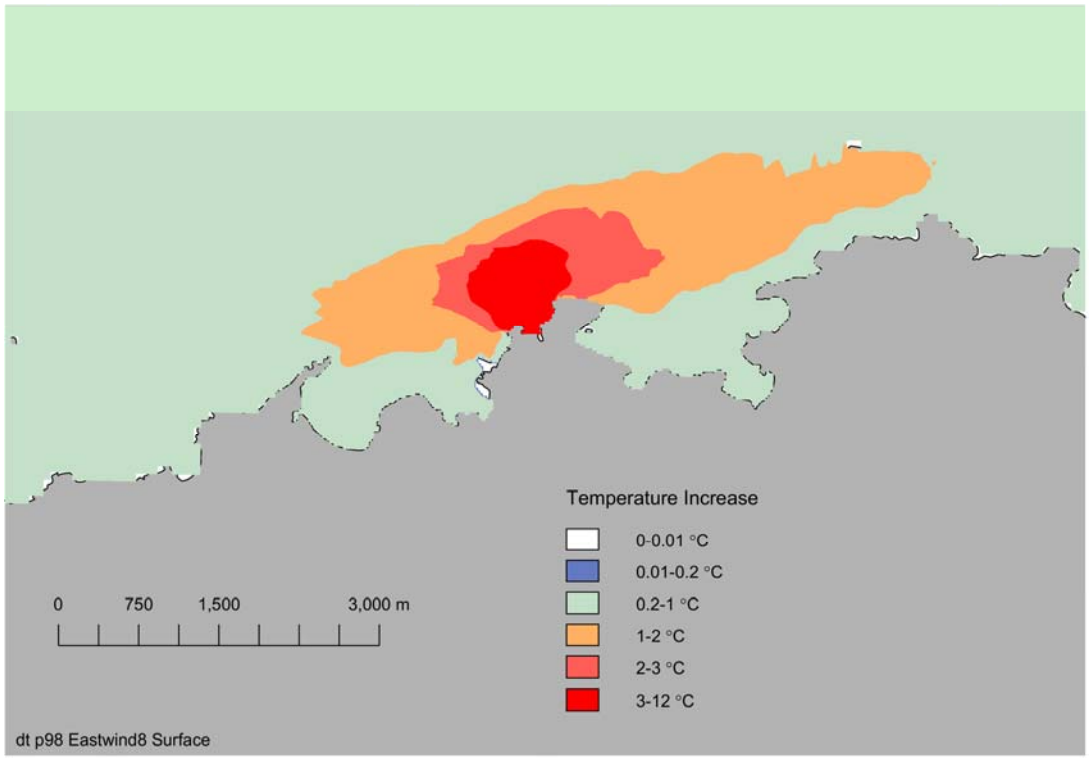

Figure 86 Surface temperature, 98 percentile – East wind case.

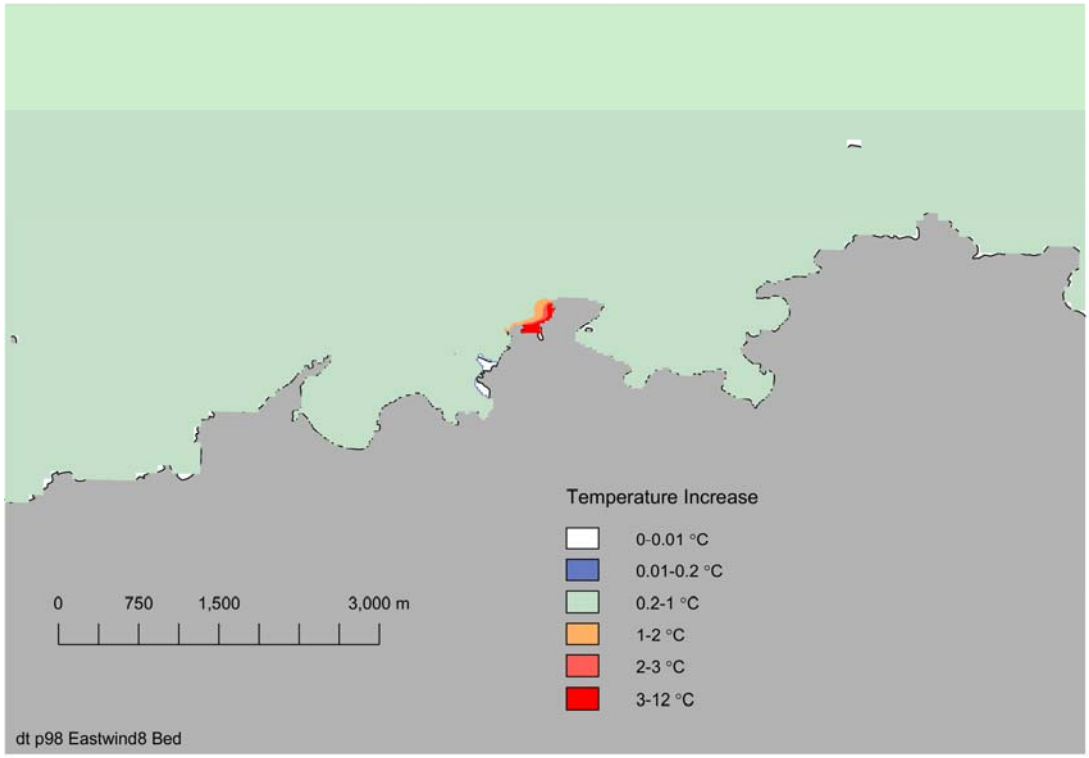

Figure 87 Bed temperature, 98 percentile – East wind case.

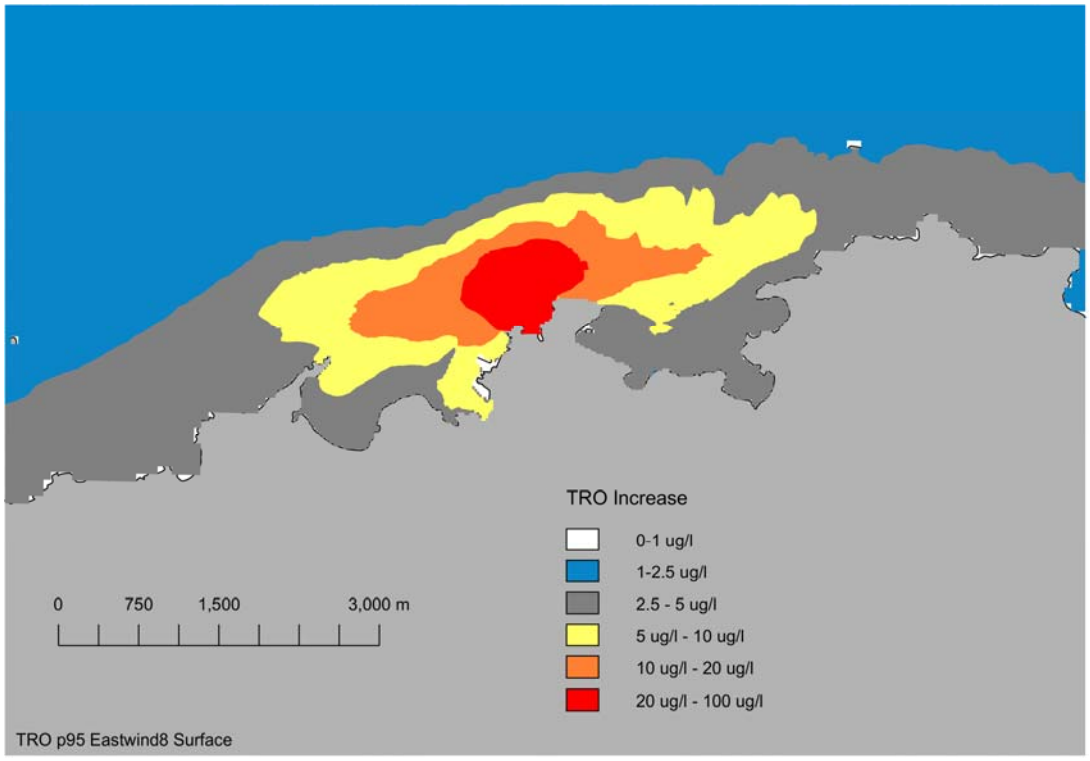

Figure 88 Surface TRO concentration, 95 percentile – East wind case.

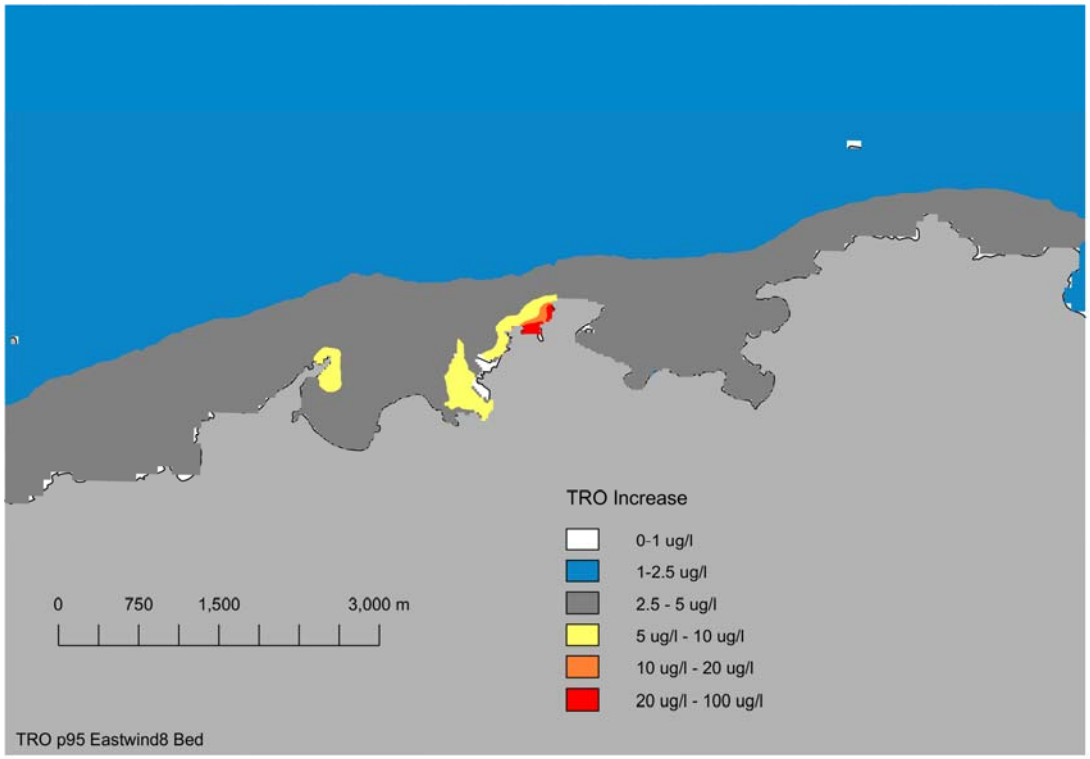

Figure 89 Bed TRO concentration, 95 percentile – East wind case.

6.9 Simulation with a variable wind

6.9.1 Selection of Representative Wind Case

Meteorology data for the period 2003 to 2012 from either RAF Valley or the Meteorological Office's Numerical Weather Prediction (NWP) are being used across the Wylfa Newydd Project. The RAF Valley data are observed whereas the NWP data are modelled. The RAF Valley data set has been selected for use with the hydrodynamic modelling as it comprises observed data and because it is considered to be representative of the marine environment.

The wind speed and direction both have a potential influence on the mixing of the CW plume. The wind speed will influence both the stress imposed on the water and the surface heat flux. The wind stress will influence the hydrodynamics while the surface heat flux can vary the temperature of the water and hence buoyant mixing. Within the plume the timescales are such that surface heat is unlikely to have a big influence on mixing processes (confirmed by the surface heat flux sensitivity studies). Wind direction has been found to influence the mixing of the CW plume as, for example, a wind from the south tends to move the plume offshore into areas with higher currents and hence greater mixing potential. Long-duration winds from any direction are relatively rare and hence a sensitivity study using a variable wind direction is necessary to complement the non-wind stress and fixed wind direction studies.

In order that the variable wind sensitivity study is as representative as possible of the long-term conditions, the simulations were undertaken using a wind record that had a similar average wind speed to the long-term average. The proportion of wind as a function of direction was also compared to the long-term average.

6.9.2 Long-term Average Wind Speed

The long-term (1982 to 2014) average wind speed from the RAF Valley data is 6.02 m/s, for 2003 to 2012 it is 6.0 m/s. The average from the NWP data (2003 to 2012) is 6.07 m/s. The average wind speed during the month of April 2008 was 6.06 m/s, close to the long-term average and hence it is a good candidate for use in exploring the influence of a variable wind on mixing. The April 2008 wind speed and direction for the RAF Valley data set are plotted in Figure 90 and Figure 91. The plots also include the NWP data for comparison.

The RAF Valley and NWP wind speeds and directions are similar with no obvious bias between them at the plotted timescales. However, a comparison of the difference in wind strength over the full 10 year records does show that on average the NWP winds are weaker for winds with a southerly direction and somewhat stronger for winds from the north. This could be explained because a southerly wind at RAF Valley would be blowing off the sea whilst a southerly wind at Wylfa Head will have travelled over land with a commensurately higher friction. Conversely winds from the north or east at Valley have travelled overland while at Wylfa Head they are from the sea. The variation in individual differences in wind strength from a given direction is several times the average difference for that direction. The variation is approximately ±5 m/s whereas the average difference is ±2 m/s from the south and around 1m/s from other directions.

Given the dominant wind direction is from the southwest, the RAF Valley data set is a better representation of the conditions (wind speed, direction, air temperature cloud cover and relative humidity) for the marine environment. In addition to the average speed over the period being representative of the long-term average, it is important that the wind direction is also representative of the long-term. The frequency of direction over the long-term (2003 to 2014) and during the period used in the modelling (2003 to 2012) are plotted alongside the April 2008 data for RAF Valley (Figure 92).

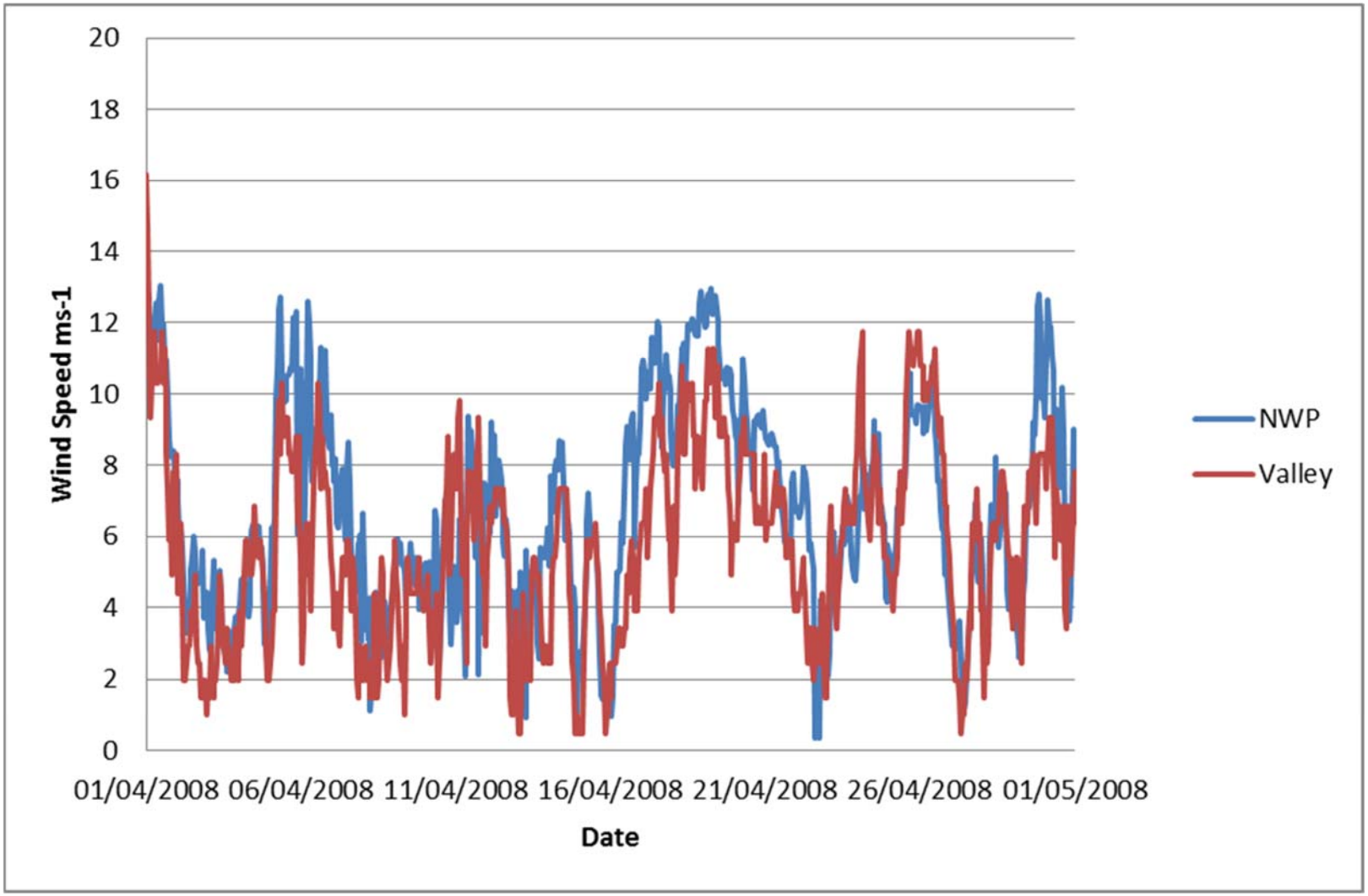

Figure 90 Wind speed for April 2008 – RAF Valley (red) and NWP (blue).

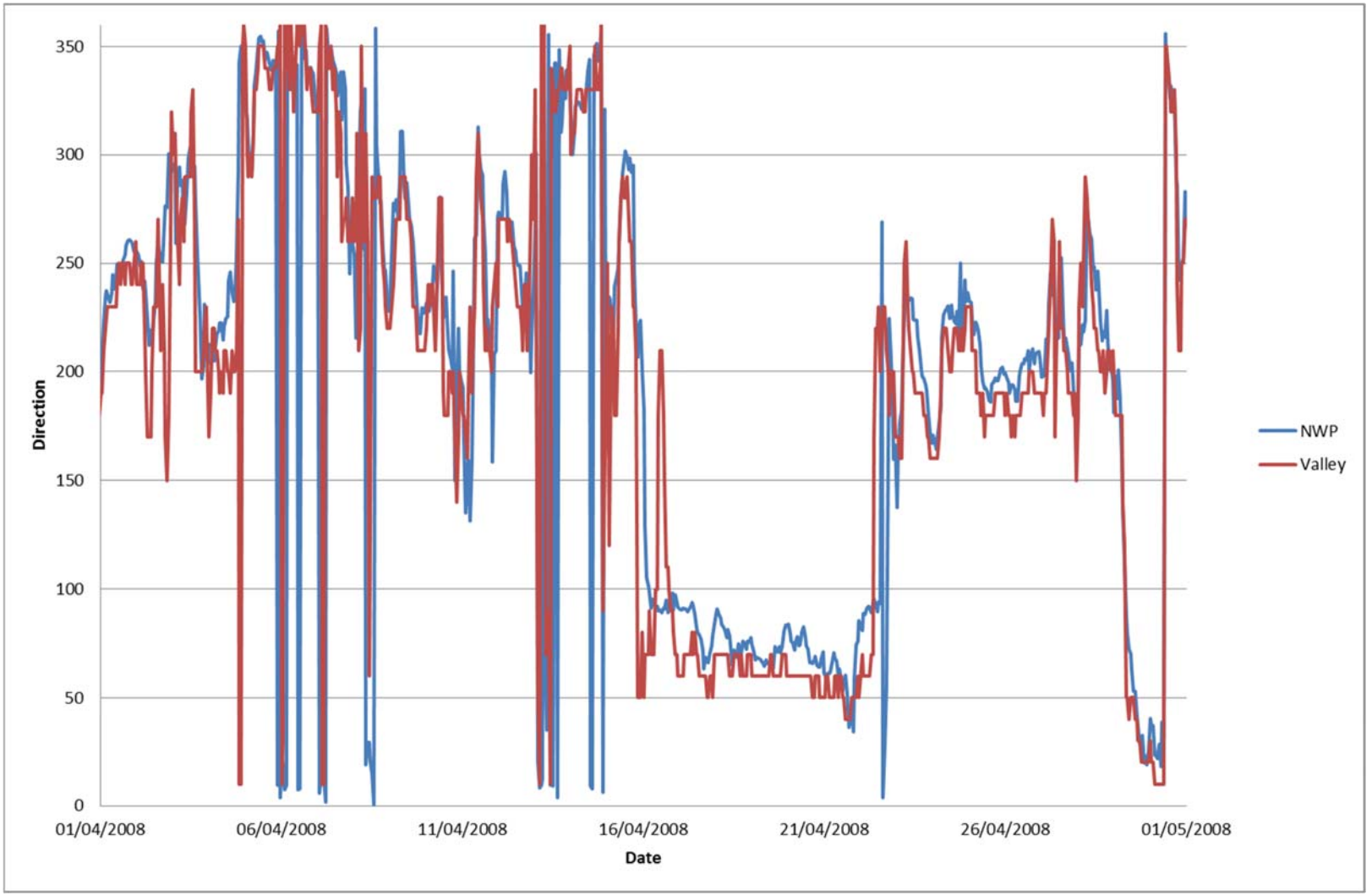

Figure 91 Wind direction for April 2008 – RAF Valley (red) and NWP (blue).

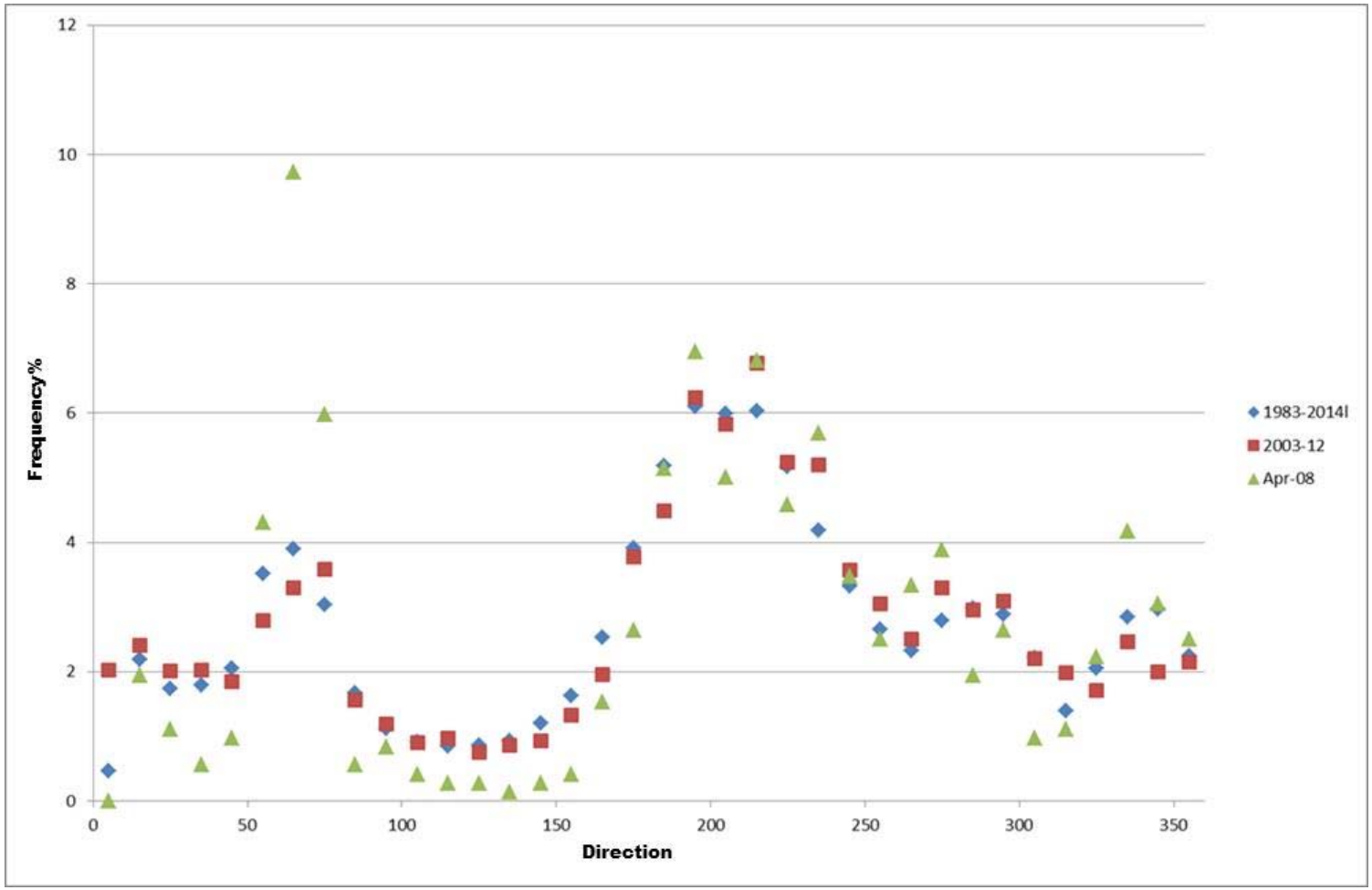

Figure 92 Frequency of wind direction at RAF Valley long-term (1983-2014 blue), period used in marine modelling (2003-2012 red) and April 2008 (green).

The frequencies of wind direction in 10° bands are plotted in Figure 92 above for the period 1983 to 2014, 2003-2012 and April 2008. The long-term record shows twin peaks in the frequency of wind direction. The most common direction in the long-term record is 195 to 215°, with a frequency of around 6% of the time. There is a second peak at 65° with a frequency of 4%. The most infrequent wind direction in the long-term record is from the direction 100 to 150° (0.8%). The wind direction in April 2008 follows the long-term trend, except that the most common direction is 65° (9.7%). Wind frequencies over 90° sectors in 2003 to 2012 and April 2008 are detailed in Table 17.

Table 17 Frequency (%) of wind direction 2003-2012 and April 2008.

Sector	2003-2012 (%)	April 2008 (%)
North	18.5	16.5
East	15.8	22.5
South	36.3	33.3
West	27.7	25.6

The wind directions in the April 2008 are within 3% of the long-term for all but the eastern sector, which is 6.7% more frequent in April 2008 than in the long-term record.

Previous studies have shown that the greatest influence on the mixing zone occurs for constant winds from the south and north, with southerly winds tending to push the plume out into the currents north of Wylfa Head where mixing is greater, while a wind from the north tends to push the plume back toward the shore.

As the overall wind magnitude and the frequency of winds from the north and south are similar in April 2008 to the long-term, the use of April 2008 wind provides a good representation of typical conditions.

6.9.3 Variable Wind Case – Temperature Rise

The mixing zone implied by the extent of the 3 °C 98 percentile rise at the surface (Figure 93) has an approximate area of 49.8 hectares, while the 2 °C 98 percentile rise has an area of approximately 97.4 hectares. The 1 °C 98 percentile rise at the surface has an approximate area of 288 hectares.

The mixing zone implied by the extent of the 3 °C 98 percentile rise at the bed (Figure 94) is limited to an area around the proposed outfall and along the western edge of Wylfa Head, with an area of approximately 3.1 hectares. The area of the 2 °C 98ile rise at the bed has an area of approximately 4.1 hectares while the 1 °C rise area is approximately 10.6 hectares.

The size of the surface mixing zone is reduced compared to the no wind stress base case, while the size of the mixing zone at the bed is increased.

6.9.4 Variable Wind Case – TRO

The mixing zone implied by the extent of the 10 µg/l 95 percentile contour (Figure 95) has an approximate area of 129 hectares.

The area of the bed with a TRO 95 percentile concentration greater than 10 µg/l is limited to the vicinity of the outfall and a strip along the western side of Wylfa Head with an area of approximately 5.7 hectares (Figure 96).

6.9.5 Variable Wind Case – Full extent

The wider extent of the plume above the background is shown in Figure 97 to Figure 100. The extent of temperature increase above the background extends for a large area (approximately 60 km north west of the

intake/ outfall area). Unlike the summer base case, this extent also moves south around Anglesey. To the east, this increase extends up towards Llandudno. However, this increase is small, with maximum increases of 0.2 °C. The same pattern can be seen for increase in TRO values; however, the extent is smaller (approximately 20 km to the north and east of Anglesey). Here the maximum increase is 2.5 µg/l.

6.9.6 Variable Wind Case – Recirculation

The depth-averaged temperature rise for a model cell (141,64) approximately in the middle of the CW forebay has been calculated from a simulation of the period 15 August 2011 to 1 September 2011.

In Table 18 the mean, 98 percentile and maximum temperature rise above ambient at the intake for summer base case and variable wind are listed.

Table 18 Recirculation statistics - Variable wind case.

Statistic	Variable Wind: Temperature rise above ambient (°C)	Summer Base Case: Temperature rise above ambient (°C)	Difference (°C)
Average	0.41	0.46	–0.05
98 percentile	0.69	0.78	–0.09
Maximum	0.88	0.84	0.04

The imposition of a variable wind reduces the average temperature rise by 0.05 °C at the CW intake and reduces the 98 percentile by 0.09 °C. The maximum CW intake temperature is increased by 0.04 °C.

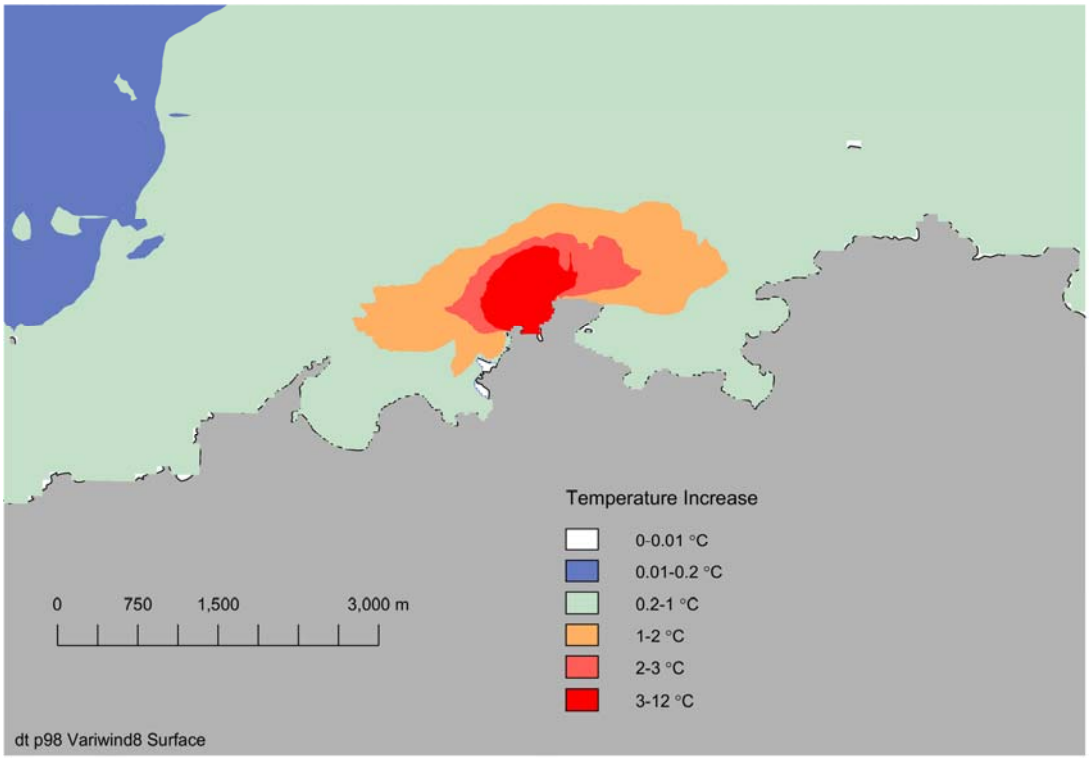

Figure 93 Surface temperature, 98 percentile – Variable wind case.

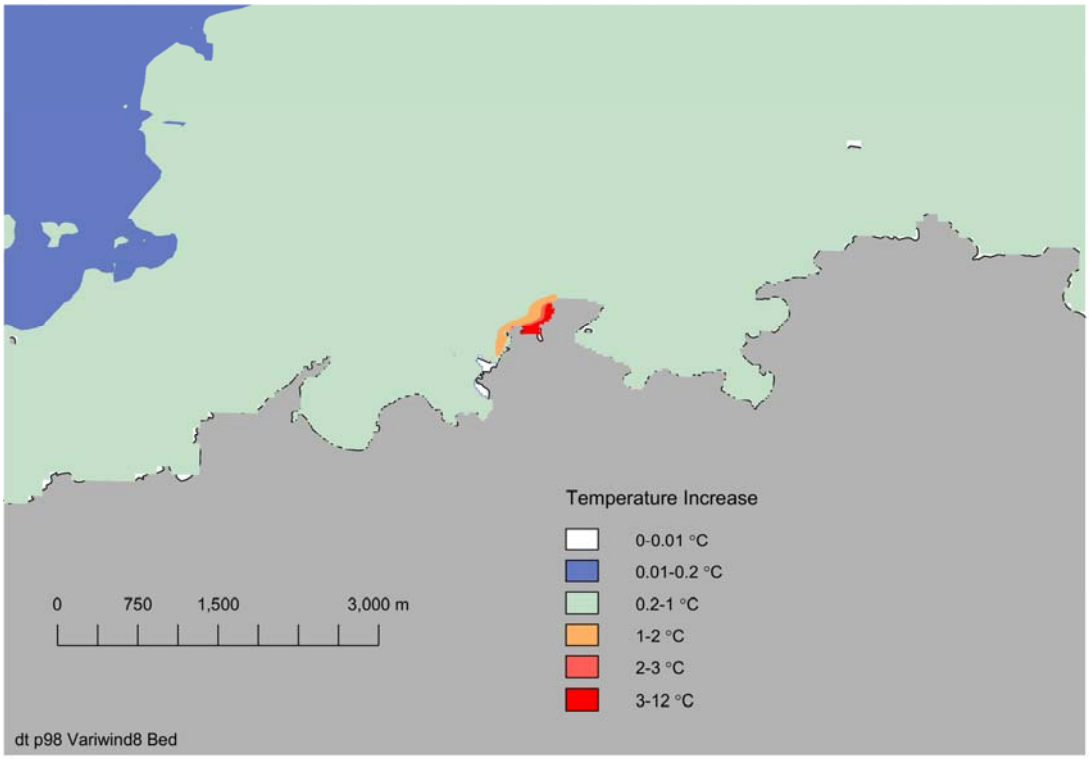

Figure 94 Bed temperature, 98 percentile – Variable wind case.

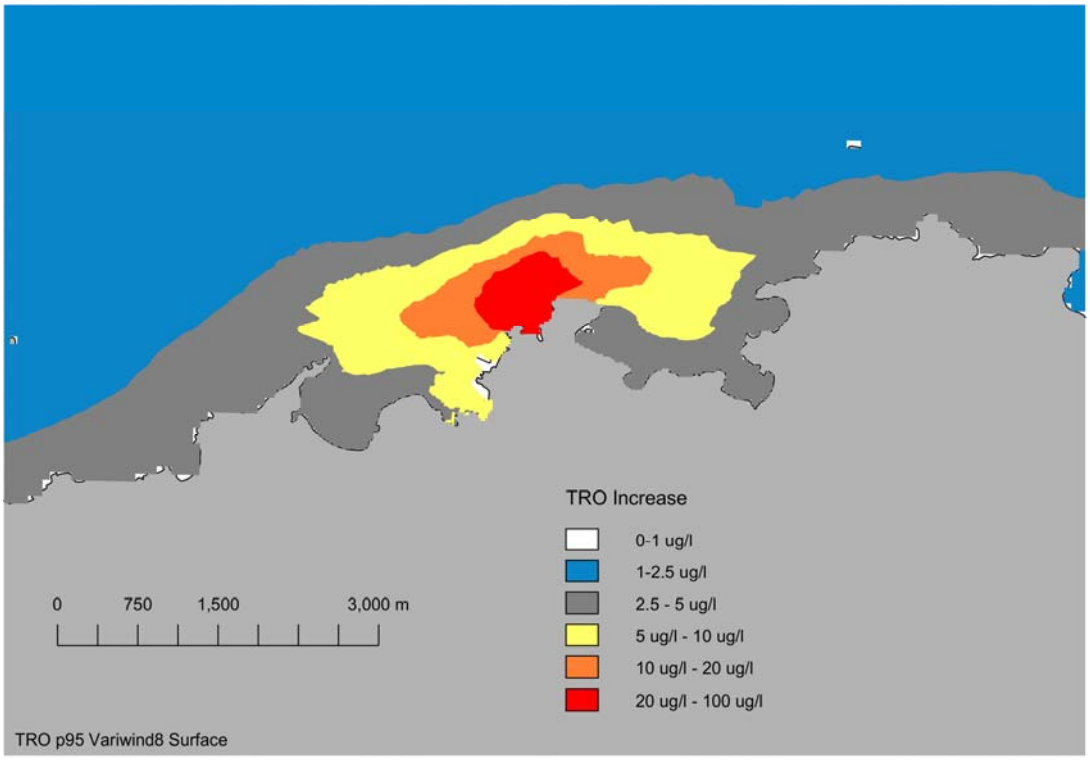

Figure 95 Surface TRO concentration, 95 percentile – Variable wind case.

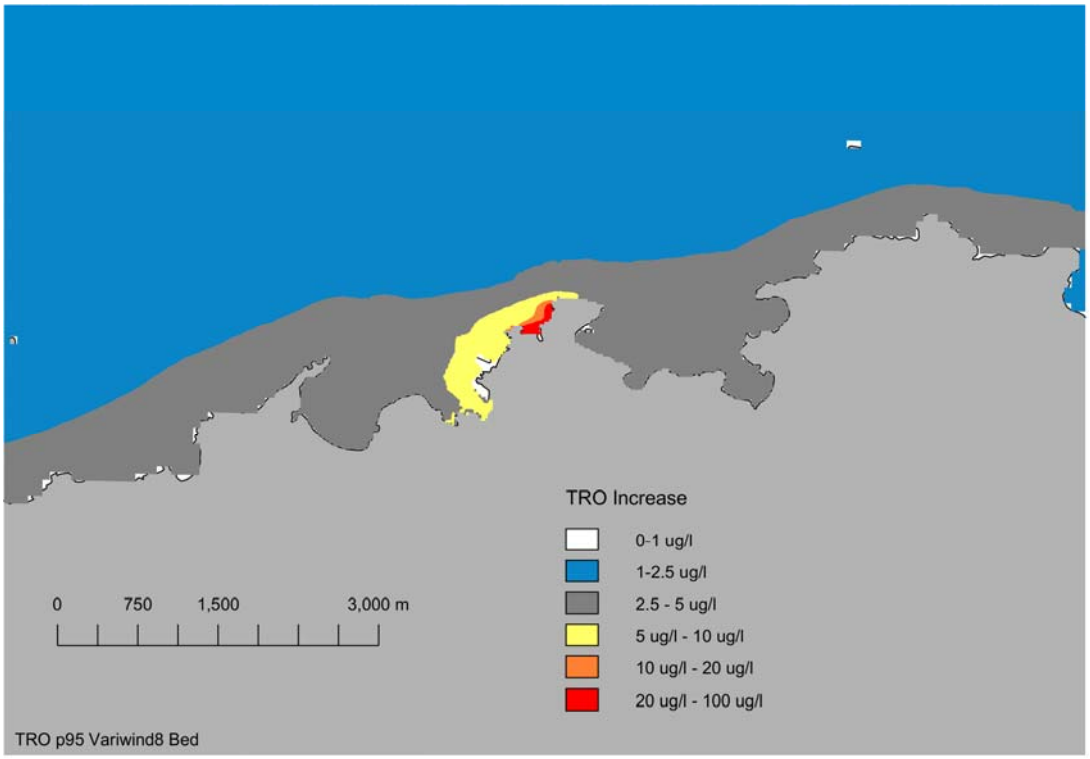

Figure 96 Bed TRO concentration, 95 percentile – variable wind case.

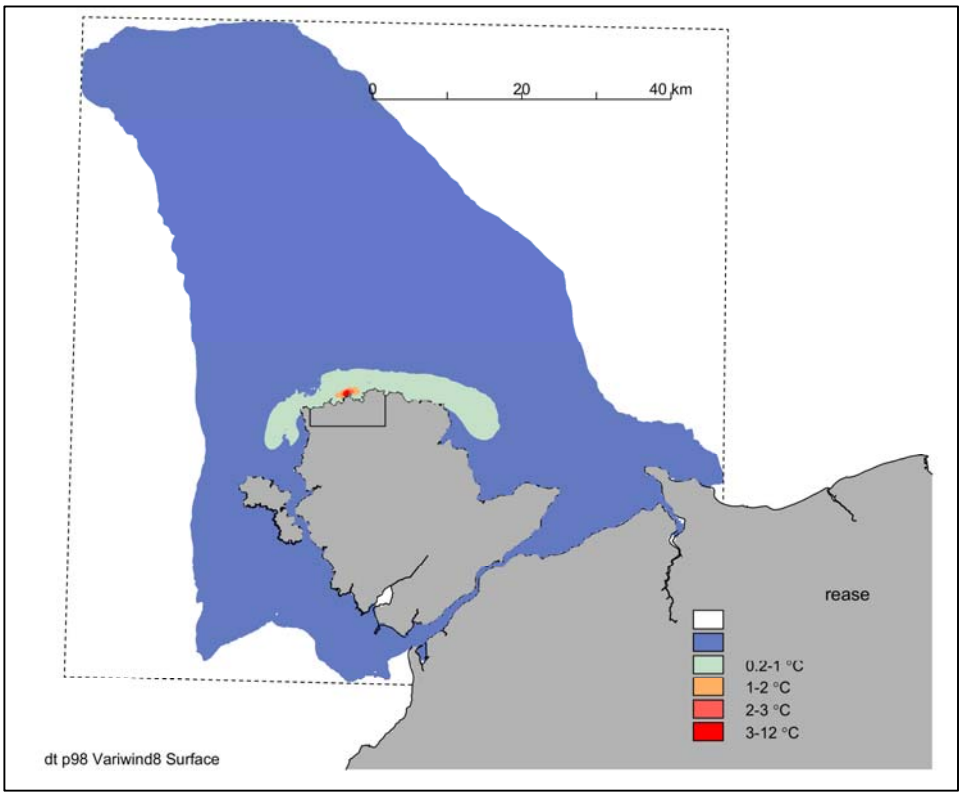

Figure 97 Surface temperature, 98 percentile – Variable wind case, wide extent.

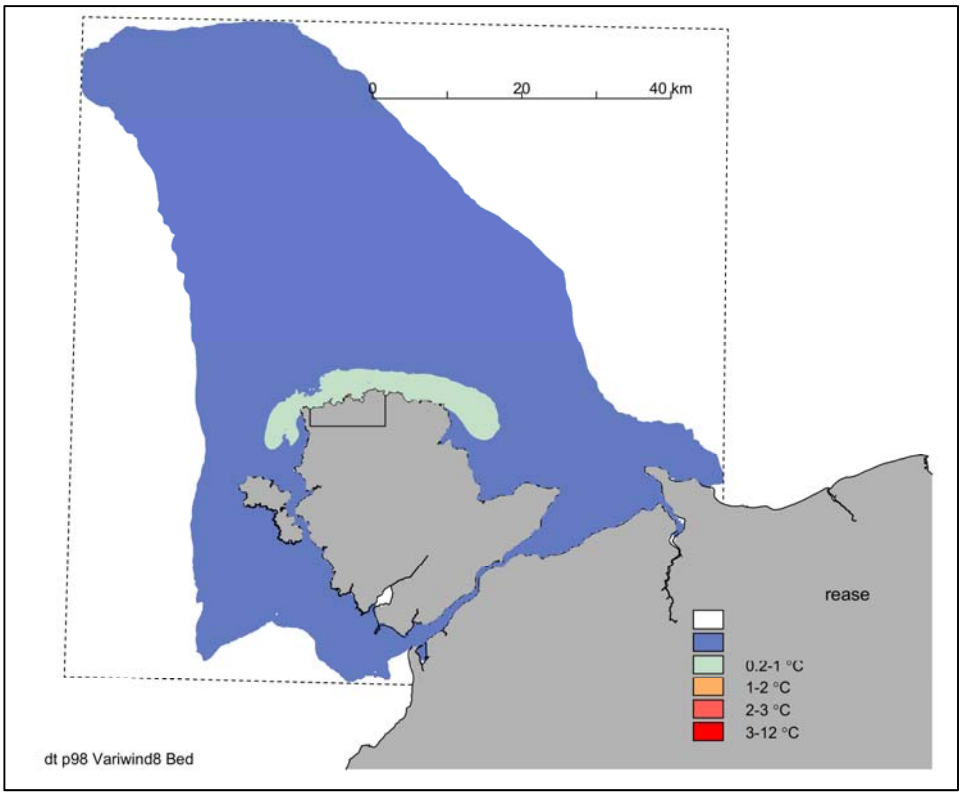

Figure 98 Bed temperature, 98 percentile – Variable wind case, wide extent.

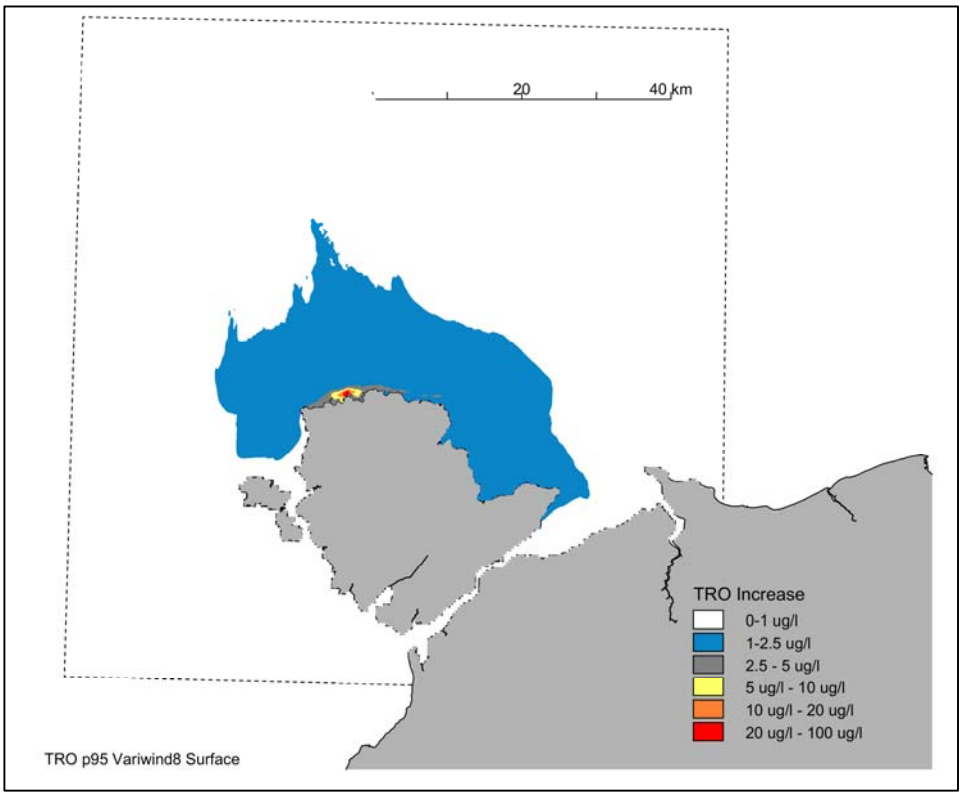

Figure 99 Surface TRO concentration, 95 percentile – Variable wind case, wide extent.

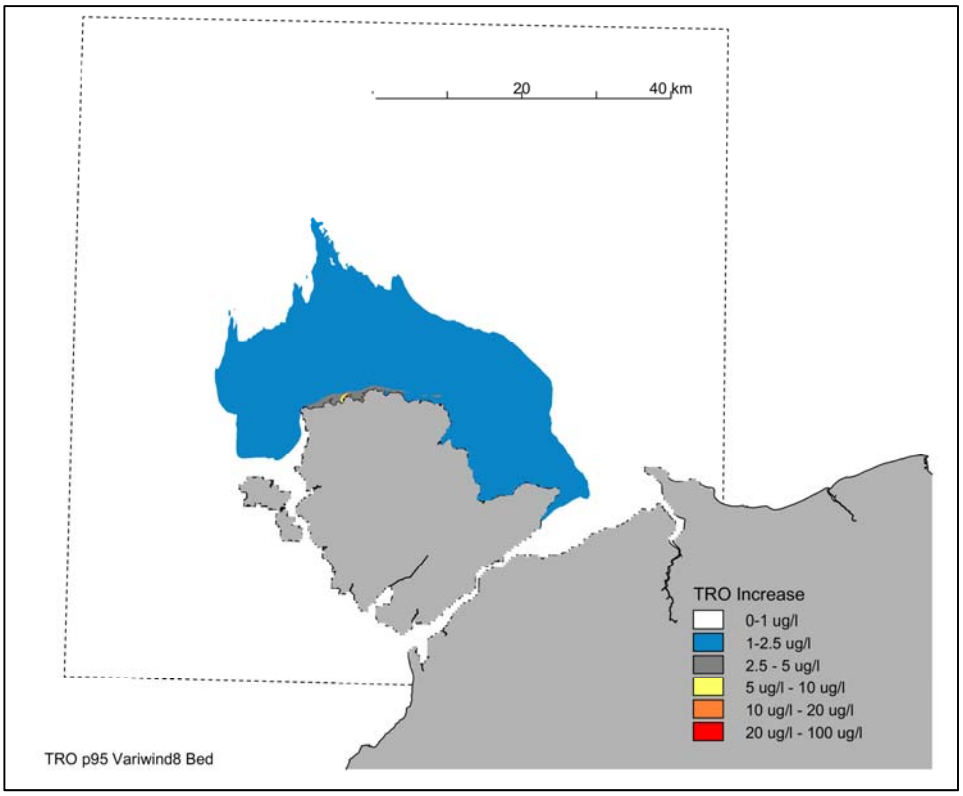

Figure 100 Bed TRO concentration, 95 percentile – Variable wind case, wide extent.

6.10 Wave Sensitivity

A simulation has been undertaken to examine the sensitivity of the predicted mixing zones to the inclusion of wave forcing in the model. Waves are known to have the potential to increase vertical mixing and bed shear stresses.

The simulation made use of a calibrated wave model developed by AMEC/HR Wallingford for Horizon. The AMEC-Wallingford wave model was created using the SWAN wave model and was calibrated/validated using wave data recorded at four sites around Wylfa Head. The model has four nested grids of increasing resolution with the innermost grid of 20 m centred on the Wylfa site and covering Cemlyn and Cemaes Bays. The other grids are 50 m, 200 m and 500 m in size. The model is driven at the outer boundary using wave and wind data from the MetOffice's WaveWatch 3 model. During calibration of the model the wave height and wind speeds were reduced by 10% from the original WaveWatch 3 data (Hawkes 2015).

AMEC/Wallingford has provided the calibrated boundary data and model grids for use in other studies. In a second phase of wave modelling the refined wave model was modified to include the changes in bathymetry and structures associated with Wylfa Newydd. These include dredging in front of the proposed CW intake and construction of breakwaters and a MOLF; these simulations were completed during 2016. In 2017 Wallingford re-ran the stage 2, with Power Station, simulations to reflect changes to the breakwater and MOLF design. At this time a decision was taken to extend the innermost, 20m, grid to cover Cemlyn and Cemaes Bays.

Horizon's hydrodynamic model has been developed within Deltares' Delft3d framework. The Delft3d modelling software allows the user to couple the hydrodynamic model to a wave model either in so-called offline or online mode. In the offline mode the wave models are run separately while in the online mode the two models are run together and the output of one can be used as conditions for another.

As waves travel they change character under the influence of wind and local hydrodynamic conditions. In particular as waves near the shore their direction and height are modified by the local bathymetry. For this study the models were run in online mode with the wave model taking the predicted water level as an input condition. Use of predicted currents as input to the wave model resulted in localised numeric instabilities in a relatively shallow area with high currents.

The AMEC/Wallingford model was a pure SWAN model that ran as a console application. It had to be adapted to conform to the Delft3d implementation of SWAN. For example the grids in the pure SWAN model are defined within the model input script but within the Delft3D framework are defined in the same way as the hydrodynamic grids. The AMEC/Wallingford model was used to define boundary conditions in the Delft3d Wave model for the desired wave condition.

The SWAN model grid extents and location of the WatchWatch 3 boundary condition are shown in Figure 101. Hawkes (2015) provides information on the wave climate predicted at five points north of Wylfa Head. The location of the central of these (Point 3) is shown in the SWAN model grids in Figure 102. The predicted wave roses at the model boundary and for Point 3 (Hawkes 2015) for 1980 to mid-2015 are shown in Figure 103 and Figure 104, respectively.

The most common direction predicted at Point 3 was 225 to 255 degrees, with the most common wave height being 0.5 to 1.0 m. Waves from a northerly direction, which would have a direct path into Porth-y-pistyll and Cemlyn Bay, are relatively rare.

In order to examine the sensitivity of the predicted mixing zone to the additional vertical mixing due to waves it is necessary to define a representative wave condition at the boundary. It is unrealistic to use an extreme wave condition for a relatively long-term simulation such as a spring-neap cycle, as extreme waves are by their nature relatively rare events; hence, a condition representative of the more common wave conditions around Wylfa Head was selected. The direction of the chosen wave was from the most common direction (southwest) with a wave height on the high side (around 1.5 m) of the most common heights (0.5 m to 1.0 m).

The approach adopted was to identify the desired wave conditions at Point 3 from the wave modelling time series output and then use the associated boundary condition data in a coupled hydrodynamic and wave

simulation. The conditions that occurred at 03:00 on 7 March 2014 were selected for use in the modelling (see Table 19).

Table 19 Wave conditions used in coupled model simulations.

Condition	Date	Time	Hsig	Period (s)	Direction
Typical – High	7/3/2014	03:00	1.48	3.45	239.4

The summer base case was used as the basis of the sensitivity study with the wave model coupled to the flow model. The wave model was called upon on an hourly basis. The coupling made use of the water depth and current in the flow model as input to the wave simulation. The boundary conditions of the wave model were set up to achieve the conditions listed in Table 19 at Point 3 (the location of which is shown in Figure 102).

6.10.1 Summer Base Case with Waves: Temperature Rise

A spring-neap simulation of the CW discharge has been carried out using a wave condition representative of a high typical wave. The hydrodynamic model was setup as per the summer base case. The models were coupled with the wave model being called upon every hour. The temperature rise at the surface and bed are plotted in Figure 105 and Figure 106.

The 2 ˚C temperature rise mixing zone at the surface has an area of approximately 150 hectares, which is smaller than the equivalent without waves included (227 hectares). The approximate area of the 2 ˚C temperature rise mixing zone at the bed is 4.0 hectares which is 0.5 hectares larger than the equivalent without waves (3.5 hectares).

The 3 ˚C temperature rise mixing zone at the surface has an area of approximately 63 hectares compared to 88.7 hectares without waves. The 1 ˚C temperature rise mixing zone at the surface has an area of approximately 300 hectares compared to 741 hectares without waves.

The 3 ˚C temperature rise mixing zone at the bed has an area of approximately 2.9 hectares compared to 2.7 hectares without waves. The 1 ˚C temperature rise mixing zone at the bed has an area of approximately 5.5 hectares compared to 6.6 hectares without waves.

6.10.2 Summer Base Case with Waves: TRO

The TRO 95 percentile mixing contour at the surface and bed with waves are plotted as Figure 107 and Figure 108.

The area of the TRO 95 percentile mixing zone defined by the 10 µg/l contour at the surface is 188 hectares which is less than the equivalent case without waves included (313 hectares).

The area of the TRO mixing zone defined by the 10 µg/l contour at the bed is 6.2 hectares which is larger than the equivalent case without waves included (4.8 hectares).

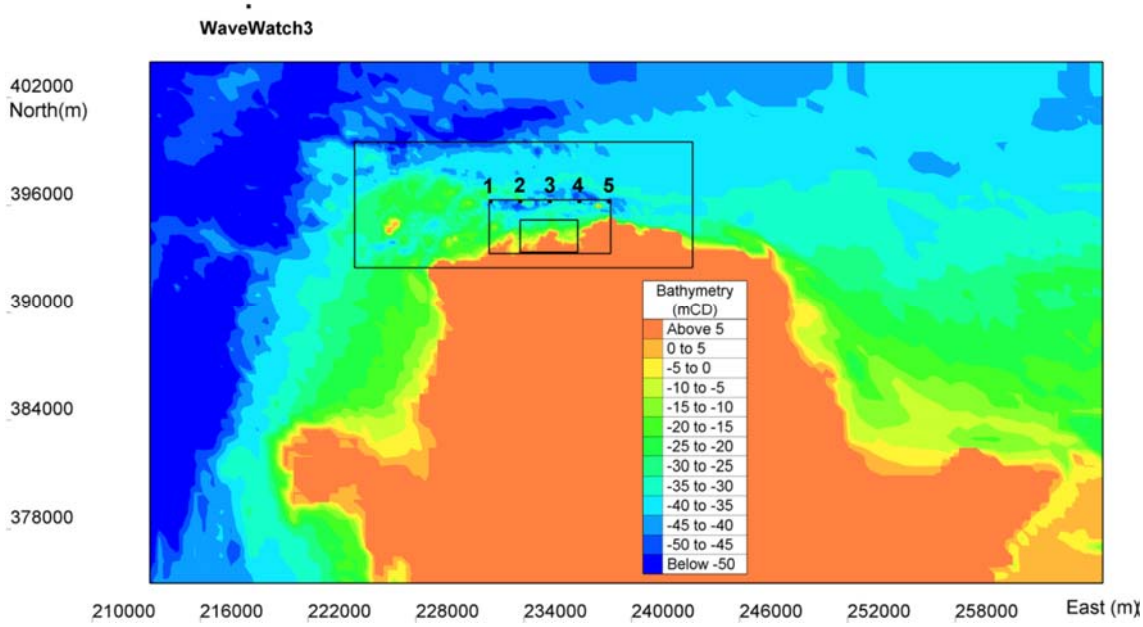

Figure 101 SWAN model grid extents (overall 500m and nested 200 m, 50 m and 20 m grids) (Hawkes 2015).

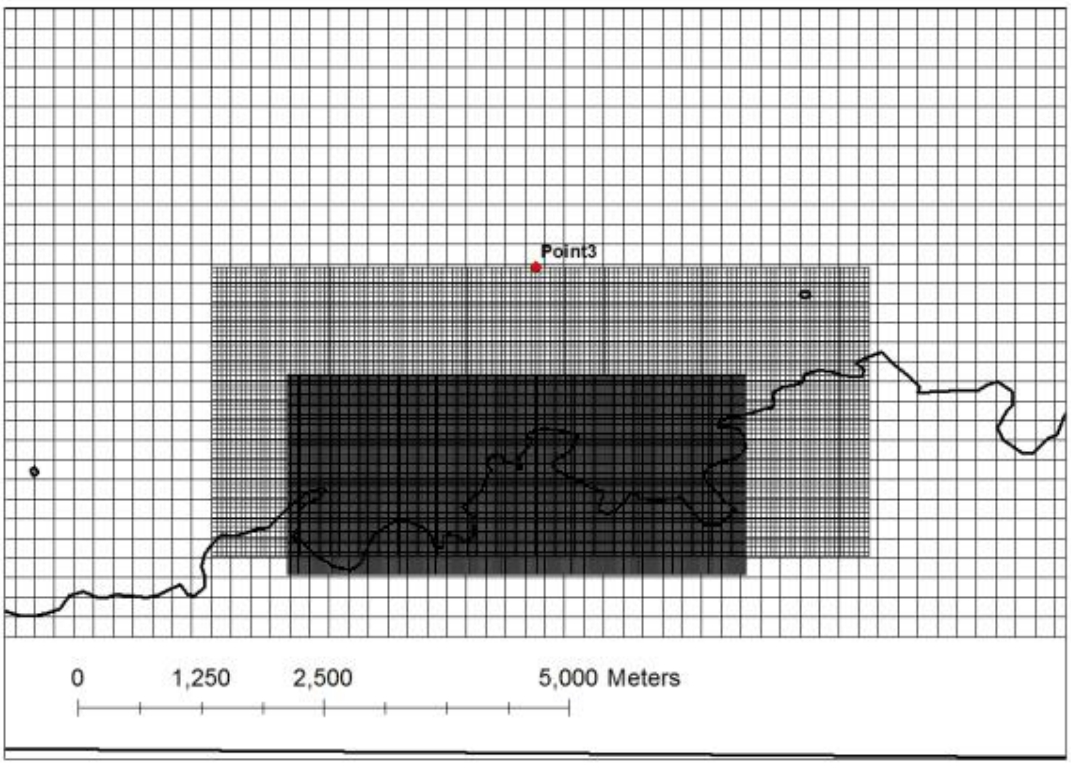

Figure 102 Monitoring Point 3 with the latest 20m grid, 50m grid and part of the 200m grid.

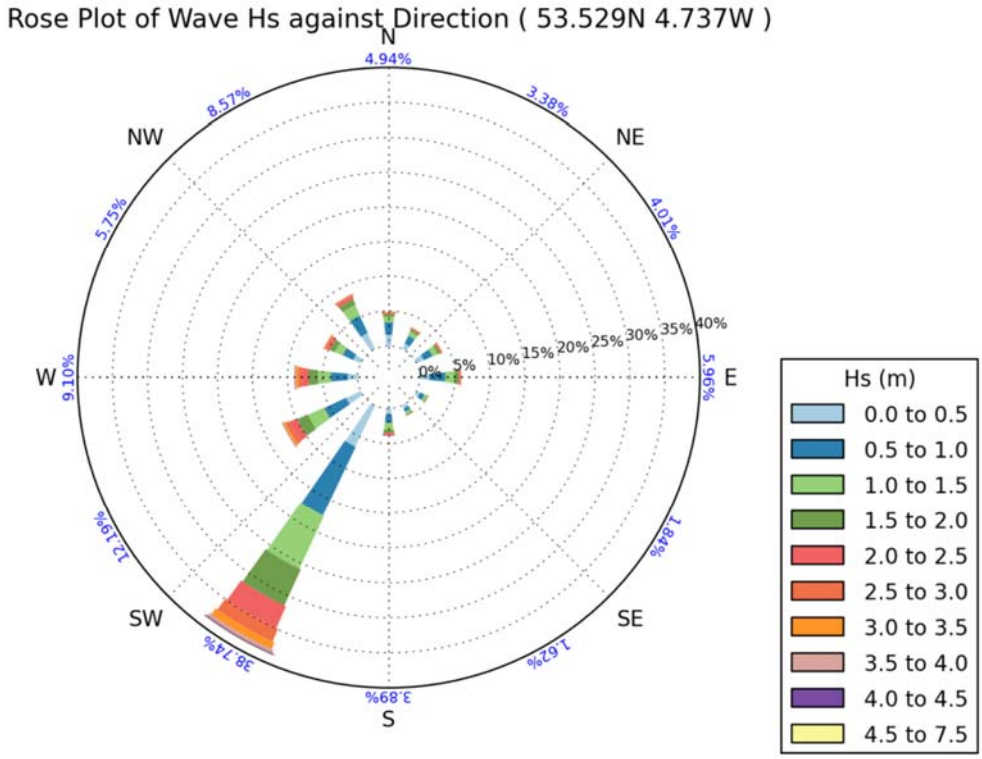

Figure 103 Wave rose at model boundary.

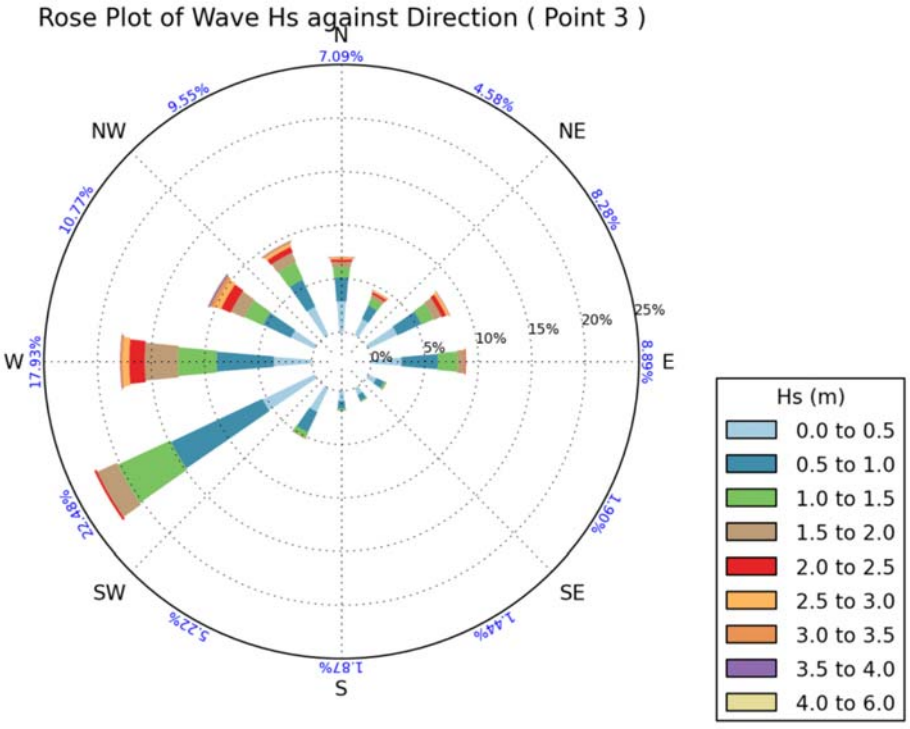

Figure 104 Wave rose – Point 3 (Hawkes 2015).

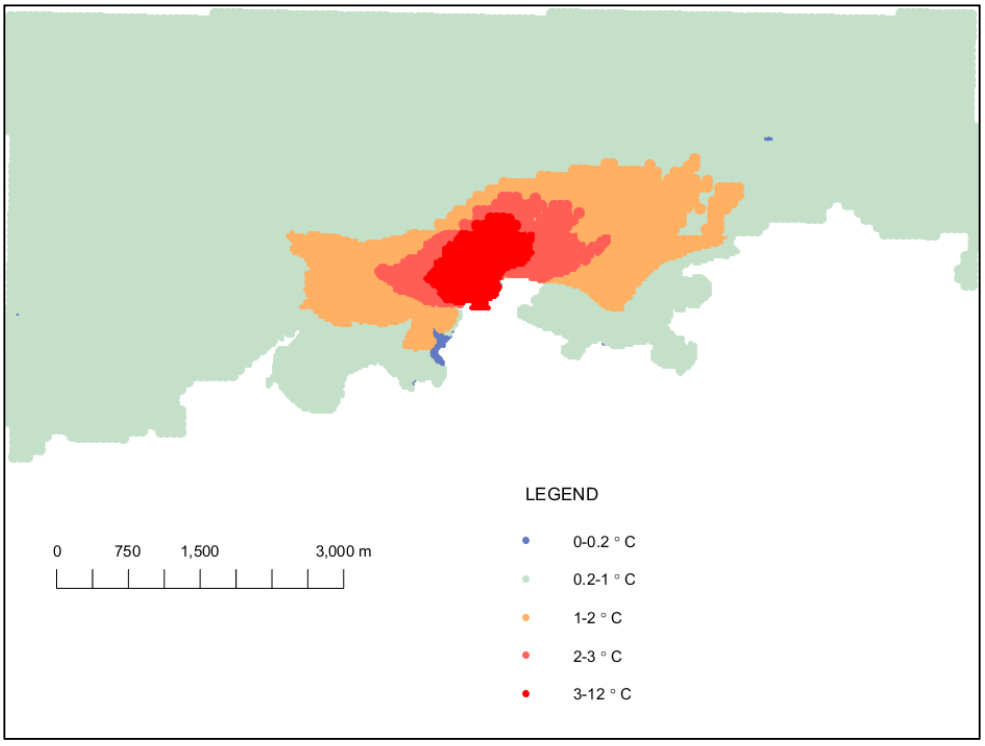

Figure 105 Surface temperature, 98 percentile – Summer base case with typical wave condition.

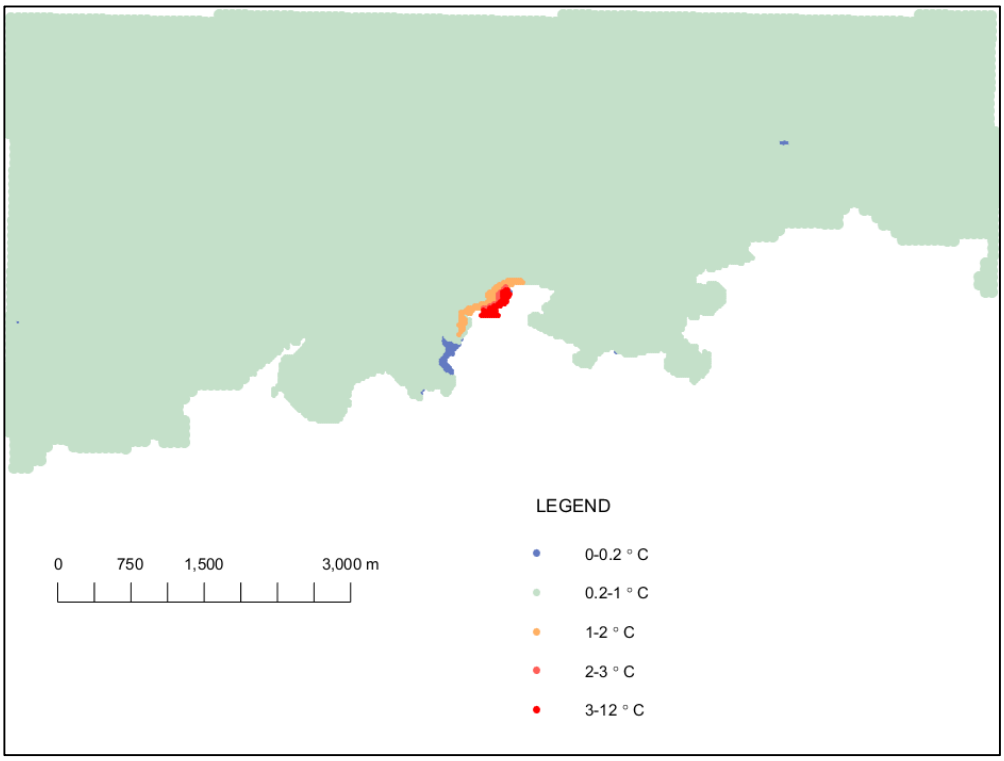

Figure 106 Bed temperature, 98 percentile – Summer base case with typical wave condition.

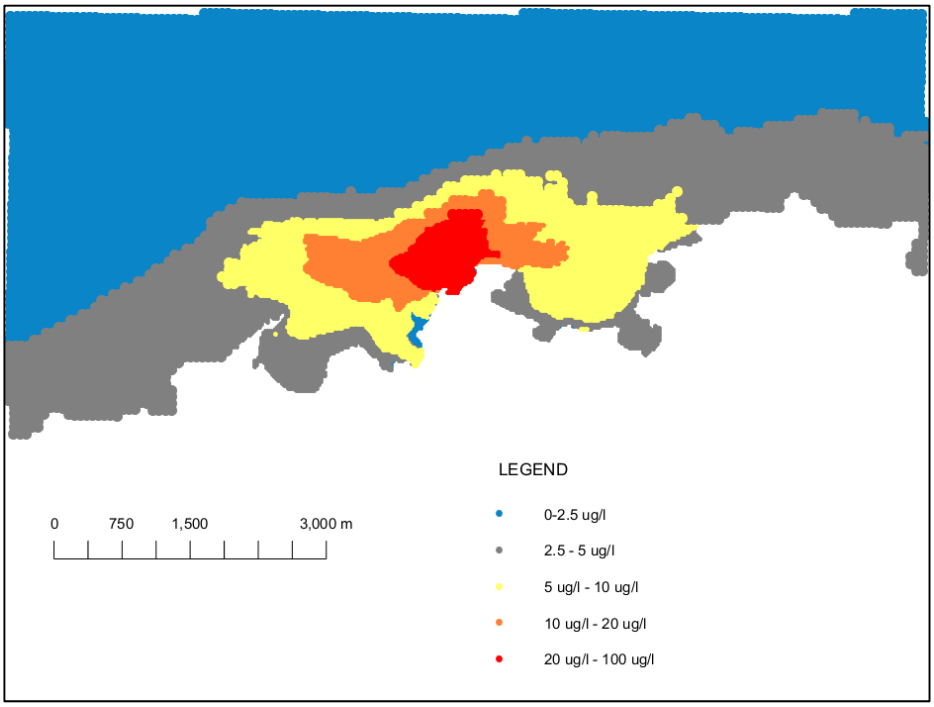

Figure 107 Surface TRO concentration, 95 percentile – Summer base case with typical wave condition.

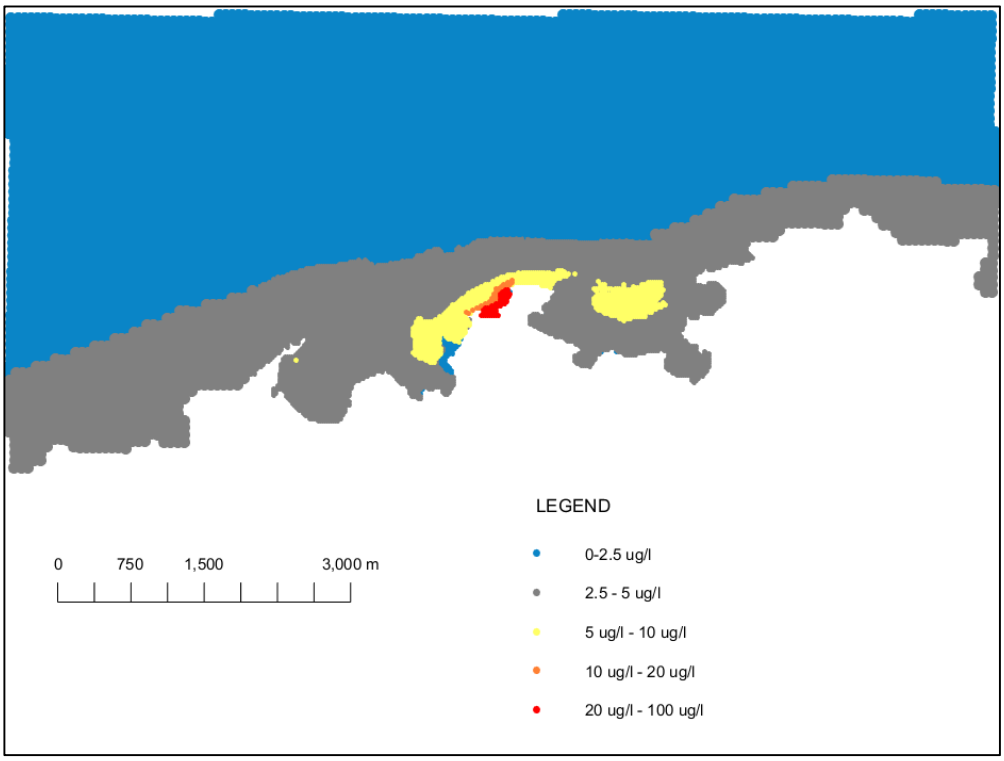

Figure 108 Bed TRO concentration, 95 percentile – Summer base case with typical wave condition.

6.11 Summary of the Wind and Wave Sensitivity Simulations

Model simulations have been completed with and without wind stress influencing the hydrodynamics. A comparison of the results provides a measure of the sensitivity of the predicted mixing zones to the inclusion of wind. The area of the 2 °C temperature rise and the 10 µg/l (0.01 mg/l) TRO mixing zone for the variable wind and summer base cases are detailed in Table 20. The tidal and surface heat flux conditions are the same for both simulations.

Table 20 Area of mixing zone: temperature and TRO for summer base case with variable wind and constant wind cases.

Metric	Mixing Zone Area (Hectares)						
	Summer Base Case	Variable Wind case	Summer South Wind	Summer North Wind	Summer West Wind	Summer East Wind	No Wind Typical wave
2°C Rise Surface	227	97.4	47.8	225	97.8	154	150
2°C Rise Bed	3.5	4.1	3.7	0.7	4.2	3.7	4.0
0.01 mg/l TRO Surface	313	129	80.0	239	139	213	188
0.01 mg/l TRO Bed	4.8	5.7	4.8	7.6	6.6	5.0	6.2

The inclusion of a wind with a constant direction from either of the north, south, east or west reduced the predicted extent of the surface mixing zones as defined in Table 20. This reduction in the area of the surface mixing zone is generally associated with a small increase at the bed, resulting from the effect of wind stress on downward mixing of the buoyant plume.

Despite the general reduction noted above, the mixing zone defined by the 3 ˚C temperature rise for winds from the north was found to increase compared to the summer base case. This is due to the winds constraining the plume more onshore, allowing temperatures close to the outfall to rise.

The imposition of a wind with variable direction (with an average magnitude equivalent to the long-term average) reduces the size of the surface mixing zones and increases the size of the mixing zone at the bed compared to the summer base case (no wind). The size of the mixing zone at the bed remains relatively small with the variable wind case.

The greatest difference is observed in the extent of the TRO mixing zone where the area at the surface is reduced from 313 to 129 hectares. The extent of the mixing zone at the bed shows an increase from 4.8 to 5.7 hectares with the variable wind case compared to the summer base case.

The variable wind mixing zones have an area between those of the no wind base case and the constant southern wind case. The variable wind case mixing zones are smaller than those for the constant north or east wind cases and are similar in size to the mixing zones from the west wind case.

The addition of a wave representative of the high end of typical conditions results in a reduced mixing zone at the surface and an increased mixing zone at the bed. The reduction in the surface mixing zone is less than that associated with a variable wind condition and similar to that for a constant wind from the north or west. The increase in the TRO mixing zone at the bed is less than the change found with a constant wind from the north. The 2 ˚C temperature rise mixing zone at the bed is similar to the base case and wind sensitivity studies.

Overall the conclusion is that the no wind base case is conservative, and that the inclusion of wind and waves reduces the size of the mixing zones at the surface, and that while the bed mixing zone increased for some sensitivity studies, the changes were small.

6.12 Simulation with a Tidally Varying CW Condition

The main CW discharge simulations have used a fixed discharge condition of 126 m^3/s and a temperature rise of 12 °C. Practical pumping systems may not deliver a constant flow, and the flow delivered by a fixed speed pump will vary with the head it provides. The head will vary at a coastal site as the delivery level will usually be fixed but the intake level will vary with the tide. While the flow will vary with tidal conditions the heat to be rejected in the plant condensers will be constant (as will the heat flux to the sea) and therefore the temperature between intake and outfall will also vary. With higher intake water levels the flow will increase and the temperature rise decrease with the opposite occurring as the intake water level falls.

A model run has been undertaken to simulate a tidally varying CW flow. The model included a representation of the proposed breakwater and intake systems. The CW discharge was introduced into the model over eight cells in-order to represent the near field mixing. The ambient seawater temperature was representative of the summer, i.e.14.6 °C.

The model was run in excess temperature mode with a wind speed of 5.6 m/s which is the mean measured at RAF Valley from the western sector. The wind drag was set to zero and therefore wind stress did not influence the hydrodynamics. The surface heat flux was 21.7 $W/m^2/K$, representative of the average for the summer season. The TRO decay rate was set to 10.08 per day.

The CW conditions were set to vary over time depending on the water level at the inlet. The CW flow and temperature rise have been defined at the Lowest Astronomic Tide (LAT) and the flow at Highest Astronomic Tide (HAT) (Table 21). Flow conditions at intermediate water levels were calculated by assuming a constant heat rejection at the condenser and a linear variation of flow with water level.

Table 21 CW flow and temperature rise for LAT and HAT.

Condition	Water Level (m OD)	Flow (m^3/s)	Temperature Rise (°C)
HAT	3.90	130	10.4
LAT	-3.60	113	12.0

For both the model spin up and main model runs, the intake water level predicted in the summer base case was used to calculate a CW flow and temperature rise every hour assuming a linear variation between the conditions listed in Table 21.

6.12.1 Tidally Varying CW – Temperature Rise

The mixing zone implied by the extent of the 3 °C 98 percentile rise at the surface (Figure 109) has an approximate area of 73.3 hectares. The 2 °C 98 percentile rise at the surface has an approximate area of 178 hectares, while the 1 °C 98 percentile rise has an area of approximately 666 hectares. Compared to the summer base case, the variable CW flow 2°C 98 percentile mixing zone is 21% smaller at the surface.

The mixing zone at the bed implied by the extent of the 3 °C 98 percentile rise area (Figure 110) is approximately 2.7 hectares and is limited to an area around the proposed outfall and along the western edge of Wylfa Head. The areas of the 2 °C and 1 °C 98ile rises at the bed are approximately 3.6 hectares and 6.2 hectares respectively. The size of the 2 °C mixing zone is similar to that for the summer base case (which was 3.5 hectares).

6.12.2 Tidally Varying CW – TRO

The mixing zone implied by the extent of the 10 µg/l 95 percentile contour (Figure 111) has an approximate area of 284 hectares. The variable CW flow mixing zone at the surface is 9% smaller than that of the summer base case.

The area of the bed with a TRO 95 percentile concentration greater than 10 µg/l is limited to the vicinity of the outfall and a strip along the western side of Wylfa Head with an area of approximately 5.2 hectares (Figure 112). The variable CW flow mixing zone is 8% larger than that of the summer base case.

6.12.3 Tidally Varying CW – Recirculation

The depth-averaged temperature rise for a model cell (141,64) approximately in the middle of the CW forebay has been calculated from a simulation of the period 15 August 2011 to 1 September 2011.

In Table 22 the mean, 98 percentile and maximum temperature rise above ambient at the intake are listed.

Table 22 Recirculation statistics – Tidally varying CW.

Statistic	Temperature rise above ambient (°C)
Average	0.42
98 percentile	0.70

Maximum	0.76

Compared to the equivalent fixed CW condition case, recirculation is reduced using a variable CW condition.

6.12.4 Summary of the Variable CW Condition Simulations

The variable CW condition simulation resulted in a reduced extent of the 2°C mixing zone at the surface and a small increase in extent at the bed. For the TRO mixing zone, a similar pattern is observed, with a reduction in area at the surface of 28.3 hectares, and increase at the bed of 0.37 hectares.

The TRO mixing zone area is similar to that of the summer base case. This might be expected because the TRO is simulated as a constant concentration unlike the temperature rise that varies with the flow rate. The average flow in the simulation is 121m^3/s which is only slightly (4%) lower than the 126m^3/s in the summer base case.

Overall it can be concluded that the use of a constant CW condition in the modelling is a conservative assumption.

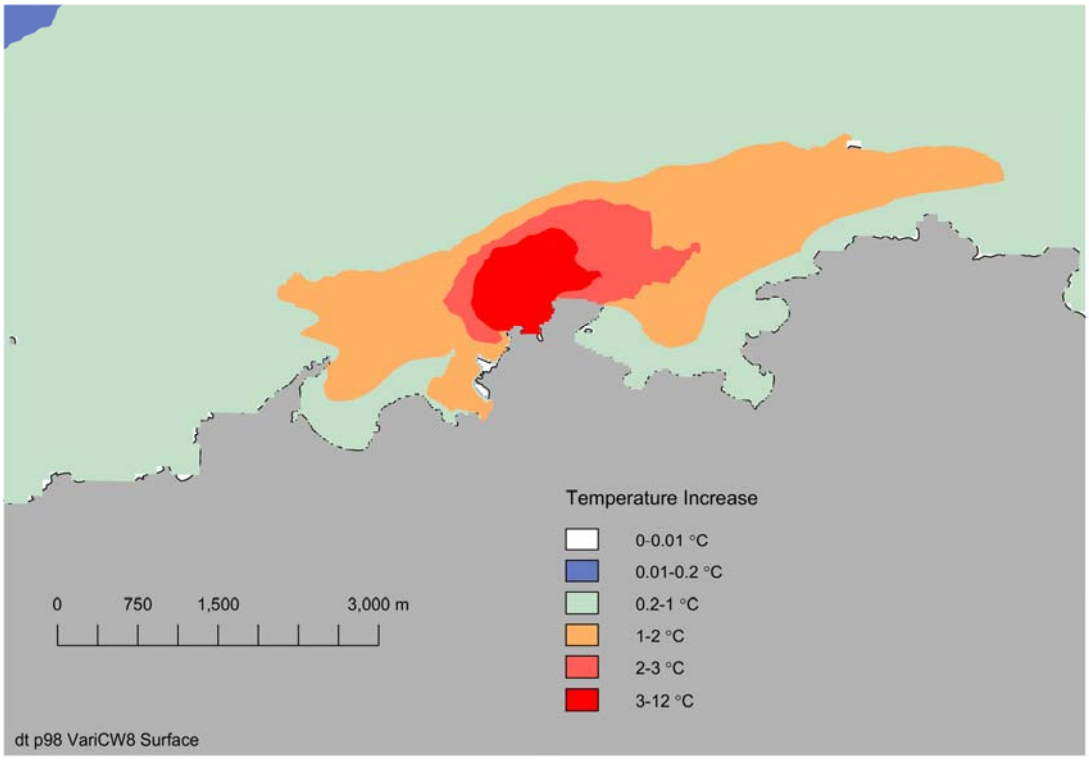

Figure 109 Surface temperature, 98 percentile – Tidally varying CW condition.

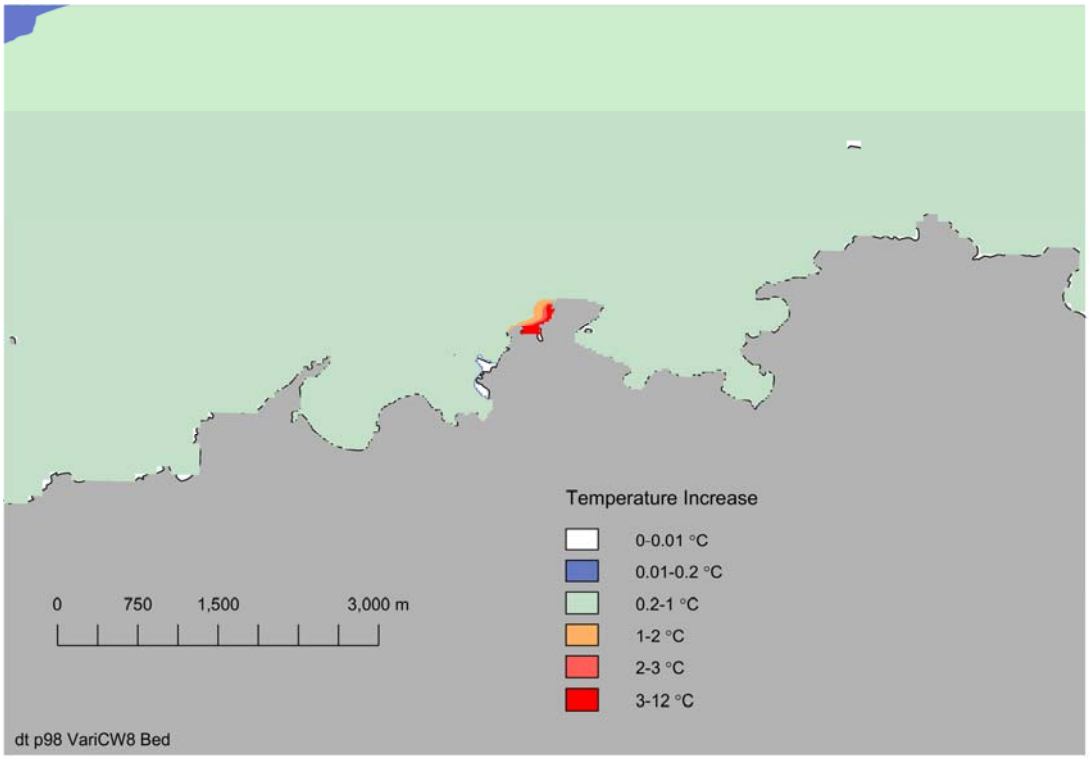

Figure 110 Bed temperature, 98 percentile –Tidally varying CW condition.

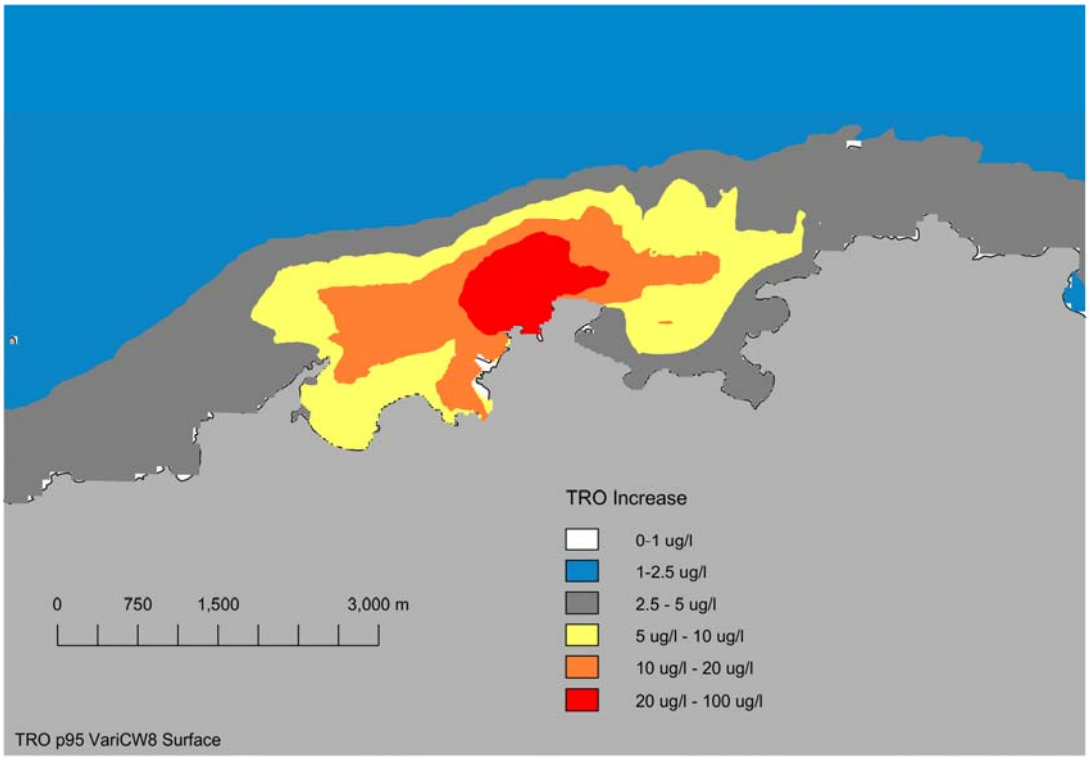

Figure 111 Surface TRO concentration, 95 percentile – Tidally varying CW condition.

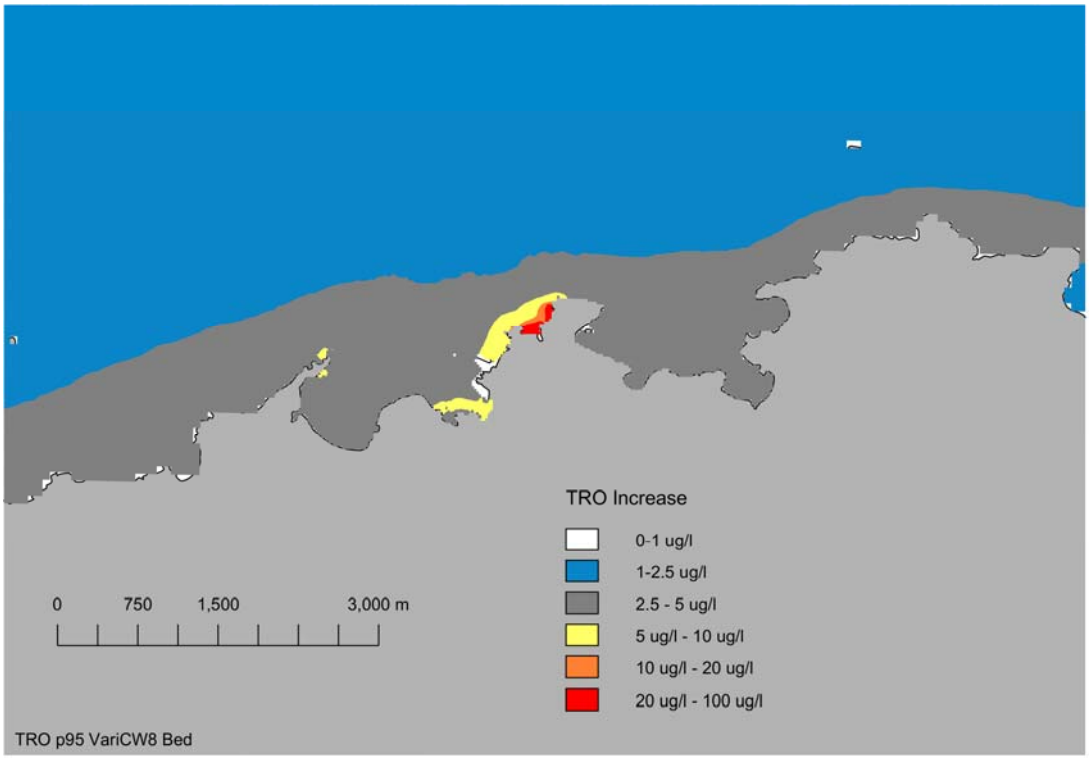

Figure 112 Bed TRO concentration, 95 percentile – Tidally varying CW condition.

6.13 Dilution Studies

Some model runs have been completed using a conservative tracer in addition to the temperature and TRO discharge. Conservative tracer runs allow the model to be used to predict dilution of the discharge, the output of which can be used in other studies such as the H1 screening.

The simulations of the summer season, including the sensitivity studies, were set up with a discharge of a conservative tracer. The tracer was discharged at a concentration of 100 units and was included in model spin up runs so that the predicted concentrations simulate the dilution with long-term operation of the CW discharge. Running the model with the tracer alongside temperature means that the model includes the influence of buoyancy on the mixing of the tracer.

The model run statistics were generated for the same period as the summer seasonal cases and therefore cover a full spring neap cycle.

6.13.1 Average Dilution

The average dilution (calculated by dividing the discharge concentration by the long-term mean concentration of the conservative tracer) at the surface and bed are plotted in Figure 113 and Figure 114 respectively.

The lowest mean surface dilution of 1.05 occurs close to the outfall. At 100 m from the outfall the mean dilution increases to 1.2. Further offshore at a distance of 500 m from the outfall, the mean dilution is 4.9.

Comparatively, at the bed the lowest mean dilution is 1.7 (again occurring close to the outfall). At 100 m from the outfall the mean dilution increases to 5.1, while further offshore at a distance of 500 m from the outfall, the mean dilution is 50.

6.13.2 Minimum Dilution

The minimum dilution (calculated by dividing the discharge concentration by the long-term maximum concentration of the conservative tracer) at the surface and bed over the summer spring neap cycle are plotted in Figure 115 and Figure 116 respectively.

The minimum dilution at the surface is 0.96 (i.e. the maximum concentration at the surface is greater than the concentration of tracer added to the discharge); this can result from recirculation (as the tracer discharge is modelled as an increment above the intake concentration) and/or stratification of the plume.

At 100 m from the outfall the minimum dilution is 1.02. Further offshore at a distance of 500 m from the outfall, the minimum dilution is 2.08.

The minimum dilution at the bed is 1.7, occurring at the outfall. At 100 m from the outfall the minimum dilution is 2.5 and at 500 m from the outfall this increases almost tenfold to 24.4.

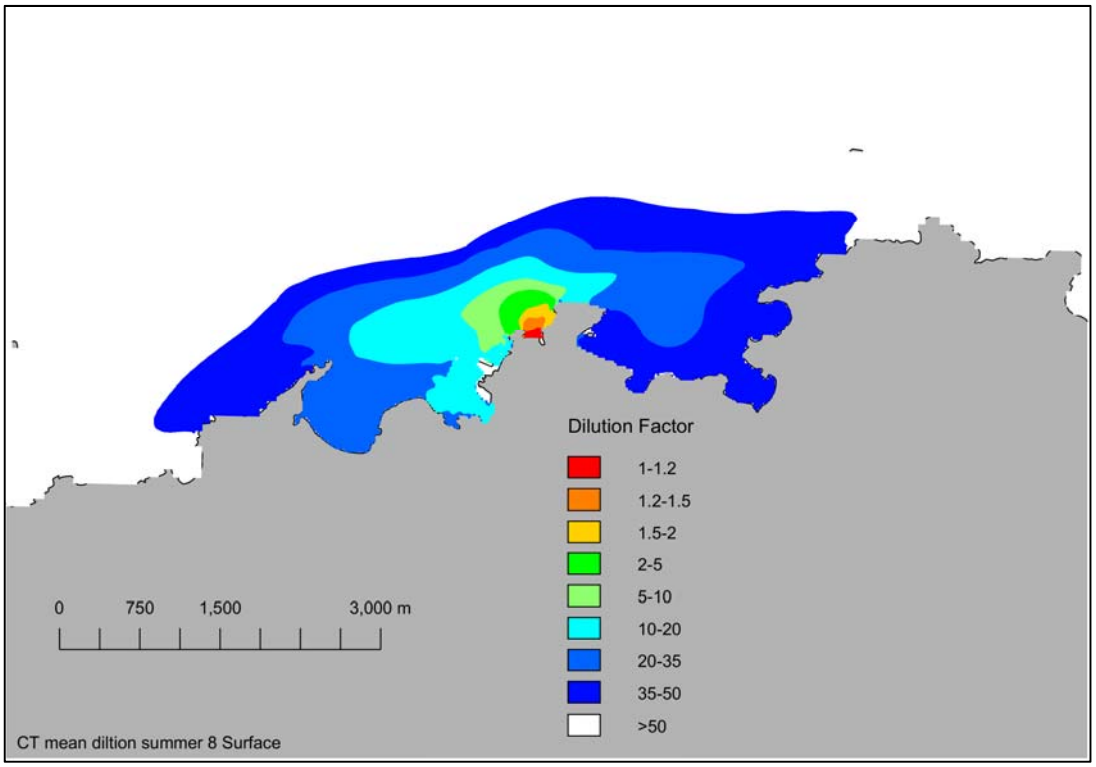

Figure 113 Average dilution: surface.

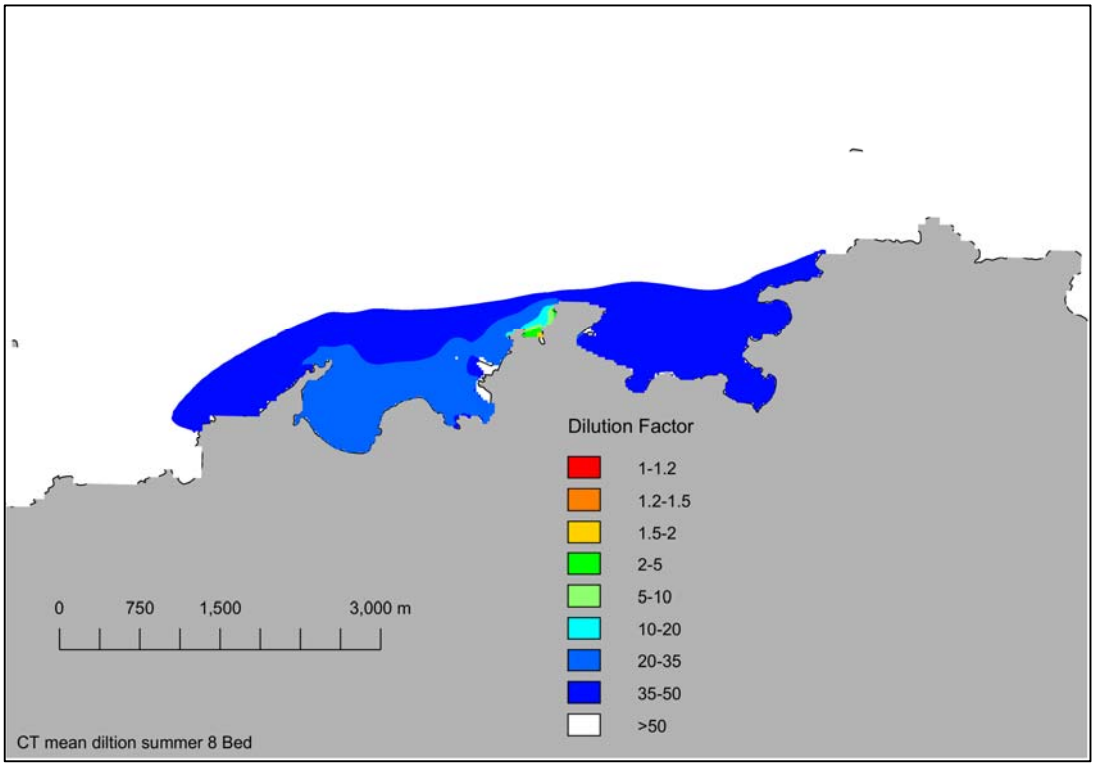

Figure 114 Average dilution: bed.

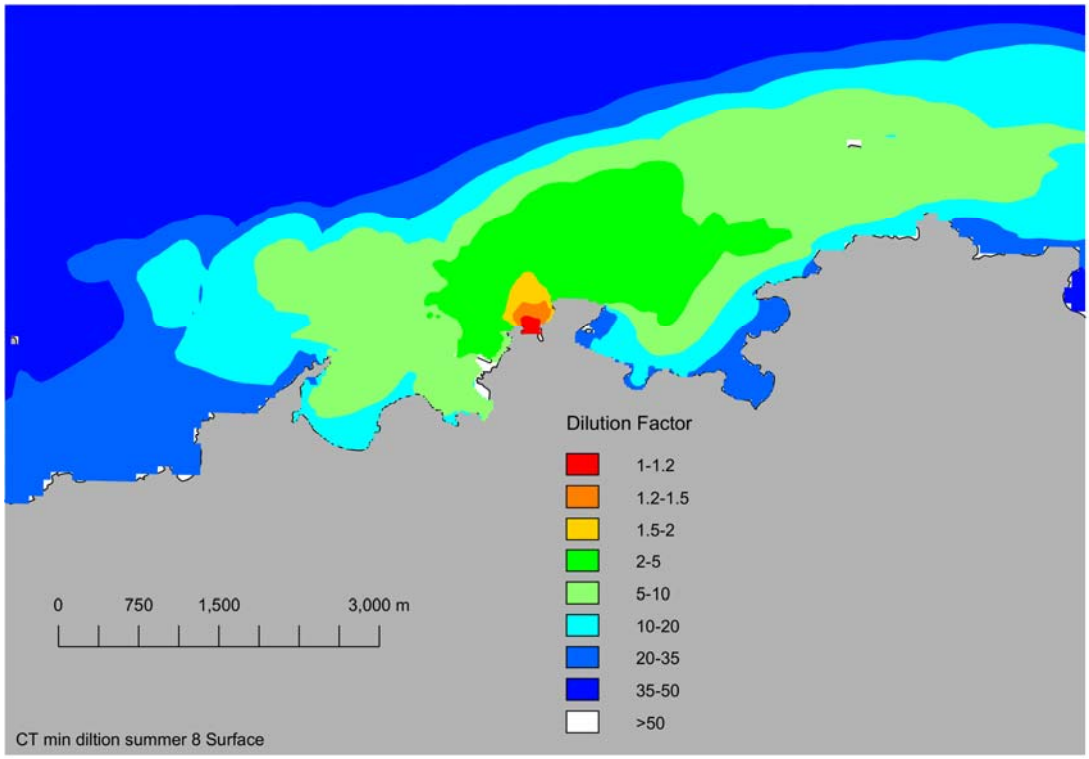

Figure 115 Minimum dilution: surface.

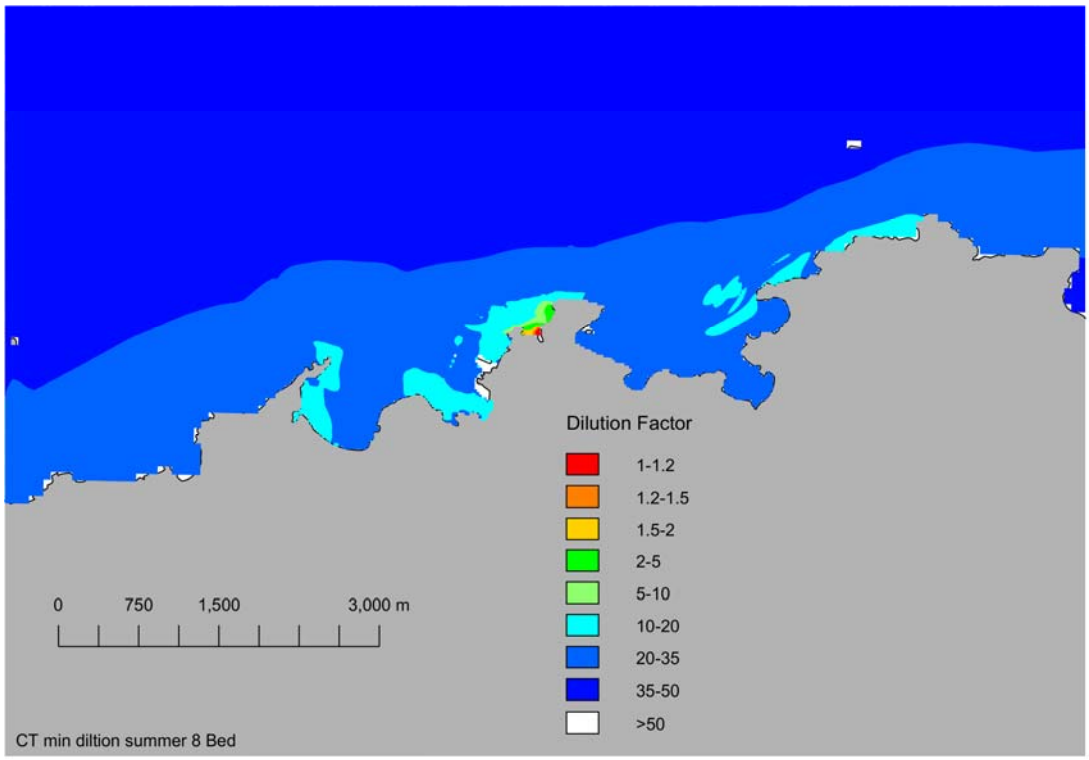

Figure 116 Minimum dilution: bed.

6.13.3 Summary of Dilution

Table 23 summarises the predicted dilution at distances of 100 m and 500 m from the outfall.

Table 23 Predicted dilutions at 100 m and 500 m from the outfall.

Location	Distance from the outfall	
	100 m	500 m
Surface Mean	1.3	8.0
Surface Minimum	1.1	2.1
Bed Mean	5.1	35
Bed Minimum	2.9	22

The mean and minimum dilution is greater at the bed than at the surface because of the buoyancy of the CW plume. Within 100 m of the outfall there is little dilution at the surface (average of 1.3 and minimum of 1.1), whilst at the bed the dilution is approximately four times greater than at the surface (average dilution at the bed at 100 m from the outfall is 5.1 and the minimum is 2.9). The buoyancy of the discharge still has an influence on dilution at a distance of 500 m from the outfall, where the mean and average dilution at the surface are around five times less than the equivalent statistic at the bed. The average of the dilution at the surface and bed is detailed in Table 24.

Table 24 Average of surface and bed dilutions at 100 m and 500 m from the outfall.

Location	100 m	500 m
Mean	3.2	21.5
Minimum	2.0	12.05

6.14 Further sensitivity studies

Model simulations were carried out to validate the outputs for a number of design change parameters. The purpose of the runs was to ensure that the existing model outputs were reflecting a worst case scenario and could be assessed as such.

The design changes considered were an increased intake length (174m as opposed to 100m), an increased intake channel dredge depth of 1m from -10m to -11m AOD and a MOLF with a continuous quay wall (as opposed to two loading berths with a revetment design between them).

An additional sensitivity scenario was completed with a 20m east/west shift in the western breakwater. The output of this run showed the surface temperature and TRO plumes to increase up to 10%, and as such was rejected.

Outputs for surface temperature and TRO are presented in

Figure 117 and Figure 118, respectively, to allow comparision between summer base case and the sensitivity scenario reflecting the three proposed design changes.

6.14.1 Extent of the temperature mixing zone

Figure 117 shows that in comparisons between the original and design change summer base case scenarios, the surface temperature plots are very similar, particularly in terms of the overall 3 ºC 98 percentile rise at the surface. A slight difference is evident in the extent of encroachment of the 2-3 ºC contour into the area behind the western breakwater which is slightly increased (to a distance of up to 75m) in the design change scenario compared to the original summer base case. There are also several small extensions / retractions of the 2-3 ºC contour border in the order of 25 to 50m at discrete points along the southern boundary as it crosses Cemaes Bay.

The changes in the 98 percentile temperature rise statistics at the surface are summarised in Table 25. The outputs show relatively small changes to the overall temperature contour areas. The changes at the bed, although not plotted, are summarised in Table 26, and again indicate minor reductions in the contour areas.

Table 25 : Sea surface temperature rise summary statistics- original and design change sensitivity summer base cases.

Surface temperature rise (98%ile)	Original summer base case area (ha)	Design sensitivity change area (ha)
1°C	741	720
2°C	227	222
3°C	89	86

Table 26 : Sea bed temperature rise summary statistics- original and design change sensitivity summer base cases.

Bed temperature rise (98%ile)	Original summer base case area (ha)	Design sensitivity change area (ha)
1°C	6.6	6.3
2°C	3.5	3.3
3°C	2.7	2.6

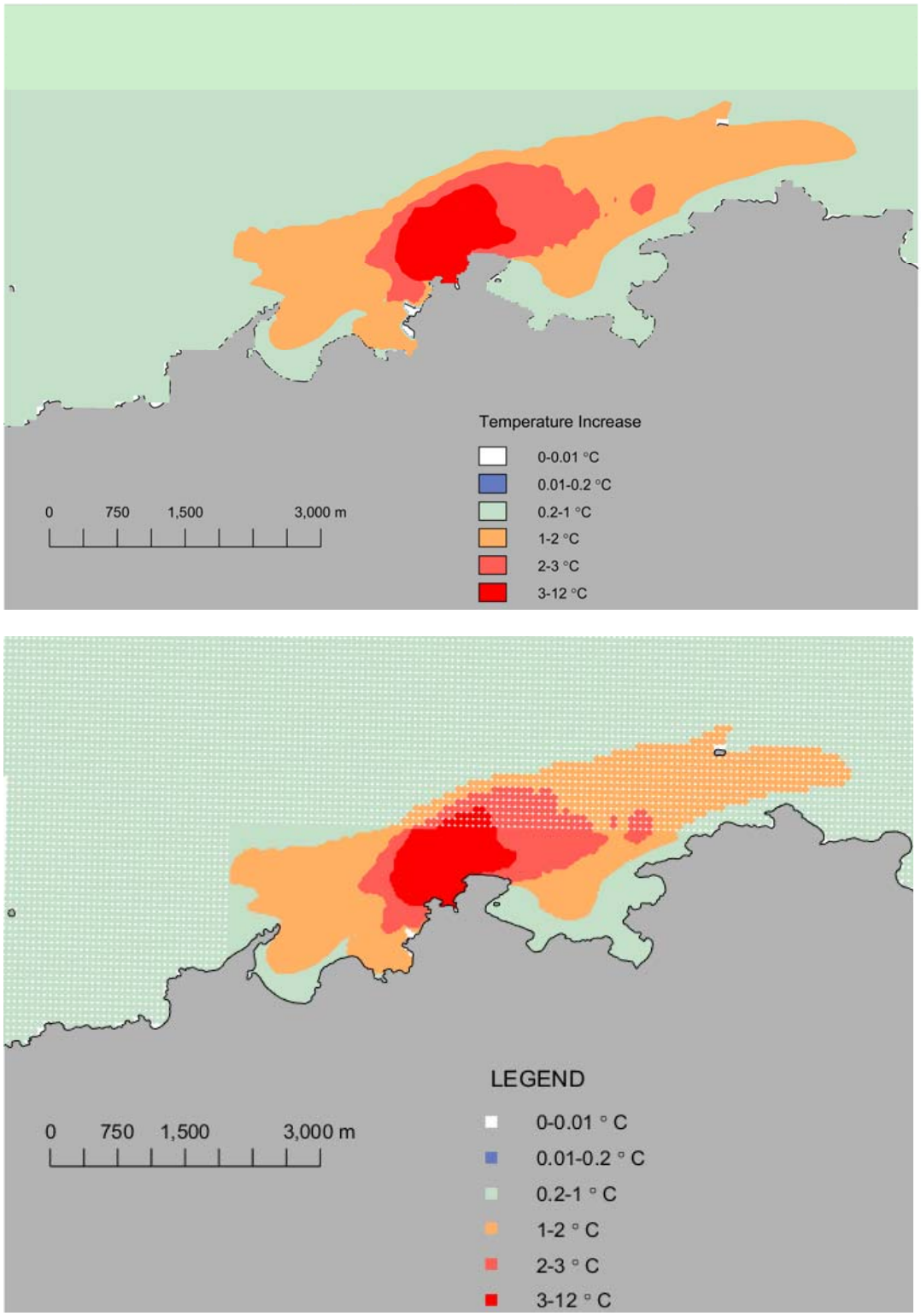

Figure 117 : Surface temperature increase- with summer base case (top) and design change sensitivity scenario (bottom).

6.14.2 Extent of TRO mixing zone

Figure 118 shows that the overall footprint of both the original and design change summer base case scenarios for surface TRO are very similar. There is a slight change to the shape of the 0.02-0.05 mg/l contour border, in the form of a narrow prominence extending towards the western coastline adjacent to the Power Station in the order 75m, but the overall extents of the TRO plots are comparable. Table 27 provides a summary of the original summer base case and the design change case. The results for the design change case indicate very little change in the area of the 0.01mg/l surface TRO contour. Although not plotted, the changes at the bed are summarised in Table 28, and again show minor reductions in the contour areas.

Table 27 : Sea surface TRO 95%ile summary statistics- original and design change sensitivity summer base cases.

Surface TRO (98%ile)	Original summer base case area (ha)	Design sensitivity change area (ha)
0.01 mg/l	313	307

Table 28 : Sea bed TRO 95%ile summary statistics- original and design change sensitivity summer base cases.

Bed TRO (98%ile)	Original summer base case area (ha)	Design sensitivity change area (ha)
0.01 mg/l	4.8	4.7

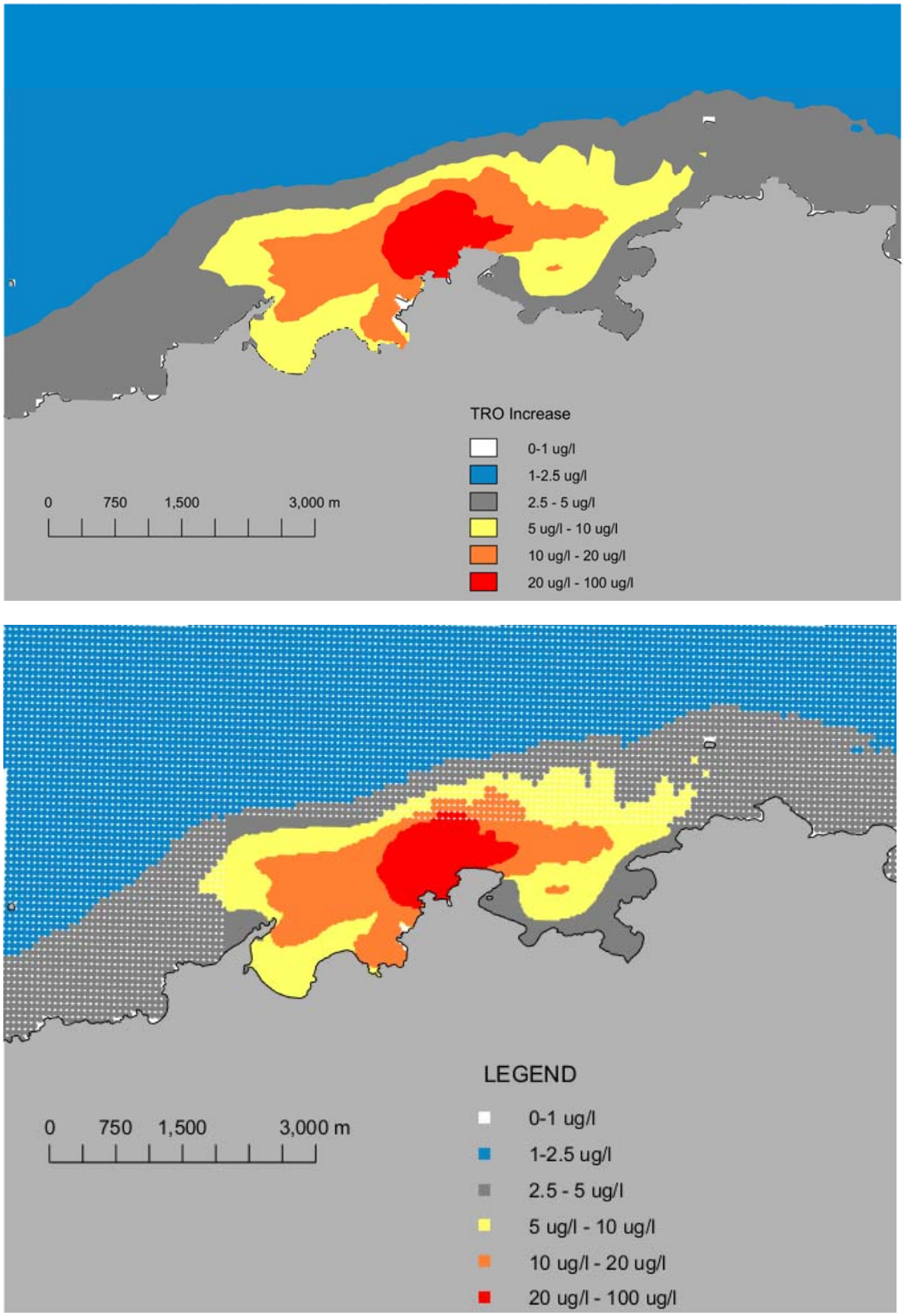

Figure 118 : Surface TRO increase plots with summer base case (top) and intake sensitivity scenario (bottom).

7. Annual Temperature Rise and TRO Statistics

7.1 Statistical Model of Seawater Temperature

Horizon has used a long-term (ten year) record of monthly average water temperature around Wylfa Head combined with temperature data sampled at ten-minute intervals to develop a statistical model of seawater temperature (Horizon, 2012e). The higher frequency data were measured at a number of moorings which were deployed over a full year.

The ambient temperature varies over a range of timescales from tidal to annual. The seasonal variation is approximately 8 °C. This is greater than the tidal variation which is at most 0.5 ˚C. The temperature was correlated with the tidal state, the relationship varying over the year.

In January the tidal range of temperature was between 0.2 °C to 0.5 °C with a peak approximately an hour before High Water (HW) and a minimum around Low Water (LW). In May the tidal range was up to 0.4 °C with peaks around HW and minimum temperature around LW. In July there was a tidal range of about 0.4 °C, with the minimum occurring an hour or so before LW. Maximum temperatures occurred either side of HW with local minima at HW, the local minimum being higher than the overall tidal minimum which occurred an hour before LW.

7.2 Hydrodynamic Modelling

The factors influencing the mixing of the CW discharge are tidally driven flows and surface heat losses for temperature and TRO decay rates for the biocide. The temperature modelling has been undertaken using the so-called excess temperature approach where the model is set up to predict the excess temperature above ambient due to the discharge rather than the actual temperature. The surface heat loss varies with meteorology and the ambient water temperatures, and hence exchange rates will vary between seasons. TRO decay rates also vary with the seasonal differences in water temperature and quality.

A range of model runs have been undertaken to both explore the sensivity of the predicted temperature rise and TRO fields resulting from long term operation of the Wylfa Newydd CW system and generate predicted changes for direct use in case making.

Where actual temperatures and TRO on an annual basis are required these have been computed by combining a statistical model of ambient water temperature with a prediction of the temperature rise over a year. To obtain the prediction of the rise over the course of the year simulations using seasonally appropriate surface heat loss rates have been combined to provide maps showing the 98 percentile annual increase in water temperature. These maps can be used directly to predict the size of the annual temperature rise mixing zone. Each of the seasonal simulations were run for long enough to allow the thermal and TRO fields to fully develop and used the average surface heat loss and TRO decay rate for the season. The seasonal simulations were run without the influence of wind stress on the water surface and with a fixed CW discharge rate and temperature rise.

The simulations used to explore the sensitivity of the predicted temperature & TRO fields to surface heat loss, wind stress, wave action, representation of the CW plume near field and CW pump characteristics were undertaken using one of the model set ups of the four seasons used in the annual case. The base case used for the sensitivity studies was the summer season- the summer being choosen because the surface heat loss coefficient is the same as the average for the year.

The sensitivity studies have shown that the base case is generally conservative (as regards the influence of wind, waves and CW flux) and fairly insensitive to the assumptions on surface heat flux and source representation.

As noted previously, the modelling has simulated a representative tidal variation for surface heat loss and TRO decay rates appropriate for the four main seasons. The relevant quality standards are expressed as annual statistics and therefore a method is required to combine the output of the individual seasonal simulations to represent the variation over a full year.

The seasonal simulations predicted temperature and TRO concentrations at each cell at an hourly resolution for a representative spring-neap cycle.The use of spring-neap cycle (approximately 14 days) captured the influence on mixing of the discharge due to variation in tidal flow. The ambient water temperature was set to a representative value for each season while the ambient TRO concentration was set to zero. For each simulation adequate time was allowed prior to storing model output for the hydrodynamics to settle and for TRO and temperature to reflect long-term operation of the Power Station CW discharge.

The annual statistics of TRO and temperature rise were calculated by combining within the Delft3d modelling environment the four seasonal results files (the temperature files were converted to rise above ambient before concatenation). The surface and bed temperature and TRO were then exported to MATLAB format and statistics calculated using the same MATLAB scripts as the seasonal simulations.

See Section 8.1. for further information on the method.

7.2.1 Annual Case: Temperature Rise

The annual 98 percentile temperature rise at the surface and bed are plotted as Figure 119 and Figure 120 respectively.

The mixing zone implied by the extent of the 3 °C 98 percentile rise at the surface has an approximate area of 88.1 hectares. The 2 °C 98 percentile rise at the surface has an approximate area of 209 hectares, while the 1 °C 98 percentile rise has an area of approximately 692 hectares. The mixing zones for the annual case are similar in extent to those for the summer base case.

The mixing zone at the bed implied by the extent of the 3 °C 98 percentile rise area is approximately 3.3 hectares and is limited to an area around the proposed outfall and along the western edge of Wylfa Head. The area of the 2 °C and 1 °C 98ile rise at the bed is approximately 4.2 hectares and 7.6 hectares respectively.

7.2.2 Annual Case: TRO

The annual 95 percentile TRO concentration at the surface and bed are plotted as Figure 121 and Figure 122 respectively. The mixing zone implied by the extent of the 10 µg/l 95 percentile contour has an approximate area of 248 hectares. The area is 80% of the equivalent for the summer base case (313 hectares).

The area of the bed with a TRO 95 percentile concentration greater than 10 µg/l is limited to the vicinity of the outfall and a strip along the western side of Wylfa Head with an area of approximately 5.6 hectares.

7.2.3 Annual Case – Full extent

The wider extent of the plume above the background is shown in Figure 123 to Figure 126. The extent of temperature increase above the background is very similar to that of the summer base case, and extends for a large area (approximately 60 km), predominantly to the north west of the intake/outfall area. However, this increase is small, with maximum increases of 0.2 °C. The same pattern can be seen for increase in TRO values; however, the extent is smaller (approximately 20 km). Here the maximum increase is 2.5 µg/l.

7.2.4 Annual Simulation: Summary

The annual 2 °C temperature rise mixing zone is 92% of that for the summer base case. The area of the TRO mixing zone is also smaller than the summer base case. The reduction in the TRO surface mixing zone is greater (80% of the base case) than the reduction in temperature rise. The areas of the annual mixing zones at the bed are similar to the summer base case.

The similarity in the annual temperature rise mixing zone and summer simulation mixing zones is probably as a result of the average flux over the four seasons being 21.7 $W/m^2/K$, which is the same as the summer flux. The difference between the size of the 10 µg/l 95 percentile TRO mixing zone reflects the influence of the seasonal variation in TRO decay rates.

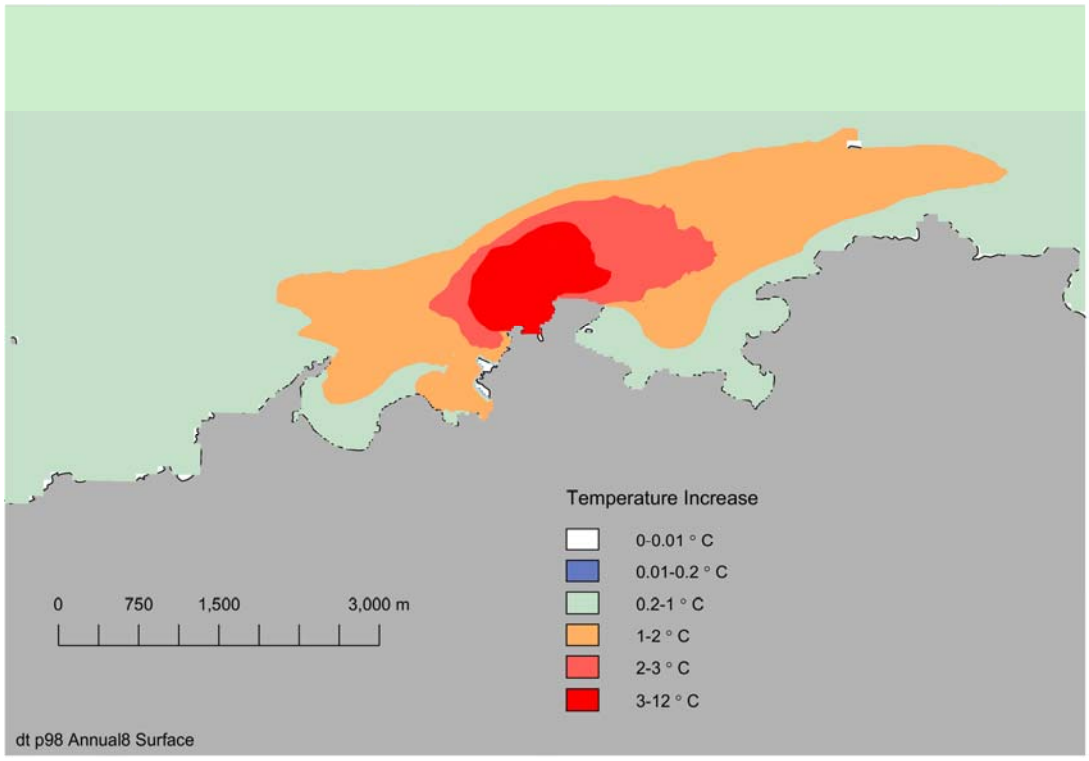

Figure 119 Annual 98 percentile temperature rise at the surface.

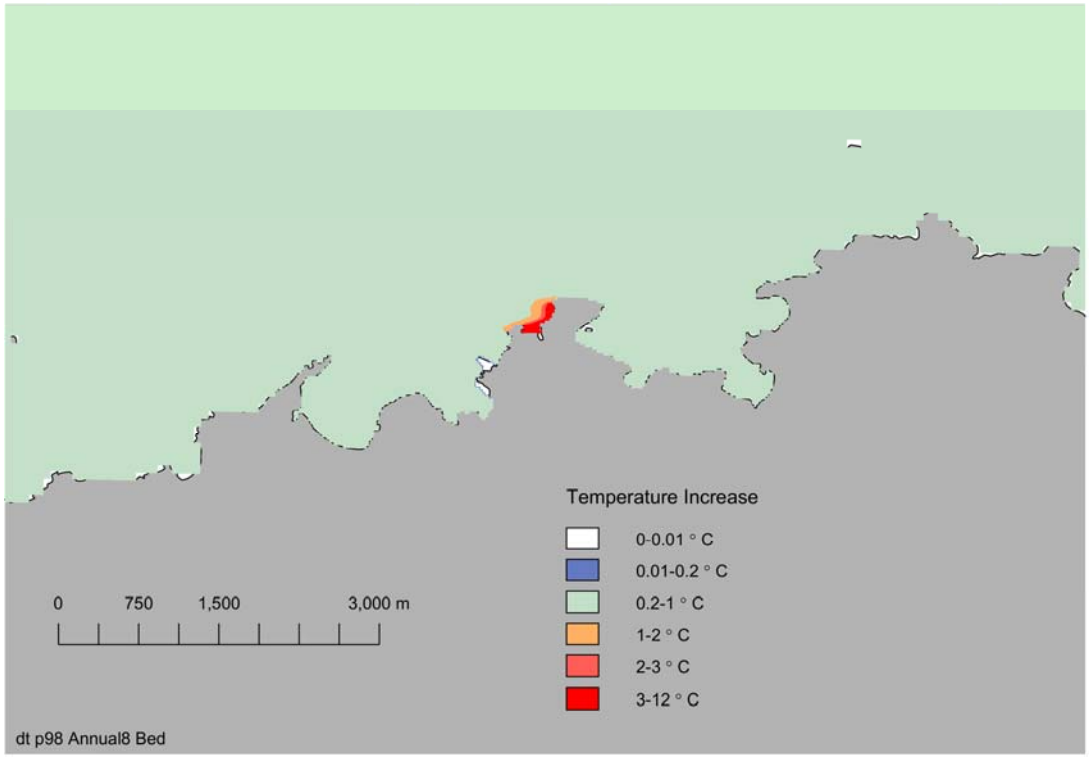

Figure 120 Annual 98 percentile temperature rise at the bed.

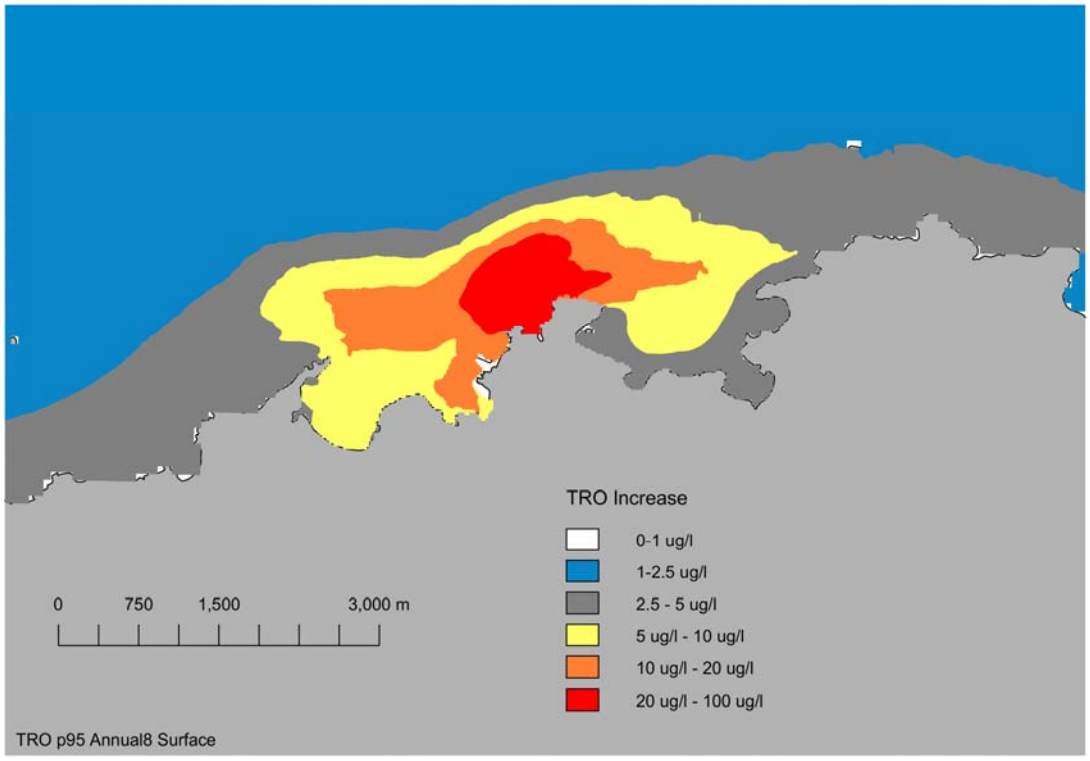

Figure 121 Annual 95 percentile TRO concentration at the surface.

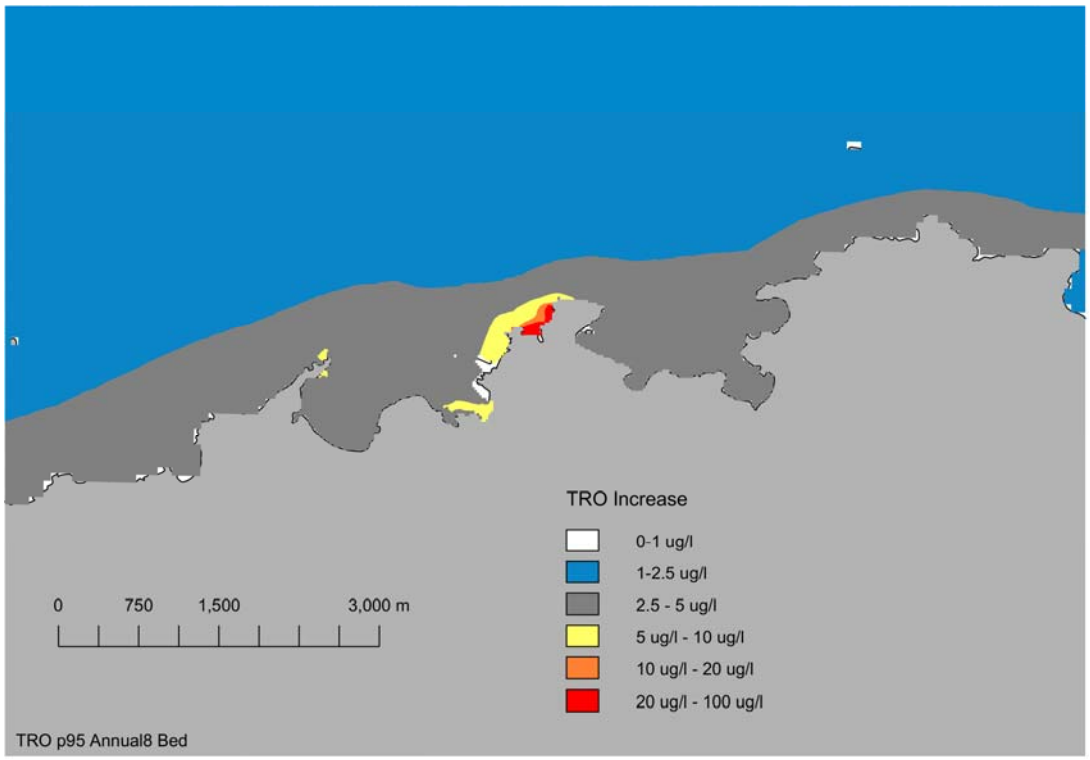

Figure 122 Annual 95 percentile TRO concentration at the bed.

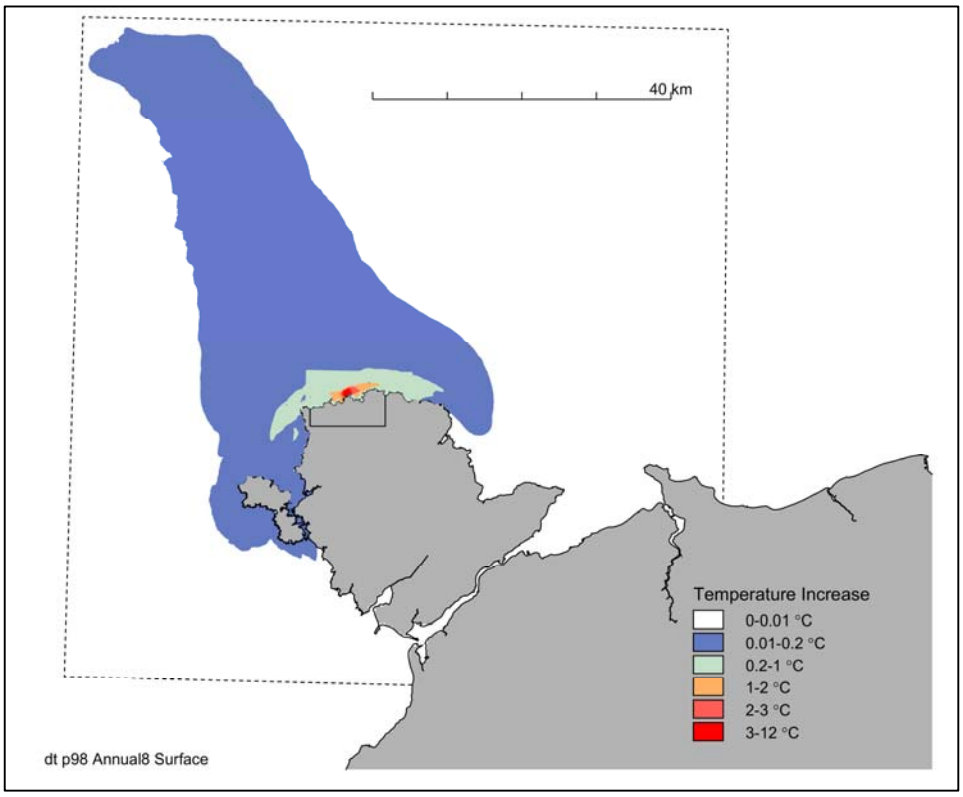

Figure 123 Surface temperature, 98 percentile - Annual case, wide extent.

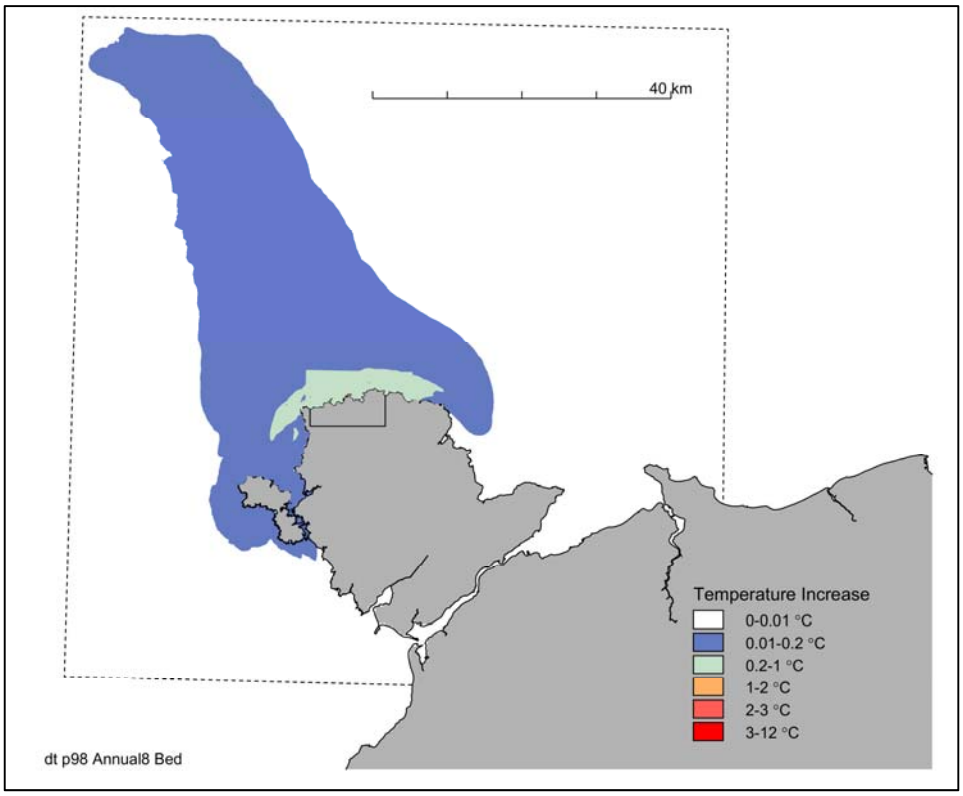

Figure 124 Bed temperature, 98 percentile - Annual case, wide extent.

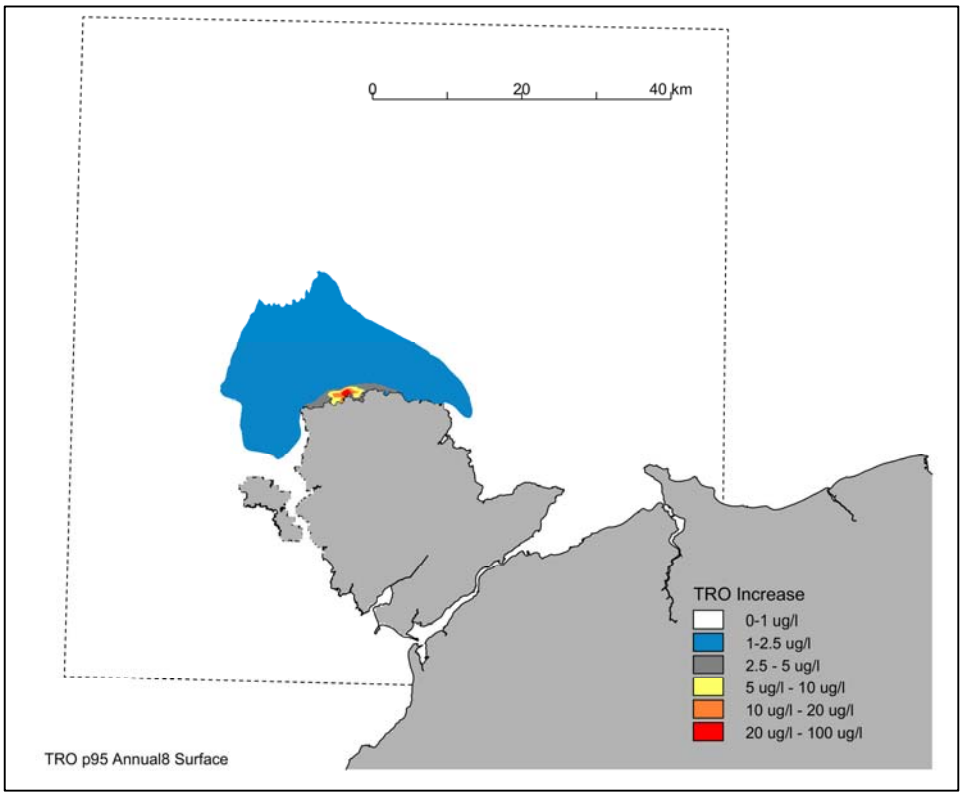

Figure 125 Surface TRO concentration, 95 percentile - Annual case, wide extent.

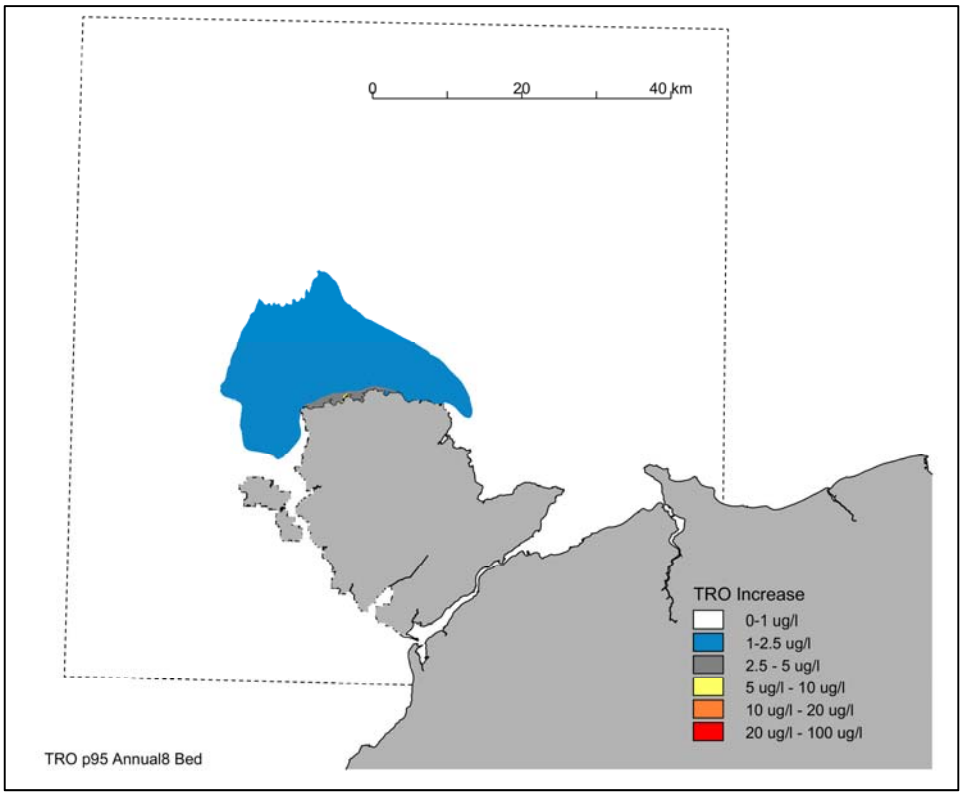

Figure 126 Bed TRO concentration, 95 percentile – Annual case, wide extent.

8. Total Temperature (ambient plus station operation)

8.1 Combining the Modelled Temperature Rise with the Statistical Model

See Section 7 for further information on the base case modelling assumptions.

Before combining the ambient temperature data and temperature rise model output, it is necessary to consider what correlations if any are likely to exist between the two data sets.

Although there is a correlation between the temperature rise and tide for the modelled temperature rise, this correlation will vary with location. For example, at a site east of Wylfa Head the CW plume will be advected past on the flood tide whereas for a site to the west of the outfall it is more likely to experience the plume on the ebb tide. The ambient temperature also shows a correlation with the state of the tide. Maximum temperatures at the offshore site tended to show a maximum around high water with a minimum around low water. The exact timing of the maximum and minimum varied over the year.

When the total temperature is calculated the annual base case simulation is used.

To combine the ambient temperature and predicted increase it is convenient to ignore any correlation between the ambient temperature and temperature rise and assume the data sets are independent. This assumption can be justified given the tidal variation in ambient temperature is relatively small compared to the increase above ambient necessary to exceed 23 °C.

For example the 98 percentile ambient from the statistical model is 16.44 °C. For the water to exceed 23 °C as a 98 percentile implies a constant rise of 6.56 °C (23 °C – 16.44 °C). This temperature rise is large compared to the tidal variation in temperature at the offshore site, which was at most around 0.5 °C.

Maps showing the predicted 98 percentile water temperature with the long-term operation of the CW discharge have been produced by combining the ambient 98 percentile with the maximum rise from the CW discharge over the year. The combination of an annual 98 percentile and the maximum rise results in a conservative estimate of the area of a given temperature 98 percentile with the Power Station in operation.

8.1.1 Predicted Annual Temperatures

The predicted annual 98 percentile temperature at the surface and bed are plotted in Figure 127 and Figure 128 respectively. The 98 percentile mixing zones with a temperature greater than 23 °C is approximately 14.6 hectares respectively. The area of the 23 °C 98 percentile mixing zones at the bed are limited to the immediate vicinity of the outfall in Porth Wnal. Close to the outfall it is likely that the design of the outfall structure will influence the mixing of the discharge and hence the size of the temperature mixing zone.

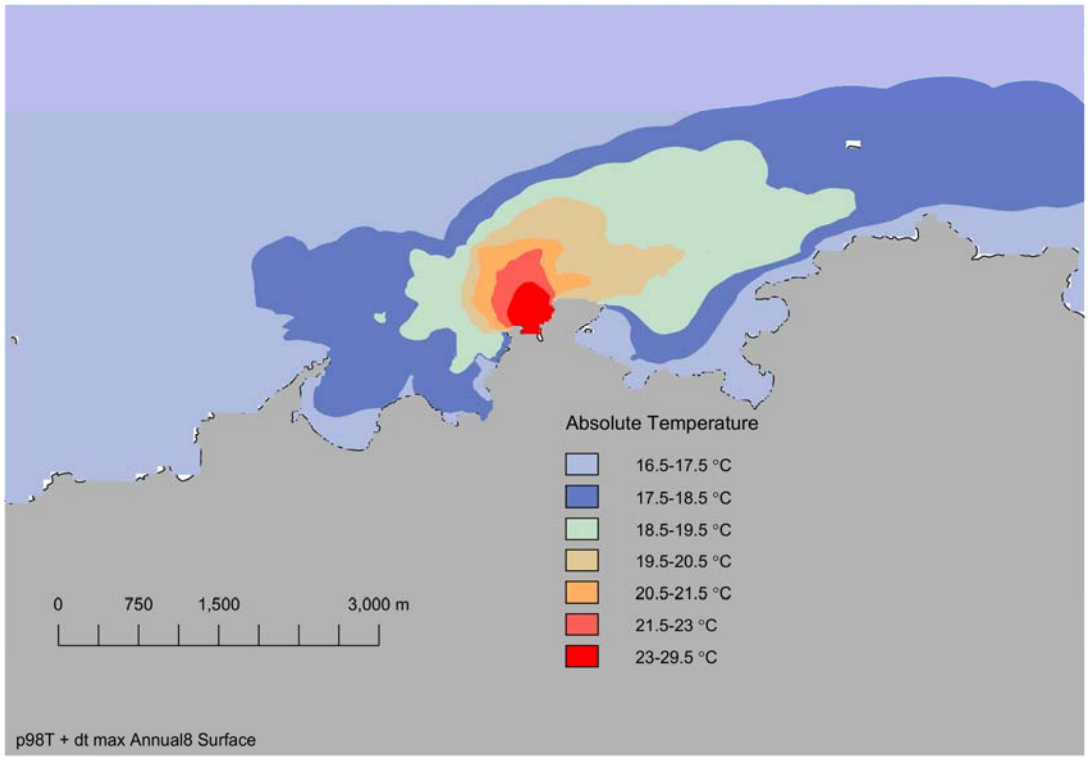

Figure 127 98 percentile ambient water temperature with maximum temperature rise: surface.

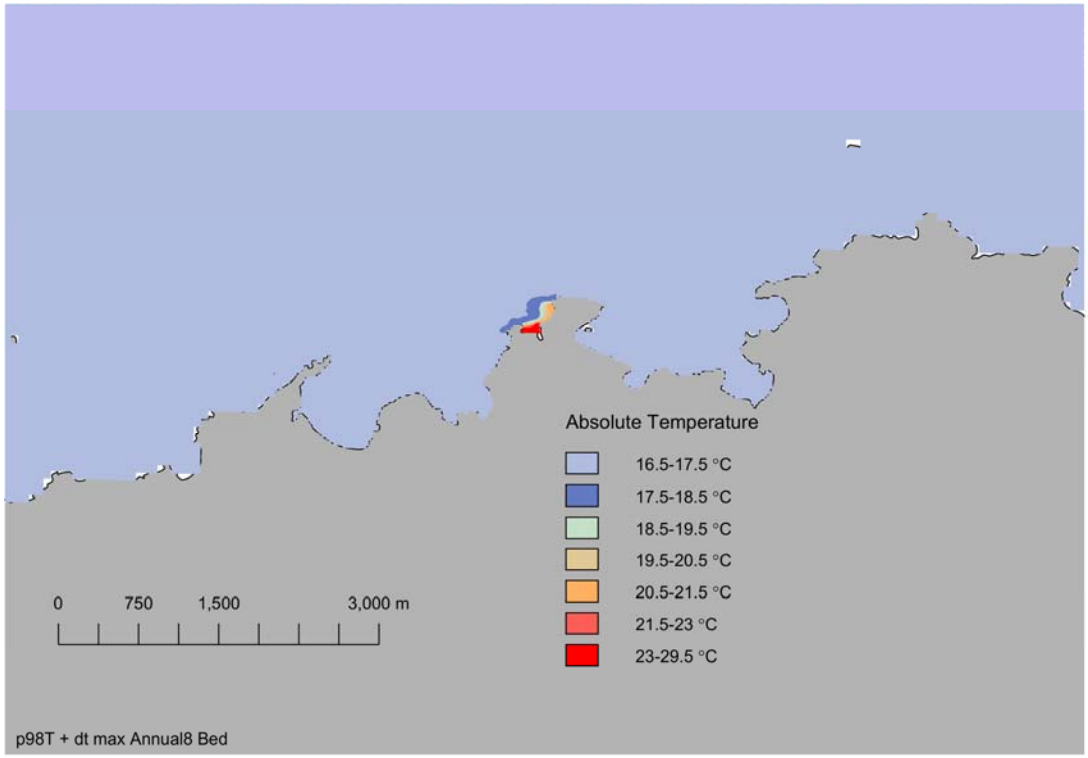

Figure 128 98 percentile ambient water temperature with maximum temperature rise: bed.

9. Indirect Influence of the Thermal Discharge on Water Quality

In addition to the direct influence of the CW discharge on water quality, the temperature increase associated with the discharge has the potential to indirectly influence the solubility of oxygen and also the ratio of ionised to unionised ammonia.

9.1 Influence of Temperature on Dissolved Oxygen

The solubility of gases including oxygen in water varies with temperature. As the temperature increases the solubility decreases. Depending on the initial dissolved oxygen (DO) concentration and the temperature increase, there is therefore potential for a reduction in DO with increased water temperatures. Temperature is one factor influencing DO concentrations, but other factors include the organic loads from agricultural runoff and sewage treatment works.

9.1.1 Dissolved Oxygen Standards

For classification under the Water Framework Directive (WFD), the UKTAG has recommended the UKTAG (2008) values as detailed in Table 29.

Table 29 UKTAG (2008) DO Classifications.

Classification	Freshwater (mg/l 95 percentile)	Seawater (salinity=35) (mg/l 95 percentile)
High	7	5.7
Good	5 to 7	4 to 5.7
Moderate	3 to 5	2.4 to 4
Poor	2 to 3	1.6 to 2.4
Bad	2	1.6

Note: UKTAG (2008) provides a figure for interpolation to intermediate salinities.

9.1.2 Measured Dissolved Oxygen in the Waters off Anglesey

DO concentrations and the percent saturation were measured at two long-term mooring buoys (2010 to 2011). The % saturation recorded is plotted in Figure 129.

The average percent saturation for the two moorings was 99.4% (S9) and 94.8% (S2- the further offshore of the two moorings). The average DO concentration at mooring S9 was 9.6mg/l with a 95 percentile of 8.8mg/l.

The observed DO concentration would be therefore be associated with a High Status water body using the UKTAG classification.

9.2 Temperature Change and Implied Change in Saturation Concentration

Modelling has been undertaken to predict the temperature increase due to the thermal discharge from Wylfa Newydd. If it is assumed that the water is saturated the modelled temperature rise can be used to predict the DO concentration at that temperature. In this way the potential for change as a result of the increased water temperature from the operation of the CW discharge can be investigated.

The DO saturation concentration as a function of temperature and salinity has been calculated using a formula due to Benson and Krause (1984) cited in HELCOM (2017)[6]. Assuming a constant salinity of 33.6 (which was the average measured at mooring S9) and a temperature equal to the 95 percentile ambient (16.04 °C) plus the maximum predicted temperature rise (Figure 130).

The minimum predicted DO concentration assuming average salinity and the maximum temperature rise is greater than the WQTAG High Status boundary value of 5.7 mg/l (WQTAG 2006) The minimum saturated DO concentration occurs in the vicinity of the outfall where the temperature increase is greatest. The operation of the CW discharge would not change the classification of the water off Anglesey on the basis of DO.

9.3 Influence of Temperature and pH on the Ratio of Ionised to Unionised Ammonia

Ammonia in water can exist in either an ionised or an un-ionised form. The un-ionised form is typically more toxic to aquatic life. The ratio of ionised to un-ionised ammonia varies with temperature and pH, with an increase in un-ionised ammonia as the temperature increases. The temperature increase from the operation of the CW discharge could alter the ratio.

While UKTAG (2007) proposed new Predicted No-Effect Concentration limits for un-ionised ammonia in UK waters which are lower than the WFD EQS, these were not adopted in the WFD Directions in 2015[7]. The relevant EQS used for un-ionised ammonia is therefore 0.021 mg/l as an annual average.

NRW water quality data collected between 2007 and 2009 in Holyhead Bay and near Turkey Shore, Holyhead reported an average filtered ammonia concentration of 0.0118 mg/l as N. No measurements for unfiltered or unionised ammonia were recorded in the dataset.

Water quality surveys conducted as part of the baseline programme measured a number of parameters between 2010 and 2016. Initially measurements were taken on both flood and ebb stages of the tide at a number of different locations in the waters around Wylfa Head. During the programme, the number of sites and samples were rationalised in response to the data, for example, when the data showed that the values on the flood and ebb tides were identical.

The average of the monthly average ammonia concentration was 0.0293 mg/l as N and for un-ionised ammonia it was 0.00058 mg/l N. The results for unionised ammonia were consistent with a High Status classification under WFD. The average concentrations of ammonia and unionised ammonia show that approximately 2% of the ammonia was in the unionised form.

The average of the filtered ammonia was 0.037 mg/l N, although the majority of values were actually <0.02 mg/l N. Therefore the NRW and baseline filtered ammonia values are reasonably consistent and show low concentrations of ammonia in the seawater.

The observed unionised ammonia ratio is similar to that calculated using the USEPA (1989) formulae[8] . The same formula has been used to calculate the unionised ammonia concentration for a range of temperature increases up to the maximum temperature rise over the CWS (Table 30).

Under all of the potential temperature conditions listed in Table 30, the unionised ammonia remains well below the classification standard of 0.021 mg/l. Therefore the proposed thermal discharge will not result in an increase in unionised ammonia that would change the classification of the local water body.

[7] The Water Framework Directive (Standards and Classification) Directions (England and Wales) 2015
[8] http://www.waterboards.ca.gov/waterrights/water_issues/programs/bay_delta/docs/cmnt081712/srcsd/engleatt2.pdf

Table 30 Unionised Ammonia Concentration as a function of temperature.

Condition	T (°C)	T (K)	pH	Salinity	Ratio- Unionised/ Total Ammonia	Unionised Concentration (mg/l)
Average ambient	11.78	284.93	8.07	34.3	0.020	0.00060
Average + 12°C	23.78	296.93	8.07	34.3	0.048	0.00142
Max Ambient	16	289.15	8.07	34.3	0.028	0.00081
Max Ambient + 12°C	28	301.15	8.07	34.3	0.065	0.00191

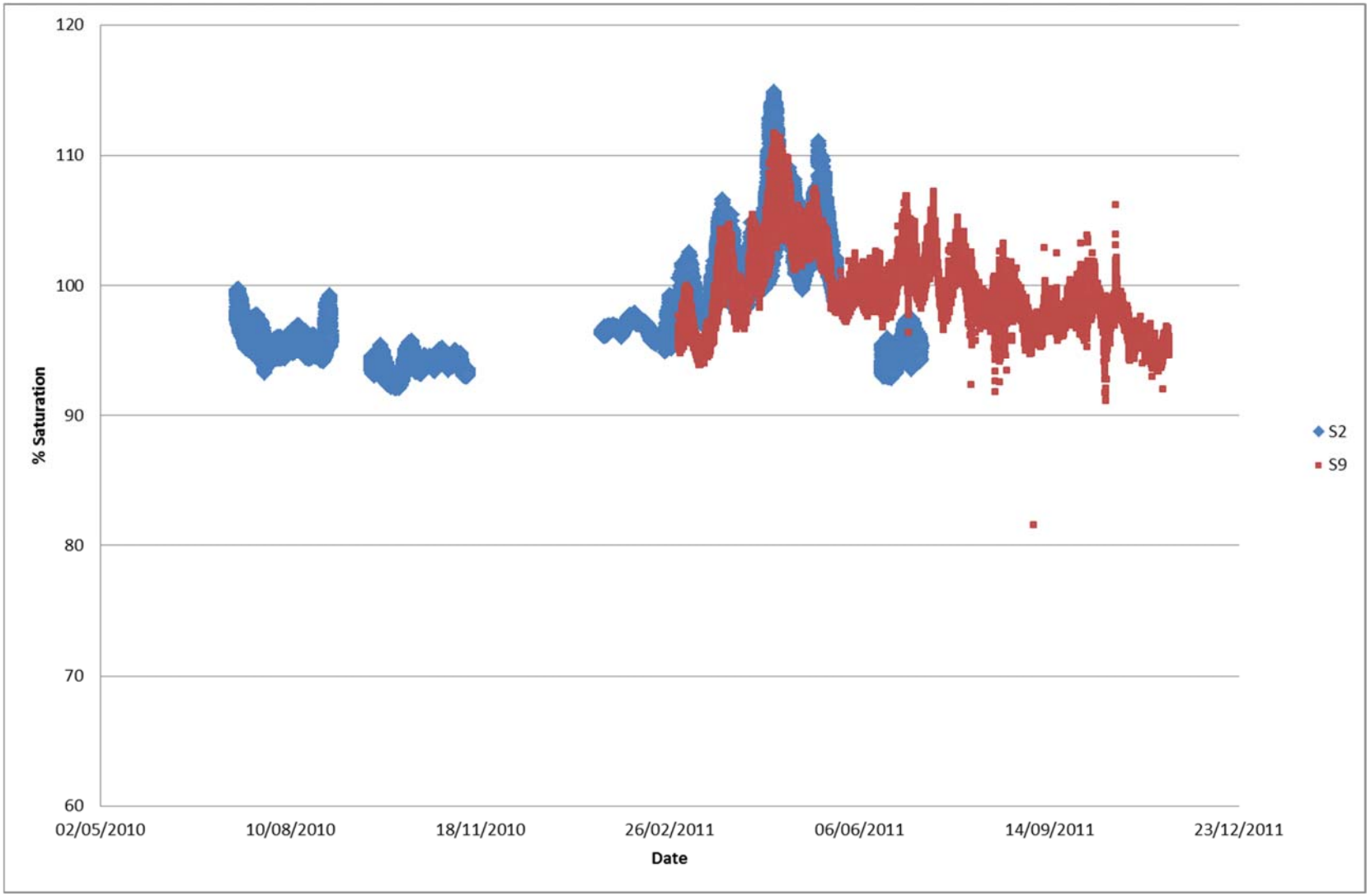

Figure 129 DO % saturation (2010-2011).

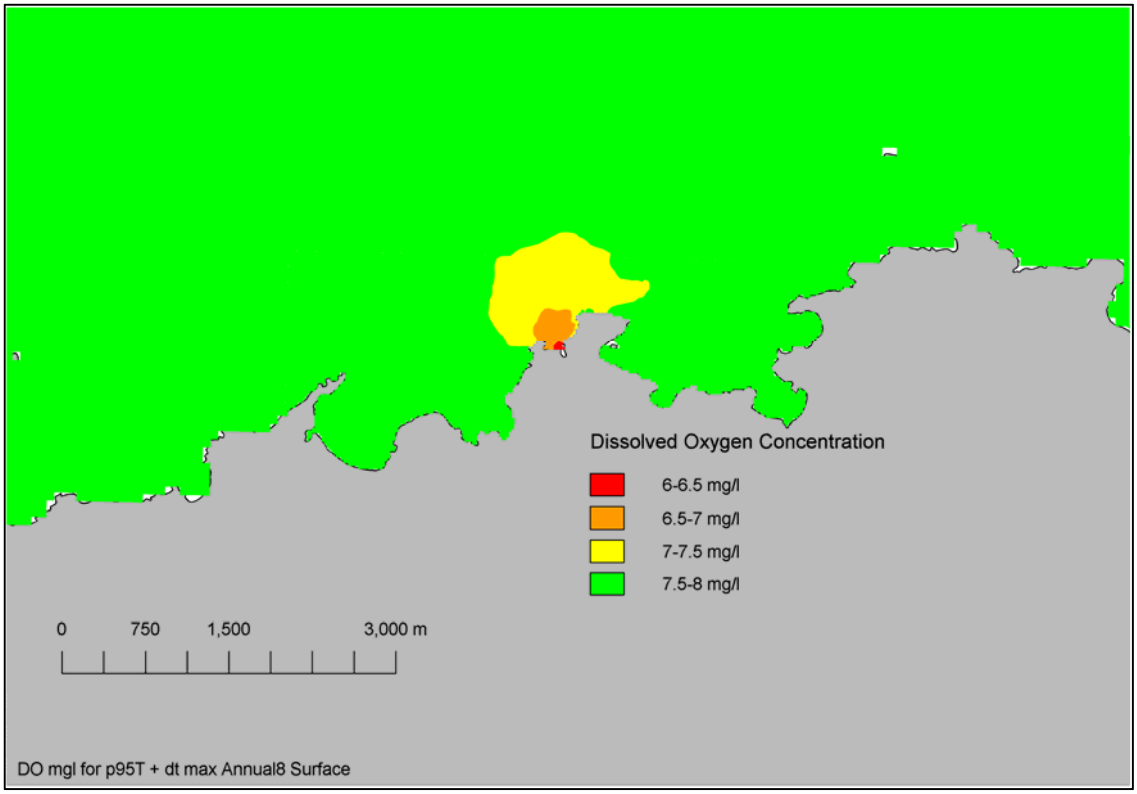

Figure 130 95 percentile DO concentration (mg/l): ambient plus maximum rise.

10. Chlorinated By-products

The dosing of chlorine-based biocides is known to give rise to a range of persistent Chlorination By-Products (CBPs). When dosing seawater with chlorine, it reacts with the bromide ion in seawater to form bromine. In coastal waters the subsequent reactions are bromine-based unless there is significant ammonia present (BEEMS 2011a).

While the oxidising constituents decay due to reactions with organic constituents of the seawater, some persistent reaction products are formed and it is these that are grouped under the term chlorination by-products (CBP). An extensive overview of the chemical reactions, toxicology and field data for CBPs in European waters was carried out in BEEMS 2011a.

10.1 Environmental Standards for Chlorination By-Products

In the BEEMS (2011a) review of chlorination by-products it is noted that there is no published European quality standard for the commonly encountered CBPs. The only relevant statutory environmental quality standard (EQS) was that for chloroform for which an EQS of 2.5 µg l^{-1} (2500 ng/l) expressed as an annual average applied. In the Netherlands an interim bromoform standard is applied in the Rotterdam area of 16 µg l^{-1} expressed as a 24-hr average over the full water column at 1,000 m from a discharge (BEEMS 2011a).

Taylor (2006) cited in EDF (2011) suggested a Predicted No -Effect Concentration value of 5 µg l^{-1} (500,000 ng/l) for bromoform which was used in the consenting of Hinkley C. This value has been adopted for the present study of Wylfa Newydd CBPs.

10.2 Chlorination By-Product data for Wylfa

Jacobs has undertaken an extensive water quality survey on behalf of Horizon. The survey included measurements of CBPs in the seawater around Wylfa during a period (2012 to 2013) when the Existing Power Station was generating electricity. The Existing Power Station, which used chlorination as a biocide, had two reactors; one ceased operation in April 2012 while the second continued operation until December 2015. Hence during the baseline water quality survey a single unit was in operation.

Figure 131 details the water quality sampling sites targeted during the baseline monitoring programme (see appendix D13-1, Water quality and plankton Report, Application Reference Number: 6.4.83 and Titan, 2012). A summary of the chloroform results is detailed in Table 31.

The chloroform concentrations measured at the near surface are consistently higher than those from deeper in the water column. Higher values near the surface would be consistent with CBPs from a buoyant CW discharge. Near surface concentrations are lower during February to April than in the other months. Assuming that the chloroform is associated with the Magnox CW discharge this could be due to either an outage or suspension of chlorination during the winter. All of the individual measured values are lower than the chloroform EQS.

A summary of the bromoform results is detailed in Table 32. The bromoform concentrations measured at the near surface are consistently higher than those from deeper in the water column. Higher values near surface would be consistent with CBPs from a buoyant CW discharge. As with the chloroform concentrations, near surface bromoform concentrations are lower during February to April than in the other months. Assuming that the bromoform is associated with the Existing Power Station CW discharge, this could be due to either an outage or suspension of chlorination during the winter.

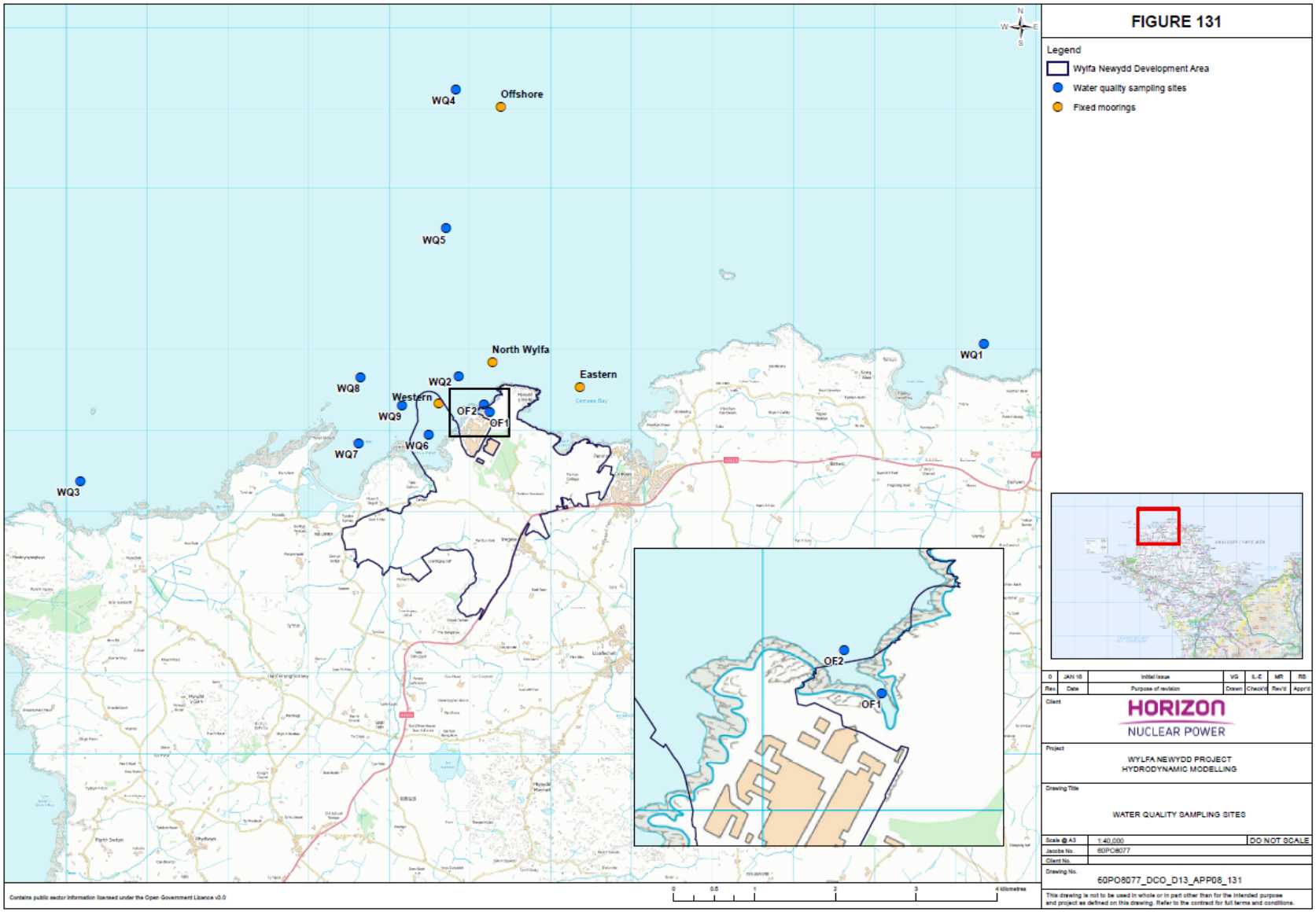

FIGURE 131

Legend

- Wylfa Newydd Development Area
- Water quality sampling sites
- Fixed moorings

Rev.	Date	Purpose of revision	Drawn	Checkd	Rev'd	Appr'd
0	JAN 16	Initial issue	VG	IL-E	MR	RB

Client: HORIZON NUCLEAR POWER

Project: WYLFA NEWYDD PROJECT
HYDRODYNAMIC MODELLING

Drawing Title: WATER QUALITY SAMPLING SITES

Scale @ A3	1:40,000	DO NOT SCALE
Jacobs No.	60PO8077	
Client No.		

Drawing No.: 60PO8077_DCO_D13_APP08_131

Table 31 Baseline chloroform (ng/l) data.

Month	WQ1	WQ1	WQ2	WQ2	WQ3	WQ3	WQ4	WQ4	WQ5	WQ5	WQ6	WQ6
Depth (m)	1	15.9	1	14.5	1	9.1	1	21.3	1	23.9	1	7.5
May-12	24	<1	11	<1	6.6	<1	8.8	<1	<1	<1	8.8	1.7
Jun-12	12	<1	7.7	<1	8.1	2.2	17	<1	10	<1	19	<1
Ju/l2	35	<1	25	1.2	31	<1	26	<1	22	<1	40	<1
Aug-12	30	<1	20	<1	29	<1	31	<1	23	<1	27	3.2
Sep-12	21	3.1	33	4	27	3.8	34	2	26	2.2	22	2.6
Oct-12	13	<1	14	<1	9.5	<1	15	<1	10	<1	17	<1
Feb-13			2.6				3.4		2		1.5	
Mar-13			1.2				3		2.4		2.7	
Apr-13			3.6				2.4		4		2.9	
May-13			16				25		20		13	
Jun-13			10				21		33		16	
Ju/l3			23				31		38		29	
Aug-13			33				40		44		26	
Sep-13			29				47		50		39	
Oct-13			26				17		21		18	

Table 32 Baseline bromoform (ng/l) data.

Month	WQ1	WQ1	WQ2	WQ2	WQ3	WQ3	WQ4	WQ4	WQ5	WQ5	WQ6	WQ6
Depth (m)	1	15.9	1	14.5	1	9.1	1	21.3	1	23.9	1	7.5
May-12	24	<1	11	<1	6.6	<1	8.8	<1	<1	<1	8.8	1.7
Jun-12	12	<1	7.7	<1	8.1	2.2	17	<1	10	<1	19	<1
Ju/l2	35	<1	25	1.2	31	<1	26	<1	22	<1	40	<1
Aug-12	30	<1	20	<1	29	<1	31	<1	23	<1	27	3.2
Sep-12	21	3.1	33	4	27	3.8	34	2	26	2.2	22	2.6
Oct-12	13	<1	14	<1	9.5	<1	15	<1	10	<1	17	<1
Feb-13			2.6				3.4		2		1.5	
Mar-13			1.2				3		2.4		2.7	
Apr-13			3.6				2.4		4		2.9	
May-13			16				25		20		13	
Jun-13			10				21		33		16	
Ju/l3			23				31		38		29	
Aug-13			33				40		44		26	
Sep-13			29				47		50		39	
Oct-13			26				17		21		18	

10.3 Production and Mixing of Bromoform and Chloroform

In the absence of predicted bromoform concentrations for the Wylfa Newydd CW discharge, an estimate has been made making use of data from other UK power plant. In BEEMS (2011a) the maximum reported bromoform concentration in a UK power plant discharge was for Heysham nuclear Power Station on the west coast (average of 29.2 $\mu g l^{-1}$). As such, a bromoform discharge concentration at Wylfa Newydd of 30 $\mu g\ l^{-1}$ has been assumed, which is likely to be a conservative assumption because the proposed use of chlorine biocide at Wylfa Newydd would be reduced compared to other power plant, as it would follow best practice with regards to tailoring dosing regimes to biofouling risk (Environment Agency, 2010). The Wylfa Newydd TRO discharge has been assumed to be 100 $\mu g\ l^{-1}$ which is half that assumed for the Hinkley C project. A TRO concentration of 20 µg /l was measured at point of discharge at Heysham Power Station; this further reduced to 10 µg /l at a distance of 1 km away (Jenner *et al*. (1997) cited in EDF (2011)).

Assuming a bromoform discharge of 30 $\mu g l^{-1}$, a six-fold dilution is required to reach the BEEMS Predicted No-Effect Concentration of 5 $\mu g\ l^{-1}$. The size of the mixing zone implied by the dilution necessary to achieve a concentration of 5 $\mu g l^{-1}$ assuming a conservative tracer discharged at 30 $\mu g\ l^{-1}$ is 432.4hectares (248.1hectares as a 98 percentile) at the surface and 3.9 hectares (2.6 hectares as a 98 percentile) at the bed.

In a survey of UK nuclear power plant (BEEMS 2011a) it was found that chloroform was below the detection limit of <0.1 $\mu g l^{-1}$ in the effluents of all but Hartlepool on the heavily industrialised Tees Estuary where a single spot sample was found to contain 1.5 $\mu g l^{-1}$. With an EQS of 2.5 $\mu g l^{-1}$, measured chloroform concentrations were all below EQS at discharge. Chloroform concentrations measured in the waters off the Existing Power Station at Wylfa Head were also well below the EQS (with a maximum concentration recorded at WQ2 of 0.033 $\mu g l^{-1}$, see Table 31) and it is therefore likely that, with the envisaged reduced biocide dosing compared to other plant, the chloroform formed in the Wylfa Newydd CW discharge would also be below the EQS.

11. Climate Change

Climate change can be expected to alter the marine environment over the life of the Wylfa Newydd Power Station. A revised set of climate predictions are expected to be released in 2018, but at present the best data set is that from UKCP09 (UKCP09, 2015). This provides a range of predictions for sea level change and the predicted change in sea and air temperature. While it is expected that other aspects of the future weather will be different to today with dryer summers and stormier winters, the changes are less reliably understood and not quantified in UKCP09.

The predicted change in sea temperature and meteorology can be used to examine the influence of climate change on the surface heat flux by adjusting the input data to the spreadsheet used to calculate the seasonal values for the base case modelling (Table 33).

The predicted changes in UKCP09 for the median emissions scenario (median probability) of UKCP09 for the 2050s are:

- Summer mean land air temperature increase: 1 to 2 °C (1.5°C)
- Winter mean land air temperature increase: 1 to 2 °C (1.5°C)
- Sea level pressure rise 0.3 hPa
- Marine rain fall: -2%
- Mean sea temperature increase: 1.5 °C
- Cloud cover change: -2%
- Mean sea level rise: 21.8 cm

Using these values the seasonal surface heat fluxes are slightly increased.

Table 33 Calculated seasonal average surface heat loss rate: current and climate change conditions.

Season	Current conditions ($W/m^2/K$)	Climate change conditions ($W/m^2/K$)
Winter	21.4	22.2
Spring	19.7	20.3
Summer	21.7	22.5
Autumn	24.0	25.1

There is little difference between the surface heat flux of the current meteorology input data and with an assumption for climate change. In the surface flux sensitivity study where the rate was changed by ±10 $W/m^2/K$, it was found that the mixing zones were fairly insensitive to the imposed rate. The surface heat loss rates used for the seasonal base cases are therefore reasonable for conditions under climate change. The increased seawater temperature will increase the area of the 23 ˚C exceedance mixing zone.

Climate induced sea temperature rises over the life of the power station would mean that DO levels and the proportion of un-ionised ammonia would be expected to reduce and increase in the future baseline, respectively.

The greatest change under the UKCP09 projections is in the sea level which is projected to increase by around 22 cm by the mid-2050s. Given the morphology of the north Anglesey coast, an increase of this scale would not be expected to change the coastline greatly. Furthermore, in the absence of climate change impacts on the tidal forcing there would not be expected to be large scale differences in mixing zones should the water level in the entire model be raised by 22 cm to simulate this aspect of climate change. For this reason no explicit modelling of the temperature and TRO mixing under climate change has been undertaken.

12. Use of the Model to Inform Coastal Process Studies

The Delft3d coupled hydrodynamic-wave model has been run for a number for different scenarios to provide the output required for impact assessment. The primary model output presented for this purpose is bed shear stress. The coupled hydrodynamic-wave model setup is detailed in Section 6.10.

The approach adopted for the current study has been to identify the desired wave conditions at Point 3 from wave model time series output (see Section 6.10) and then use the associated boundary condition data in a coupled hydrodynamic and wave simulation.

Two typical wave conditions have been used – the first condition adopted was 6 March 2014 at 12:00 when a predicted wave of 0.9m from 228.1° occurred at Point 3. A somewhat greater wave (Significant wave height (H_{sig})1.48m, T_{m02} 3.45s from 249.2°) occurred a few hours later at 03:00 on 7 March 2014. This condition, which has been termed High Typical, was used in simulations of the CW plume the results of which are included in this report.

Waves in the winter months tend to be higher than during the summer. The use of a wave height of 2m was used to represent typical winter conditions. The conditions that occurred on 27th February 2011 were selected to provide a typical winter wave climate.

Hawkes (2016) tabulated extreme wave conditions at the monitoring points. The 1 in 10 year wave at Point 3 is predicted to be 5.3m in height with a direction of 285° to 15°. Extreme waves are relatively rare but in the 3 hourly time series a wave of 5.22m from 274.9° was predicted at Point 3 on 12th February 2014 at 18:00.

The 98 percentile wave height predicted at Point 3 between 1980 and 2015 is 2.85m. On the 15th April 1992 at 9:00 a wave of 2.85m with a direction of 358.3 was predicted at Point 3. This 98 percentile wave condition from the North has therefore been used to represent the Extreme wave modelled as it represents an appropriate magnitude for this wave type and direction. The different Typical and Extreme wave conditions are tabulated in Table 34.

Table 34 Wave conditions at Point 3 used in coupled model simulations.

Condition	Date	Time	Hsig	Direction
Typical	6/3/2014	12:00	0.9	228.1
Typical – High	7/3/2014	03:00	1.48	239.4
98 percentile (Extreme wave from the North)	15/4/1992	09:00	2.85	358.3
Typical Winter	27/2/2011	18:00	2.0	343.7

Two versions of the wave model were required one with and one without the Wylfa Newydd Power Station breakwaters and MOLF. For the model the bathymetry and obstacle file in the wave model was updated to reflect the design with a 400m long western breakwater (drawing No: PB5659-300-008).

The simulations to predict changes to bed shear stress with the Project were undertaken with three wave conditions; Typical; High Wave from the North; and Typical Winter wave. The simulations of sediment discharges used the Typical wave (see Section 13) while those to examine the influence of waves on mixing of the CW plume made use of the Typical High wave (see Section 6.10). The High Typical wave was used for the CW influence study as it was intended as a sensitivity study rather than a prediction of long-term behaviour.

12.1 The Coupled Model

In a turbulent flow the boundary layers at the bed associated with the waves and the current interact nonlinearly (see for example Soulsby and Clarke, 2005, Soulsby et al 1993) which has the effect of enhancing both the mean and oscillatory bed shear-stresses. The current profile is also modified, because of the extra turbulence generated close to the bed. The change to the vertical current profile is equivalent to that from an enhanced bed roughness and therefore the combination of waves and currents enhances the bed shear stress. The non-linearity of the interaction results in a greater maximum bed shear stress that a simple addition of the pure current and wave bed shear would imply.

There are a number of different models available for the wave current boundary layer and the resulting virtual roughness available in Delft3D. For the present study the Delft3D default method of Fredsoe (1984) has been used. For the Fredsoe model the non-linear interaction between waves and currents can result in an increase of maximum bed shear stress, which determines entrainment, of up to 70% above that obtained by assuming a linear combination. Depending on the conditions the non-linear combination of waves and current bed shear can be an important phenomena for sediment transport. Soulsby et al (1993) concluded that the non-linearity was most important under wave dominated conditions.

Whilst SWAN is a widely used tool for modelling near shore waves it has limitations. The phase-decoupled approach employed in SWAN does not fully handle diffraction in harbours or in front of reflecting obstacles. The SWAN sourceforge website (http://swanmodel.sourceforge.net/online_doc/swantech/node26.html) discusses these limitations but considers that the “SWAN diffraction approximation can be used in most situations near absorbing or reflecting coastlines of oceans, seas, bays, lagoons and fjords with an occasional obstacle such as islands, breakwaters, or headlands but not in harbours or in front of reflecting breakwaters or near wall-defined cliffwalls”. Behind breakwaters (which may be reflecting), it is noted on the SWAN website that results “seem reasonable”. Holthuijsen (2007), one of the initial SWAN developers provides (Figure 8.9 pp 267) evidence that away from reflecting obstacles where standing waves can develop SWAN can reasonably reproduce diffraction. The proposed Wylfa Newydd MOLF design includes some vertical walls as well as solid revetments and therefore the SWAN predictions in the vicinity of the these features, which are within the harbour, should be treated with a degree of caution. However, away from the vicinity of these features, the coupled model should be capable of predicting changes of interest for coastal processes.

The Delft3D software package can be used to model the bed load and suspended transport of non-cohesive materials and the suspended transport of cohesive and non-cohesive material.

The suspended transport is calculated by solving the 3D advection diffusion equation for each of the sediments with the flow field and eddy diffusivities being derived from the hydrodynamic solution.

The solution of the sediment transport is more complex than that for a tracer material as the solution requires the settling of the sediment under the action of gravity to be modelled as well as the exchange of material with the bed.

The Delft3D code can include the effect of sediment density damping turbulence and the interaction of sediment fractions. For non-cohesive sediments the model uses a modified turbulence model to account for the influence of waves on the turbulent mixing of sediment. When settling up a simulation the user is required to define a settling velocity for cohesive sediment while Delft3D calculates the velocity for a non-cohesive material. In a similar fashion the user has to define a shear stress for the onset of deposition and erosion for a cohesive material but these are calculated for non-cohesive sediments.

In the following subsections, both the predicted depth averaged current and bed shear stress at mid ebb and flood are plotted for a neap and spring tide below for the three wave conditions. Before presenting results with waves, predicted currents and bed shear stresses have also been plotted for a simulation without waves in order that the influences of waves on the predicted flow field and bed shear stress can be identified. Note that the currents and bed shear stress are obtained from the hydrodynamic model and therefore the extent of the plotted data, which is the innermost hydrodynamic grid, differs to that of the significant wave heights obtained from the 20m wave model grid.

The model was run in 3D with 10 layers in the vertical for both the with and without waves cases. The bed friction was represented using the Chezy coefficient. The plots in the following sections show the bed shear stress due to current alone or current combined with waves (for the with waves cases). The plots also show the depth averaged current vectors; this is in order to represent the flow field (rather than to imply that depth averaged velocity was used to calculate the bed shear).

The coupled model was used to simulate flows and waves for the period 24 August 2011 and 31 August 2011. In the following results presented for a neap tide are from the 23 August 2011 when the tidal range was 2.45 m and the results for the spring tide are from the 30 August 2011 when the tidal range was 6.2 m.

Note that the date and time of the hydrodynamic and the wave conditions are not coincident and that therefore the results are not intended to be a hindcast of the conditions at a single instant in time but rather are representative of the range of conditions that can occur.

12.2 No Wave Condition

The no wave depth-averaged current and bed shear stress are plotted for a neap tide in Figure 132 to Figure 135 and for a spring tide in Figure 136 to Figure 139.

The bed shear stress and currents for the neap tide at the time of mid flood is similar for the model simulation without (Figure 132) and with (Figure 133) the Power Station. South of a line joining the headlands either side of Wylfa Head currents and bed shear stress are relatively low. North of this imaginary line the currents and hence bed shear stress is higher. South of the line the bed shear stress is less than 2 N/m^2, which is approximately the stress required to suspend material with a diameter of 1.5 mm (van Rijn 2016).

The mid ebb depth-averaged currents and bed shear stress (Figure 134) are in general somewhat higher than the mid flood on a neap tide (Figure 132). The higher bed shear stress on mid ebb compared to mid flood is more apparent north of an imaginary line connecting the headlands.

For both the with and without Power Station cases (Figure 135 and Figure 134) the predicted bed shear stress during the time of mid ebb on a neap tide is higher offshore away from the influence of the headlands. The Power Station modifies the flow field in the bay to the west of Wylfa Head which is reflected in small, localised, changes in bed shear stress.

Compared to the equivalent neap tide results (Figure 132) the bed shears stress and currents at mid flood on a spring tide (Figure 136) are higher.

As with the neap tide simulation the bed shear stress is similar for the without and with Power Station spring tide simulations (Figure 136 and Figure 137). Offshore north of the line joining the headlands, which separates the sheltered low current and bed shear stress areas from the higher current and bed shear stress zones the bed shear stress is greater on the spring tide than on the equivalent neap tide (compare for example Figure 137 and Figure 132).

The depth-averaged current and bed shear stress are, away from the breakwaters and MOLF, similar for the no wave mid ebb conditions with (Figure 139) and without (Figure 140) the Power Station. The bed shear stress and currents and relatively low southwards of a line drawn between the headlands.

Comparing the no wave mid ebb and mid flood results from a spring and a neap tide it will be noted that overall bed shear stress is higher on the spring tide than on the neap because the spring tide gives rise to higher current velocities. For a given tide the mid ebb tide currents are higher than at mid flood which is reflected in higher bed shear stress.

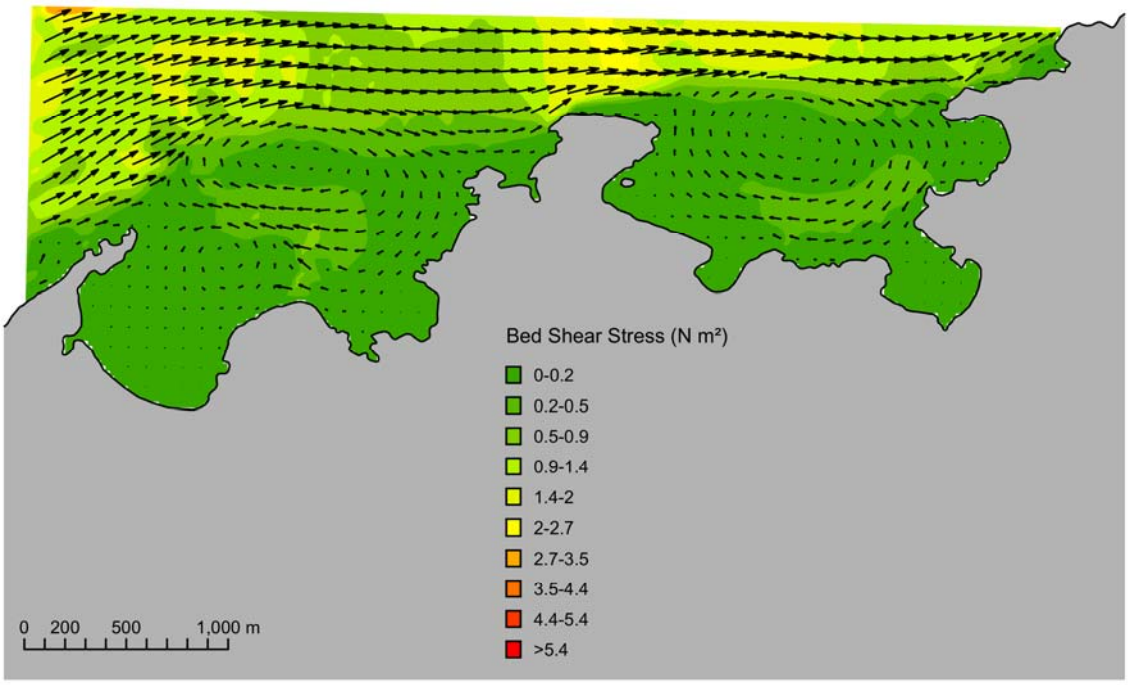

Figure 132 Neap tide no wave mid flood – No Power Station. Arrows represent current vectors.

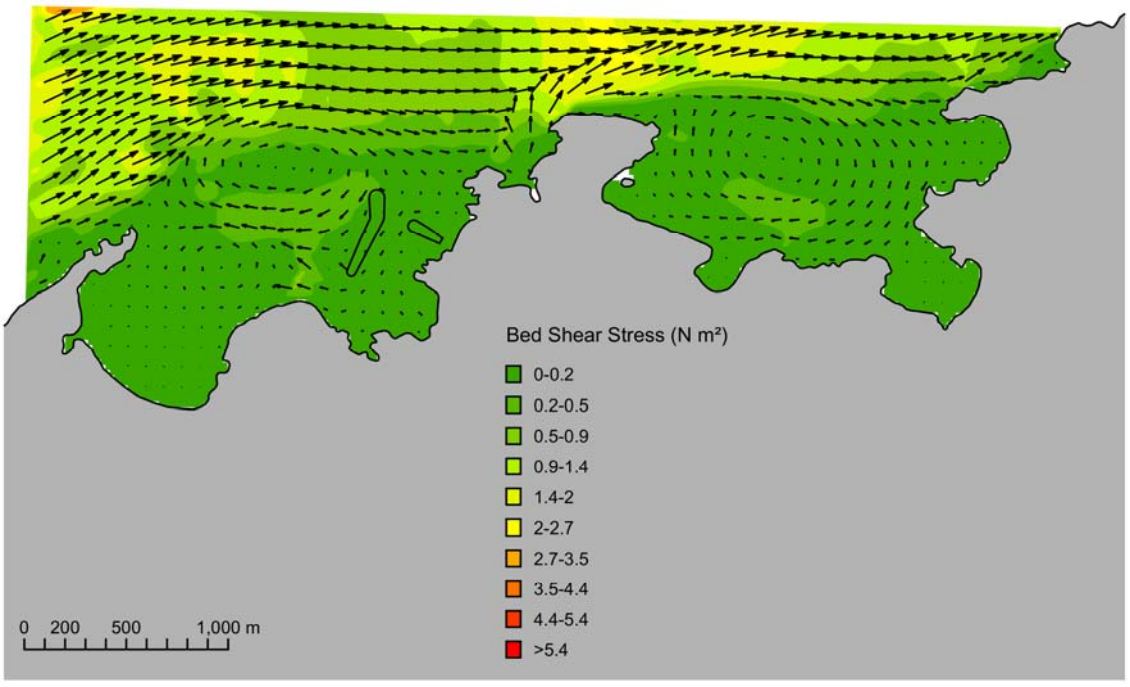

Figure 133 Neap tide no wave mid flood – With Power Station. Arrows represent current vectors.

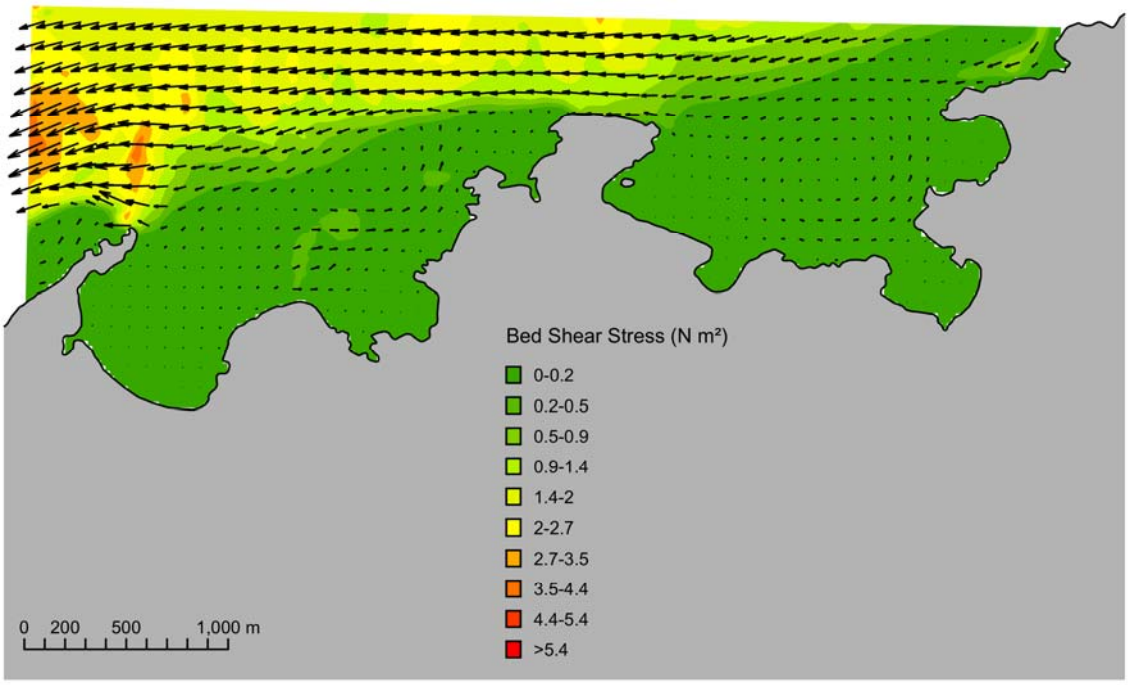

Figure 134 Neap tide no wave mid ebb – No Power Station. Arrows represent current vectors.

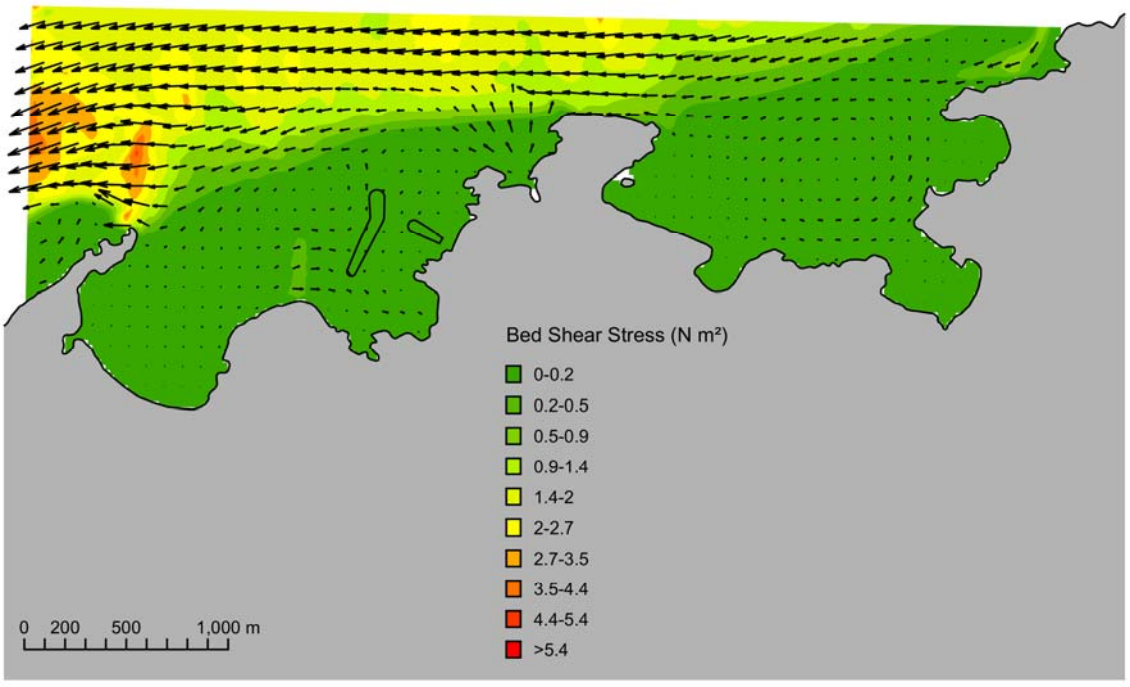

Figure 135 Neap tide no wave mid ebb – With Power Station. Arrows represent current vectors.

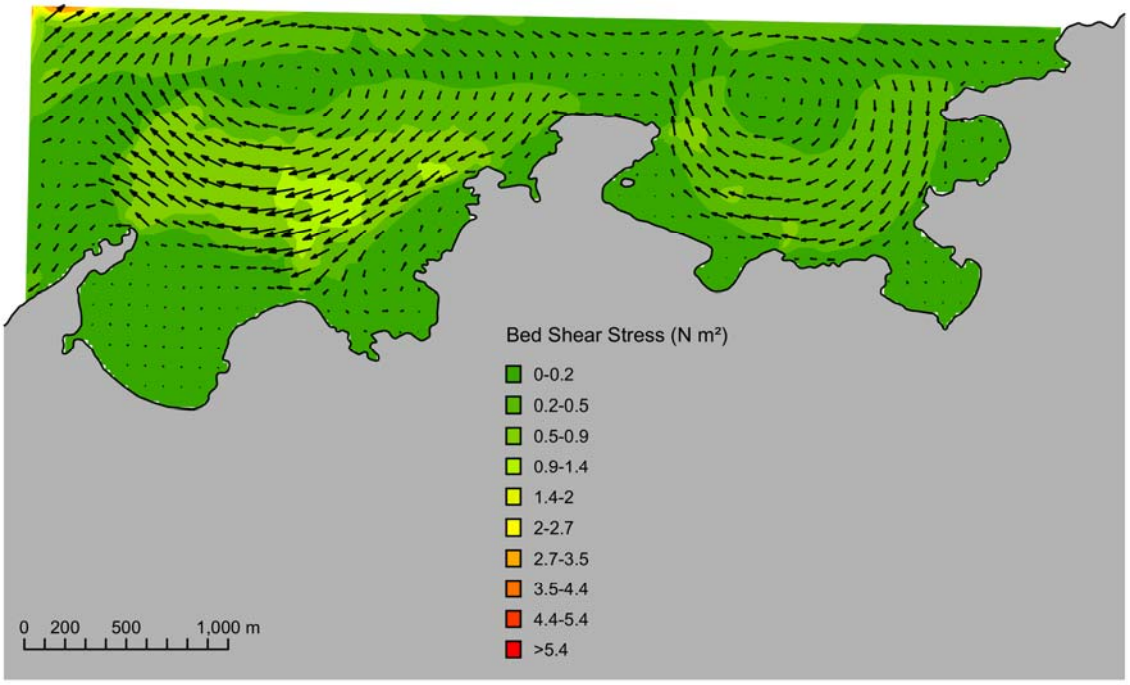

Figure 136 Spring tide no wave mid flood – No Power Station. Arrows represent current vectors.

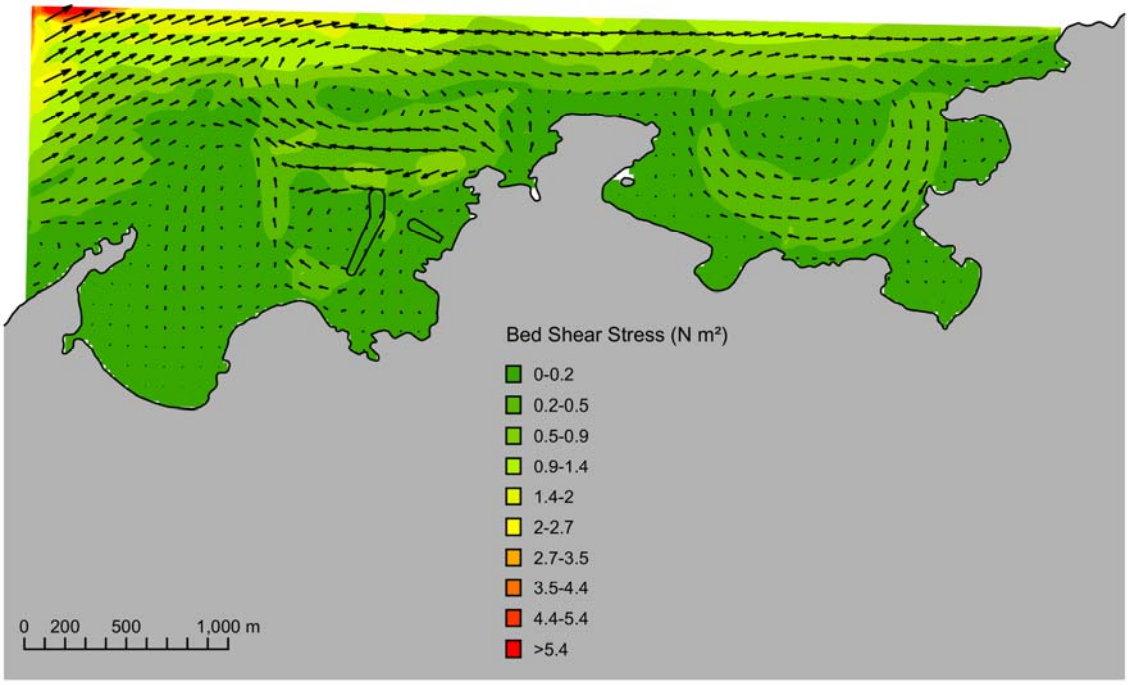

Figure 137 Spring Tide no wave mid flood – With Power Station. Arrows represent current vectors.

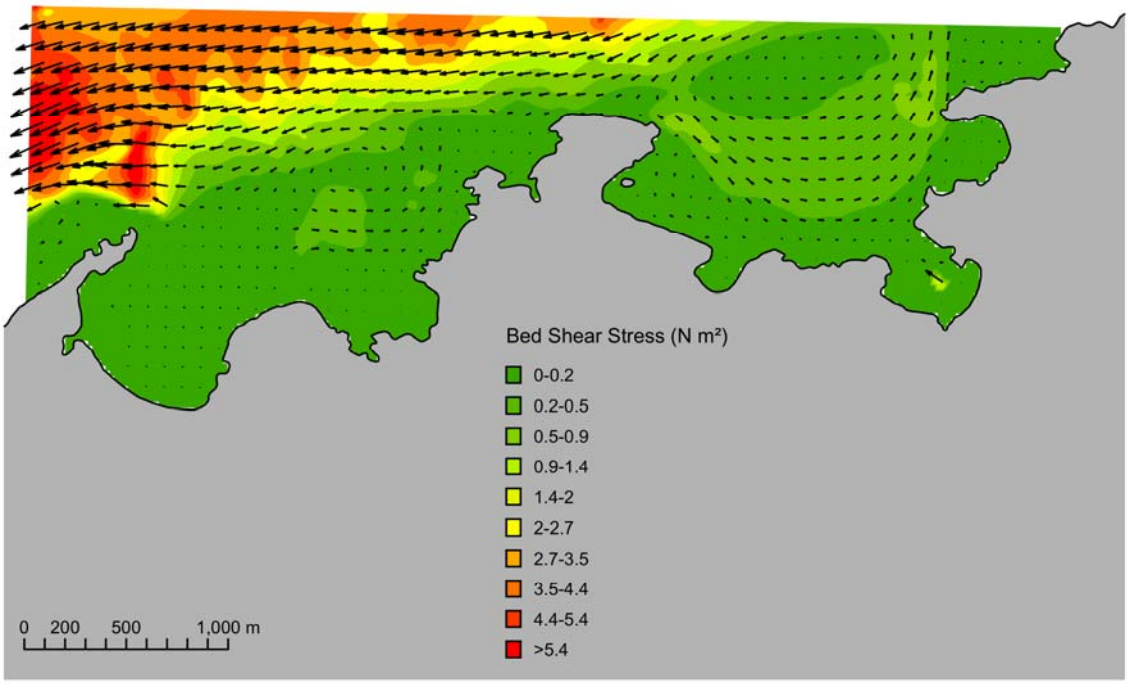

Figure 138 Spring tide mid ebb no wave – No Power Station. Arrows represent current vectors.

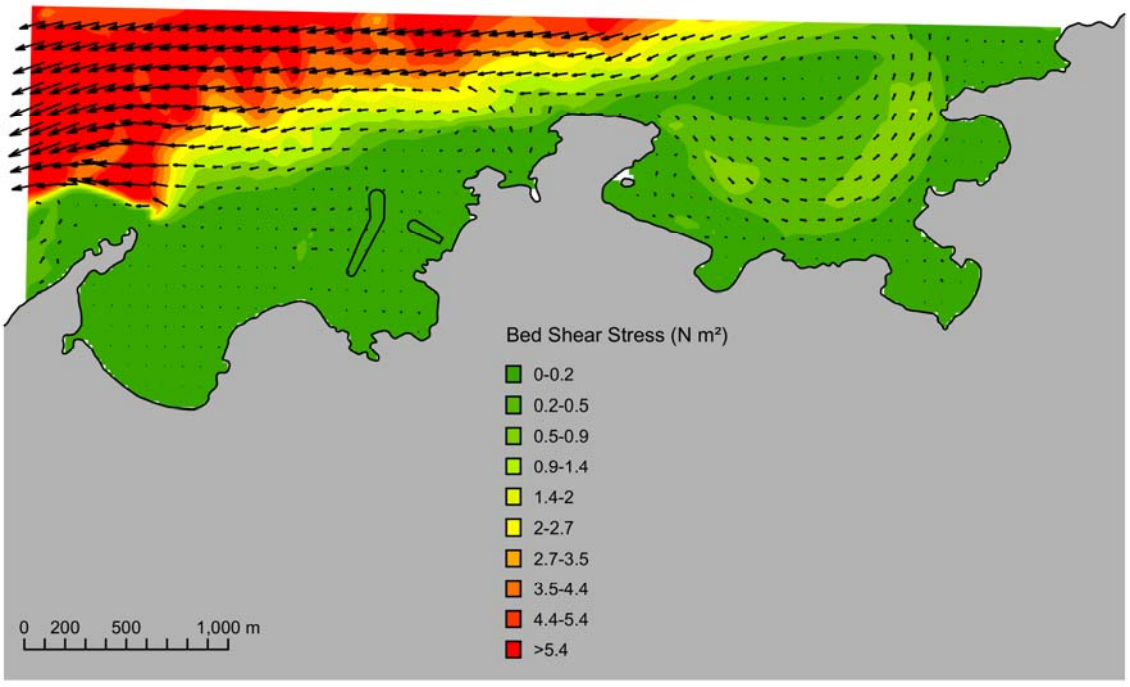

Figure 139 Spring tide mid ebb no wave – With Power Station. Arrows represent current vectors.

12.3 Typical Wave Conditions

The depth average current and bed shear stress at mid flood on a neap tide with the Power Station and a typical wave (Figure 141) is similar to the results without the Power Station (Figure 140). The bed shear stress for the typical wave condition is also similar to the bed shear stress without waves included (Figure 132).

Similarly, there are limited differences in the depth-averaged current and the bed shear stress for the neap tide at the time of mid ebb (Figure 142) with a typical wave condition included and those without the waves included (Figure 134).

The inclusion of the typical wave condition results in a small increase in the predicted bed shear north of the headland to the west of Cemlyn Bay. Given the direction of the typical wave (from the south west) the bays tend to be sheltered from the waves but the shallower water off of this headland allows the wave to influence bed shear stresses.

There are differences in the depth-averaged flow field resulting from the development of the western breakwater. However, except for the vicinity of the western breakwater the bed shear stress for the with (Figure 144) and without Power Station (Figure 144) spring tide mid flood typical wave conditions are similar.

In general there are limited differences in either the depth-averaged current or the bed shear stress in the spring tide simulations with a typical wave condition included and those without. There is some increase in the predicted bed shear north of Trwyn Cemlyn (the headland to the west of Cemlyn Bay) with the wave included. Given the direction of the typical wave (from the south west) the bays tend to be sheltered from the waves but the shallower water off of Trwyn Cemlyn allows the wave to influence bed shear stresses.

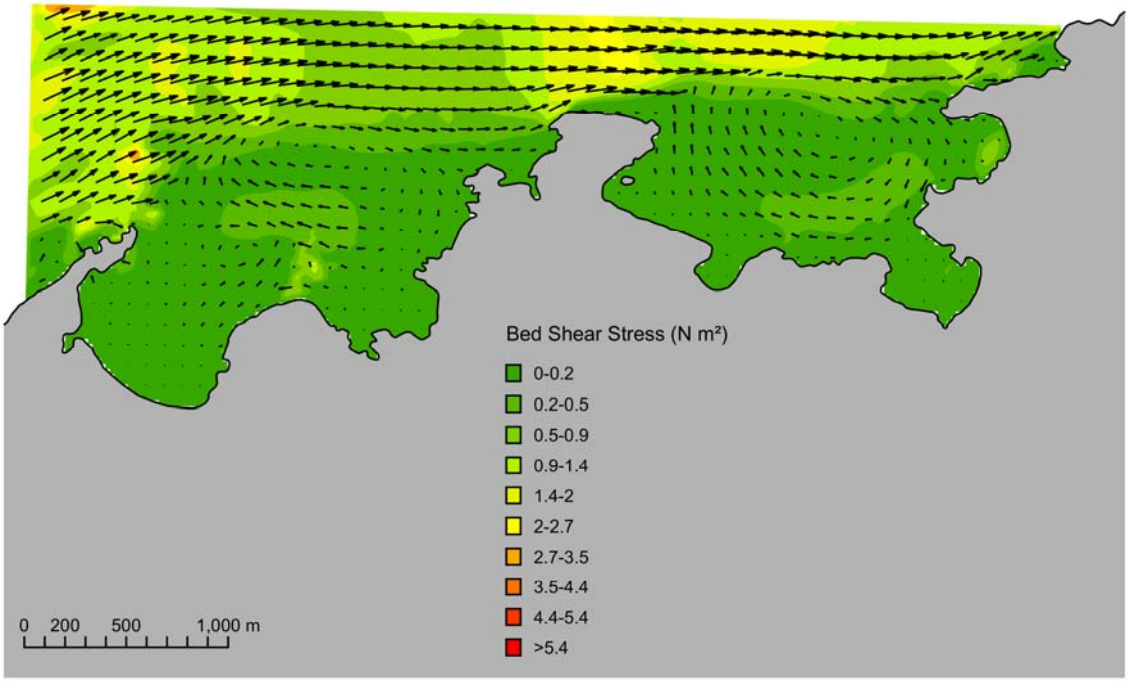

Figure 140 Neap tide mid flood typical wave – No Power Station. Arrows represent current vectors.

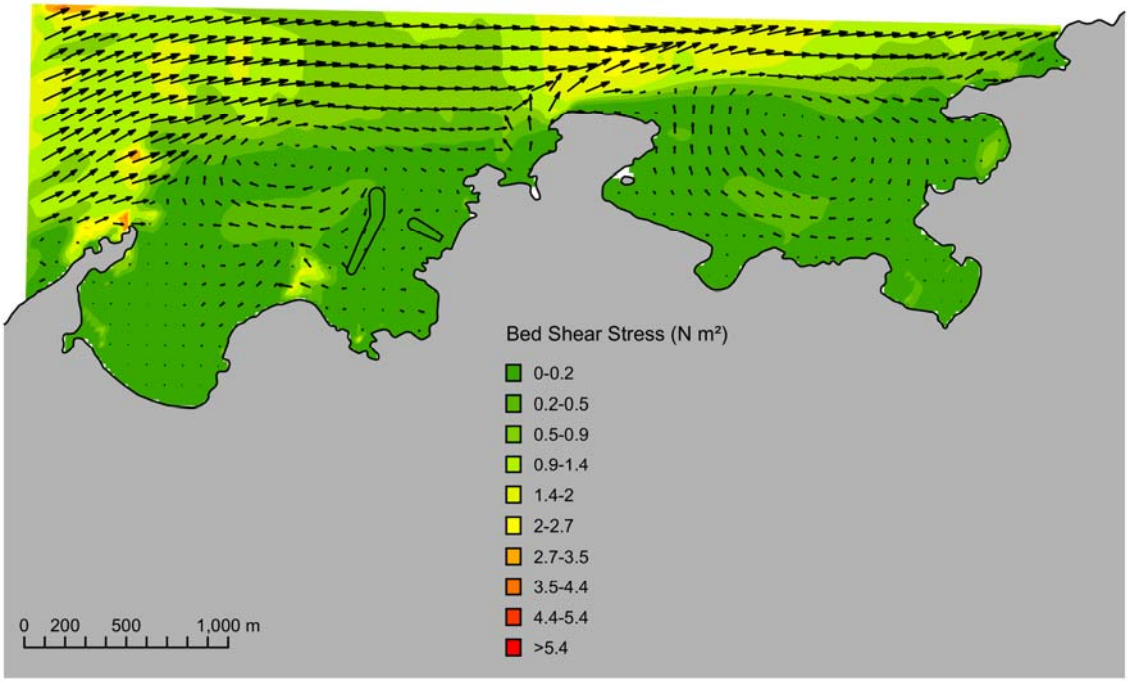

Figure 141 Neap tide mid flood typical wave – With Power Station. Arrows represent current vectors.

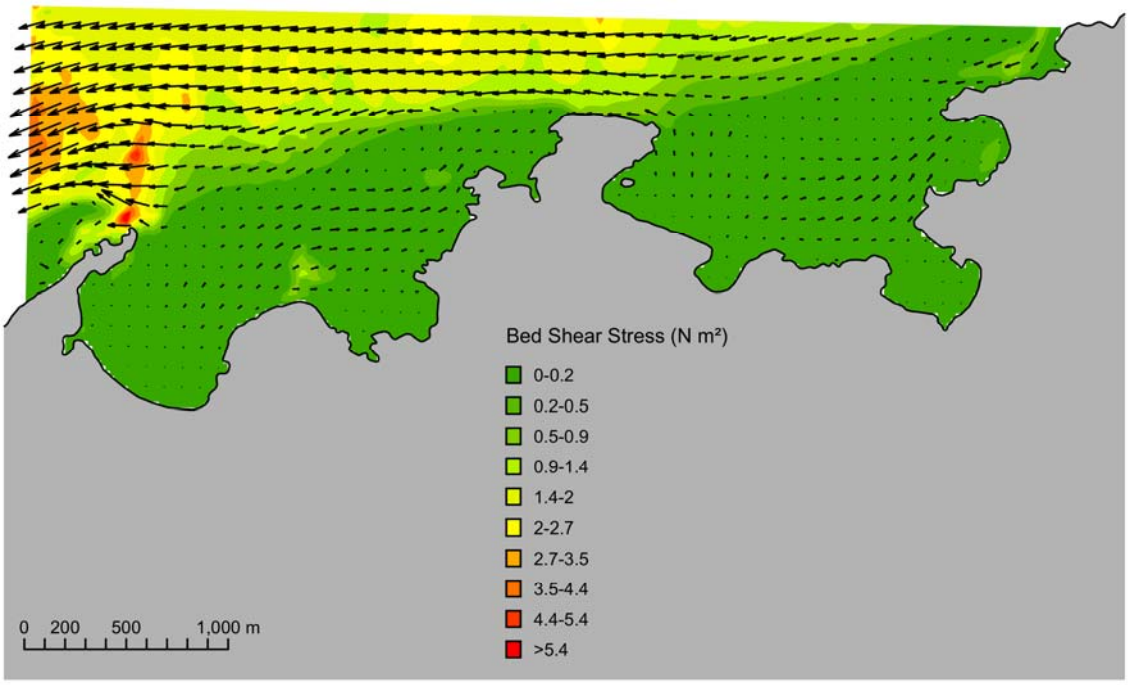

Figure 142 Neap tide mid ebb typical wave – No Power Station. Arrows represent current vectors.

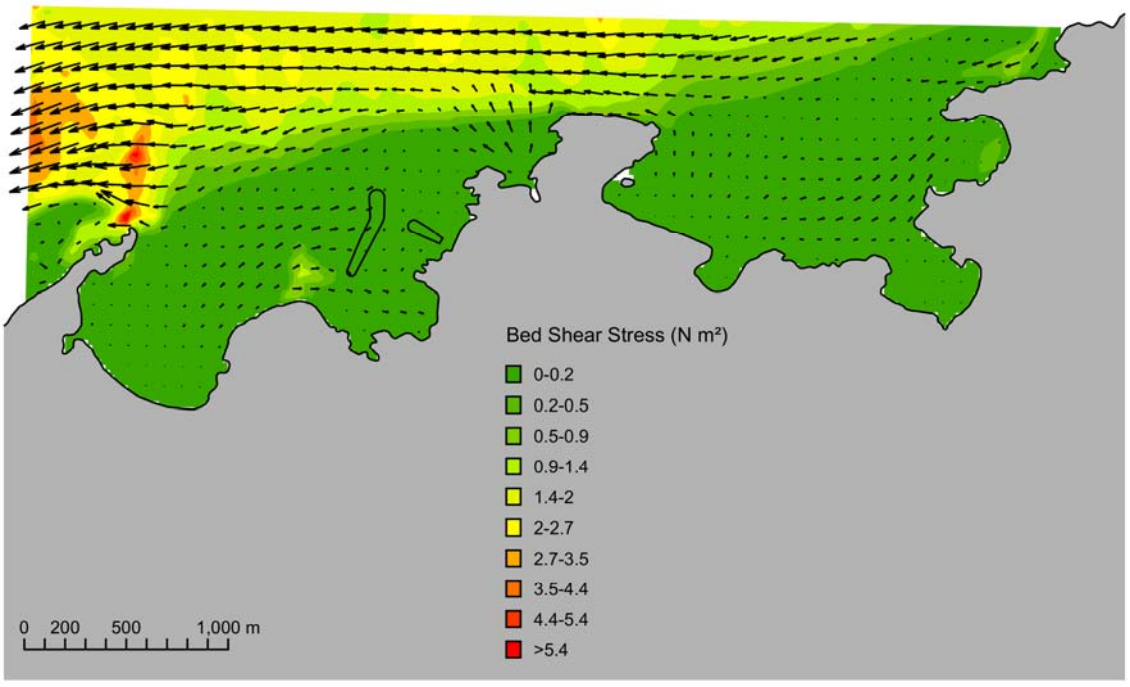

Figure 143 Neap tide mid ebb typical wave – With Power Station. Arrows represent current vectors.

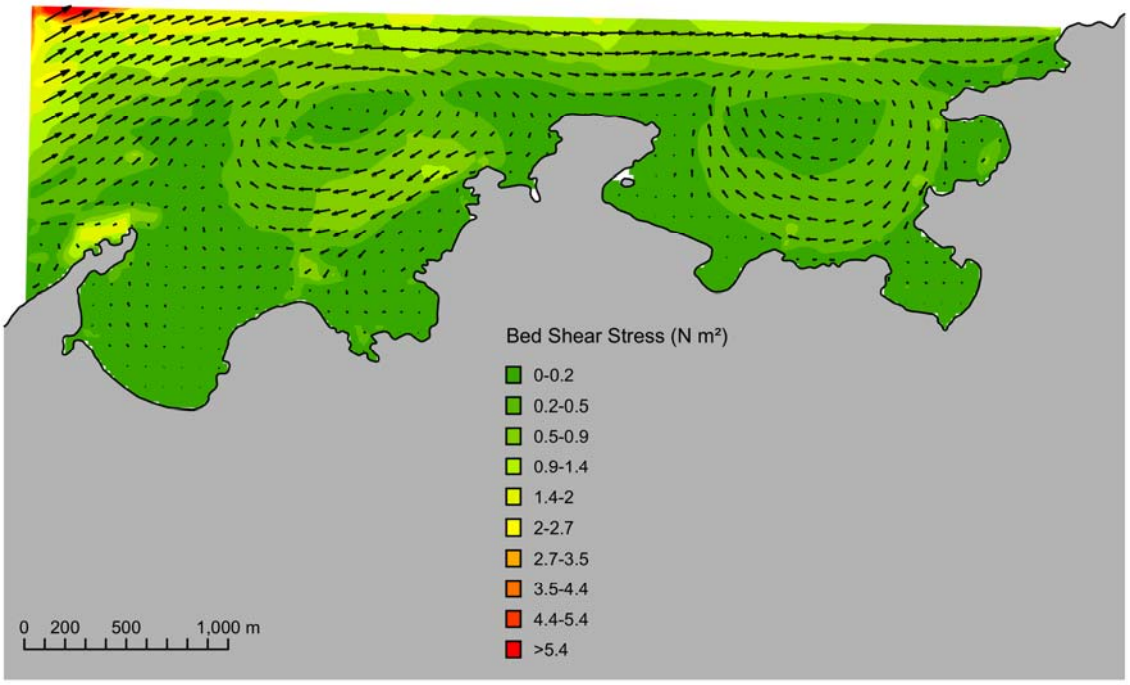

Figure 144 Spring tide mid flood typical wave – No Power Station. Arrows represent current vectors.

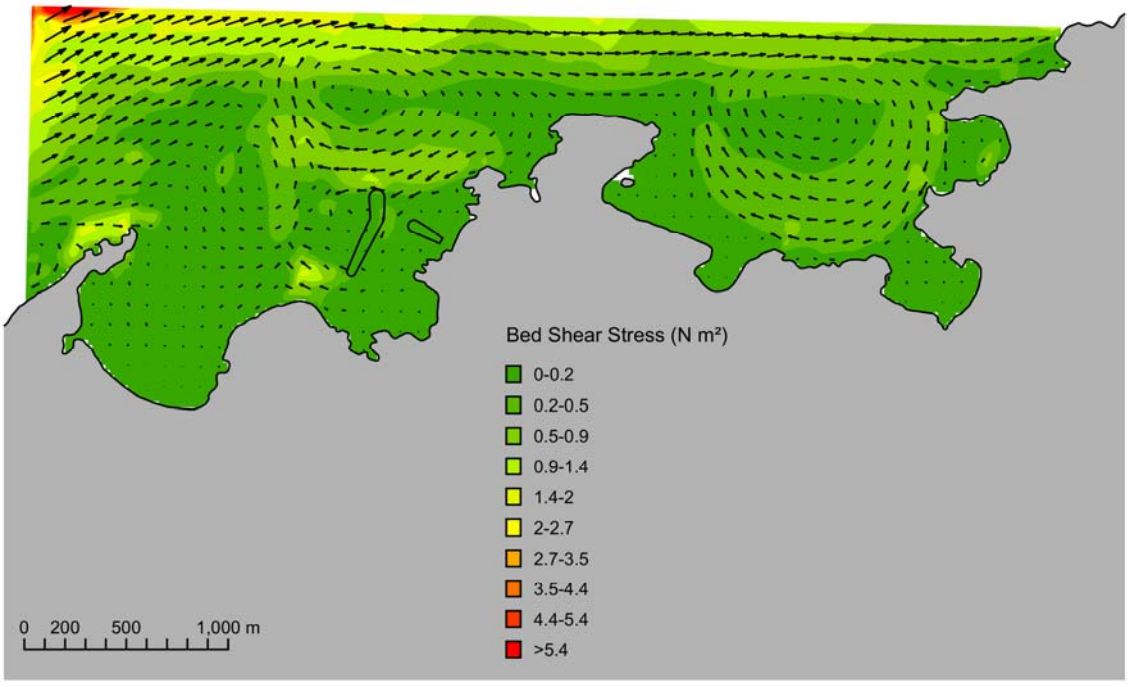

Figure 145 Spring tide mid flood typical wave – With Power Station. Arrows represent current vectors.

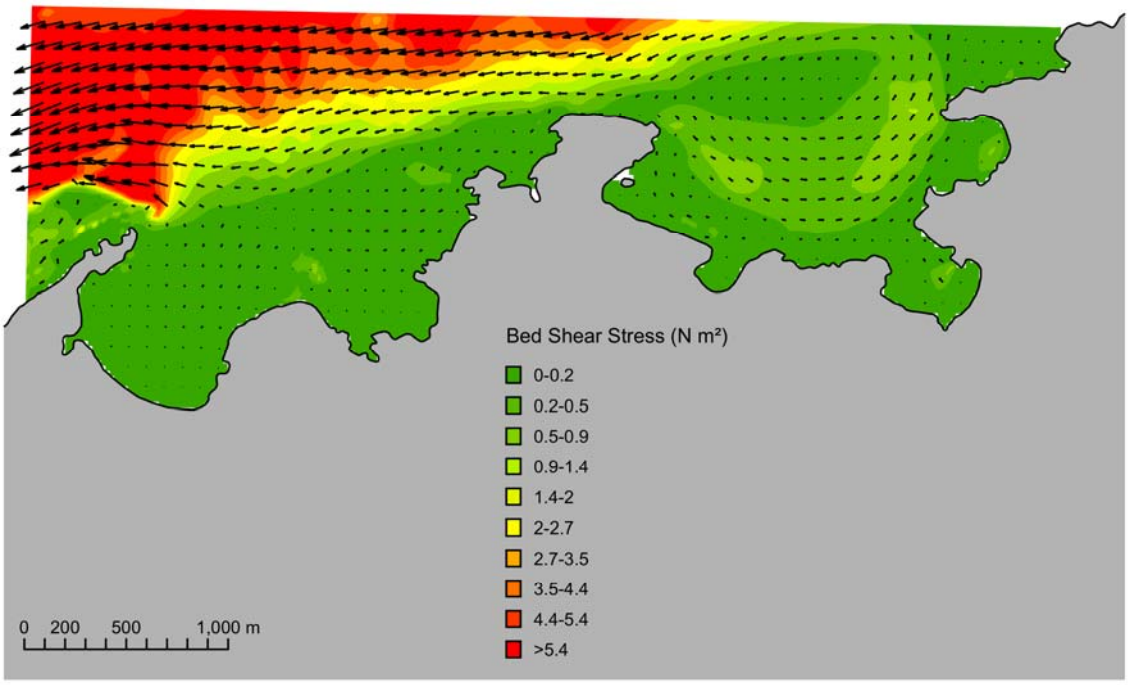

Figure 146 Spring tide mid ebb typical wave – No Power Station. Arrows represent current vectors.

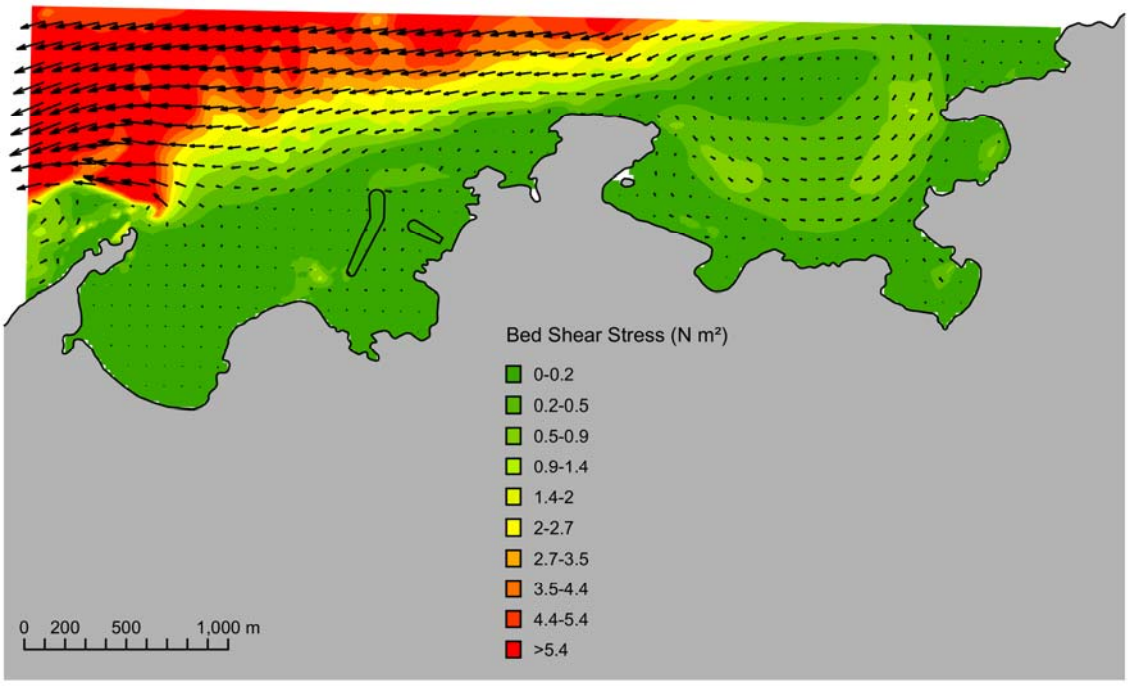

Figure 147 Spring tide mid ebb typical wave – With Power Station. Arrows represent current vectors.

12.4 Typical Winter Wave Conditions

Examples of the predicted depth-averaged current and bed shear stress for the typical winter wave conditions (Table 34) are plotted for a spring tide in Figure 148 to Figure 151.

Compared to the no wave cases the inclusion of a typical winter wave in the model increase the bed shear stress in the inshore areas either side of Wylfa Head. The typical winter waves appear to drive near shore currents, an example being seen in the vicinity of Cemaes Bay where there is a flow into and out of the innermost part of the bay with the waves included (Figure 149) but not with a typical wave condition (Figure 145). Where previously the maximum bed shear stress was less than $2N/m^2$ this value is exceeded over most of Porth-y-pistyll with areas predicting up to $8N/m^2$. The bed shear stress in the vicinity of the shingle bank that forms Cemlyn lagoon is still low, as Cemlyn Bay is protected from direct wave action except for waves from the north east sector.

The influence of the western breakwater in reducing the wave heights and hence the bed shear stress is notable when comparing the with (Figure 149, Figure 151) and without (Figure 148, Figure 150) Power Station plots. However, the influence of the western breakwater appears to reduce the shear stresses in the lee of the structure but not on the seaward side of the breakwater. High shear stresses are maintained particularly at the southern tip of the breakwater in the narrow opening to the harbour.

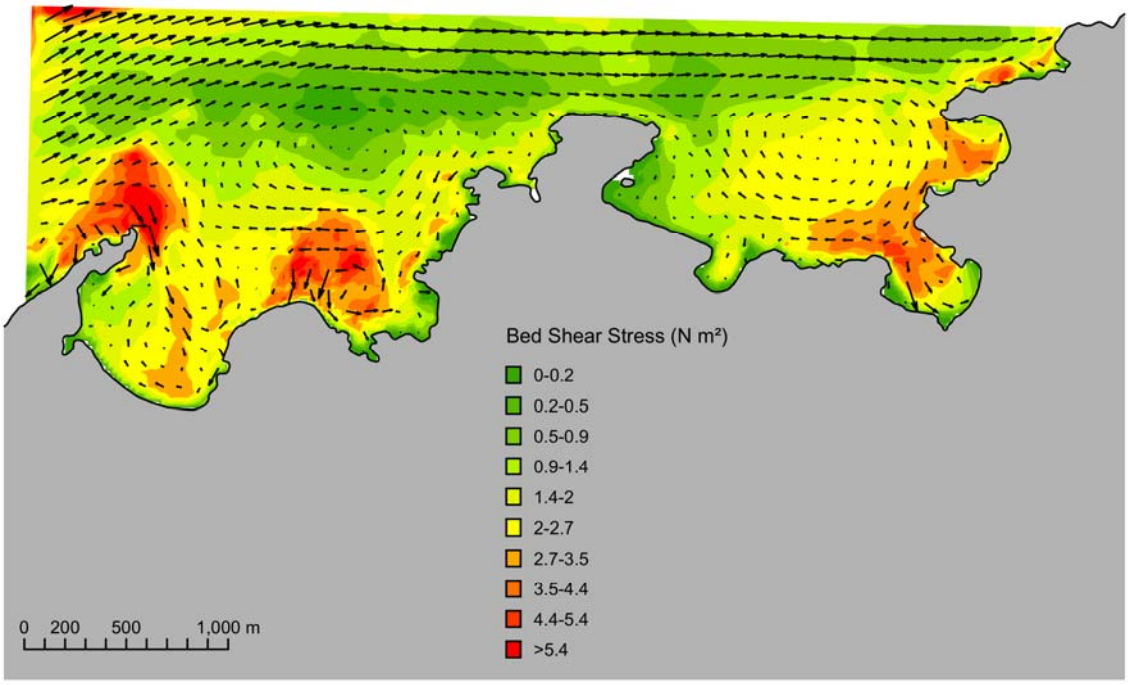

Figure 148 Spring tide mid flood winter wave – No Power Station. Arrows represent current vectors.

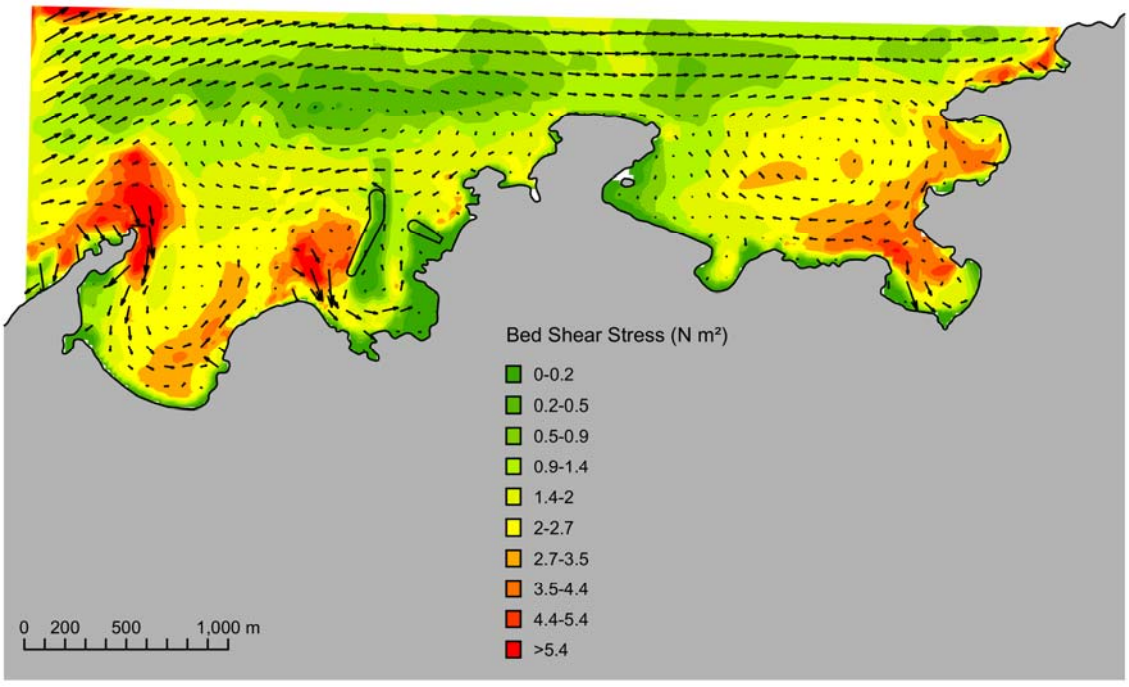

Figure 149 Spring tide mid flood typical winter wave – With Power Station. Arrows represent current vectors.

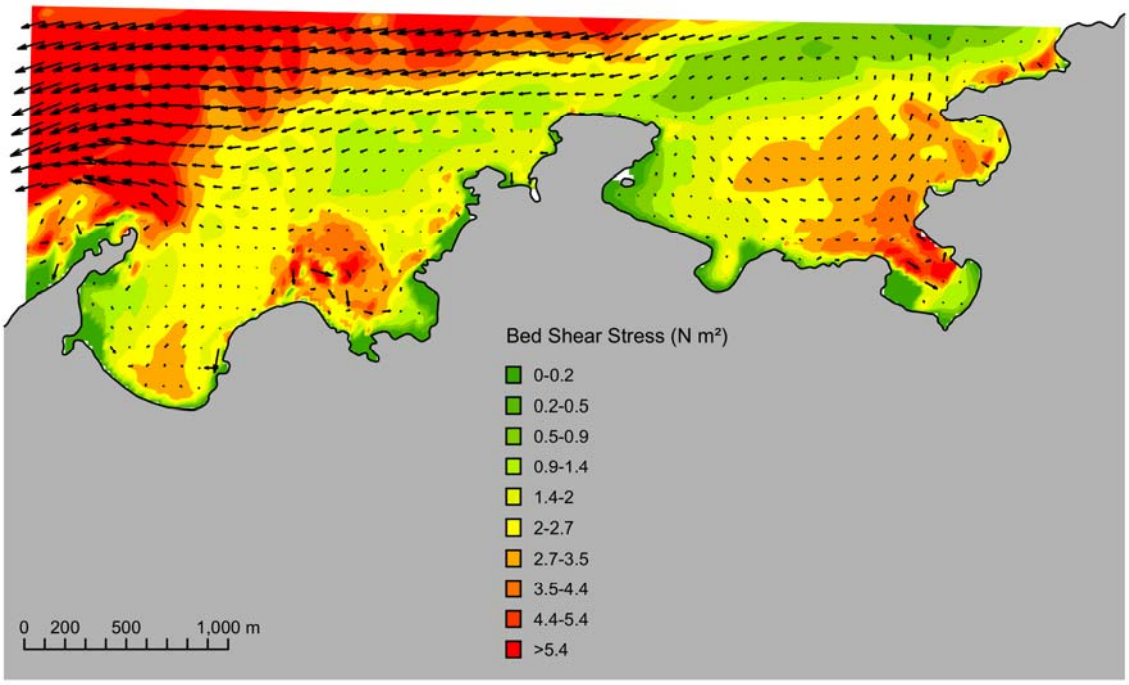

Figure 150 Spring tide mid ebb winter wave – No Power Station. Arrows represent current vectors.

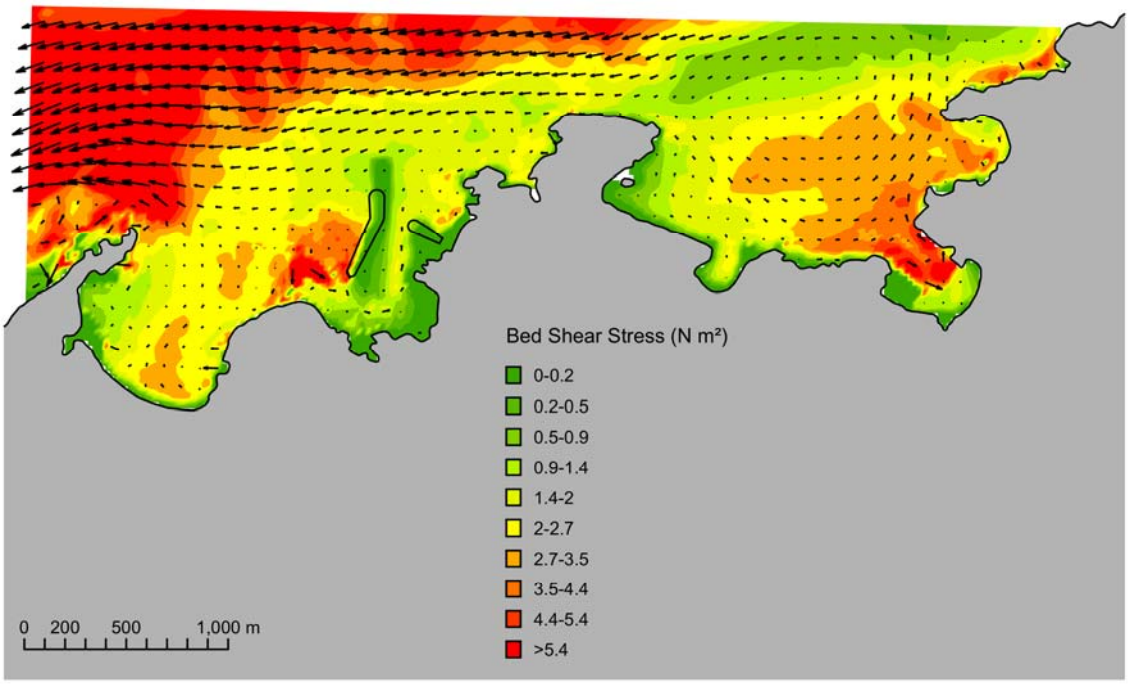

Figure 151 Spring tide mid ebb winter wave – With Power Station. Arrows represent current vectors.

12.5 Extreme (98 percentile) Wave Conditions

Examples of the predicted depth-averaged current and bed shear stress for the hydrodynamic model coupled to a wave model run with an extreme wave condition (98 percentile) from the north on the spring tide are presented in Figure 152 to Figure 155.

The maximum bed shear stress and depth-averaged current data for a spring tide mid flood with the extreme wave from the north with the Power Station plotted as Figure 153 when compared to the same conditions without the Power Station (Figure 152, Figure 154) shows a reduction in bed shear stress in the lee of the breakwater. There is also a modification of the wave driven flow in Porth-y-pistyll because of the breakwater. Away from the vicinity of the Power Station there appears to be little change in either the flow field or the bed shear stress.

The maximum bed shear stress and depth-averaged current data for a spring tide mid ebb with the extreme wave from the north with the Power Station plotted as Figure 155 when compared to the same conditions without the Power Station (Figure 154) shows a reduction in bed shear stress in the lee of the breakwater. There is also a modification of the wave driven flow in Porth-y-pistyll because of the breakwater. Away from the vicinity of the Power Station there appears to be little change in either the flow field or the bed shear stress.

As with the winter wave condition discussed above the extreme wave has a direction from the north and thus the near shore area of Cemlyn and Cemaes Bays are more exposed to the waves than is the case with the typical wave which comes from the south west.

The addition of the extreme wave increases bed shear stress in the near shore and drives near shore currents. With increasing wave height the influence of the waves will be felt in increasingly deeper water.

There is a band of lower bed shear in line with the north of Wylfa Head. This is probably the zone between the offshore where currents are extreme and water deep so that the current is the dominant factor in the bed shear stress and the inshore region where wave action is dominant.

In addition to the bed shear stress plots presented at the time of mid ebb and mid flood, maximum bed shear stress simulated over a 24 hour period on the spring and neap tides have also been generated for a typical wave (Figure 156 and 157) and for an extreme wave (Figure 161 and 162). Difference plots are shown for spring and neap tides for the typical wave model simulation only (Figure 158 and 159).

These plots of maximum bed shear stress indicate similar trends in bed shear stress as the plots showing bed shear stress at the times of mid flood and mid ebb and a detailed discussion of them is therefore not included.

Figure 158 shows reductions in bed shear (greens and blues) for a spring tide either side of the northern extent of the western breakwater, but increases off Trwyn Cemlyn and Cerrig Brith, and north west of Wylfa Head. These locations tend to have high bed shear, and the bed is characterised by bare rock.

The average difference between the developed and undeveloped case during a neap tide is plotted in Figure 159. As with the spring tide case there are areas of reduced bed shear either side of the western breakwater (although these are small) and increased shear off Trwyn Cemlyn and Cerrig Brith. The relevance of these changes to coastal processes is outside the scope of this report, but the increased stress occurs in areas where the bed shear stress is predicted to be high and the sea bed characterisation (Figure 160) which identified the areas north of Trwyn Cemlyn and Cerrig Brith as being bare rock.

12.5.1 Spring Tide Extreme Wave Condition

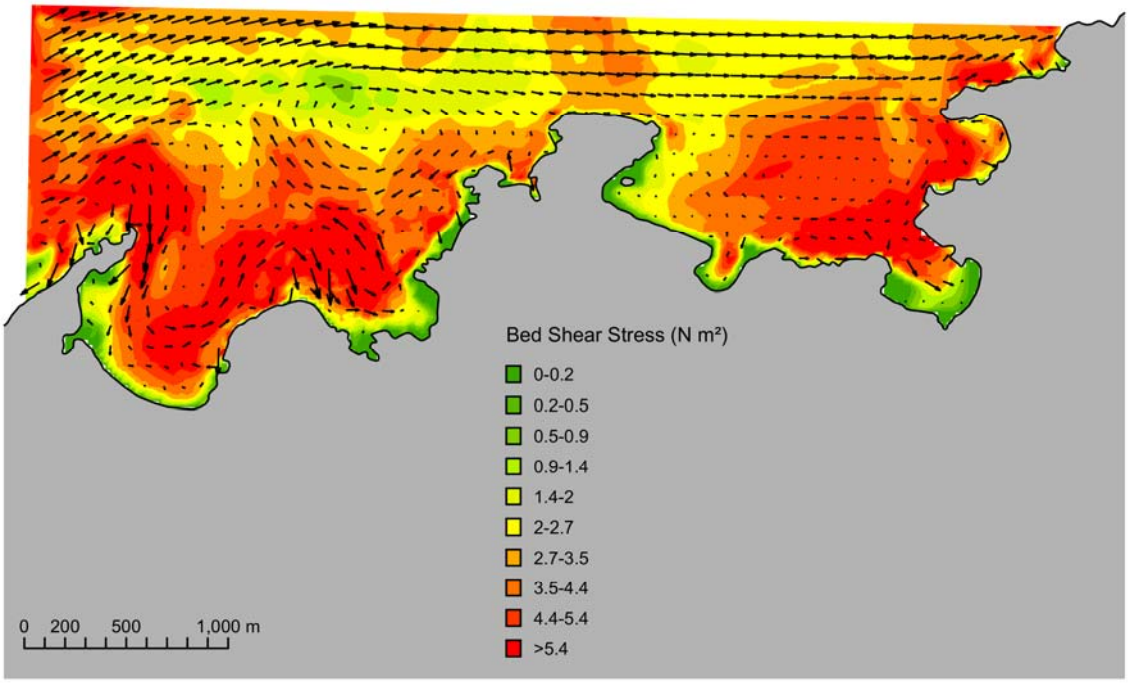

Figure 152 Spring tide mid flood Extreme wave – No Power Station. Arrows represent current vectors.

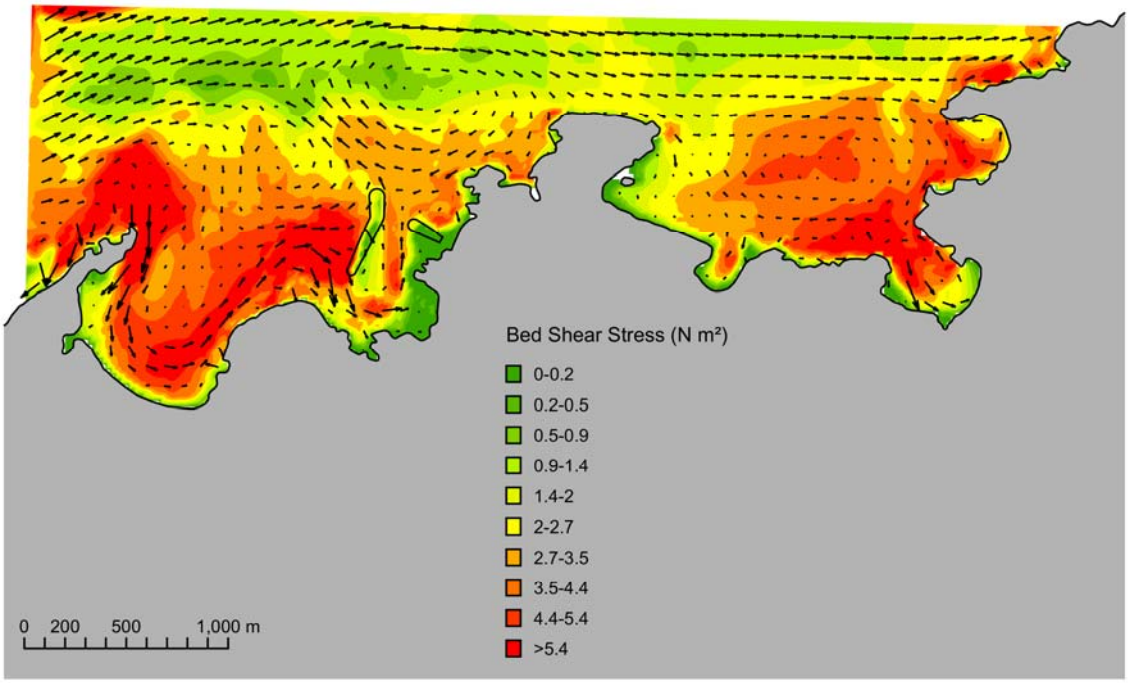

Figure 153 Spring tide mid flood Extreme wave condition – With Power Station. Arrows represent current vectors.

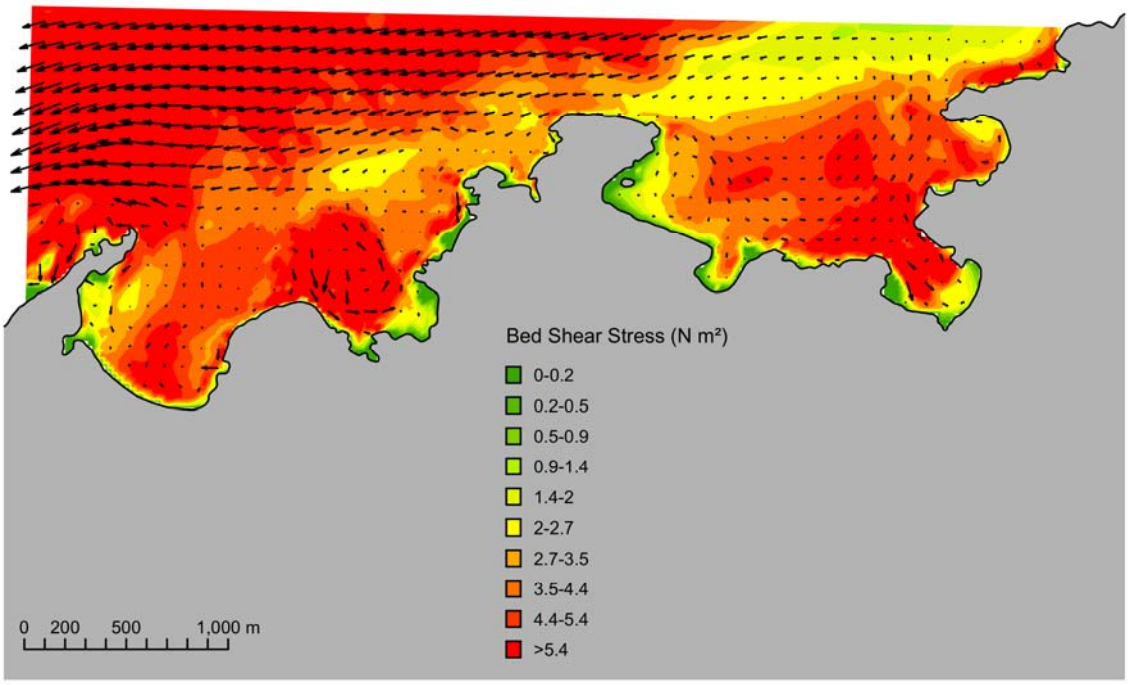

Figure 154 Spring tide mid ebb Extreme wave – No Power Station. Arrows represent current vectors.

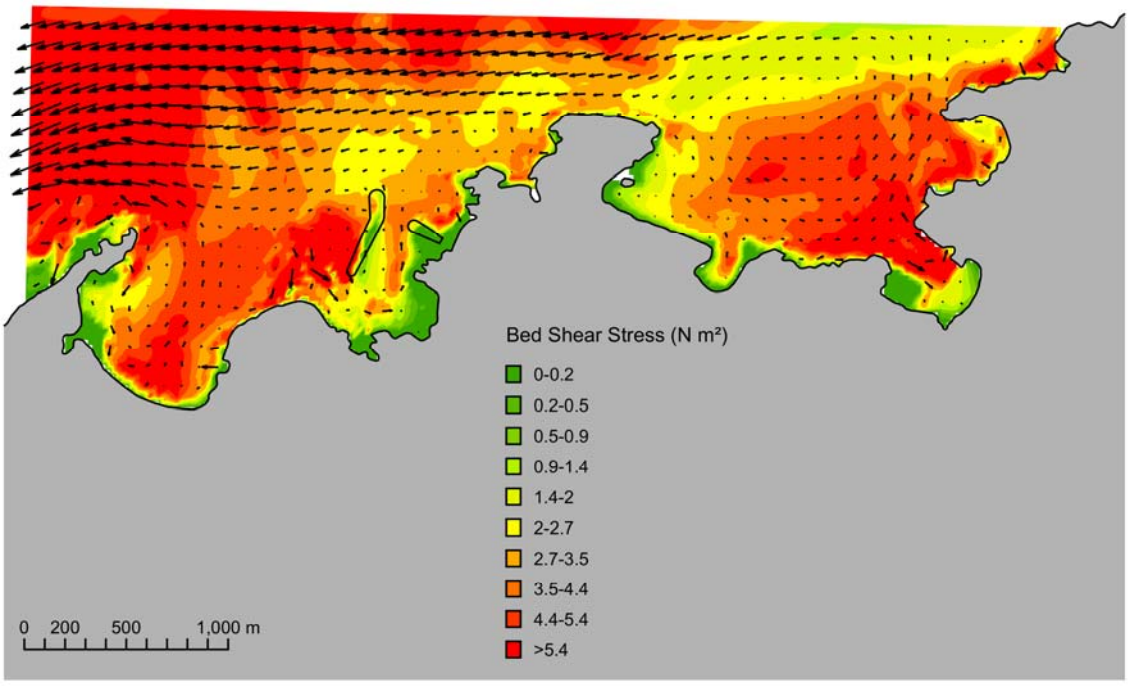

Figure 155 Spring tide mid ebb Extreme wave – With Power Station. Arrows represent current vectors.

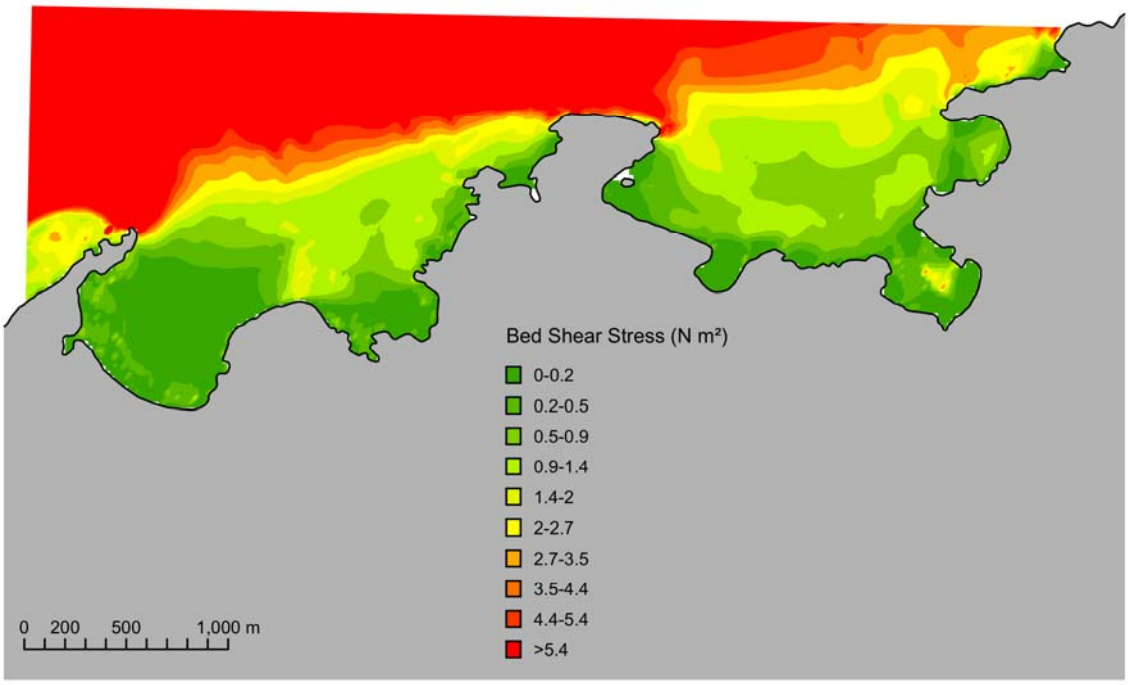

Figure 156 Maximum bed shear stress – Baseline spring tide typical wave.

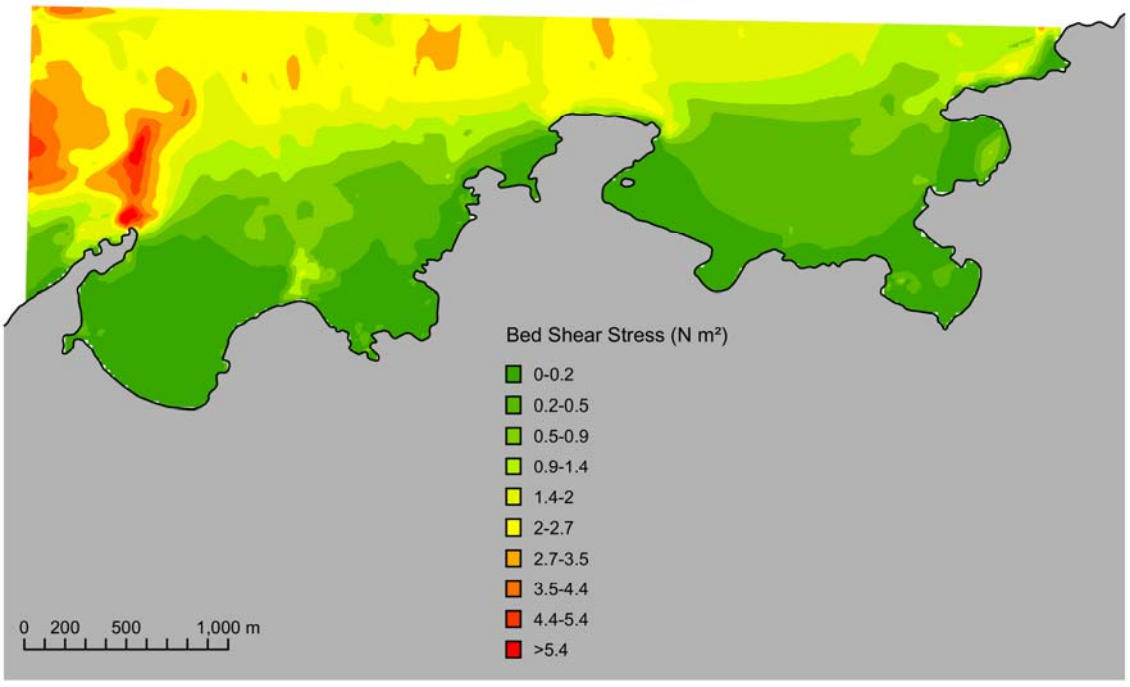

Figure 157 Maximum bed shear stress: – Baseline neap tide typical wave.

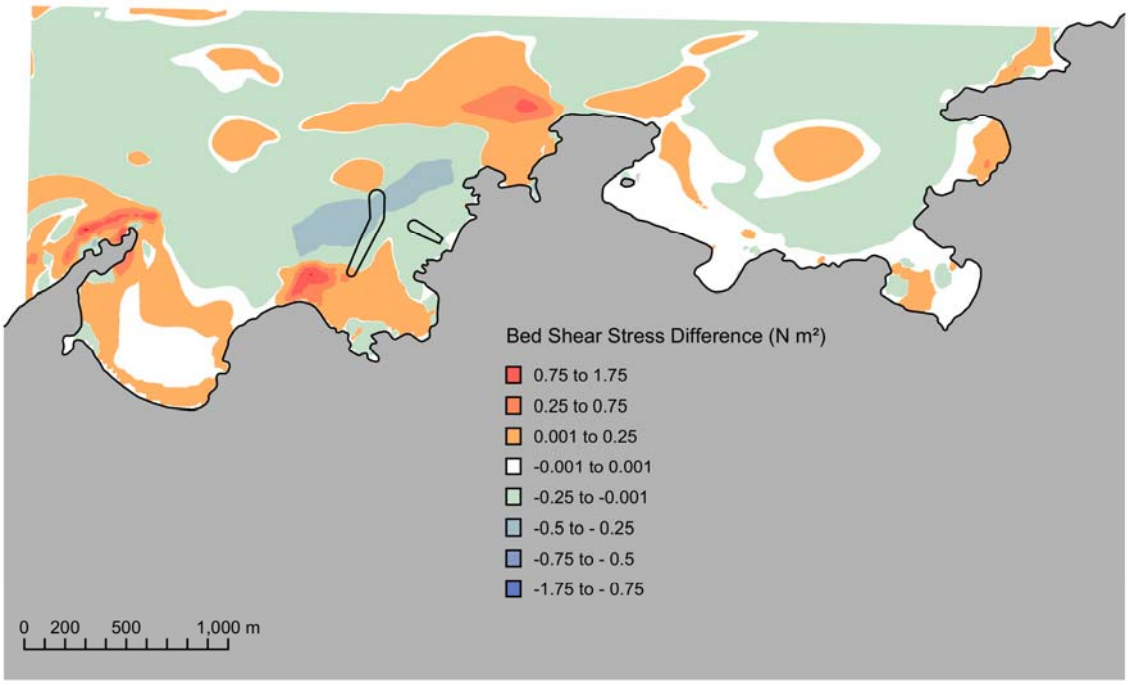

Figure 158 Average difference in bed shear stress – With and without Power Station for a spring tide typical wave.

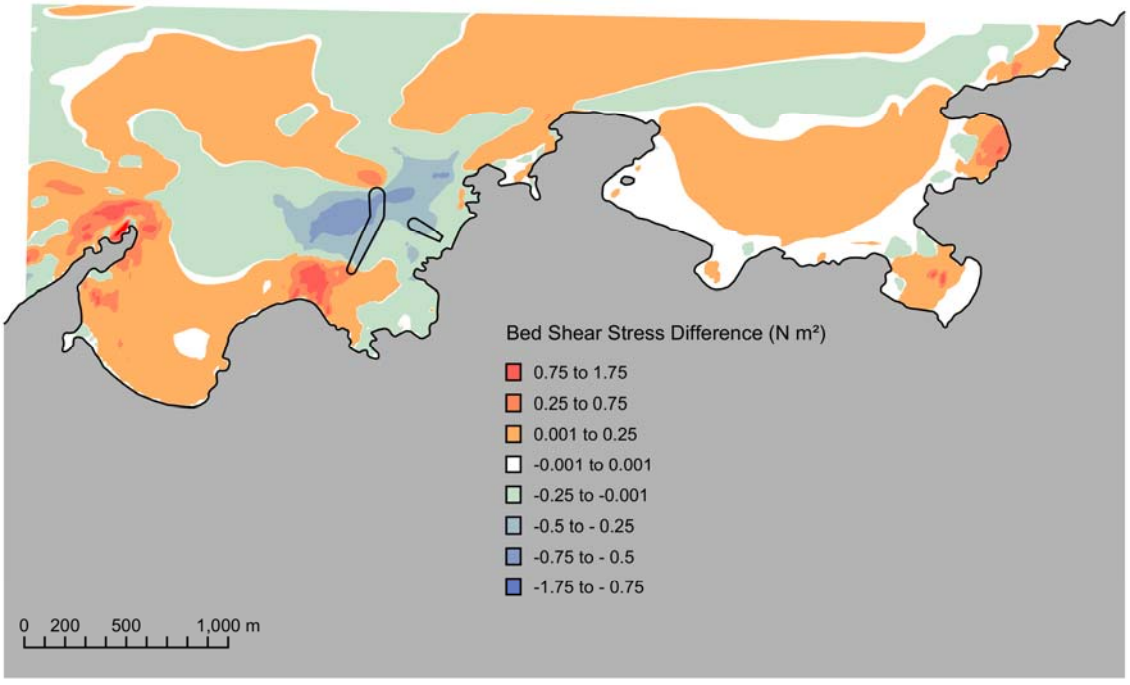

Figure 159 Average difference in bed shear stress – With and without Power Station for a neap tide typical wave.

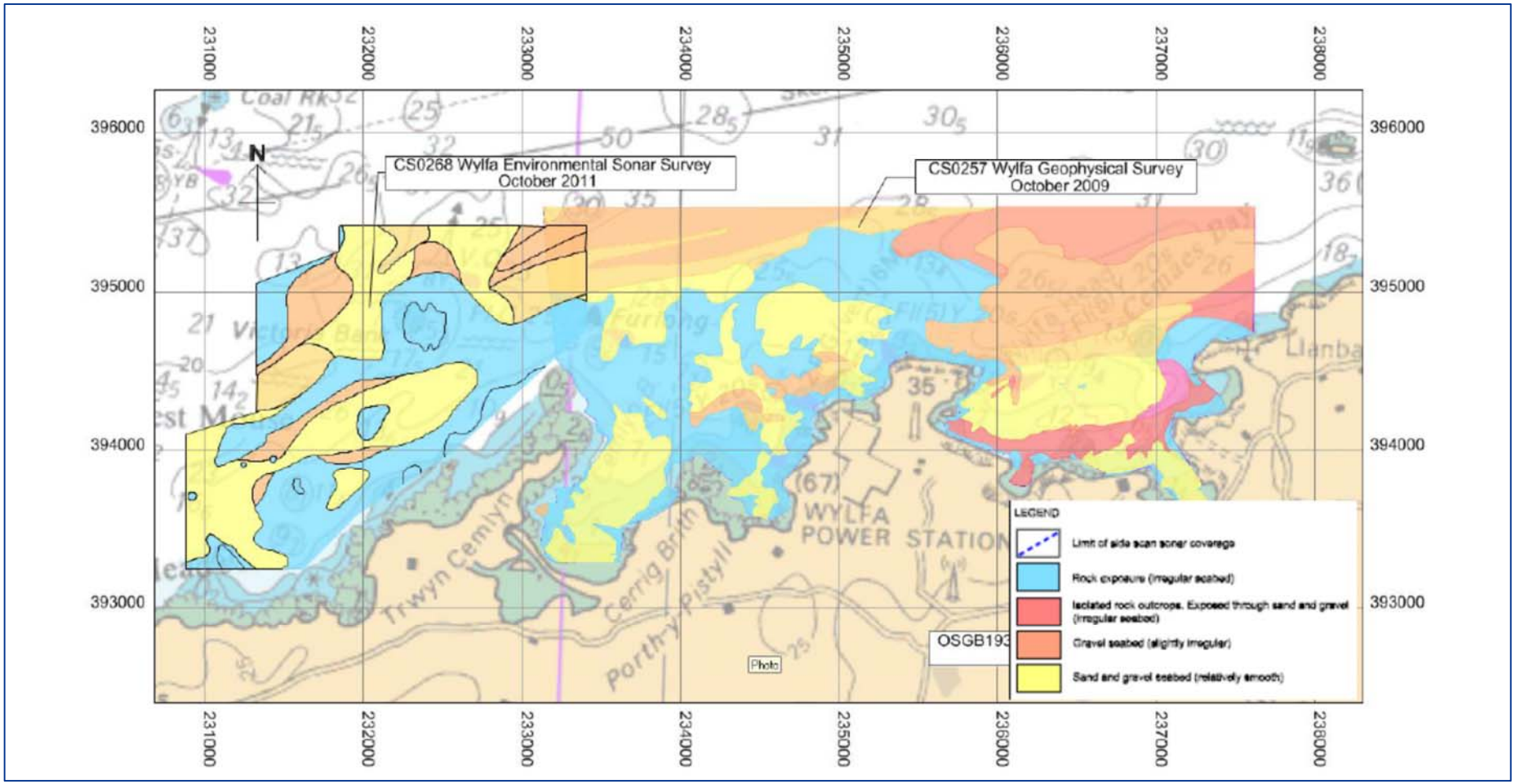

Figure 160 Seabed map (Titan, 2012).

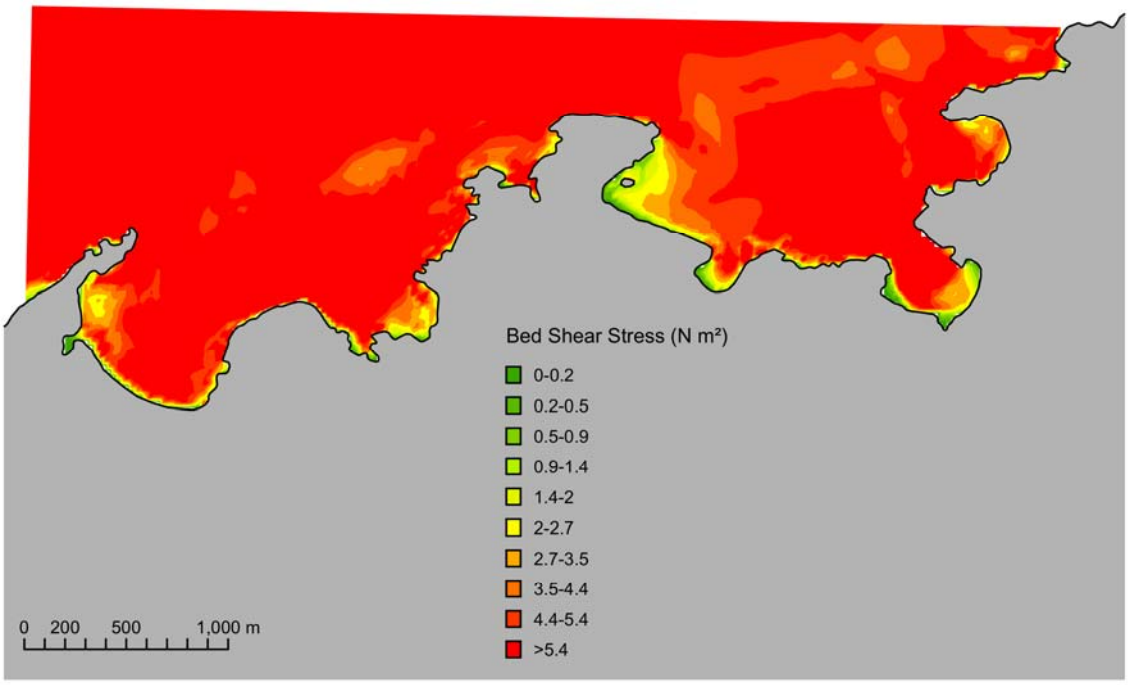

Figure 161 Maximum bed shear stress: Spring Tide Extreme North Wave – Without Power Station.

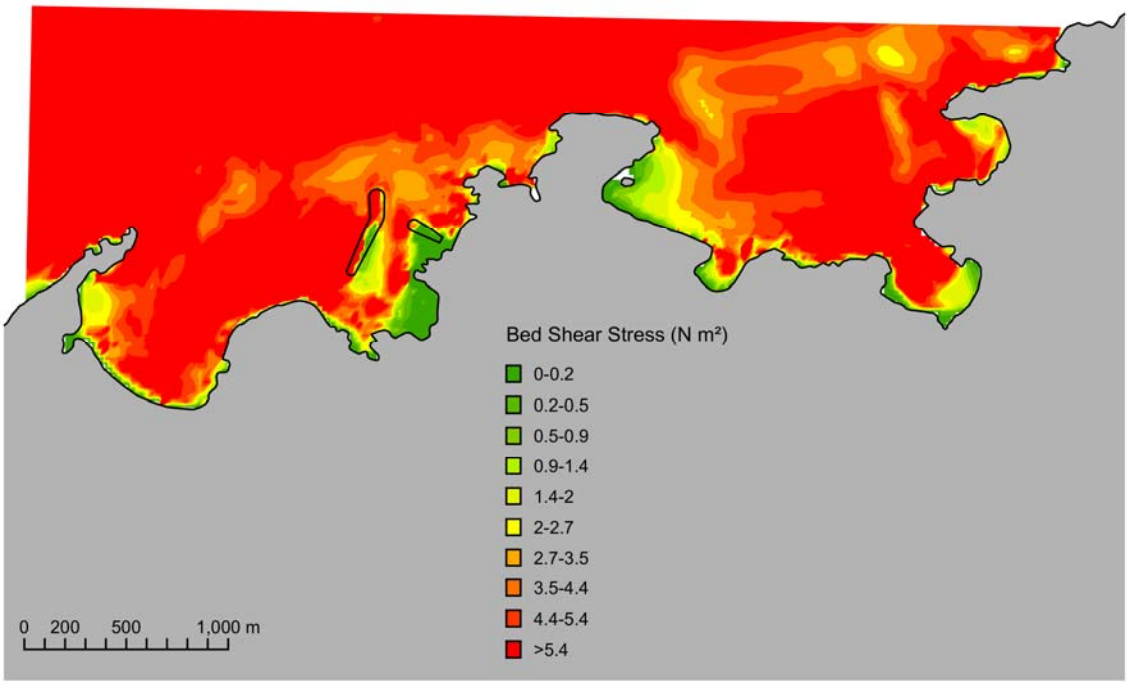

Figure 162 Maximum bed shear stress: spring tide Extreme north wave – With Power Station.

12.6 Discussion of Bed Shear Stress Simulations

Simulations without the Power Station have been undertaken with and without waves which allows for an assessment of the sensitivity of bed shear stress to waves. The results suggest that offshore currents are the dominant factor in bed shear stress as there is little difference in the predicted bed shear stress with wave action included.

However, inshore within the bays waves can be an important influence on bed shear stresses. There is limited influence on bed shear with the typical wave condition, and an increasing influence as the wave height is increased. Wave direction is key influencing factor because of the orientation of the coastline and because the presence of headlands tends to reduce the potential for waves from the most common south westerly directions to impact on the bays around Wylfa.

The construction of the breakwaters results in differences in the depth-averaged flow field but has limited impact on the bed shear stress for the typical wave condition simulation (e.g. a small increase in the predicted bed shear north of the headland to the west of Cemlyn Bay). However,there are differences in the bed shear for the stronger winter wave condition. The bed shear conditions immediately seaward of the shingle bank that forms Cemlyn lagoon are not affected by the Power Station.

13. Drainage Discharge and Dredge Spill Sediment Modelling

13.1 Construction Drainage Discharges- Input Data and Assumptions

The input data and assumptions that underlie the construction phase drainage modelling simulations are summarised in Table 35. The discharges considered include fluvial sources, deep excavation dewatering, cofferdam dewatering, tunnel dewatering and sewage effluent sources. The locations of the drainage discharges are shown in Figure 163. These conditions are representative of a worst case owing to the 1 in 2 storm flows being used as the base flow with a 1 in 30 storm event part way through the 2-week simulation. In addition, the model assumes that the landscape mounds of the Wylfa Newydd Development Area are unvegetated. The model also assumes no wind or waves present.

Table 35 Summary of the drainage discharge modelling assumptions

Drainage discharge	Component freshwater discharges	Source of flows at each point	Suspended solids conc. (mg/l) (1 in 2 yr flows)	Suspended solids conc. (mg/l) (1 in 30 yr flows)	Notes
1S - Cemaes Bay	A3 via Nant Cemaes	Only surface drainage Base flow taken as the peak 1 in 2 storm flow = 1.53m^3/s 24hr storm flow taken as the peak 1 in 30= 2.85m^3/s	40	110	Base flow taken as the 1 in 2 flows Inclusion of a 24hr storm event using the 1 in 30 flows
A2 – Cemaes Bay	A2 direct to sea	Only SW drainage Base flow taken as the 1 in 2= 0.0009m^3/s 24hr storm flow taken as the 1 in 30= 0.146m^3/s	70	300	Base flow taken as the 1 in 2 flows Inclusion of a 24hr storm event using the 1 in 30 flows
2S - Porth y Wylfa	A1 and B1 via Tre'r Gof outfall channel	Only SW drainage Base flow taken as the peak 1 in 2 storm flow (estimated from flood modelling output) = 0.50m^3/s 24hr storm flow taken as the peak 1 in 30 (estimated from flood modelling output) = 0.80m^3/s	70	400	Base flow taken as the 1 in 2 flows Inclusion of a 24hr storm event using the 1 in 30 flows
PB and PC	Direct to sea	1. SW drainage. From each discharge point, 1 in 2 (0.005m^3/s) and for 1 in 30 (1.174m^3/s) Plus, 2. Groundwater from dewatering of deep excavations (0.0014m^3/s) Plus, 3. Groundwater from tunnelling (PC only - does	70	300	Base flow taken as the 1 in 2 flows Inclusion of a 24hr storm event using the 1 in 30 flows

Drainage discharge	Component freshwater discharges	Source of flows at each point	Suspended solids conc. (mg/l) (1 in 2 yr flows)	Suspended solids conc. (mg/l) (1 in 30 yr flows)	Notes
		not get discharged at PB) (0.07 m^3/s) TOTAL flow- PB: 1 in 2- 0.0064m^3/s & 1 in 30-1.1754m^3/s PC: 1 in 2- 0.0764m^3/s & 1 in 30 1.2454m^3/s			
3S – from the Afon Cafnan into Porth-y-pistyll	C1, D1, D2 and E1 via Afon Cafnan	SW drainage Peak 1 in 2 storm flows= 5.62m^3/s Peak 1 in 30 storm flow= 7.83m^3/s	40	200	Base flow taken as the 1 in 2 flows Inclusion of a 24hr storm event using the 1 in 30 flows
OCD- Outfall cofferdam	N/A	Drainage from cofferdam. 1 in 2 rainfall= 0.000983796m^3/s plus seawater infiltration = 0.005555m^3/s, and 1 in 30 year flow = 0.00179398m^3/s plus seawater infiltration = 0.005555m^3/s 2. Groundwater from tunnelling (0.07 m3/s) TOTAL flow- 1 in 2- 0.076539m^3/s / 1 in 30- 0.077349m^3/s	70	300	Discharge split btw rainfall, marine and tunnel GW Base flow taken as the 1 in 2 flows Inclusion of a 24hr storm event using the 1 in 30 flows
MCD- Main cofferdam (Porth-y-pistyll)	N/A	Flow comprises- GW (0.002315m^3/s), marine water (0.0083333m^3/s), and rainfall (0.043449m^3/s) for 1 in 2 flow Total flow of 0.05409722m^3/s GW (0.002315m^3/s), marine water (0.0083333m^3/s), and rainfall (0.078704m^3/s)for 1 in 30 flow Total flow of 0.08935185m^3/s	70	300	Discharge split btw rainfall, marine and GW Base flow taken as the 1 in 2 flows Inclusion of a 24hr storm event using the 1 in 30 flows
CSD- Sewage discharge at tip of northern		0.0185m^3/s for 15 hour duration	30	n/a	Assumed to be an open pipe bed discharge

Drainage discharge	Component freshwater discharges	Source of flows at each point	Suspended solids conc. (mg/l) (1 in 2 yr flows)	Suspended solids conc. (mg/l) (1 in 30 yr flows)	Notes
breakwater					
SCSD- Sewage discharge for Site Campus just east of the outfall cofferdam		0.0185m^3/s for 12 hour duration	30	n/a	Assumed to be an open pipe bed discharge, ~50m off the coast

JACOBS

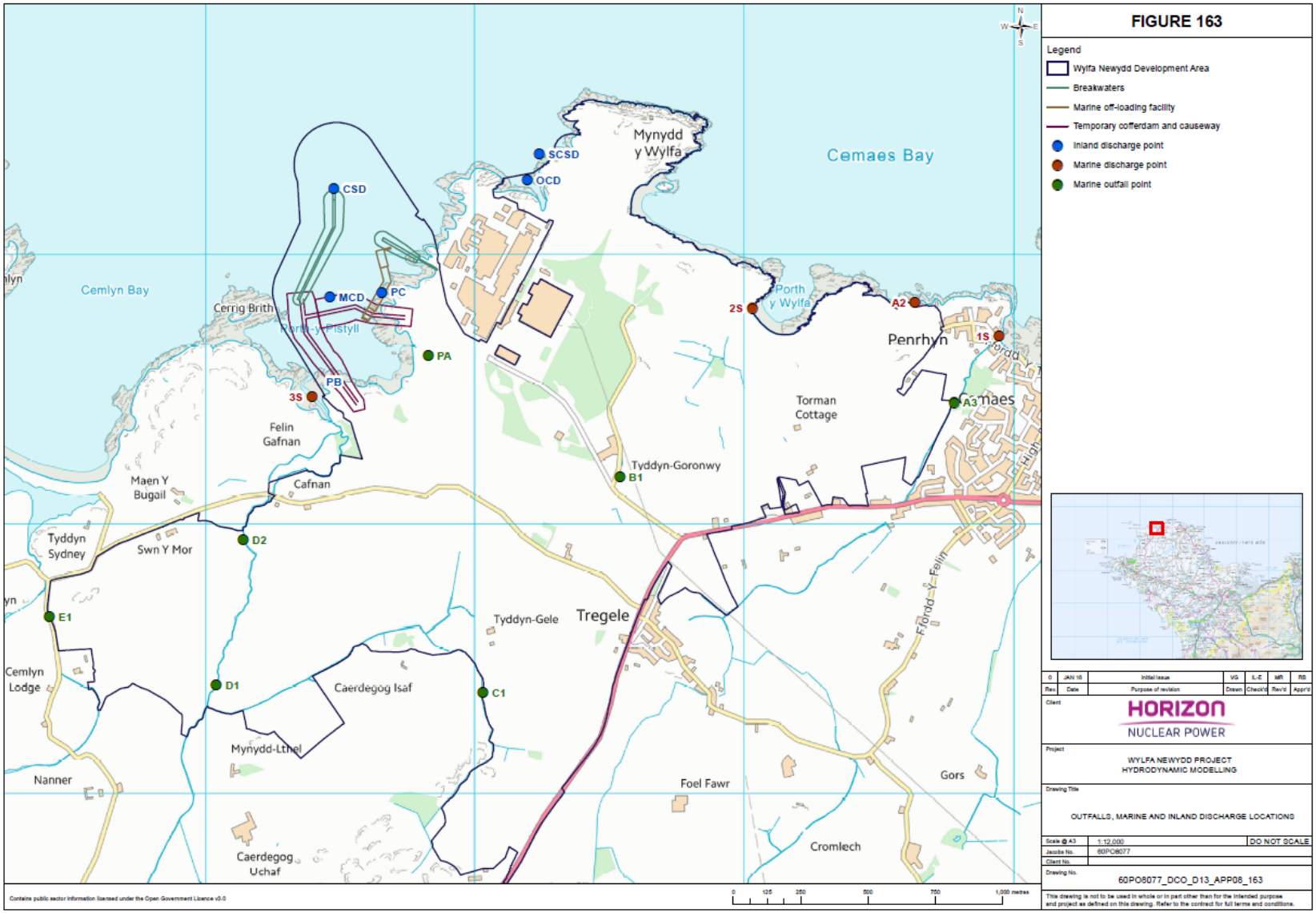
FIGURE 163
Legend
Wylfa Newydd Development Area
Breakwaters
Marine off-loading facility
Temporary cofferdam and causeway
Inland discharge point
Marine discharge point
Marine outfall point
Cemaes Bay
Mynydd y Wylfa
SCSD
OCD
CSD
MCD
PC
PA
PB
3S
2S
A2
1S
A3
Cemlyn Bay
Cerrig Brith
Porth y Wylfa
Penrhyn
Cemaes
Torman Cottage
Felin Gafnan
Maen Y Bugail
Cafnan
Tyddyn-Goronwy
B1
Tyddyn Sydney
Swn Y Mor
D2
E1
D1
C1
Tyddyn-Gele
Tregele
Caerdegog Isaf
Mynydd-Lthel
Cemlyn Lodge
Nanner
Foel Fawr
Gors
Cromlech
Caerdegog Uchaf
Ffordd-y-Felin
HORIZON NUCLEAR POWER
WYLFA NEWYDD PROJECT
HYDRODYNAMIC MODELLING
OUTFALLS, MARINE AND INLAND DISCHARGE LOCATIONS
1:12,000
DO NOT SCALE
60PO8077
60PO8077_DCO_D13_APP08_163

13.2 Dredging Activities- Input Data and Assumptions

The main dredging activity will occur in the region of the western breakwater where there is the greatest volume of over burden to be removed. The release of fine material from dredging activity was represented by three releases along the length of the western (400m) breakwater plus two additional releases within the dredged area of the harbour. The duration of the spill followed that adopted for previous studies, which assumed a longer (541m) breakwater, and hence a larger proportion of the overburden. With a shorter breakwater there will be less material to remove and hence the simulations were conservative in terms of the fugitive spill.

It was assumed that the vessel works the following pattern every 24hrs:

- 2hrs on site to load 3500m3 of dredge material
- 4hrs transit time to the Disposal Site
- 2hrs to offload the dredge material
- 4hrs transit time back to the dredge site
- 2hrs on site to load 3500m^3 of dredge material
- 4hrs transit time to the Disposal Site
- 2hrs to offload the dredge material
- 4hrs transit time back to the dredge site

Hence the total dredged material in any one 24 hour period would be 7000m^3.

For the proposed semi dry approach there is 160 000m^3 of material to remove by dredging. Of this material it is estimated that 20% is soft material (sand and silt) for which there is potential for 5% to be lost from the dredging barge as a spill. In addition there is estimated to be 120 000m^3 of soft material under the breakwaters that may be required to be removed. The maximum quantity of soft material to be removed is then 220 000m^3.

Using the assumed working pattern of 7000m^3 per day of material the soft material will take approximately 31 days (17 for the breakwater and 14 for the remainder). In practice it may be that for areas where the soft material is a relatively thin layer over the rock there will not be a separate soft and hard removal process. In this case the soft material was removed alongside the hard and while the volume remained the same the removal rates were reduced.

The simulated scenarios provide a conservative prediction of the dredge fugitive sediment based on the available information.

13.3 Suspended Solids Particle Size

The suspended solids particle sizes from project discharges is assumed to consist of fine clay sediments which have a particle size of 2 µm or less. Such fine particles have a very low Stokes settling velocity. In freshwater a 2 µm sphere takes nearly eight hours to settle 0.1 m, with such a low settling velocity the discharge could be represented by a conservative tracer. However, in saline water and in higher concentrations the settling of clay is less straightforward and can exhibit flocculation (Lintern 2003, Sutherland *et al*., 2014). Flocculation increases the particle size and hence settling velocity; the settling of clay is therefore influenced by the concentration of the sediment as at low concentrations the potential for particle collisions and hence flocculation is lower. At low concentrations (Filostrat 2014 Figure 2.5) the settling velocity is that for individual particles, as the concentration increases flocculation results in an increase in settling velocity. Above a threshold concentration further increases result in reduced velocities as particles hinder each other's settling.

Two further model simulations were undertaken with cohesive sediment included in the hydrodynamic model. The settling velocity was set to 0.2mm/s for both of these simulations. This velocity was measured by Sutherland *et al*. (2014) for a clay settling in water with a marine salinity. The concentration of clay in their experiments was much greater than proposed at 14.7g/l. Flocculation, settlement and resuspension levels are relevant here in terms of the subsequent assessment of the outputs in terms of environmental effects. Filostat (2014) suggests that the proposed concentration of 100mg/l in the pond effluent is on the border between free settling and flocculation (given as 100 to 300 mg/l). The modelled settling velocity is therefore conservative as it assumes flocculation is occurring and therefore higher settlement velocity, which could show higher local sedimentation in local sensitive habitats e.g. Cemlyn Ridge. However, in practice the lower free settling velocity may well be applicable; therefore lower sedimentation than predicted would likely occur in local sensitive habitats.

The model requires a critical bed shear stress at which the sedimented material is re-suspended. As with settling the behaviour of clay material is relatively complex and the critical shear stress can vary with the age of the deposited material. Beaulieu *et al.* (2003) conducted experiments that involved both measuring the settling velocity and critical bed shear stress for clay material settling in saline waters. Their values of bed shear stress were used as they measured the stress required to re-suspend recently deposited clays. The critical shear stress measured for deposits of three to 24 hours age was 0.07 to 0.09 N/m^2. A value of 0.1 N/m^2 was used in the modelling study as a conservative estimate of the critical bed shear stress (as there would be reduced resuspension, and therefore potential to be carried away from local sensitive habitatsof sedimented material with a higher critical stress).

13.3.1 Dredge particle size fractions

The particle size distribution assumed for the dredge activities was represented by four particle sizes covering both sand and fine particles; these are the same proportions as used in the Holyhead Deep dredge disposal study.

Table 36 Dredge spill particle size fractions

Sediment fraction name	Percentage of total (%)	Diameter (µm)
Coarse Sand	56	1000
Medium Sand	12	300
Fine Sand	9.6	100
Silt (Cohesive)	22.4	63

13.4 Representation Drainage Discharges

Drainage discharges were represented in the model as an inflow at the appropriate location in the model. Deflt3D's Walking Discharge was used as necessary. In the Walking Discharge the model will move the inflow to the nearest active cell which is useful for discharges in the intertidal region. The dewatering flows from the two coffer dams was introduced into a model cell mid-way along the seaward side of the coffer dam.

13.5 Wave Condition

The most common wave condition (Hawkes 2015) is for a wave with a significant wave height of 1m from the southwest. As the simulations will occur over a long duration a typical wave condition is the most appropriate to use.

13.6 Dredge Scenario

The dredge model simulation was set up to run from 1 July 2011 to 17 July 2011 as a spin up period, and during this period the baseline fluvial discharges were in operation but the wave model was not coupled to the hydrodynamics nor was the dredging spill included. The dredge activities were simulated for the period between the 17 July and 21 August. After the 21 August, there was a six-day post dredge period with the baseline fluvial discharges still in operation. The wave model was run coupled to the hydrodynamics hourly starting on the 17 July until the end of the simulation. Model results were stored for the full period following the spin up (17 July to 27 August).

The fugitive spill from the dredging was included at five locations, three along the western breakwater and two within the harbour area.

13.7 Drainage Scenario

The drainage simulation included a spring-neap-spring cycle as spin up. During the spin up the drainage discharges were in operation and hence the spin up allowed both the hydrodynamics and suspended solids concentrations to settle.

The flows used in the scenario were the 1:2 year flows with the relevant concentrations of suspended solids included as per Table 35 (i.e. ranging from 30 to 70 mg/l). The model ran from 17 June 2011 to 28 August 2011 with the discharge in operation from the outset (a total of 72 days). A 24 hour storm event (1:30 year flow) with suspended solid concentrations as per Table 35 was introduced on the 19 August and the output of this has been presented separately.

During the simulation, the wave model was coupled to the hydrodynamics to allow the maximum sediment deposition to be demostrated. In addition the breakwater, temporary causeway and main coffer dam were in place to give a worst case in terms of sediment deposition as a result of restricting mixing in the near shore area.

13.8 Results

The predicted suspended soilds concentrations and thickness of deposited material are detailed in the following sections.

13.8.1 Dredging activities- worst case suspended solids

The four suspended solids size fractions have been summed and the resulting total concentration plotted in Figure Figure 164 to Figure 166 for 1 hour post the final dredge event at the near bed, mid depth and near surface layers in the model.

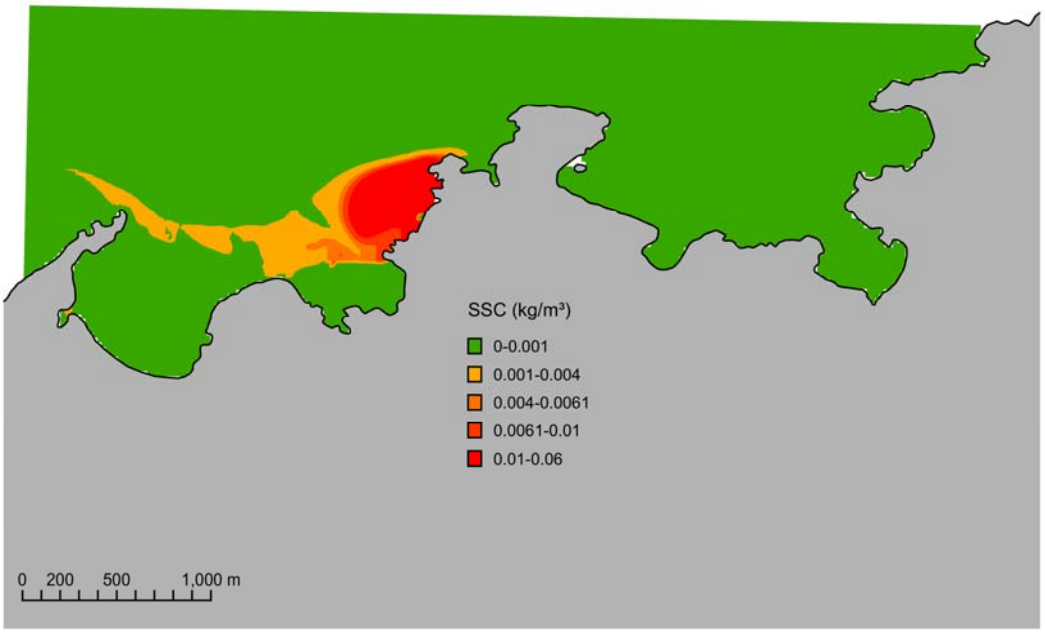

Figure 164 Suspended solids concentration (kg/m3) an hour after the final dredge: Surface

The near surface area with an increase of suspended solids greater than 6.1mg/l (measured ambient SCC between May 2010 and August 2012, Jacobs 2012) an hour after the final dredge ends is 18.5hectares (Figure 164).

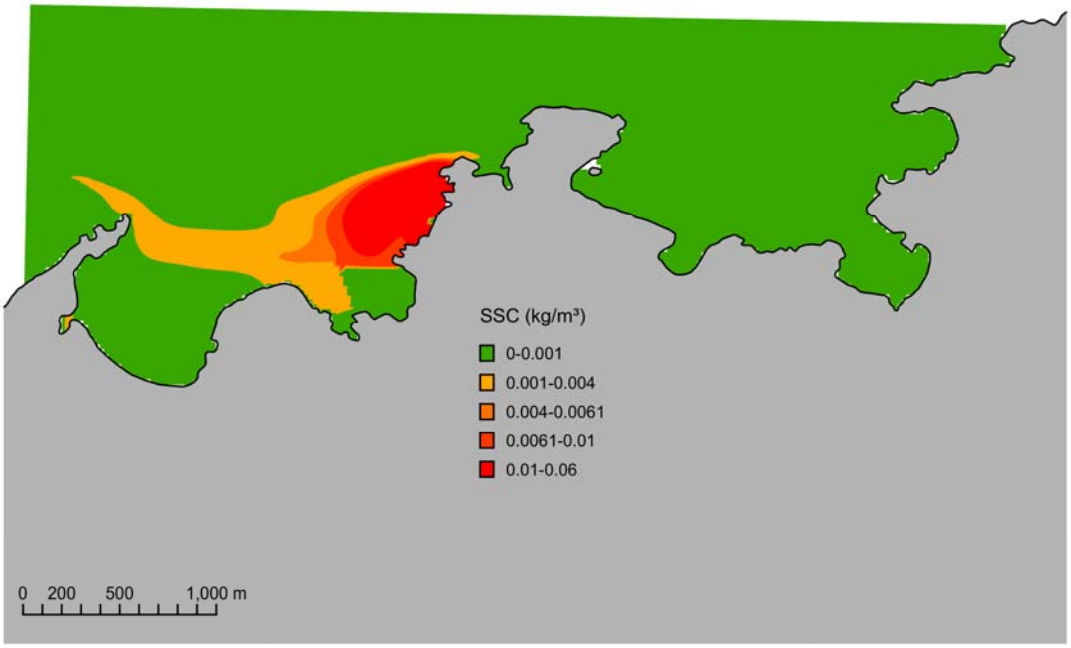

Figure 165 Suspended solids concentration (kg/m³) an hour after the final dredge: Mid depth

The mid depth area with an increase of suspended solids greater than 6.1mg/l an hour after the final dredge ends is 24.5hectares (Figure 165).

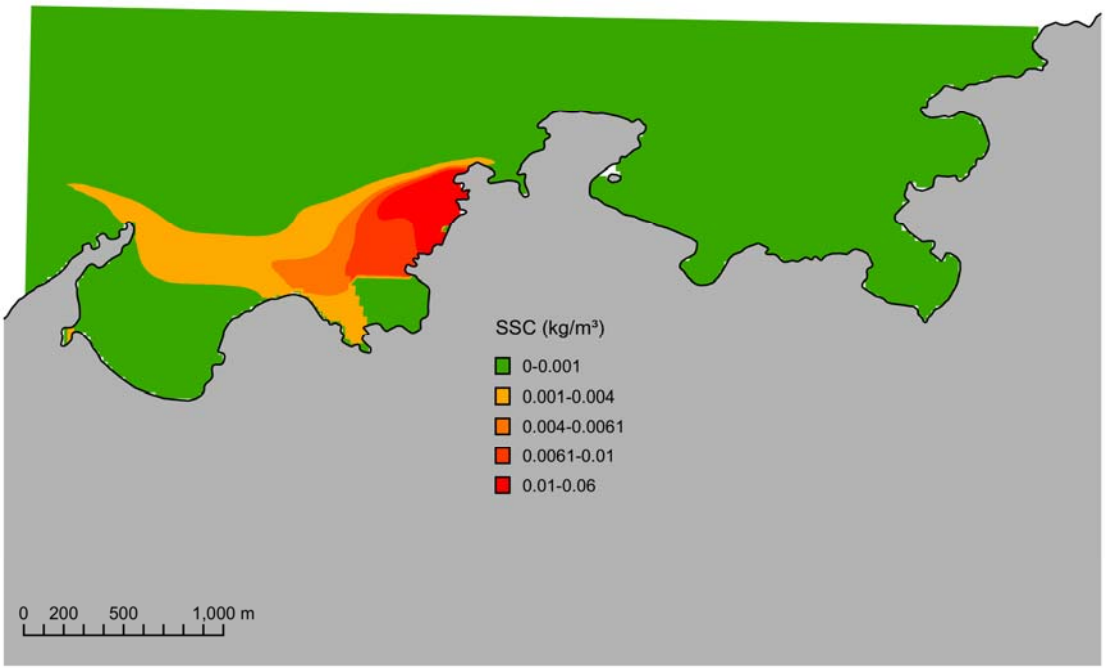

Figure 166 Suspended solids concentration (kg/m³) an hour after the final dredge: Near bed

The near bed area with an increase of suspended solids greater than 6.1mg/l an hour after the final dredge ends is 20.7hectares (Figure 166).

13.8.2 Dredging activities- worst case deposition of suspended solids

The modelled deposition of suspended solids on the bed an hour and six days after the last dredge event are plotted in Figure 167 and Figure 168. Differences in the distribution of the material at these two times reflect the potential for transport of the deposited sediments.

The data shown in Figure 167 have been plotted using the MarLIN thickness bands. The model predicts 0.9mm to 4mm of deposition in parts of Cemlyn Bay with less than 0.9mm around the shingle bank that forms Cemlyn Lagoon. The highest concentrations are at the spill locations. The predicted heights at these locations are unrealistic because in practice the vessel will not return to the same five locations over the course of the 35-day dredge program. The model also ignores the action of the dredger which will remove any deposited material in the active work areas.

Figure 167 and Figure 168 show very little difference between an hour after the last dredge and six days later at the end of the simulation. The only changes (i.e. a reduction in sediment thickness) involve a narrow band (<100m in width) hugging the coastline around Porth-y-pistyll between Porth Wnal and the area to be designated as the MOLF. There are also very slight decreases in sediment thickness in discrete areas to the north east of Cemlyn Bay.

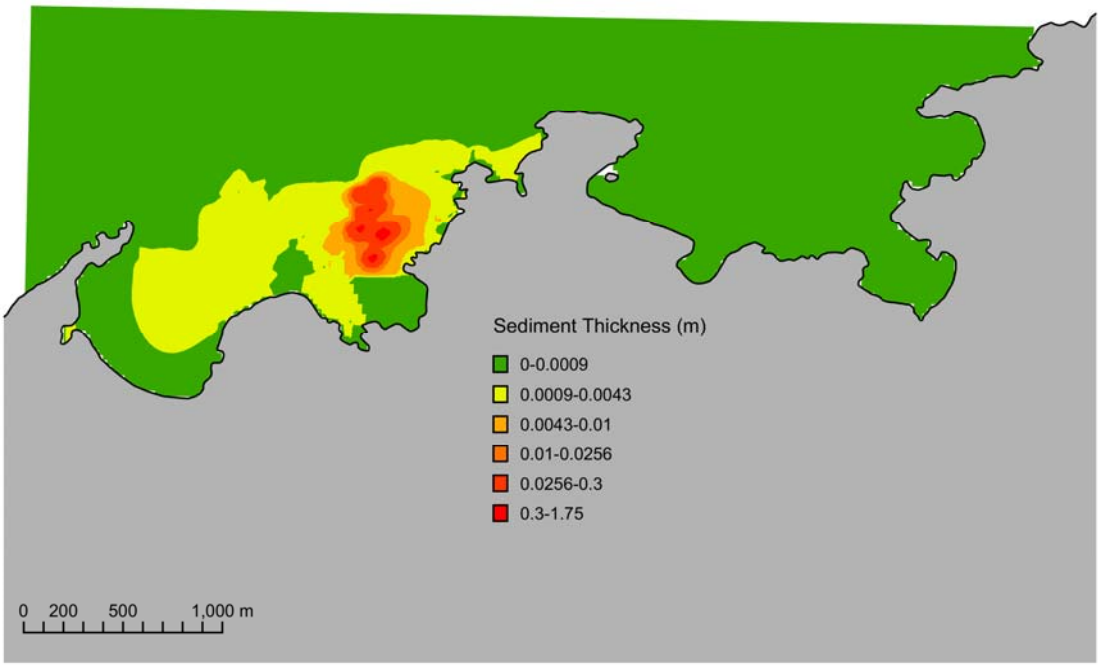

Figure 167Predicted sediment thickness one hour post dredging at end of 17 July-21 August simulation

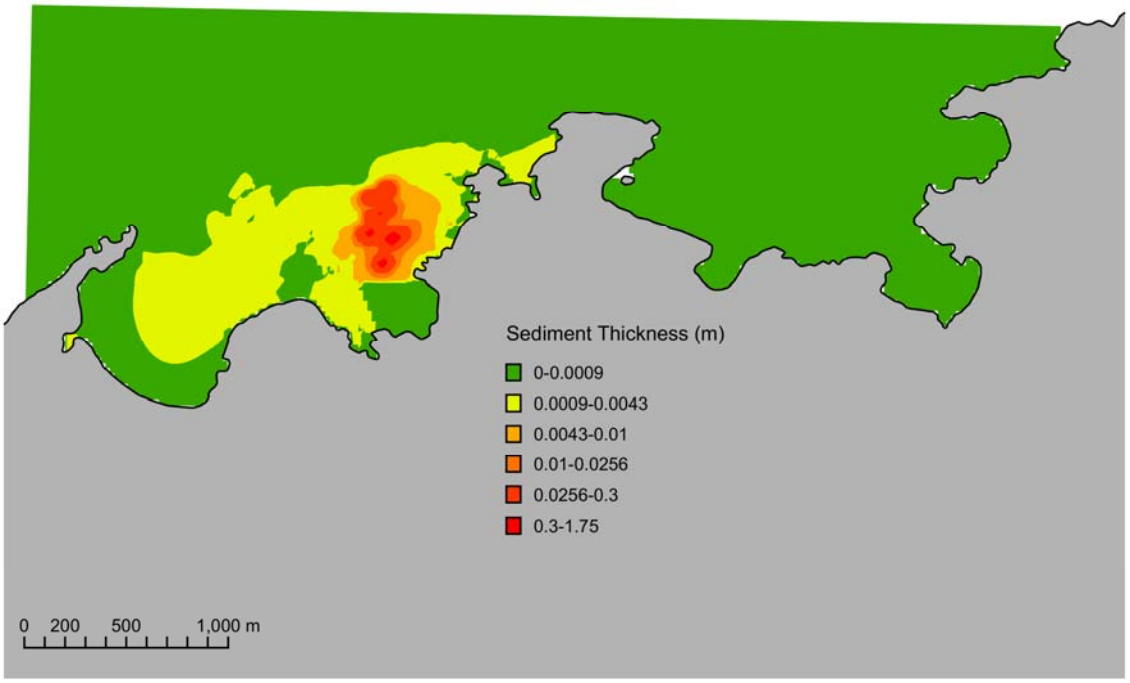

Figure 168 Predicted sediment thickness post dredging (+6 days) at the end of the simulation- 27 August.

13.8.3 Construction drainage- worst case suspended solids

The mid depth, worst case suspended solids concentration data for the peak 1 in 2 storm flows with a 1 in 30 peak storm flow are plotted in Figure 169 (end of simulation, representing a 2-week period) and Figure 170 (end of a 1 in 30 storm event part way through the simulation). The scenarios are a worst case owing to the use of peak flows during the simulation, assumption of no vegetation on all mounds within the Wylfa Newydd Development Area, as well as the absence of wind or waves during the simulation.

The maximum predicted concentration is 0.106 kg/m^3 which falls within the extreme lower end of the Water Framework Directive classification of turbid (i.e. 6 mg/l outside the intermediate turbid classification boundary). These areas classified as turbid were within close proximity to the outfall near Cerrig Brith covering an area of 0.05ha. The ambient total suspended solids as recorded *in situ* between 2010 and 2016 (see appendix D13-1, Application Reference Number: 6.4.83) were classified as intermediate turbid. The low suspended solids concentrations predicted by the model over the wider area reflect the relatively low flux of silt from the drainage discharges and the high levels of dilution in the bays either side of Wylfa Head.

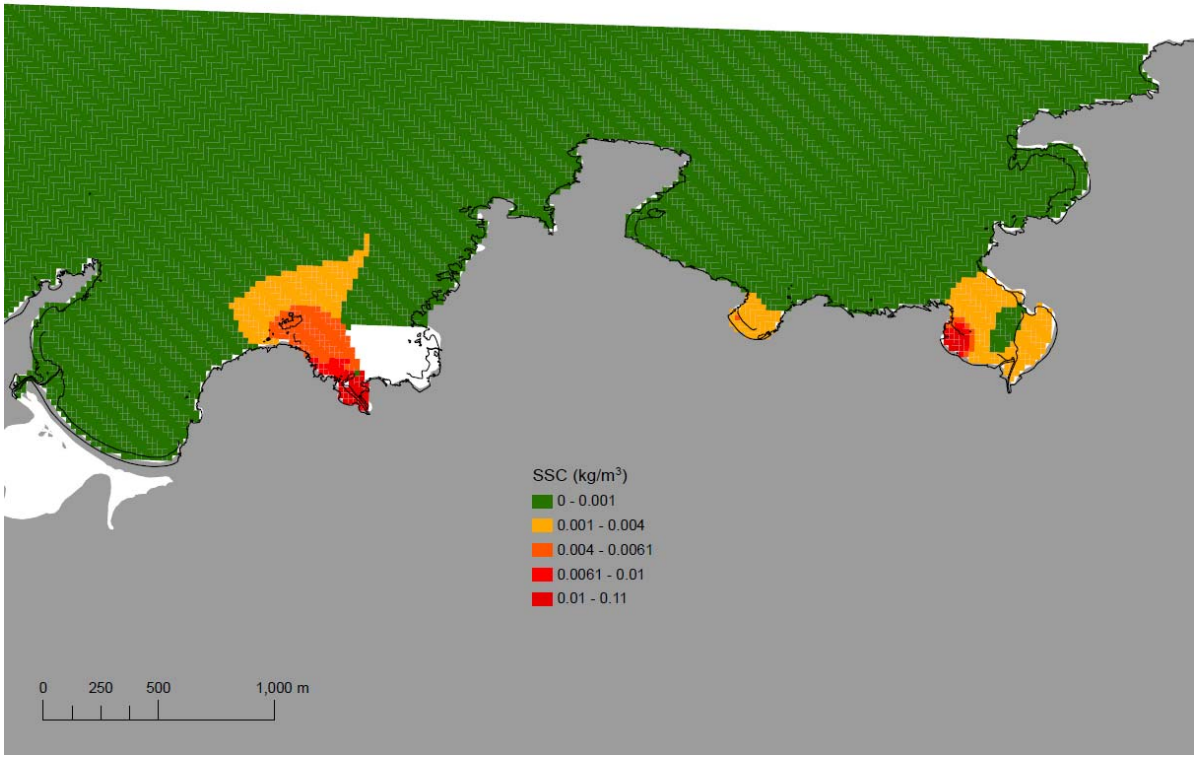

Figure 169 A worst case end of model simulation: a 1 in 2 storm with a 1 in 30 storm event part way through (no wind or waves) construction drainage suspended solids concentration (kg/m^3). Blanked out area represents the main coffer dam area.

After the storm event (Figure 170), there was an increase in both the extent of areas of elevated suspended solids concentration adjacent to the outfalls, and the maximum suspended solids concentration (0.115kg/m^3), although the latter is still within the extreme lower end of the WFD turbid classification (the area within this classification totalled 0.22ha).

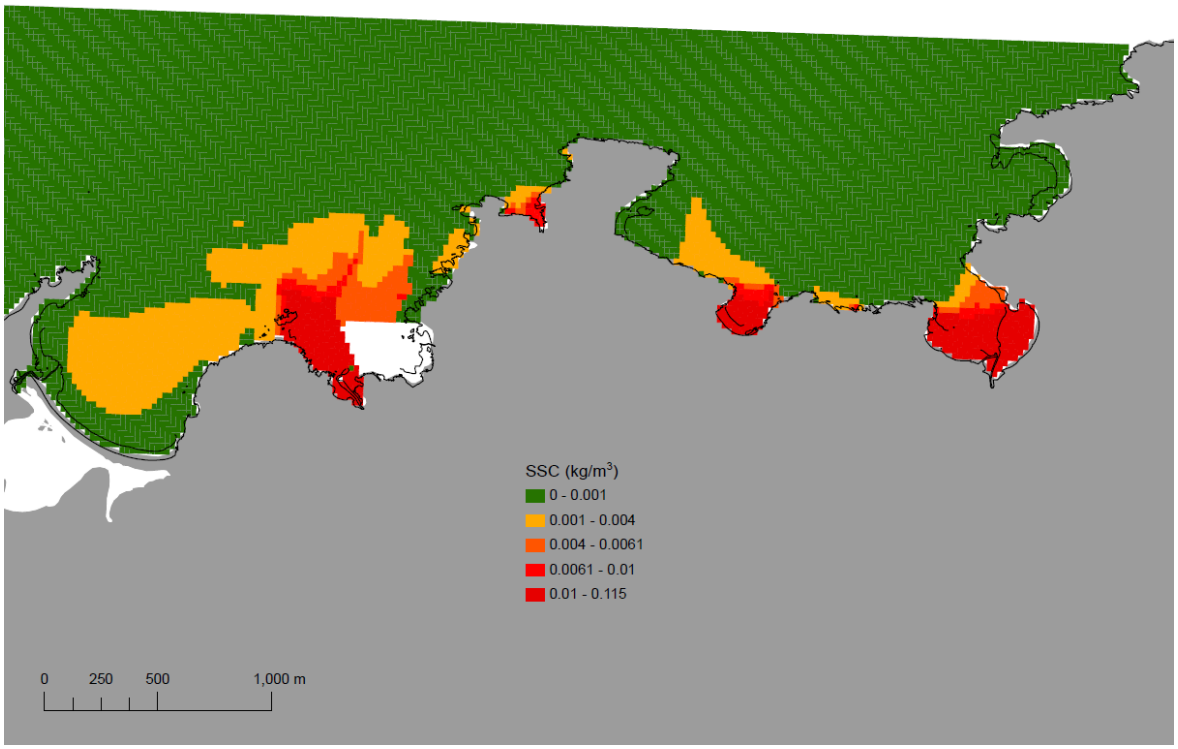

Figure 170 A worst case model simulation: part way through model simulation at the end of 1 in 30 storm event (no wind or waves) construction drainage suspended solid concentration (kg/m^3). Blanked out area represents the main coffer dam area.

13.8.4 Construction drainage- worst case deposition of suspended solids

The predicted thickness of suspended solids deposited on the bed as a result of the construction drainage at the end of the worst case modelling simulation is plotted as Figure 171.

It should be noted that the sediment thicknesses presented are a worst case as they do not incorporate wind or wave stress and are for a 1 in 2 storm event with a 1 in 30 storm peak flows occurring mid-way through with mounds unvegatated. The figures show there to be very low levels of deposition of suspended material from the construction drainage discharges over the majority of area towards Cemlyn Lagoon (<0.2cm). There is an area of higher deposition around Cerrig Brith, partly as a result of the breakwater, which in reality would not reach the sediment depth indicated (<6.3cm) as there would be the added dispersion owing to wave action. The coupled hydrodynamic and wave modelling studies have shown that for wave conditions which represent typical winter and higher (98 percentile) waves, bed shear stress in the near shore is dominated by the wave induced stress.

According to the MarLIN Marine Evidence based Sensitivity Assessment (MarESA) criteria, deposition of up to 5cm in a single event is classified as light smothering with heavy smothering being up to 30cm in a single discrete event (Tillin and Tyler Walters 2014; 2015a; 2015b). Deposition of up to 1cm in a single event is assumed to represent smothering comparable to natural events and the deposition within Cemlyn Bay (excluding the area of Cerrig Brith) is therefore considered to be of negligible magnitude. This assumption is based on extensive literature which contains studies relating to natural sedimentation processes and ecological effects (Miller *et al*., 2002).

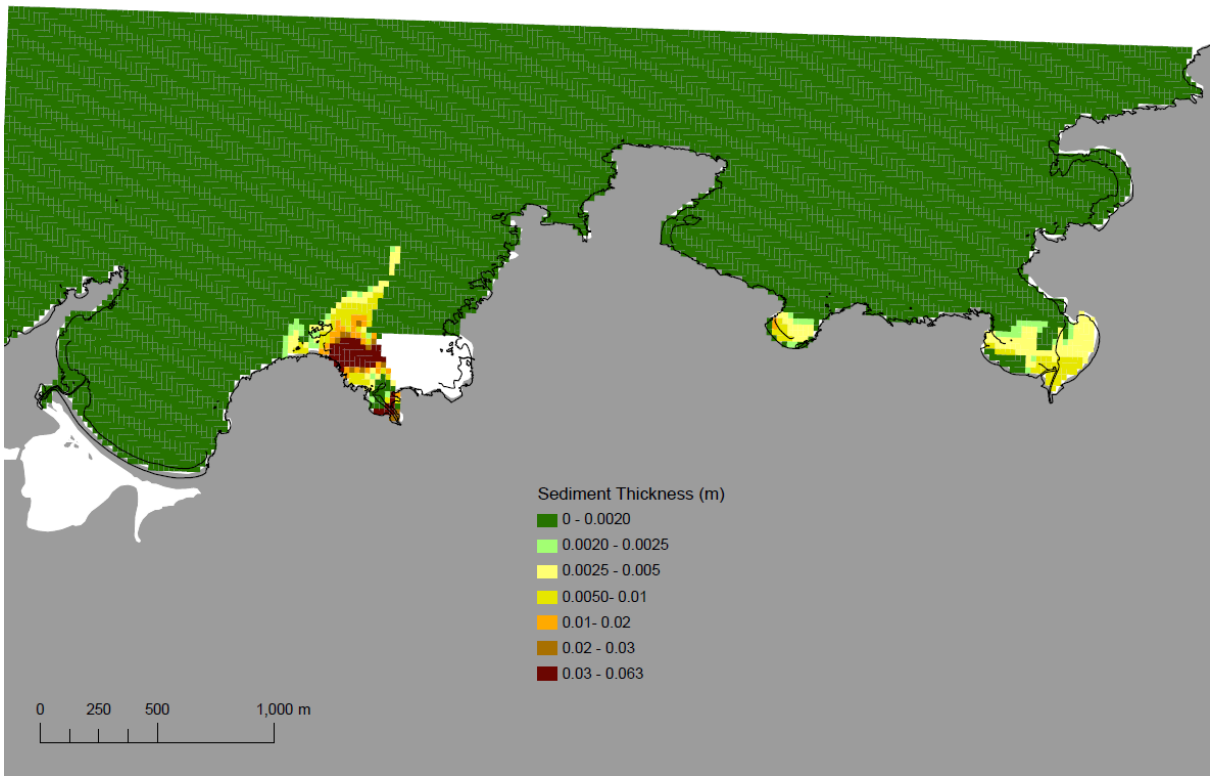

Figure 171 A worst case model simulation: end of model simulation for a 1 in 2 storm with a 24-hour 1 in 30 storm event part way through (no wind or waves) predicted thickness of deposited material (m). Blanked out area represents the main coffer dam area.

14. References

ABPMer (2016). Audit of the Wylfa Hydrodynamic Model, Second Review, R.2583 P2, September 2016.
APEM Ltd (2012). Infra-Red Survey. Draft Report No. WYB0890.

Atkins (2017). Preliminary Design for Construction Surface Water Drainage and Concept Design. Atkins report to Horizon Nuclear power Ltd. Ref: 5151821-301-002; Revision 03. 183 pp.

Beaulieu, S.E., Sengco, M.R. and Anderson, D.M. (2003). Using clay to control harmful algal blooms: deposition and resuspension of clay/algal flocs, Woods Hole Oceanographic Institution, Woods Hole, MA 02543.

BEEMS (2011a) Chlorination by-products in Power Station cooling waters. British Energy Estuarine and Marine Studies, Scientific Advisory Report Series 2011 no. 009.

BEEMS (2011b). Thermal standards for cooling water from new build nuclear power stations. British Energy Estuarine and Marine Studies, Scientific Advisory Report Series 2011 no. 008.

Department of Energy and Climate Change (DECC) (2011). National Policy Statement for Nuclear Power Generation (EN-6). Available from: https://www.gov.uk/government/uploads/system/uploads/attachment_data/file/37051/2009-nps-for-nuclear-volumeI.pdf [Accessed January 2016].

EDF (2011). Predicted Effects of New Nuclear build on Water Quality at Hinkley Point. Cefas Report to EDF Energy. 162 pp.

Environment Agency (2010). Cooling Water Options for the New Generation of Nuclear Power Stations in the UK. Report SC070015/SR3. 214pp.

Environment Agency (2011). H1 Annex D-Basic Surface water discharges. Report No. GEHO0810BSXL-E-Ev2.2. 50 pp.

Filostrat, J. E. (2014). Estimation of Sediment Resuspension and Deposition in Coastal Waters, University of New Orleans Theses and Dissertations. Paper 1796.

Fredsoe (1984). Turbulent boundary layer in wave-current interaction." Journal of Hydraulic Engineering 110: 1103-1120.

Hawkes (2015). Wylfa Newydd Wave Modelling: Phase 1 DER5524-RT001-R01-00 December 2015.

Hawkes (2016). Wylfa Newydd Wave Modelling: Phase 2 DER5524-RT005-R01-00 October 2016.

HELCOM (2017). HELCOM Monitoring Manual. Appendix 3. Available at http://www.helcom.fi/Documents/Action%20areas/Monitoring%20and%20assessment/Manuals%20and%20Guidelines/Manual%20for%20Marine%20Monitoring%20in%20the%20COMBINE%20Programme%20of%20HELCOM_PartB_AnnexB8_Appendix3.pdf [Accessed August 2017]

Holthuijsen, L.H. (2007). Waves in Oceanic and Coastal Waters Cambridge University Press ISBN 978-0-521-12995-4

Horizon (2014). Marine Modelling and Assessment Methodology HNP-S5-PAC-REP-00033, Rev.0.2.

Horizon (2011a). Hydrodynamic Modelling for Wylfa: Wind and Heat Transfer (WYL-PD-PAC-REP-0007).

Horizon (2011b). Chlorine Decay Measurements in Saline waters from Wylfa Power Station during Autumn (TECH/GCA/146/11).

Horizon. 2012b. Chlorine Decay Measurements in Saline waters from Wylfa Power Station during Winter (TECH/GCA/155/12).

Horizon (2012a). Wylfa Hydrodynamic and Water Quality Modelling: Phase 2 model build, Calibration and Validation (WYL-PD-PAC-REP-00015).

Horizon (2012c). Chlorine Decay Measurements in Saline waters from Wylfa Power Station during Summer (TECH/AOS/1884/12).

Horizon (2012d). Chlorine Decay Measurements in Saline waters from Wylfa Power Station during Spring (TECH/GCA/159/12).

Horizon (2012e) Development of a statistical model of seawater temperature, DCRM Ref Number: WYL-PD-PAC-REP-00012.

Jacobs (2017a). Summary of Marine Hydrodynamic Modelling: Cooling Water Abstraction- 126m^3/s; Breakwater length- 541m, Jacobs Ref: 60PO8077/AQE/REP/004, 26 May 2017, Client Ref: WN0902-JAC-OS-REP-00029, Rev 0.1.

Jacobs (2012). Consultancy Report Wylfa Water Quality Surveys. Jacobs UK Ltd report to Horizon Nuclear Power Ltd. (W202.01-S5-PAC-REP-00008).

Jacobs (2014). Hydrology Modelling and Assessment Methodology Memo (60PO8007/HYD/REP/002).

Lintern, D.G. (2003). Influences of flocculation on bed properties for fine-grained cohesive sediment, PhD Thesis, University of Oxford.

Miller, D.C., Muir, C.L. and Hauser, O.A. 2002. Detrimental effects of sedimentation on marine benthos: what can be learned from natural processes and rates? Ecological Engineering. 19, pp.211-232.Moores, A. (2011a). Wylfa Hydrodynamic Survey: Development of a statistical model of seawater temperature. Report to Horizon Nuclear Power Ltd No WYL-PD-PAC-REP-00012.

Moores, A. (2011b). Hydrodynamic Modelling for Wylfa: Phase 1 Calibration Study. Report to Horizon Nuclear Power Ltd No. WYL-PD-PAC-REP-00009.

Moores, A. (2011c). Hydrodynamic modelling of Wylfa wave enhanced mixing. Report to Horizon Nuclear Power Ltd No. WYL-PAC-PD_REP-00009.

Moores, A. (2014). Simulating the Decay of TRO: Model formulation and set up in Delft3d RWENpower report ENV/545/2014.

Moores, A. (2016a). A Note on a CORMIX analysis of the Hitachi Outfall design. Report to Horizon Nuclear Power Ltd WNHM002.

Moores, A. 2016b. Selection of Wind Sensitivity Conditions. Report to Horizon Nuclear Power Ltd WNHM008.

Moores, A. (2016c). Summer Source Study. Report to Horizon Nuclear Power Ltd WNHM010.

Moores, A. (2016d). Summer Long Near-Field Case Study Note. Report to Horizon Nuclear Power Ltd WNHM011.

Moores, A. (2016e). Surface Heat flux for Wylfa Newydd modelling 220915. Report to Horizon Nuclear Power Ltd WNHM007.

Soulsby, R.L. and Clarke, S. (2005). Bed Shear Stresses under Combined Waves and Currents on Smooth and Rough Beds Report TR137 Wallingford August 2005.

Soulsby, R.L, Hamm, L. Klopman, G, Myrhaug, D. Simons R.R., and Thomas, G.P.(1993). Wave-current interaction within and outside the bottom boundary layer Coastal Engineering, 21.41-69.

Sutherland, B.R., Barrett, K.J. and Gingras, M.K. (2014). Clay settling in fresh and salt water, Environ. Fluid Mech., DOI 10.1007/s10652-014-9365-0.

Tillin, H. and Tyler-Walters, H. 2014. Assessing the sensitivity of subtidal sedimentary habitats to pressures associated with marine activities. Phase 2 Report – Literature review and sensitivity assessments for ecological groups for circalittoral and offshore Level 5 biotopes. JNCC Report No. 512B, 260 pp. [Online]. [Accessed: October 2016]. Available at: http://jncc.defra.gov.uk/PDF/Report%20512-A_phase1_web.pdf

Tillin, H.M. and Tyler-Walters, H. 2015a. List of definitions of pressures and benchmarks for sensitivity assessment. Discussion document Jan 2015. [Online]. [Accessed: October 2016]. Available at: http://www.marlin.ac.uk/assets/pdf/Pressure-and-benchmark-definition-jan2015-v9-web.pdf.

Tillin, H.M. and Tyler-Walters, H. 2015b. Finalised list of definitions of pressures and benchmarks for sensitivity assessment. May 2015. [Online]. [Accessed: October 2016]. Available at: http://www.marlin.ac.uk/assets/pdf/Finalised-pressure-benchmarks-May2015.pdf.

Titan (2012). Wylfa Oceanography Interpretive Report (WYL-TES-PAC-REP-00024).

UKCP09 (2015). UK Climate Projections. Available at: http://ukclimateprojections.metoffice.gov.uk/21678[Accessed August 2017]

UKTAG (2007). Proposed EQS for Water Framework Directive Annex VIII substances: ammonia (un-ionised) Science Report: SC040038/SR2 SNIFFER, Report: WFD52(ii), SCHO0407BLVT.

UKTAG (2008). UK environmental standards and conditions (phase 2), SR1 2007. Available from: http://www.wfduk.org/sites/default/files/Media/Environmental%20standards/Environmental%20standards%20phase%202_Final_110309.pdf [Accessed July 2017].

van Rijn, L.C. (2016). Initiation of motion and suspension; critical bed-shear stress for sand-mud mixtures. Available from: http://www.leovanrijn-sediment.com/papers/Thresholderosion2016.pdf.[Accessed July 2017].

Water Framework Directive (2015). Water Framework Directive (Standards and Classification) Directions (England and Wales) 2015. 66 pp.

Wither, A., Bamber, R., Colclough, S., Dyer, K., Elliott, M., Holmes, P., Jenner, H., Taylor, C. and Turnpenny, A. (2012). Setting new thermal standards for transitional and coastal (TraC) waters. Marine Pollution Bulletin, 64, pp. 1564 1579.

WQTAG (2006). Guidance on assessing the impact of thermal discharges on European Marine Sites Report No. WQTAG160, 2006.